Faculty of Engineering and Science

Experimental Characterization and Modeling Microwave Heating of Oil Palm Fruits and Bunches

Jessie Chang Sze Ling

This thesis report is presented for the Degree of
Master of Philosophy (Mechanical Engineering)
of
Curtin University

January 2017

DECLARATION

To the best of my knowledge and belief, this thesis contains no material previously published by any other person except where due acknowledgements have been made. This thesis contains no material which has been accepted for the award of any other degree or diploma in any university.

Signature: ……

Name: Jessie Chang Sze Ling

Student ID: 14425859

Date:

LIST OF PUBLICATIONS

Following are the journal papers that have been submitted from current work:

1. J.S.L. Chang, M.C. Law, Y.S. Chan, C.P. Leo, (2015) “Effects of Microwave heating on oil palm mesocarp”, Chemical Engineering Transactions, 45. 1633-1638
2. M.C. Law, E.L. Liew, S.L. Chang, Y.S. Chan, C.P. Leo, (2016) “Modelling microwave heating of discrete samples of oil palm kernels”, Applied Thermal Engineering, 98, 702-726.

ACKNOWLEDGEMENT

This work is supported by the Fundamental Research Grant Scheme (FRGS/2/2014/TK06/CURTIN/03/1) from the Ministry of Education, Malaysia. I would like to express my appreciation to the thesis committees, Associate Professor Dr Perumal Kumar, Associate Professor Dr Chua Han Bing, Dr Law Ming Chiat and Dr Stephanie Chan Yen San for giving me the opportunity to work on this project.

A great thank to my supervisors, Dr Law Ming Chiat and Dr Stephanie Chan Yen San, for their supports, encouragement and valuable guidance at various stages of my master program, that is, during the project introduction, experimental works, modeling developments and thesis writing.

I would also like to acknowledge some collaborations in acquiring data for this thesis dissertation. Firstly, the dielectric properties of the samples are provided by Dr You Kok Yeow, Universiti Teknologi Malaysia (UTM), the SEM images of microwave heated samples are provided by Dr Leo Choe Peng, Universiti Sains Malaysia (USM) and the appearances of microwave heated samples are provided by Mr Bernard Pui from Curtin University Sarawak. Gratitude also goes to Sarawak Oil Palm Bhd for supplying the oil palm fresh fruit bunches for this research work. Special thanks also to the lab technicians, Mr Michael Ding, Mr Aspindy and Mr Andyson, whom have helped and supported me in the preparation of experimental works.

Last but not least, I would also like to thank my parents, siblings, friends and colleagues at Curtin Sarawak for their remote love and support.

ABSTRACT

The implementation of microwave in oil palm processing operations offers numerous advantages. It provides extensive heat generation to accelerate the removal of moisture compared to the conventional heating and drying methods. Consequently, microwave also reduces processing time, which in turn results in energy-saving. Although microwave technology is beneficial in the oil palm milling process, the effects of microwave on the oil palm fruits and bunches are still poorly understood. Therefore, this study aims to investigate the microwave energy interaction with the oil palm fruits and bunches using a multi-physics model. The physical, dielectric, thermal and mechanical are characterized for the prediction of microwave power density and heat-mass transports during microwave heating process in the modelling.

The dielectric properties, thermal conductivity and thermal behavior of the oil palm fruits and bunches are determined using dielectric probe, thermal constant analyzer and Thermogravimetric anlaysis respectively. On the other hand, the effects of microwave energy on fruits detachment during the milling process are dependent on the mechanical behavior and the microstructure changes of the oil palm fruits are investigated using compression testing and Scaning Electron Microscope respectively.

The experimental results show that empty fruit bunches has high dielectric properties but a poor thermal conductivity compared to kernel and mesocarp. Dielectric properties are proportional to the samples' moisture content, whereby lower dielectric properties are attained at lower moisture content. It is found that empty fruit bunches (EFB) have the highest moisture content (485.49 % d.b.), followed by the kernel (28.2 % d.b.) and mesocarp (25.9 % d.b.). Hence, EFB with a highest moisture content are found to have a broader range of dielectric constant ($3.09 \leq \varepsilon_r^{'} \leq 24.4$) and loss factor ($0.68 \leq \varepsilon_r^{''} \leq 12.8$) compared to mesocarp ($3.28 \leq \varepsilon_r^{'} \leq 4.7$, $0.29 \leq \varepsilon_r^{''} \leq 1.10$) and kernel ($2.88 \leq \varepsilon_r^{'} \leq 6.2$, $0.36 \leq \varepsilon_r^{''} \leq 1.08$). It is found that the thermal conductivity for kernel, mesocarp and EFB is 0.68, 0.458 and 0.028W/(m·K) respectively. In order to avoid the decomposition of the oil palm fruits and bunches, thermal analysis is conducted. The analysis show that the decomposition temperature for mesocarp, kernel and fruit bunches starts from 100 °C.

The experiments show that microwave heating increased the mechanical properties. On the other hand, the micrographs show no physical damage is found after the samples are subjected to microwave treatment for 2 mins at 100 W and 200 W.

Electromagnetic coupled heat-mass transfer model is developed to describe the microwave heating and drying process of the oil palm kernel, mesocarp and EFB. Maxwell's equation, Fourier heat conduction and Fick's law are used in the developed of the model by modeling the interaction between electromagnetic, heat and mass transfer equations. The model shows good agreements between the experimental and the simulation results.

Electric field, temperature and moisture distributions are analyzed. The microwave power density generation in the EFB, mesocarp and kernel samples is not only dependent on the electric field intensity but also on the dielectric properties of the samples. Among the samples, EFB generated the highest microwave power density due to its larger dielectric properties compared to the kernel and the mesocarp. Subsequently, higher temperature is obtained in the EFB. On the other hand, the simulation result shows a small difference between the volume-averaged and surface average temperature of the kernel and the mesocarp, thus the surface temperature can be an approximation to predict volumetric temperature.

Surface convection, radiation and evaporation reduce the sample surface temperature rapidly, thus minimum temperature is found on the sample surface. Among the mechanisms, radiation is the dominant cooling mechanisms to reduce the sample surface.

The interaction of microwave with FFB is studied. The simulation shows that hot spot occurs in EFB. Mesocarp is quicker heated by this hotspot. High thermal and moisture concentration gradients are observed between the EFB, mesocarp and kernel. These increase heat and moisture transfers in the FFB which lead to a faster heating and drying process.

TABLE OF CONTENTS

Nomenclature IV

Abbreviations VI

List of Figures VII

List of Tables XII

Chapter 1 1

1.1 Background....1

1.2 Problem Statement....6

1.3 Significance and novelty of the study....6

1.4 Objectives of this research....7

1.5 Thesis structure....7

1.6 Conclusions....8

Chapter 2 9

2.1 Fundamentals of microwave heating....9

2.2 Microwave heating and drying for agricultural products....14

2.2.1 Microwave drying....14

2.2.2 Application of microwave heating in oil palm industry....14

2.3 The effects of heating and drying....16

2.3.1 The effect of heating on thermal properties....16

2.3.2 The effect of heating and drying on mechanical properties....18

2.3.3 The effects of heating on microstructure, texture and appearance...19

2.4 Mathematical modelling of drying process....20

2.4.1 Convective drying models....20

2.4.2 Microwave drying models....25

2.5 Summary....28

Chapter 3 29

3.1 Assumptions and limitations....29

3.2 Materials preparation....29

3.2.1 Determination of size....29

3.2.2 Determination of moisture content....30

3.3 Characterization experimental procedures....31

3.3.1 Permittivity measurement....31

3.3.2 Characterization of thermal properties of Kernel, Mesocarp and EFB32

3.4 Microwave heating and drying experiment....33

3.5 Effects of microwave irradiation....35

3.5.1 Determination of Mechanical properties of Kernel, Mesocarp and EFB 35
3.5.2 Microstructure analysis 37
3.6 Summary 38
Chapter 4 39
4.1 Characterizations 39
4.1.1 Initial moisture content 39
4.1.2 Permittivity measurement 40
4.1.3 Thermal conductivity measurement 46
4.1.4 Thermal behavior characterization 47
4.2 Microwave heating and drying 50
4.3 The effects of microwave heating and drying 57
4.3.1 Mechanical behaviour characterization 57
4.3.2 SEM analysis 62
4.4 Summary 68
Chapter 5 69
5.1 Introduction 69
5.2 Assumptions and limitations 69
5.3 Computational domain 70
5.4 Governing equations 75
5.4.1 Electromagnetics field 75
5.4.2 Conservation of moisture content 75
5.4.3 Conservation of energy 76
5.4.4 Initial and boundary conditions 76
5.5 Input parameters 81
5.6 Numerical procedures 82
5.7 Mesh generation 84
5.8 Summary 86
Chapter 6 87
6.1 Model validations 87
6.2 Electric field distributions 97
6.3 Microwave power density generation and power lost 105
6.4 Temperature and moisture distributions 108
6.5 Summary 124
Chapter 7 125

7.1 Computational domain....125
7.2 Mesh generation....128
7.3 Electric field distributions....130
7.4 Microwave power density generation and power lost....133
7.5 Temperature and moisture distributions....136
7.6 Summary....143
Chapter 8 144
8.1 Characteristics of kernel, mesocarp and EFB....144
8.2 Effects of microwave heating and drying on kernel, mesocarp and EFB....144
8.3 Heat and mass transfers of oil palm kernel, mesocarp and EFB....145
8.4 Heat and mass transfers of FFB....146
8.5 Significance of the current work....146
8.6 Recommendations for future work....147
Reference 149
Appendix 163

NOMENCLATURE

A	frequency factor	1/s
A_s	area	m^2
c	moisture concentration	mol/m^3
c_o	speed of light	m/s
c_e	equilibrium moisture concentration	mol/m^3
$\dot{c}_{evap}$	moisture evaporation rate	$mol/(m^3s)$
C_p	heat capacity	J/(kg·K)
d_p	penetration depth	m
d_m	geometric mean diameter	m
d_{cater}	diameter of circular crater	mm
d_{silica}	diameter of the silica body in the circular crater	mm
d_{starch}	diameter of granular starch	mm
D	diffusivity	m^2/s
D_o	pre-exponential factor	m^2/s
D_{eff}	effective moisture diffusivity	m^2/s
$\mathbf{E}$	electric field strength	V/m
E_a	activation energy of sample's evaporation process	J/mol
E_d	activation energy of sample's moisture diffusivity	J/mol
E_m	elastic stress	MPa
f	microwave frequency	Hz
h_m	mass transfer coefficient	m/s
h_t	surface convective heat transfer coefficient	$W/(m^2·K)$
$\mathbf{H}$	magnetic flux magnitude density	V·s
H_{evap}	enthalpy of heat formation	J/mol
J	electric current density	A/m^2
k	thermal conductivity	W/(m·K)
l	length	m
L	characteristic length	m
M_{H_2O}	molecular weight of water vapor	g/mol

MC	moisture content	kg/kg d.b.
MC_e	equilibrium moisture content	kg/kg d.b.
MC_o	initial moisture content	kg/kg d.b.
MC_t	moisture content at drying time t	kg/kg d.b.
Nu	Nusselt number	dimensionless
Pr	Prandlt number	dimensionless
P	microwave power	W
q_{cond}	heat flux by conduction	J/m^2s
Q	rate of heat flow	W
$\dot{Q}_{evap}$	evaporative moisture cooling per unit volume	W/m^3
$\dot{Q}_{MW}$	volumetric heat generation per unit volume	W/m^3
$\dot{Q}_{rad}$	heat loss due to radiation per unit volume	W/m^3
R	universal gas constant	J/(K·mol)
R^2	linear coefficient of determination	dimensionless
t	time	s
t_h	thickness	m
T	temperature	°C
$T_{\exp}$	experimental transient temperature	°C
T_s	ambient temperature	°C
T_{sim}	simulated transient temperature	°C
V	volume	m^3
V_o	sample's initial volume	m^3
V_t	sample's volume at drying time t	m^3
w	width	m
w_{cell}	width of cell structure	mm
W	weight	kg
W_{bd}	sample's bone-dry weight	kg
W_o	sample's initial weight	kg
W_t	sample's weight at drying time t	kg
ε_r	permittivity of the material	dimensionless
ε_o	permittivity of free space	F/m

$\varepsilon_r^{'}$	dielectric constant	dimensionless
$\varepsilon_r^{''}$	dielectric loss factor	dimensionless
ρ	density	kg/m^3
$\tan\delta$	loss tangent	dimensionless
μ	relative permeability of the material	dimensionless
δ_{luikov}	thermogradient coefficient in Luikov's system	dimensionless
σ_{luikov}	phase conversion factor from liquid to vapor	dimensionless
σ_y	yield stress	MPa
σ_T	Stefan-Boltzmann constant	W·m/K^4
α	attenuation factor	1/s
ω	angular wave frequency	rad/s
γ_T	emissivity of sample	dimensionless

ABBREVIATIONS

d.b.	dry basis
EFB	Empty fruit bunches
FFA	Free Fatty acid
FFB	Fresh fruit bunches
POME	Palm oil mill effluents

LIST OF FIGURES

Figure 1.1: Structure of a typical oil palm fruit (*Elaeis guineensis*) 1
Figure 1.2: Flow chart of palm oil processing redrawn from Ohimain and Izah (2014) 3
Figure 3.1: Keysight 85070E Dielectric Probe 31
Figure 3.2: Experimental setup for microwave heating and drying 33
Figure 3.3: Schematic diagram showing the locations of fiber optics (P1 and P2) in determination of sample surface temperature during microwave heating. 35
Figure 3.4: Stress-strain curve of kernel at moisture content of 10 % dry basis... 37
Figure 4.1: Dielectric properties of the kernel at various moisture contents at 2.45 GHz. 41
Figure 4.2: Dielectric properties of mesocarp at various moisture contents at 2.45 GHz. 42
Figure 4.3: Dielectric properties of EFB at various moisture contents at 2.45 GHz. 42
Figure 4.4: Loss tangent and penetration depth of (a)kernel, (b)mesocarp and (c)EFB at various moisture contents at a frequency of 2.45 GHz. 45
Figure 4.5: TGA and derivative weight analysis of fresh kernel 48
Figure 4.6: TGA and derivative weight analysis of fresh mesocarp 48
Figure 4.7: TGA and derivative weight analysis of fresh EFB 48
Figure 4.8: Temperature of (a)kernel, (b)mesocarp and (c)EFB subject to various microwave power levels 52
Figure 4.9: (1) Moisture content and (2) drying rate of (a)kernel, (b)mesocarp and (c)EFB subject to various microwave power levels 53
Figure 4.10: Physical appearance of microwave treated oil palm kernel (a) before and after exposure to (b)100 W, (c)180 W, (d)300 W and (e)2 mins at 180 W. .. 56
Figure 4.11: Physical appearance of microwave treated oil palm mesocarp (a) before and after exposure to (b)100 W, (c)180 W, (d)300 W and (e)2 mins at 180 W. 56
Figure 4.12: Physical appearance of microwave treated oil palm EFB (a) before and after exposure to (b)100 W, (c)180 W, (d)300 W and (e)2 mins at 180 W. .. 57
Figure 4.13: (a) Elastic modulus and (b) Yield stress of kernel at different moisture content levels dried at 180 W 58

Figure 4.14: (a) Elastic modulus and (b) Yield stress of mesocarp at different moisture content levels dried at 180 W 59
Figure 4.15: (a) Elastic modulus and (b) Yield stress of EFB at different moisture content levels dried at 180 W 60
Figure 4.16: SEM micrographs at 500x and 1500x magnifications of (a) fresh and microwave treated kernel at powers of (b) 100 W and (c) 200 W under 500x and 1500x magnifications. 63
Figure 4.17: SEM micrographs of (a) fresh mesocarp and that subjected to (b) 100 W and (c) 200 W under 500x magnification. 64
Figure 4.18: SEM micrographs at x1000 and x5000 magnifications of (a) fresh, microwave treated EFB at power level of (b) 100 W and (c) 200 W under 1000x and 5000x magnifications. 67
Figure 5.1: Computational domain of model 71
Figure 5.2: Temperature points of (a) kernel, (b) mesocarp and (c) EFB measured in simulation 72
Figure 5.3: Cut plane 1 of the kernel, mesocarp and EFB models. The horizontal plane is set at the center of the samples; the plane taken for (a) kernel at z=0.0062 m (x–y plane 1), (b) mesocarp at z=0.001775 m (x–y plane 2) and (c) EFB at z=0.0049 m (x–y plane 3) from the conical flask surface. 73
Figure 5.4: Cut plane 2 of the kernel, mesocarp and EFB models. The vertical plane is set at the center of the samples; the plane taken for (a) the kernel, (b) the mesocarp and (c)the EFB at y=0.145 m (x-z plane). 74
Figure 5.5: Flow chart of simulation steps 83
Figure 5.6: Temperature and moisture content of (a) kernel, (b)mesocarp and (c)EFB at t=600 s, with a total number of elements in the model. 85
Figure 6.1: Simulated and experimental temperature of kernel subject to microwave power of (a)100 W, (b)180 W and (c)300 W 88
Figure 6.2: Simulated and experimental temperature of mesocarp subject to microwave power of (a)100 W, (b)180 W and (c)300 W 89
Figure 6.3: Simulated and experimental temperature of EFB subject to microwave power of (a)100 W, (b)180 W and (c)300 W 90
Figure 6.4: Simulated and experimental moisture content of kernel subject to microwave power of (a)100 W, (b)180 W and (c)300 W 91

Figure 6.5: Simulated and experimental moisture content of mesocarp subject to microwave power of (a)100 W, (b)180 W and (c)300 W 92
Figure 6.6: Simulated and experimental moisture content of EFB subject to microwave power of (a)100 W, (b)180 W and (c)300 W 93
Figure 6.7: Distribution of electric field inside the microwave cavity with (a) kernel, (b) mesocarp and (c) EFB viewed on x-y plane. 98
Figure 6.8: Distribution of electric field inside the microwave cavity with (a) kernel, (b) mesocarp and (c) EFB viewed on x-z plane. 99
Figure 6.9: Standing waves in the microwave cavity at z_1=6.2mm, z_2=62mm and z_3=142mm. 100
Figure 6.10: The electric field intensity which is (a) around and (b) inside the kernel through the microwave exposure. 101
Figure 6.11: The electric field intensity which is (a) around and (b) inside the mesocarp through the microwave exposure. 102
Figure 6.12: The electric field intensity which is (a) around and (b) inside the EFB through the microwave exposure. 103
Figure 6.13: Generated microwave power density and power lost per unit area of (a) a kernel, (b) a mesocarp and (c) an EFB due to various mechanisms when subject to 180 W microwave power. 106
Figure 6.14: Electric field intensity in the kernel throughout the microwave heating and drying durations. 109
Figure 6.15: Generated microwave power density in the kernel after (a) 1 min and (b) 5 mins of microwave heating and drying. 109
Figure 6.16: Surface and interior temperature distributions in the kernel after (a) 1 min and (b) 5 mins of microwave heating. 110
Figure 6.17: Electric field intensity in the mesocarp throughout the microwave heating and drying durations. 111
Figure 6.18: Generated microwave power density in the mesocarp after (a) 1 min and (b) 5 mins of microwave heating and drying. 111
Figure 6.19: Surface and interior temperature distributions in the mesocarp after (a) 1min and (b) 5 mins of microwave heating. 112
Figure 6.20: Electric field intensity in the EFB throughout the microwave heating and drying durations. 112

Figure 6.21: Generated microwave power density in the EFB after (a) 1 min and (b) 5 mins of microwave heating and drying. 113
Figure 6.22: Surface and interior temperature distributions in the EFB after (a) 1min and (b) 5 mins of microwave heating. 114
Figure 6.23: Temperature distribution in the center (h/2) of the (a) kernel, (b) mesocarp and (c) EFB during the microwave OFF phase, t = 12-30s. 115
Figure 6.24: Dielectric loss factors of the kernel on the viewed after (a) 1 min (60 s) and (b) 5 mins (600 s) of microwave heating..... 116
Figure 6.25: Dielectric loss factors of the mesocarp viewed on after (a) 1 min (60 s) and (b) 5 mins (300 s) of microwave heating..... 116
Figure 6.26: Dielectric loss factors of the EFB viewed on after (a)1 min (60 s) and (b)5 mins (300 s) of microwave heating. 117
Figure 6.27: Temperature history of (a) a kernel, (b) a mesocarp and (c) an EFB subject to microwave power of 180 W. 118
Figure 6.28: Moisture content history of (a) a kernel, (b) a mesocarp and (c) an EFB subject to microwave power of 180 W. 119
Figure 6.29: Moisture content profiles of kernel after subject to cyclic microwave heating at 180 W for (a) 1 min, (b) 5 mins and (c) 10 mins. 121
Figure 6.30: Moisture content profiles of mesocarp after subject to cyclic microwave heating at 180 W for (a) 1 min, (b) 5 mins and (c) 10 mins..... 122
Figure 6.31: Moisture content profiles of EFB after subject to cyclic microwave heating at 180 W for (a) 1 min, (b) 5 mins and (c) 10 mins. 123
Figure 7.1: (a) Computational model of FFB and the (b) details of FFB. 125
Figure 7.2: The red line (line 1) as indicated is used for result comparisons. 126
Figure 7.3: Cut plane 1 of the FFB models. The horizontal plane is set at the center of the samples; the plane is located at z = 0.0162 m (x-y plane 4) from the cavity surface. 127
Figure 7.4: Cut plane 2 of the FFB models. The vertical plane is set at the center of the samples; the plane is located at y = 0.145 m (x-z plane 4) from the cavity surface. 127
Figure 7.5: Effects of element numbers on estimated (a) temperature and (b) moisture content of kernel, mesocarp and EFB at t=600s. 129

Figure 7.6: Electric distribution (a)in the microwave cavity, (b)around the FFB and (c)within the FFB viewed on x-y plane. The arrows in the figures indicate the direction of the electric fields for the 2.45 GHz incident waves. 131
Figure 7.7: Electric distribution (a)in the microwave cavity, (b)around the FFB and (c)within the FFB viewed on x-z plane. The arrows in the figures indicate the direction of the electric fields for the 2.45 GHz incident waves. 132
Figure 7.8: Power absorbed and lost for (a) a kernel, (b) mesocarp and (c) EFB due to various mechanism when subject to 180 W microwave power. 134
Figure 7.9: The microwave power density of FFB after (a) 5 s, (b) 1 min (60 s) and (c) 5 mins (300 s) of microwave heating. 135
Figure 7.10: Electric field intensity and microwave power density absorbed by mesocarp, kernel and EFB at microwave exposure for 5 s, 60 s and 300 s. 136
Figure 7.11: The temperature distributions in the FFB after (c) 1 min (60 s) and (d) 5 mins (300 s) of microwave heating. 137
Figure 7.12: Average temperature of the kernel, mesocarp and EFB subjected to 180 W microwave power. 138
Figure 7.13: Average moisture content of (a) kernel, (b) mesocarp and (c) EFB subjected to 180 W microwave power. 139
Figure 7.14: Moisture content in mesocarp, kernel and EFB at microwave exposure for the 50 s, 100 s and 300 s. 140
Figure 7.15: Average penetration depth of kernel, mesocarp and EFB during microwave heating and drying. 141
Figure 7.16: Loss tangent of kernel, mesocarp and EFB during microwave heating 142

LIST OF TABLES

Table 1.1: Productivity of the major oil crops in year 2016 (Mielke, 2017) 2
Table 2.1: Approximate ranges of moisture diffusivity in some materials (Mujumdar, 2006) 23
Table 3.1: Duration of ON/OFF state for 1 cycle for microwave power levels at 100 W, 180 W and 300 W..... 34
Table 3.2: Range of sample's moisture content used in the mechanical strength experiment..... 37
Table 4.1: Initial moisture content of kernel, mesocarp and EFB (*Elaeis Guineensis*)..... 40
Table 4.2: Regression equations relating dielectric properties to the moisture content in the kernel, mesocarp and EFB at 2.45 GHz. 43
Table 4.3: Thermal conductivity of mesocarp and EFB slices 47
Table 4.4: Analysis of weight loss of mesocarp, kernel and EFB in four stages with its chemical constituents 49
Table 4.5: Total moisture loss and drying time required to dry oil palm mesocarp, kernel and EFB to reach equilibrium. 54
Table 4.6: Regression equations relating the mechanical strength to the moisture content in the kernel, mesocarp and EFB..... 61
Table 4.7: Width of the cell structure of the fresh and microwave treated kernel. 64
Table 4.8: Width of the cell structure of the fresh and microwave treated mesocarp. 65
Table 4.9: Diameter of the silica bodies, circular crater and granular starch in fresh and microwave treated EFB 66
Table 5.1: Initial moisture content of kernel, mesocarp and EFB. 77
Table 5.2: Mass transfer coefficient of the kernel, mesocarp and EFB. 79
Table 5.3: Properties of oil palm kernel, mesocarp and EFB 81
Table 5.4: Element size and total element numbers of the kernel, mesocarp and EFB case studies for various mesh options..... 84
Table 6.1: Correlation analysis for the simulated and experimental results of samples' temperatures. 94
Table 6.2: Correlation analysis for the simulated and experimental results of samples' averaged moisture content. 94

Table 6.3: Steady state simulated temperature of the kernel, mesocarp and EFB subjected to 100 W, 180 W and 300 W microwave power levels. 95
Table 7.1: Dimensions of the kernel, mesocarp and EFB constructed in the model. 126
Table 7.2: Element sizes and total element numbers of the geometry for various mesh options. 128

CHAPTER 1

INTRODUCTION

1.1 Background

Oil palm trees in Malaysia are mainly from the family of the *Elaeis guineensis* which originates from West Africa and it consists of *Dura* and *Pisifera* species. The *Dura* and *Pisifera* are chosen for interspecific hybrids to form *Elaeis guineensis* for its outstanding yields and it is currently used in Malaysia oil palm industry (Nair, 2010). A typical oil palm fruit consists of three major parts. They are the mesocarp (flesh of the fruit), shell and kernel. Palm oil and kernel oil can be obtained from the mesocarp and kernel respectively. An *Elaeis guineensis* oil palm fruit possesses a thick mesocarp, thin shell and large kernel as shown in Figure 1.1.

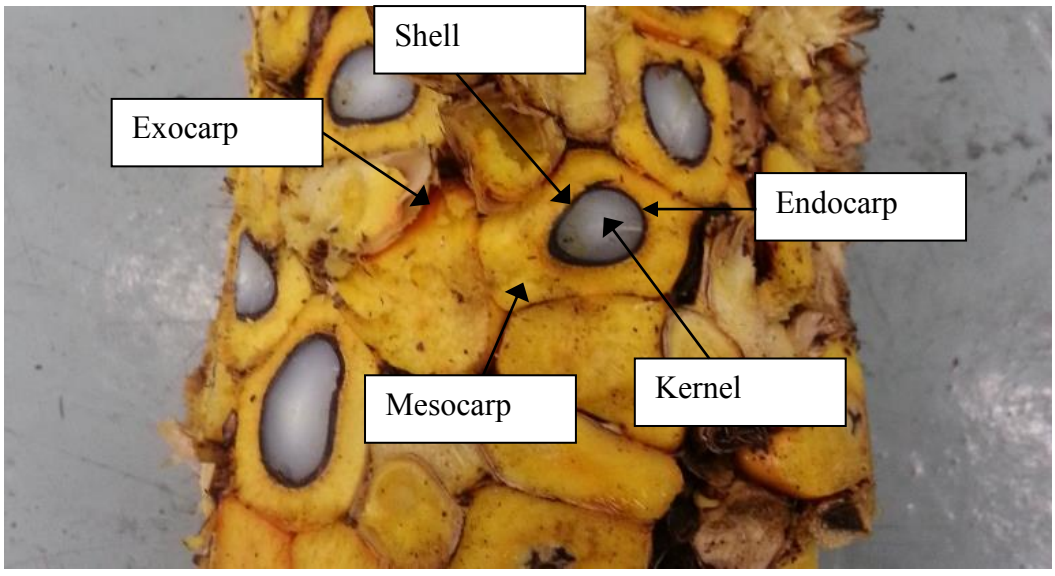

Figure 1.1: Structure of a typical oil palm fruit (*Elaeis guineensis*)

Malaysia is one of the largest producers and exporters of palm oil in the world. As a leading palm oil exporter in the oil palm industry, Malaysia palm oil has been exported to more than 100 countries. According to the statistics (Hassan et al., 2014), an average of 16.04 million tonnes of palm oil and 0.92 million tonnes of kernel oil were exported worldwide in the year 2016.

The usages of palm and kernel oil are very extensive. Palm oil is widely used in food products such as cooking oil, margarine and non-dairy creamers as well as feedstock for biofuel. On the other hand, palm oil has a longer shelf life compared to other vegetable oils. Palm kernel oil is a raw material for the production of non-food products such as soaps, detergents, toiletries, cosmetics and candles. In 2012, palm oil has the highest world consumption among all the oils and fats products (Darby, 2014). Besides palm oil and palm kernel oil, Malaysia also produces other major oil crops as shown in Table 1.1. Mielke (2017) reported that in the year of 2016, oil palm had the highest edible oil production.

Table 1.1: Productivity of the major oil crops in year 2016 (Mielke, 2017)

Oil crop	**Oil content (%)**	**Oil production (million tons)**
Palm oil (mesocarp)	20.1	20.98
Sunflower	41.2	4.37
Rapeseed	39.7	2.17
Palm kernel oil	45.4	1.45
Coconut	66.1	0.82
Groundnut	43.2	0.14
Cottonseed	14.7	0.09

Palm and kernel oils are extracted from oil palm fruits through physical and mechanical processes in palm oil milling process. Figure 1.2 shows a typical palm oil milling process. The milling process includes the pre-treatment of fresh fruit bunches (FFB), seed pressing process, oil refinery and fractional process.

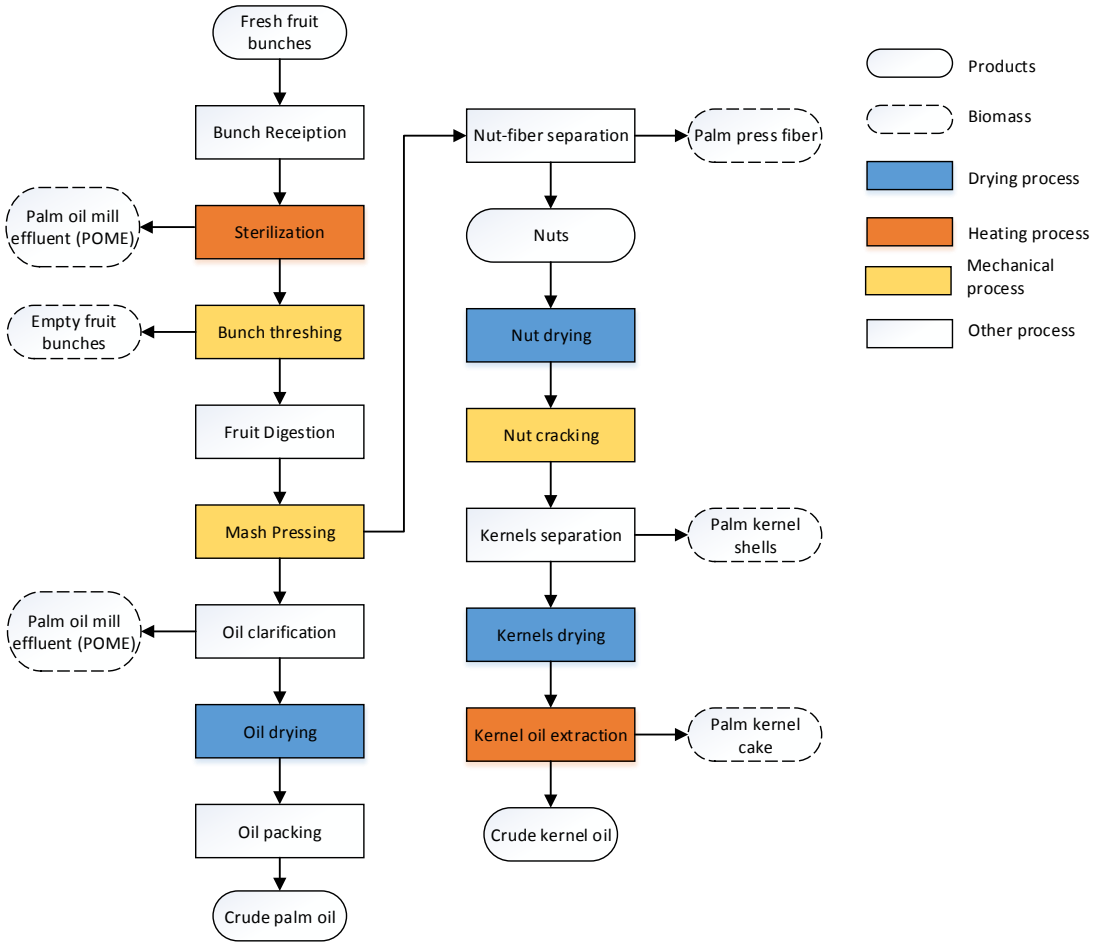

Figure 1.2: Flow chart of palm oil processing redrawn from Ohimain and Izah (2014)

Sterilization is the first stage of the milling process where FFBs are exposed to heat rendering operation with high-pressure steam operated at 15-45 psi for about 90 mins in horizontal cylinder autoclaves (Sivasothy and Rohaya, 2000). Sterilization aims to soften the fruits which allow easy detachment from the FFBs and to improve the quality of fruits by deactivating the enzymatic activities that cause an increase in Free Fatty Acid (FFA). For trading purposes, FFA content in crude palm oil must not exceed 5 %, according to the Malaysian Palm Oil Association (MPOA) (Nor'aini and Siew, 1990). The sterilized fruits are then detached from the FFBs through the threshing process in rotating thresher. After the threshing process, the detached fruits are further softened and mashed in a steam-heated digester at 95-100 °C for 20 mins. After digesting, the palm fruits enter into a screw oil expeller in order to press and obtain the palm oil and pressed cake (nut and fiber). The pressed cakes obtained from the pressing process contain nuts and fibers. The nut and fibers are separated by

using a cyclone system. The fibers are relatively light and carried away by an upward air flow, while the nuts that are relatively heavy fall into a rotary drum. The nuts are then dried in a silo and are sent to a cracker to crack the nut, before transporting them to hydrocyclones to separate its kernel and kernel shell. The kernels have to be dried to achieve a moisture content of less than 7 % for storage purposes, before extracting the crude palm kernel oil from the kernels. The last step of the milling process is to separate the palm oil from impurities (i.e. clarification and purification processes). The crude palm oil is then dried to achieve a moisture content of about 0.1 % to 0.25 % before storage which aimed to maintain the oxidation stability (Igwe and Onyegbado, 2007).

The palm oil milling process generates a large amount of wastes such as processed empty fruit bunches, palm fiber, palm kernel shells and palm oil mill effluents (POME). Among all, the oily wastewater, POME, is considered as the most harmful waste if left untreated. POME is generated when hot steam is used in the processes such as sterilization, hydrocyclone and clarification processes. According to Kamyab et al. (2015), POME is one of the major environmental pollutants as it contains a high biochemical oxygen demand, chemical oxygen demand, nitrogen and phosphorus contents. These contents accelerate bacteria growth and require a high oxygen level to oxidize the organic matters of POME and consequently contaminate the aquatic environment. Therefore, POME requires an expensive and challenging treatment process before disposal as pointed by Madaki and Seng (2013). Brezing (1986) estimated that an oil palm mill with a capacity of 10 tons of FFB per hour would require a water treatment plant that is sufficient to sustain for half a million of inhabitants. Therefore, there is an urge to look for alternatives.

In addition to the environmental issue due to the current sterilization process, the existing milling process also consumes an enormous amount of energy (Sivasothy and Rohaya, 2000). This is due to the convective heating process which the heat energy is transferred from the dried air to the fruits by convection, conduction and radiation mechanisms. Thostenson and Chou (1999) recommended that a slow heating rate should be used to minimize a sharp thermal gradient between the surface and the interior of the fruit to achieve a more uniform surface and interior temperatures. This resulted in a longer heating process and a higher energy consumption for oil palm fruit sterilization. Besides, as shown in Figure 1.2, heating

and drying processes are carried out separately during the conventional oil palm milling process. At the sterilization process, the hot steam used in supplying heat to the FFB would concurrently increase the moisture content of the FFB. Consequently, additional drying process would be required in removing the moisture.

Microwave energy, on the other hand, is perceived to be capable of delivering equivalent result under a single process yet capable of improving the process efficiency. The interaction between microwave and polar solvents, e.g. water, causes molecular motion through rotation of dipoles inside a food sample. This phenomenon is known as dipolar rotation. The rapid molecular motion of the dipoles results in molecular frictions which in turn produces heat inside the food sample. The adoption of microwave technology has offered a number of advantages such as volumetric heating, short process time, energy savings and non-contact heating. Moisture is a major constituent in fresh food and it serves as a good microwave energy absorber. As water is present throughout the material, heat is generated volumetrically. This leads to a faster heating rate and a shorter process time. In addition, an intense microwave heating results in a faster drying process that promotes intensive moisture evaporation.

Besides, microwave heating process provides rapid and energy-efficient heating process compared the conventional heating process. Cheng et al. (2011) reported that the microwave heating process achieved energy efficiencies of 5.41-11.01 %. The energy efficiency was higher than the plant efficiency in the current palm oil mills (2.84 – 3.25 %) as reported by Nasrin et al. (2011). Moreover, Decareau and Peterson (1986) reported that the microwave heating process dramatically reduces the pretreatment duration by 10 times less compared with other heating systems, which decreases the energy consumption. Moreover, Cheng et al. (2008) reported that microwave heating process has better energy efficiency in water removal process and 22.5 times of unit energy consumption lower than conventional heating.

Chow and Ma (2007) stated that microwave heating technology could be a potential energy to replace the conventional sterilization process. This is because not only the microwave heating is a fast process, it also reduced energy consumption compared to the conventional sterilization process. Furthermore, POME can be eliminated as hot steam is not required in the microwave heating process. In addition,

Cheng et al. (2011) showed that a palm oil production process with microwave assisted solvent extraction pre-treatment could replace the conventional palm oil milling process which only involved the physical and mechanical approaches.

1.2 Problem Statement

The current milling process has not changed much since 1970s when the palm oil was commercialised (Ujang et al., 2010). The milling process is not only a time-consuming process, but also environmentally unfriendly as it generates a large amount of waste. Heating and drying are carried out separately during the milling process which aims to supply heat and reduce the moisture content. Microwave has been shown to provide a better alternative for heating, drying and eliminating the POME production.

1.3 Significance and novelty of the study

The microwave heating efficiency of oil palm fruits is affected by its inherent properties such as dielectric and thermal properties. The dielectric properties determine the ability of oil palm fruits to store and convert microwave energy into heat energy (Mudgett, 1986, Umesh Hebbar and Rastogi, 2012, Magee et al., 2013). The thermal properties determine temperature distributions of oil palm fruits during microwave heating process. The dielectric and thermal properties for kernel, mesocarp and fresh empty fruit bunches (EFB) are different. Hence, it is crucial to determine the optimum microwave heating conditions to avoid thermal runaway.

In order to design a microwave heating and drying system, it is important to characterize the dielectric and thermal properties of oil palm fruits. However, the information of various properties of the oil palm fruits are limited. The measurement in this work provide new contribution for the physical, dielectric, thermal and mechanical characterization of oil palm kernel, mesocarp and EFB. This measurement are important to predict the generated microwave power density and heat-mass transports during microwave heating process. In addition, due to the complex interactions between microwave and oil palm fruits, a multi-physics model of microwave heating and drying of the oil palm fruit fruits is needed. The

experimental characterizations of the dielectric and thermal properties of oil palm fruits will be used as the input to the multi-physic model. The model will accelerates the design process of a microwave heating system for oil palm fruits and the product can be brought to market quicker.

1.4 Objectives of this research

The objectives of the current research are as follows:

1. To characterize dielectric and thermal properties of oil palm fruits and EFB.
2. To determine the effects of microwave heating and drying on mechanical strength and microstructure of oil palm fruits and EFB.
3. To develop and validate a microwave heating and drying model.

1.5 Thesis structure

This thesis consists of 8 chapters and is organized as follows:

This chapter is mainly on the introduction of the research topic, where the problem, proposed method and objectives are identified.

Chapter 2 of this thesis consists of four sections. The first section provides an introduction on the microwave heating. The second section discusses the characteristics of microwave heating and drying and also reviews the microwave heating and drying technique applied in the oil palm sterilization process. The third section discusses the effects of microwave heating on food products in general. This is followed by an overview and development of modelling of microwave heating and drying.

Chapter 3 presents the equipment, setups and experimental procedures. The experiments aim to characterize thermal and dielectric properties, to obtain heating and drying behaviors. Besides, the effect of microwave heating on the mechanical strength and microstructure analysis of oil palm kernel, mesocarp and EFB were studied.

Chapter 4 presents and discusses the experimental data.

Chapter 5 outlines the numerical models developed in this study. The models used to validate and to describe the microwave heating and drying of oil palm kernel, mesocarp and bunches. The numerical procedure and mesh independent study of the model are described.

Chapter 6 discusses and compares the temperature and moisture content between the experimental and simulation results. Temperature and moisture distributions in the samples are illustrated and discussed. The microwave power absorption and lost in the sample provide an understanding of the heating mechanism. In addition, temperature and moisture distributions during microwave off-phase (when the supplied microwave source is stopped) will be discussed in this chapter.

Chapter 7 investigates the application of microwave heating on the FFB. A mesh generation will be presented on this new geometry. Temperature and moisture content history associated with the microwave power absorption and loss rates will be discussed in this chapter.

Chapter 8 provides main findings and conclusions based on the conducted studies. Besides, future works and recommendations are also presented.

1.6 Conclusions

This chapter introduces the importance of the oil palm industry to the country's economy. The drawbacks of the current oil palm milling process are also discussed. To improve the efficiency and environmental issues due to the existing milling process, microwave heating is suggested as an alternative. This chapter defines the scopes of the current research and highlights the contributions of the work to the current knowledge. The overview of the thesis structure is also presented. The fundamental of microwave heating and the relevant literature reviews will be presented in the next chapter.

CHAPTER 2

LITERATURE REVIEW

This chapter will give an overview of the physics of microwave heating, followed by its application in the food industry in general. Later on, the discussion will shift to the potential of microwave heating in oil palm industry. The effects of microwave energy on the food quality also will be discussed. The last part of the review will be on mathematical modelling works of microwave heating.

2.1 Fundamentals of microwave heating

Maxwell discovered that electric field components are aligned perpendicular to magnetic field components (Meredith, 1998). When an electric or magnetic in a medium changes its position in space, the corresponding field that it produces also changes. These changes produce oscillating waves which is called the electromagnetic waves. All electromagnetic waves have two components, i.e. electric field and magnetic field.

The electromagnetic field distribution can be described by Maxwell's equation as follows:

$$\nabla \cdot \varepsilon_r \mathbf{E} = 0 \tag{2.1}$$

$$\nabla \cdot \mu \mathbf{H} = 0 \tag{2.2}$$

$$\nabla \times \mathbf{E} = -\frac{\partial(\mu \mathbf{H})}{\partial t} \tag{2.3}$$

$$\nabla \times \mathbf{H} = \mathbf{J} + \frac{\partial(\varepsilon \mathbf{E})}{\partial t} \tag{2.4}$$

where **E** is electric field strength (V/m), ε_r is the permittivity of the material (dimensionless), **H** is magnetic flux magnitude density (V·s), μ is the relative permeability of the interacted material (H/m) and **J** is the electric current density (A/m^2). These equations describe the propagations and the interactions of the electrics and magnetics fields. Equation (2.1) and equation (2.2) are the Gauss' law and the Gauss' magnetism law respectively. Gauss' law describes the movement of

electric charges around electric fields, whereas Gauss' magnetism law describes the strength of magnetic flux which based on the permeability of the interacted material. Then, the relationship between sinusoidal time-varying electric and magnetic fields are described by equation (2.3) and equation (2.4). Equation (2.3) is the Faraday's law of induction which describes that relationship between a changing magnetic field and the electric field created by the change. Ampere's law as shown in equation (2.4) stated that a flowing electric current and time-varying electric flux density give rise to magnetic field. The rapidly varying electric and magnetic fields lead to the molecular motions in a biological product, thus providing the heat sources.

Microwave is a form of electromagnetic radiation with the wavelengths ranging between the infrared and radio waves. The use of microwave energy has been introduced widely in numerous food processing industries since the 1990s (Rahman, 2007). The microwave frequencies used for industrial and domestic purposes are 915 MHz and 2450 MHz. Nowadays, microwave heating processes have widely been used for processes in production industries such as pasteurization, sterilization, tempering, thawing, vacuum drying and continuous baking. Microwave heating technique is desired due to its volumetric heating, rapid increase in temperature, controllable heat and easy cleanup that provides a uniform, fast and environmentally friendly heating process. According to McConnell (1974), microwave heating had shown a power saving of up to 74.5 % as compared to the conventional thermal heating process. In addition, Lupinska et al. (2009) stated that microwave heating not only consumed much less energy than the conventional process conducted with hot air but also improved the process efficiency. The authors stated that a higher microwave power provided a faster drying rate in the microwave-treated samples.

In the heating process, the microwave is absorbed by food and it is converted into thermal energy through interactions between microwave, polar water molecules and charged ions in food. Microwave causes polar water molecules in food to constantly rotate and couple with the electromagnetic field, where heat is generated by the molecular friction. The ability of a material absorb and convert it to heat energy depends on its material permittivity (ε_r) which is often expressed by a complex number. It can be expressed as:

$$\varepsilon_r = \varepsilon_r^{'} - j\varepsilon_r^{''} \tag{2.5}$$

where $\varepsilon_r^{'}$ and $\varepsilon_r^{''}$ are known as dielectric constant and loss factor.

Dielectric constant, $\varepsilon_r^{'}$, is the ability of a material to store electric energy in an applied electrical field. The dielectric loss factor, $\varepsilon_r^{''}$, is associated with the capacity of the material to dissipate electric energy in response to an applied electric field, which results in heat generation. The efficiency of a material responds to the microwave energy is described by loss tangent and is given by (Mandal et al., 2007):

$$\tan\delta = \frac{\varepsilon_r^{''}}{\varepsilon_r^{'}} \tag{2.6}$$

The loss tangent, $\tan\delta$, is defined as the ratio of dielectric loss factor and dielectric constant which describes the ability of a material to absorb microwave energy and dissipate heat within the material. A high loss tangent corresponds to a dielectric material with better absorbability to the electromagnetic wave. The loss tangent is dependent on the dielectric properties and the properties were reported to be influenced by several variables such as frequency, temperature, sample geometry and the sample's compositions (Lovás et al., 2010, Liu et al., 2013, Salema et al., 2013, Torgovnikov, 1993, Sosa-Morales et al., 2010).

Lovás et al. (2010) studied the effect of temperature on the dielectric properties for three different organic samples such as andesite, sulphide and carbonate samples. The authors reported that the dielectric properties of the samples were highly dependent on temperature. In addition, moisture content is also one of the parameters that affects the sample's dielectric properties. Sipahioglu and Barringer (2003) stated that water is a strong polar solvent which reoriented itself in response to changes in field polarity. Therefore, moisture content plays a role in affecting the dielectric properties of a sample. In addition, Liu et al. (2013) reported that the temperature-dependent dielectric properties of mashed potato did not change significantly during the first 10s of heating time and therefore would not significantly change the electric field distribution.

Moreover, Salema et al. (2013) had investigated the dielectric properties of oil palm biomass and biochar at frequencies ranging from 0.2 to 10 GHz using a coaxial probe attached to a network analyzer. The authors reported that the dielectric

constants of oil palm biomass and biochar were inversely proportional to frequency. On the other hand, their dielectric loss factors were directly proportional to the frequency. The decrease in dielectric constant was reported to be caused by the effect of polarization and decrease in dipole movement according to Torgovnikov (1993).

In a recent study, Sosa-Morales et al. (2010) reviewed and gathered dielectric property data from literatures for a wide range of foods, including fruits and vegetables, starch, nuts, grains, meats, egg products and liquid fluids, at various temperature and frequency ranges. While the dielectric properties of different moisture contents had been reported for a whole oil palm FFB (Sukaribin and Khalid, 2009), processed oil palm EFB (Omar et al., 2011), oil palm trunk core (Jie et al., 2015), honey (Guo et al., 2011) and tropical fruits (Sacilik and Colak, 2010a). The researchers reported that dielectric properties positively correlated with moisture content. This is because the moisture affects the interaction between the dielectric material and electromagnetic fields (Ramasamy and Moghtaderi, 2010).

The dielectric properties and loss tangent also determine the extent of the microwave penetration inside a material. The penetration depth, d_p, is defined as the depth where the microwave power is reduced to 1/e (e = 2.718) of the power entering the material's surface and can be calculated by (Hippel, 1954):

$$d_p = \frac{c_o}{2\pi f \sqrt{2\varepsilon_r' \left(\sqrt{1+\tan^2 \delta} - 1\right)}} \tag{2.7}$$

This quantity also indicates the region of the material where the microwave field can be effectively penetrated (Metaxas and Meredith, 1983). However, when the dimensions of a material is larger than the penetration depth, the microwave energy is rapidly attenuated, thus, the food material will not heat volumetrically and heating from the material's surface will dominate (Datta and Anantheswaran, 2001). Thus, microwave heating may not be homogeneous through the heating process, which in turn leads to overheating or uneven heating. Overheating of a microwave-treated material was reported to be related to the dielectric and transport properties of the material, the geometry of the system and the electromagnetic distribution in the system (Barba and d'Amore, 2012). The complex interaction between an electromagnetic field with a microwave-treated material gives a hot and cold spots

within the material which in turn lead to overheating. The effects of combining microwave with convective drying (Kumar et al., 2014), the use of rotating turntable (Zhou et al., 1995) had been studied to improve the microwave heating uniformity.

Li et al. (2011) discussed the factors causing heating non-uniformity of a biological material when exposed to microwave. It depends mainly on the uniformity of the material absorption of the microwave, which is affected by the electromagnetic field distribution in the material and its dielectric properties. The author proposed several methods for improving the issue of microwave heating non-uniformity, i.e. modifying microwave cavity, increasing microwave power feed port, installing a mode stirrer, designing the shape and size of the microwave cavity, changing the frequency of microwave and change the material's location by equipping microwave oven with a rotating turntable. However, changing the microwave frequency is not effective for industrial systems because of the strictly allocated frequency bands. The uniformity of microwave heating is also affected by the material's shape, size and dielectric properties. Birla, Wang, and Tang (2008) reported that a spherical object was heated more evenly compared to cylindrical and cubical objects. This behavior can be explained when the electric fields enter the rounded edges and is converged from one direction rather than two or three directions in the sharp edges of the cylindrical and rectangular shaped object. As a result, the more evenly electric field distributions in a spherical object provide a more uniform heating.

Ho et al. (2002), Soysal et al. (2006) and Lupinska et al. (2009) studied the intermittent microwave drying on corn, parsley and rapeseeds, respectively. Lupinska et al. (2009) suggested that a low microwave power level or intermittent or cyclic heating operation should be provided to reduce the temperature gradients, which in turn decrease the risk of damaging the drying material. Soysal et al. (2006) also reported that intermittent microwave drying able to reduce temperature gradient of parsley, however, a lower drying rate was provided compared to continuous drying. Furthermore, Ho et al. (2002) reported that intermittent microwave heating reduced the surface temperature of potatoes but enhanced product quality by minimizing the vitamin loss and product color.

2.2 Microwave heating and drying for agricultural products

2.2.1 Microwave drying

Microwave heating is often used as a pre-treatment process to speed up the drying process. It was reported to be capable of reducing the initial moisture content and improving the quality of dried fruits as discussed by Sobhy and Chaouki (2010). Drying is a mass transfer process that removes moisture content through evaporation from a solid or liquid object. Drying is a complex operation involving transient heat and mass transfers. The main aims of drying products are to allow for a longer period of storage, minimizing packaging requirements and reducing transportation weights (Maroulis and Saravacos, 2003).

Alibas (2007) studied the drying kinetic of nettle leaves under the microwave, vacuum and convective drying methods. It was reported that microwave drying was the fastest process and consumed the least energy of around 0.07 kWh. Magee (2003) carried out drying experiments for slab and cylindrical-shaped potato samples under convective, microwave and combined microwave-convective conditions. The author revealed that there were three distinct drying periods, i.e. an initial heating-up period and two falling rate periods. The drying curve (moisture content versus time) for each falling-rate period was described by an exponential model. Drying behavior was found to be a function of air temperature, air velocity, microwave output power and sample geometry. The same pattern of drying curve was also reported on mircrowave-treated biological products such as macaroni (Altan and Maskan, 2005), garlic (Sharma and Prasad, 2001, Vázquez et al., 1999), apple(Bilbao-Sa´inz et al., 2006, Jun et al., 1998, Krokida and Maroulis, 1999), wheat (Walde et al., 2002), carrot (Sumnu et al., 2005, Wang et al., 2002, Wang and Xi, 2005, Stanisławski, 2005, Cui et al., 2008), parsley (Soysal et al., 2006), mushroom (Rodríguez et al., 2005), cabbage (Yanyang et al., 2004), mint (Özbek and Dadali, 2007) and basil (Demirhan and Özbek, 2009).

2.2.2 Application of microwave heating in oil palm industry

A number of researchers explored the suitability of microwave heating in oil palm milling process. Some of the aspects that were studied included sterilization, microwave-solvent assisted oil extraction and palm oil quality.

Sterilization is an essential pre-treatment step as to retain the quality, to soften the fruit for the ease of fruit detachment and to minimize the enzymatic activity within the fruits. Vincent et al. (2014) presented a review of the methods of sterilization including the current and other proposed sterilization methods such as continuous sterilization, microwave heating and drying heating. The authors concluded that microwave heating is capable of replacing the current sterilization process to be an environment technology yet yields a better quality of palm oils.

Chow and Ma (2007) observed that the microwave-heated palm fruits had higher carotene and oil contents and a lower amount of FFA than those from other drying methods such as batch sterilization, continuous sterilization and oven drying. Moreover, the experiment also showed that microwave heating increased fruits detachment from the spikelets compared to other methods. The authors suggested that microwave technology had the potential of replacing the current steam-assisted sterilization process. The better efficiency on fruit detachment using microwave heating was also observed by Sukaribin and Khalid (2009). The better efficiency is explained because the abscission region (the region between fruits and EFB) could absorb 5-7 times more microwave energy per volume compared to other parts of the fruits, due to the higher moisture content in that region. This actually helps in fruit detachment from bunches without overheating the palm fruits.

Besides, Sarah and Taib (2013) sterilized the oil palm fresh fruits and bunches (FFB) using microwave irradiation. The oil from palm fruits was obtained by using the screw pressing method. The microwave-heated palm oil of the experiment showed better quality contents, such as a low FFA (0.7 %) which was below the standard requirement (3.5 %) and a higher vitamin E content of 1300 ppm than the commercial crude palm oil (600-1000 ppm). However, carotenoid was found to be lesser than the commercial palm oil due to the degradation of carotenoids which was due to elevated temperature. Nevertheless, lipase in the oil palm fruits was found to have been successfully inactivated after microwave irradiation. Furthermore, Cheng et al. (2011) showed that a better crude palm oil (CPO) quality was obtained from palm fruits treated with microwave heating compared to the current commercial CPO, such as low FFA of 0.26 %, low moisture content of 0.05 % and a higher vitamin E content. In addition, Hadi et al. (2012) reported the effects of oven-dried oil palm fruits has reduced the sterilization time to 3 mins. It also improved oil quality and

obtained a lower FFA (1.02-2.19 %) compared with the commercial crude palm oil (3.4 %). Besides, Umudee et al. (2013) indicated that microwave treatment provided a low FFA increment in an oil palm fruit, and this ensured the quality. Moreover, a higher power level is also shown to further reduce the FFA growth in the fruits.

The adoption of microwave technology in the oil palm mills and palm oil production processes can significantly improve the environmental friendliness of the sterilization process by eliminating the conventional usage of steam as well as improving the yield and quality of the production. Therefore, microwave heating is a promising process to greatly enhance the efficiency and quality of the current conventional process. Despite the great potential, the microwave application in oil palm industry is still limited.

2.3 The effects of heating and drying

When a food sample is subject to an elevated temperature, this will have an effect on its thermal and mechanical properties. In this section, the effects of heating and drying of food samples are reviewed.

2.3.1 The effect of heating on thermal properties

Thermal analysis has become an important method used in the thermal properties characterization of material. Thermal gravimetric analysis (TGA) is widely accepted as a suitable analysis to evaluate the thermal behavior of food due to its fast and convenient method and it requires only a small sample size for the analysis. TGA is capable of identifying the characterization and the decomposition stages in a sample. Each decomposition stage is related to the sample's weight loss trend which can be obtained from the thermal analysis. The rate of weight loss of the material sample in a specific temperature range in the analysis provides an indication of its thermal stability from the decomposition reactions. The analysis is necessary to determine the degradation temperature of the material.

Nabinejad et al. (2015) studied the thermal behavior of oil palm shell powders by using TGA. The authors indicated that there are five stages of thermal events in the palm shell powders which are the moisture evaporation, lower molecules lignin decomposition, hemicellulose decomposition, cellulose decomposition and longer molecule lignin decomposition. The decomposition stages were identified from the

weight loss pattern of the palm shell. A similar finding is also observed by Abdullah et al. (2016) on composted EFB.

Otálora et al. (2015) observed three thermal events of cactus fruits which are the moisture evaporation, the decomposition of starch and carbohydrate chains and the volatilization of the melted fruit. This is also observed by Nascimento et al. (2012) on passion fruit flours and Fan et al. (2013) on rice starches which were treated by conventional and microwave heating. In addition, the authors noticed higher activation energy in the microwaved samples than the fresh sample. The authors suggested that the microwave heating could provide a higher thermal stability to the organic foods.

Generally, heat transfer of food depends on three major parameters according to Singh and Heldman (2014), which are the thermal properties of food, geometry of food and thermal processing condition.

The thermal properties such as thermal conductivity and specific heat capacity, give a clear illustration of the temperature distribution in the heated food. The knowledge of these properties is essential to understand the heat transfer behavior when subjected to thermal treatments in the food industry. It is crucial in designing and optimizing of heating processes to provide accurate engineering solutions in the initial system analysis in order to prevent equipment faults and to achieve process specification. The thermal conductivity is a property which describes the ability of a substance to conduct heat. It allows the estimation of the conductive heat transfer rate, thus heat distribution in a material. Once the distribution is known, the heat flux at any point in the body may be computed using Fourier's law which depends on the thermal conductivity, the temperature gradient and the size of the body (Lewis et al., 2008). Besides, Hansen (1992) reported that the relatively low thermal conductivity values of fruits had limited the heat conduction rate in the fruits. A prolonged heat exposure is required for the fruits to be cooked, hence results in a quality loss. From the literature review conducted, there is no published data on the *Elaeis guineensis* oil palm fruits, particularly on mesocarp and the EFB. Hence, there is a need to determine the thermal conductivity of fresh oil palm mesocarp and EFB.

2.3.2 The effect of heating and drying on mechanical properties

The thermal cracking due to drying and shrinkage will have an impact on the mechanical strengths of the material. Oloyede and Groombridge (2000) studied the mechanical properties of dried wood specimens using oven and microwave. The microwave drying process was able to dry the specimens to the desired moisture content quicker. It was also found that the failure strength, Young's modulus and yield strength of the dried woods were reduced by as much as 60 %. However, microwave drying increases the mechanical strength of other materials such as paper (Kumar et al., 1990), carbon fiber composite (Papargyris et al., 2008) and tungsten alloy (Prabhu et al., 2014).

Several investigators studied the mechanical properties of different agricultural and food materials. Anazodo and Norris (1981) noted that the elastic modulus and crushing strength of corncob decreased with increasing moisture content. Misra and Young (1981) showed the elastic modulus of soya bean decreased parabolically with increasing moisture content. Similar results were reported for cowpea (Pappas et al., 1988), yellow dent corn kernels (Waananem and Okos, 1988), cashew nuts (Oloso and Clarke, 1993) and wheat (Kang et al., 1995) and hazelnut (Güner et al., 2003).

In fruit processing, Contreras et al. (2008) investigated the effect of convective drying and microwave-assisted convective drying methods on the mechanical characteristics of apple and strawberry. Both drying processes promoted the mechanical rigidity and resistance of the dried samples. However, fruits dried by the microwave-assisted convective drying obtained a greater mechanical resistance to fracture and deformation which improved firmness and rigidity. Krokida and Maroulis (1999) studied the effect of microwave drying on biological products. The authors reported that the microwave drying decreased the maximum stress and strain of dried products but increased the elasticity. Nevertheless, the quality of a microwave dried food was similar to those of conventional air dried food.

Besides, the information on the mechanical strengths of FFB is important in the oil palm milling process. According to Raji and Favier (2004), pressing or compression force is one of the main factors which influenced the energy demand of the oil extraction process. The correct estimation of the food's mechanical properties will minimize the energy required to crack the oil palm kernel shells (Kabutey et al., 2013).

On the other hand, Abbas et al. (2006) studied the relationship between the sterilization and the texture properties, i.e. fracturability, hardness, adhesiveness and cohesiveness of oil palm fruits. In their work, compression force was applied using an instrumental texture profile analysis (TPA) to obtain the force-time curve to analyze the texture properties of fresh and sterilized palm fruits. Their study found that the sterilization reduced the fracturability, hardness and adhesiveness properties of palm fruits significantly. This resulted in the better detachment of palm fruits from EFB and also the easy separation of mesocarp from palm kernel nuts.

In the published literature, there is no information on the mechanical quality properties of oil palm fruits as a function of moisture content. This information is important to identify the mechanical performance in fruits detachment and oil extractions of the kernel, mesocarp and EFB.

2.3.3 The effects of heating on microstructure, texture and appearance

The internal structure of food will be deformed and locally damaged during a drying process. Law et al. (2016) stated that the cracks occurred at the core oil palm kernel and then propagated to the surface of the kernel during microwave heating and drying process. In addition, Bilbao-Sa´inz et al. (2006) observed that some of the cells of microwave-treated apple were destroyed due to changes of sample's volume whereby the rate of free water diffused out to the surface is faster than the evaporated water thus increases of internal pressure during the falling periods of the drying process. Besides, Lupinska et al. (2009) stated that a high drying rate could damage the dried material, thus lower levels of microwave power should be used to minimize the risk of damaging the drying biological material.

On the other hand, Fazaeli et al. (2012) stated that changes in food structure have an influence on its textural, quality and nutritional attributes. However, Lorenz and Decareau (1976) concluded that microwave heated foods have the same magnitude of nutritional and chemical changes as those processed by conventional methods. Moreover, the degree of destruction of vitamins and pigments for microwave heated food was no greater than that heated by a conventional heat process. Therefore, the food structure is too an important factor in determining the food quality.

2.4 Mathematical modelling of drying process

There are numerous mathematical models available in the open literatures which describe the microwave drying process. In this section, the importance of mathematical models pertaining the current research is reviewed. The first section will discuss the mathematical models of a general drying process. After that, the mathematical models for microwave heating will be presented. Outstanding results from the modelling work will also be reviewed.

2.4.1 Convective drying models

There are several methods in the open literature that are used to model the moisture removal from a solid material. The first method is the analytical solution of Fick's diffusion equation. Crank (1975) provided an overview and developed a mathematical mass transfer model based on Fick's diffusion model, including many types of initial and boundary conditions for different geometries. The analytical solution is only applicable for simple geometries and it is not versatile. This method is also known as one-equation model where only the moisture content is solved.

The second method is called the two-equation model because both moisture content and solid temperature are solved. Two approaches are available in this category, namely Luikov's model and the coupled Fick's law and energy conservation equations. According to Luikov (1975), moisture content not only is transferred via volumetric moisture concentration gradient but also via temperature gradient. The author showed that moisture transport and temperature distributions inside a material are mutually correlated. Both the moisture concentration and temperature gradients contributed to the heat and mass transfer fluxes. Hence, the author developed the interrelated differential equations to model the heat and mass transfers in capillary porous bodies and are given as (Wang et al., 2007):

$$\rho C_p \frac{\partial T}{\partial t} = \nabla \cdot \left(q_{cond} \right) + H_{evap} \sigma_{luikov} \rho \frac{\partial MC}{\partial t} + \left(-D \nabla MC + D \delta_{luikov} \nabla T \right) C_p \nabla T \qquad (2.8)$$

$$\rho \frac{\partial MC}{\partial t} = -\nabla \cdot \left(-D \nabla MC + D \delta_{luikov} \nabla T \right) + \sigma_{luikov} \rho \frac{\partial MC}{\partial t} \qquad (2.9)$$

In the equation (2.8), the temperature prediction is estimated from the heat fluxes due to the conduction, the evaporation of internal moisture and the

temperature and moisture concentration gradients which are represented by the first, second and third term of the equation, respectively. The moisture content in equation (2.9) is predicted from the mass fluxes due to the moisture content and temperature gradients and the internal moisture evaporation.

The model gave a satisfactory simulation result. Various researchers have applied Luikov's model to predict the temperature changes and moisture diffusion of the biological products such as apple (Jun et al., 1998), milk (Wang et al., 2005) and barley (Ranjan et al., 2002). In addition, Haghighi and Segerlind (1988) employed modified Luikov's equations to solve simultaneously the heat and mass diffusion equations to obtain temperature and moisture distributions of biological materials during forced drying. The predicted drying curve for soybean model agreed well with the experimental data.

However, the major limitations of the model include the determination of the process related variables, the assumption of the constant thermophysical properties and the complexity of solving the solutions. The Luikov's model involves parameters which are difficult to determine experimentally such as absorption and desorption of moisture parameters and process related variables. Barbosa-Cánovas and Vega-Mercado (1996) stated that the absorption and desorption of moisture parameters needed in the Luikov's model are lack of a firm theoretical fundamental and thus require to be identified experimentally. Moreover, Wang et al. (2007) and Kemp and Oakley (2002) pointed out that process related variables such as the phase conduction between liquid and vapor (σ_{luikov}) and the thermogradient coefficient (δ_{luikov}) are difficult to be obtained theoretically and must be determined experimentally. Furthermore, Rossen (1977) pointed out that thermophysical properties in the Luikov's model are assumed to be a constant value. Thus, the solutions of the model would become exceedingly complex when the thermophysical properties, e.g. specific heat capacity, density, thermal conductivity and specific volume are functions of moisture content and temperature. In addition, solving the model and analyzing the solution are challenging because complex eigenvalues are included in the analysis although Liu and Shun (1991) and Pandey et al. (1999) presented an analytical method for solving the Luikov's equations for heat and mass transfers.

Due to the complexities and the limitations of Luikov's model, the coupled Fick's diffusion and Fourier's heat conduction equations which is a simpler model is used to solve the temperature and moisture concentration of a material. The Fourier's heat conduction and Fick's diffusion are given by Berk (2013):

$$q_{cond} = -kA_s \cdot \nabla T \tag{2.10}$$

$$\frac{\partial c}{\partial t} = \nabla \cdot \left(D \nabla c \right) \tag{2.11}$$

In the Fourier's heat conduction, as shown in equation (2.10), the rate of heat flux in a material, q_{cond}, is proportional to the negative temperature gradient, $-\nabla T$ and the area, A_s. The change in moisture concentration, as shown in equation (2.11), c, at time t is predicted by the diffusion coefficient, D, of the sample.

The advantage of this model over Luikov's model is that the input parameters such as liquid diffusion coefficients and solid thermal properties can be found experimentally or through widely-accepted correlations. Some of the works which adopted this approach are summarized as below.

Hawlader et al. (1999) developed a mathematical model to describe heat and mass transfers within the material during drying that accounted for the effect of shrinkage, moisture dependent of diffusion rate. Both heat and mass transfers were solved using the Fourier's heat conduction equation and Fick's law respectively. The study showed the coupled model predicted well with the experimental results.

Besides, Ho et al. (2002) included the effect of surrounding air flow to obtain the mass transport of a food product. The authors developed a mathematical model based on Darcy and Fick's law of diffusion to represent liquid and vapor flow within a food product, under cyclic air temperature variations for cyclic heating applications. In their model, vapor migration took place due to convection and diffusion phenomena. However, low porosity material such as food materials, vapor migration due to convection can be considered insignificant.

On the other hand, Mujumdar (2006) provided a fundamental overview of the simple liquid diffusion model based on Fick's second law. Effective moisture diffusivity of fruits, seeds, grains and polymers are shown in Table 2.1.

Table 2.1: Approximate ranges of moisture diffusivity in some materials (Mujumdar, 2006)

Material	Diffusivity (m^2/s)
Animal feed	$1.8\times10^{-11} – 2.8\times10^{-9}$
Apple	$1.0\times10^{-11} – 3.3\times10^{-9}$
Banana	$3.0\times10^{-13} – 2.1\times10^{-10}$
Carrot	$1.2\times10^{-10} – 5.9\times10^{-9}$
Biscuit	$8.6\times10^{-10} – 9.4\times10^{-8}$
Raisin	$5.0\times10^{-11} – 2.5\times10^{-10}$
Starch gel	$1.0\times10^{-10} – 1.2\times10^{-9}$
Wheat	$6.9\times10^{-12} – 2.8\times10^{-10}$
Wood	$5.0\times10^{-10} – 2.5\times10^{-9}$

Magee (2003) evaluated moisture diffusivity and moisture transfer coefficient of the slab and cylinder samples using an one dimensional transient moisture diffusion model which was proposed by Dincer and Dost (1995). Their study indicated that the model was an efficient method to estimate the moisture diffusivity and mass transfer coefficient values for convective, microwave and combined convective-microwave drying of the slab and cylinder samples. Besides, Guiné et al. (2012) determined the mass transfer properties of pears for convective air drying based on a diffusional model from Fick's second law and the analytical model of one dimensional transient moisture diffusion proposed by Dincer and Hussain (2002).

Hii et al. (2013) investigate the kinetics of heat pump drying of cocoa beans from their developed model that coupled heat and mass transfers. The model has incorporated with shrinkage factor. Their study showed that shrinkage played an insignificant role in the model due to small shrinkage ratio observed before and after drying. Mass transfer coefficient and heat transfer coefficient were predicted from Nusselt and Prandtl number correlations.

Mercier et al. (2014) developed a model which accounted for water evaporation during pasta drying to obtain its moisture profile. The authors reported that diffusivities and mass transfer coefficients were the most important parameters to accurately predict the drying time and internal moisture profile. On the other hand, Kumar et al. (2016) and Zhao et al. (2016) stated that the evaporation effect played an important role in heat and mass transfers and is accounted for the effect in both the heat and moisture transfers. In addition, various parameters included in the Fourier's equations and Fick's law are dependent on temperature and moisture content such as the heat and mass transfer coefficients (Dumas and Mittal, 2002, Xanthopoulos et al., 2012), evaporation rate (Zhao et al., 2016), diffusion coefficient (Ghazanfari et al., 2006) and drying rate constant (Alibas, 2009, Hemis et al., 2011). These parameters used in the coupled Fourier's equation and Fick's law could accurately predict the heat and mass transfers because water vapor evaporation and moisture diffusion are both function of temperature and moisture content.

Generally, food can be considered a porous medium, which contains void, gas and liquid. A more accurate model is to apply porous medium theory in the drying process.Whitaker (1977) introduced volume averaging method to predict heat and mass transfer coefficients for porous materials. The method took into account mass transfer by liquid flow due to capillary forces, vapor diffusion in a porous structure, moisture diffusion and internal evaporation of moisture, whereas heat transfer is by convection and conduction. Younsi et al. (2007) used Whitaker's volume averaging method to solve the liquid and vapor migrations within a wood that was treated with high temperature heat treatment. Free water, bound water and water vapor of moisture phase were considered in the mass transfer. Navier-Stokes and conservations of energy with Whitaker's method were solved and the result was comparable to the experimental data. Moreover, Plumb et al. (1985) solved the heat and mass transfer of a soft wood by using Whitaker's volume averaging method. The model accounted for liquid diffusion through capillary movement and the heat transfer included conduction, convection and cooling effect due to evaporation. Excellent results were obtained from this modelling work.

The mass transfer included diffusion and liquid movements transported through capillary movement, whereas the heat transfer is by conduction, convection

and evaporation. The obtained numerical results have agreed well with the experimental data.

2.4.2 Microwave drying models

Microwave drying models are similar to the convective drying models which were discussed earlier. The only exception is that the microwave heating has to be accounted for. There are generally two ways to model the microwave power absorption of a sample, which is the source of the microwave heating. The first method is to adopt the so-called Lambert's law and the second method is to solve the full Maxwell's electromagnetic equations.

Maxwell's equations are used to describe the interaction of electromagnetic field on a sample and to obtain the electromagnetic field distribution insides the sample.

Lambert's law is widely used because of its simplicity and is given by:

$$P(x) = P_o e^{-2\alpha(L-x)} \tag{2.12}$$

In Lambert's model, the microwave heating is accounted for by including a heat source in the energy equation (2.12). The heat source is an exponentially decaying term, $P_o e^{-2\alpha(L-x)}$. The microwave power on the material surface is denoted as P_o. The absorbed power inside the material decreases as the distance x increases. The constant, α, is a function of the material's dielectric properties (Arballo et al., 2010). Lambert's model is easy to solve, but the main disadvantage is that the microwave power has to be known and it is difficult to estimate. The disadvantage of Lambert's model can be overcome by solving the full Maxwell's equations. This approach allows modelers to know the electromagnetic distribution in the whole computational domain. The following discusses some of the important modelling approaches and results from the open literature.

Ayappa et al. (1991) provided an overview to solve for the electromagnetic and temperature distributions of a finite slab through Lambert's law and Maxwell's equations. The authors reported that Lambert's law was only valid for thick samples.

The temperature obtained from Lambert's law were within 0.5 % of those estimated using Maxwell's equation.

Jun et al. (1998) developed a microwave drying model using Luikov's and Lambert's equations. The authors included the effect of heat on moisture diffusion, internal evaporation and internal heat generation in the model. However, Lambert's law was dependent on the knowledge of empirical parameters such as the amount of radiation transmitted at the sample surface that must be evaluated experimentally.

Yang and Gunasekaran (2004) investigated and compared the temperature distributions inside the agar gel cylinder by solving Lambert's law and Maxwell's equations. The predicted temperature distribution profiles in the sample based on both methods were statistically accurate. However, the authors found out that Maxwell's equations were more accurate in predicting the temperature distribution, especially around the sample's edge. This is due to semi-infinite sample assumption of Lambert's law where the standing wave was disregarded, thus overestimated the temperature of the sample with a smaller radius. The result was consistent with that obtained by Oliveira and Franca (2002), who compared the use of Maxwell's equation and Lambert's law in predicting power distribution inside a food sample. Yang and Gunasekaran (2004) and Oliveira and Franca (2002) found that power distributions predicted using Lambert's law tend to agree with Maxwell's equation as the radius of the sample increased. The authors observed the absorbed power concentrated at the centre of the sample with a smaller radius. As the sample's radius increased, the amount of absorbed power at centre decreased, but increased on the surface of the sample. Lambert's law could cause a significant error when applied to samples with smaller radii.

Oliveira and Franca (2002) developed a microwave heating model which coupled Maxwell's equation and transient heat conduction to solve for electromagnetic wave and temperature distributions. The authors found that the efficiency of microwave heating depended on sample size, shape and the radiation frequencies. The authors observed that power absorption and radiation penetration were more effective at lower frequencies than at higher frequencies as the values of the dielectric properties were higher at lower frequencies. The authors also modelled an intermittent microwave heating model and the effect of turntable rotation was accounted for. This resulted in a more uniform temperature profile. Wang et al.

(2002) modelled a fluidization bed drying of carrots with different patterns of microwave heating (intermittent and continuous modes). The authors reported that the temperature of the carrot subjected to intermittent microwave heating was found to be lower compared to continuous heating. The intermittent heating overcame the overheating problem that usually occurred with continuous microwave heating.

Liu et al. (2005) developed a microwave thawing model of frozen food by coupling electromagnetic field and transient heat equations. Maxwell's equations and Lambert's law were used to compare the temperature and power distributions within the sample. Their models showed that the simulated temperature distributions by using both equations were accurate. However, concerning the power distribution in a sample, Maxwell's equation performed better than the Lambert's law. Rattanadecho (2006) illustrated the influence of wave frequencies and sample size on microwave power absorption within wood samples. The author developed a coupled Maxwell's equations and heat conduction model to predict the power absorption in the sample. It was observed that microwave power absorption increases with smaller sample size and higher microwave frequency. In addition, the power absorption was also reported to be affected by the change in the sample's properties due to the incorporation of osmotic medium (Arballo et al., 2010) and the moisture loss (Funebo and Ohlson, 1999) during the microwave drying process.

Hussain et al. (2013) developed a microwave model for EFB to predict the temperature distribution using transient heat equation. The authors used neither Maxwell's equations nor Lambert's law. Instead, the microwave input was merely modelled as a known heat source. The author indicated a linear relationship between microwave power density with the temperature distribution of EFB.

Law et al. (2016) had modelled a microwave heating and drying of discrete samples of oil palm kernels in a 2.45 GHz microwave oven. Maxwell's equation, transient heat conduction and mass transfer equations were solved for the electromagnetic field, temperature and moisture content distributions in a group of discrete kernels. The authors reported that local electric field pattern, the arrangement of samples and heat transfer mechanisms affected the heating pattern of the samples.

2.5 Summary

Current research works have shown that microwave sterilization offers a number of advantages over the conventional sterilization. Microwave heating provides a fast and uniform heating for the drying process of FFB. In addition, the POME that are generated vigorously in the current oil palm milling process could be eliminated by employing the microwave heating technology. However, their works were limited to laboratory studies and there is a lack of fundamental understanding in microwave heating of FFB.

The interaction between the electromagnetic field and material depends on a material's dielectric properties. Other parameters such as thermal conductivity, diffusivity, evaporation rate and drying rate are used to predict the heat and mass transfer phenomena in the FFB. The properties of the kernel, mesocarp and EFB such as thermal conductivity and dielectric properties are not known, especially as a function of moisture content. These properties are essential for accurate model prediction.

On the other hand, fruit detachment and oil extraction processes depend on the size and mechanical performance of the fruits and bunches, whereas the quality of the microwaved fruits can be observed from their structural changes. Researchers suggested that heating or drying has a significant effect on microstructure, mechanical and thermal behavior. Nevertheless, the effects on oil palm kernel, mesocarp and EFB are yet to be fully understood. Therefore, the effects of microwave heating and determination of microstructure, mechanical and thermal properties will be pursued. The description of the experimental work will be presented in the next chapter.

CHAPTER 3

EXPERIMENTAL STUDY

The previous chapter gave the fundamental and literature review on microwave heating of food. Particular attention was paid to the application of microwave in the oil palm industry. In this chapter, a number of experimental procedures are presented. These experiments are used to characterize the mechanical, the permittivity and the drying kinetics of fresh fruit bunches (FFB).

3.1 Assumptions and limitations

Several assumptions had been made during the experimental works. The assumptions were as follows:

1. Moisture content of the stored samples remained similar as the fresh samples.
2. Moisture was lost during microwave heating and drying only.
3. Kernel was assumed as homogeneous spheroid, while mesocarp and EFB were assumed as homogenous rectangular bodies.

3.2 Materials preparation

Fresh fruit bunch of oil palm (*Elaeis guineensis*) were obtained from a local oil palm supplier, Sarawak Oil Palm Berhad Sarawak, Malaysia. The unprocessed EFBs were collected after the palm fruits detachment from the fruit bunches. The EFB was cut into 11.5 mm x 10 mm x 24 mm cubes by using a hacksaw (Stanley 15-265) and a cutter. Mesocarp and kernel were obtained by cutting the palm fruit with a cutter and a diagonal plier. Mesocarp samples with dimensions of 24 mm x 13 mm x 4 mm and kernel samples with a mean diameter of 12.5 mm were used in the experiments. The samples were stored in a fridge prior to experiments.

3.2.1 Determination of size

The sizes of the cubic samples were determined by using a vernier caliper to measure the length, thickness and width which are denoted as l , t_h and w respectively. The sizes of the ellipsoid kernels were expressed in geometric mean diameter, d_m , which was determined according to Aremu and Fadele (2011) as:

$$d_m = \left(l \times t_h \times w\right)^{1/3} \tag{3.1}$$

The volume of the mesocarp and EFB was calculated based on equation (3.2), whereas equation (3.3) was used to calculate the volume of the kernel.

$$V = l \times t_h \times w \tag{3.2}$$

$$V = \frac{1}{6}\pi {d_m}^3 \tag{3.3}$$

3.2.2 Determination of moisture content

Moisture content at any drying time t (MC_t) was determined as follows:

$$MC_t = \frac{W_t - W_{bd}}{W_{bd}} \times 100 \tag{3.4}$$

where W_t is the sample weight at any drying time t and W_{bd} is the bone-dry weight. The equilibrium sample weight was achieved when a material equilibrates with air temperature and water vapor pressure.

The initial moisture contents of the three components of FFB, namely kernel, mesocarp and EFB were determined by using the oven-drying method. The initial moisture content was obtained according to the ASAE Standard S352.1 (ASAE, 1982) under selected conditions of time and temperature. The samples were placed in a crucible and dried at 105 °C using an oven for 24 hours. The weights of the bulk samples before and after oven-drying were recorded. The difference between the weights gave the quantity of moisture evaporated during drying on a dry weight basis (d.b.). Three repetitions were conducted to confirm the obtained initial moisture content. The initial moisture content is given by:

$$MC_o = \frac{W_o - W_{bd}}{W_{bd}} \times 100 \tag{3.5}$$

where W_o is the sample's initial weight.

3.3 Characterization experimental procedures

3.3.1 Permittivity measurement

Relative permittivity of the EFB, mesocarp and kernel were measured using a dielectric probe (Keysight, 85070E Dielectric Probe Kit) as shown in Figure 3.1. The measurement system consists of a computer-controlled vector network analyzer (VNA) (Keysight, E5071C) and the dielectric probe. Air, metal short and deionized water were used as three dielectric references for calibration at the aperture of the dielectric probe.

Figure 3.1: Keysight 85070E Dielectric Probe

The measurements were performed at room temperature. During the measurements, the kernel and EFB samples were directly in contact with the probe aperture. On the other hand, part of the fresh mesocarp of the fruit was sliced in the longitudinal direction to ensure a good contact between the surface of the mesocarp and the dielectric probe. Permittivity of EFB, mesocarp and kernel samples was measured as a function of moisture content. Samples were dried using a domestic microwave and the moisture contents are determined according to Section 3.2.2. The moisture ranges of EFB, mesocarp and kernel samples used were 31 % to 465 % d.b., 0 % to 12.7 % d.b. and 0 % to 17.1 % d.b. respectively. To increase the accuracy and validity of the experimental data, the measurement of dielectric properties for each testing was repeated five times. Dielectric constants ($\varepsilon_r^{'}$) and dielectric loss factors ($\varepsilon_r^{''}$) were obtained from each measurement and average values are reported in Section 4.1.1.

3.3.2 Characterization of thermal properties of Kernel, Mesocarp and EFB

Generally, the methods of measuring thermal conductivity are classified into two categories, namely the steady state heat transfer method and the unsteady state (transient) heat transfer method. The steady state conduction method has disadvantages such as required longer processing time and increases the possibility of moisture migration due to temperature differences across a sample (Shepherd and Bhardwaj, 1986, Wang et al., 2016). These disadvantages can be avoided by using transient conduction method to determine thermal conductivities of different fruits which often contain a higher moisture content. A line heat source method based on transient heat transfer has been widely used to measure the thermal conductivity of a biological material due to its fast measurement, convenience and small sample sizes requirement. This method is most suitable for biological materials that are heterogeneous and often contain high moisture content.

Samples for oil palm mesocarp and EFB of dimensions of 10 mm x 10 mm x 2 mm were prepared. The thermal conductivities were measured with a thermal constant analyzer (Hot Disk TPS 2500S). Due to the stringent requirement on sample size, kernel was not suitable for the experimental testing because of its rigid structure which does not meet the sample's size requirement. Hence, the thermal conductivity of kernel was taken as 0.68 W/(m·K) as reported by Koya and Fono-Tamo (2013). Based on the transient heat source method, the analyzer is capable of measuring thermal conductivity within the range of 0.005 to 1800 W/(m·K) with a tolerance of less than 5 % and it meets ISO 22007-2 standard. The measurement was conducted at room temperature. The thermal conductivity was measured by placing the sensor probes on both of the flat sample surfaces until a constant value of thermal conductivity was obtained. Two sets of mesocarp and EFB samples were prepared for the measurement of thermal conductivity.

Thermogravimetric analysis (TGA) was performed to study the decomposition and thermal stability characteristics of the fresh samples. The TGA analysis was carried out using Perkin Elmer STA 6000 simultaneous thermal analyzer. Each sample with 20 mg was placed in a platinum crucible. The experiments were carried out in an inert atmosphere by flowing nitrogen at 20ml/min with a constant heating rate of 20 °C/min from room temperature to 900 °C.

3.4 Microwave heating and drying experiment

Figure 3.2 shows the experimental setup which a modified domestic microwave oven (Samsung ME711K), fiber optic thermometer (Luxtron, USA) and weight balance (AA-160 Denmer) are included. Appendix 1 shows the set-up in the actual experimental setting. The fiber optic sensor and weight balance were used to measure the sample's temperature and mass or weight respectively.

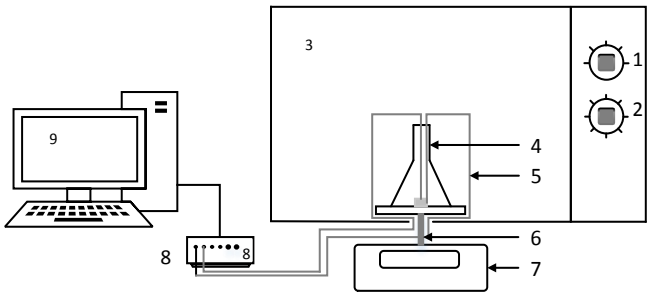

Figure 3.2: Experimental setup for microwave heating and drying

Experimental setup, (1) Microwave power level control ; (2) Microwave time control; (3) Microwave cavity; (4) Quartz conical flask; (5) Fiber optic sensor; (6) Holder; (7) Electronic weight balance; (8) Data logger and (9) Personal computer

The domestic microwave oven has a volume of 30.8 cm (width) x 29 cm (depth) x 18.5 cm (height) and an adjustable power output ranging from 100 W to 800 W. A hole was drilled from the bottom of the microwave oven to allow an aluminium holder to be inserted into the cavity and to hold a conical flask which was placed in the cavity. The sample was placed in the conical flask and its weight was measured using a weight balance.

Various microwave power levels (100 W, 180 W and 300 W) were investigated on the kernel, the mesocarp and the EFB. The microwave powers were selected because the powers were the three lowest power levels available in the microwave oven (Samsung ME711K). It is suggested that a low microwave power could provide a more uniform temperature distribution of the sample (Ho et al., 2002). Each sample was placed in a conical flask and located at the center of the microwave cavity throughout the experiments. In the current study, cyclic

microwave irradiation was supplied by the domestic microwave oven ("ON"/"OFF" state for every cycle of 30s). Although the cyclic microwave exposure resulted in temperature fluctuation, an overall logarithmic temperature increase was observed because microwave energy supplied was converted into heat. The "ON" state indicates that the microwave was generated by the magnetron and was supplied to the sample, hence, the sample's temperature increase was due to microwave heating. On the other hand, during the "OFF" state, the magnetron of the microwave oven does not generate microwave and this resulted in the decrease of the sample's temperature due to cooling by evaporation, convection and radiation. The durations of ON and OFF states for power levels of 100 W, 180 W and 300 W were listed in Table 3.1.

Table 3.1: Duration of ON/OFF state for 1 cycle for microwave power levels at 100 W, 180 W and 300 W.

Microwave power level, P (W)	**ON state, t_{on} (s)**	**OFF state, t_{off} (s)**
100	10	20
180	12	18
300	13	17

The weight reading of the flask along with the sample was periodically taken. Moisture content of the sample was assumed to have achieved equilibrium when it reached a constant weight. The moisture content was calculated according to equation (3.4).

Besides, the sample's surface temperatures were measured by using two fiber optic probes, namely P1 and P2, as indicated in Figure 3.3. A multipurpose adhesive was used to hold the fiber optic probes on the wall of the conical flask to allow the probes contact on the sample surface for temperatures measurements.

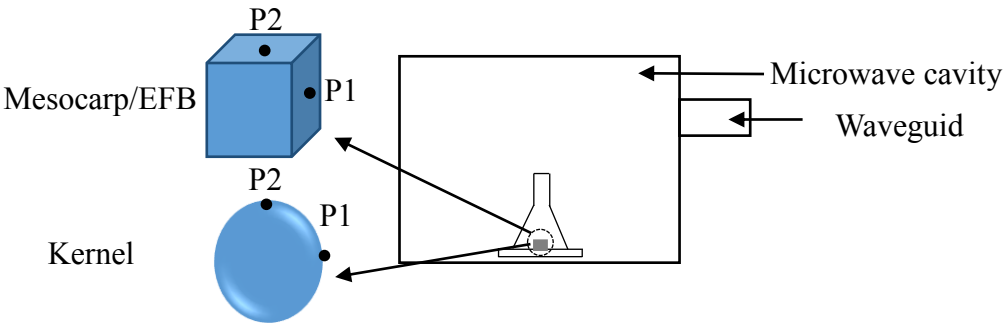

Figure 3.3: Schematic diagram showing the locations of fiber optics (P1 and P2) in determination of sample surface temperature during microwave heating.

P1 was placed at the side of the sample's surface that is closest to the waveguide, while P2 was positioned on top surface of the sample. These locations were selected because these locations are the potential hot spot locations during microwave irradiations as reported by Navarrete et al. (2012), Law et al. (2016), Chen et al. (2016), Kumar et al. (2014), and Birla, Wang, Tang, et al. (2008).

The fiber optic probes were attached to the data acquisition unit which were connected with the personal computer. The temperature data were sampled at 1 second interval using Luxtron TruTemp software. A microwave leakage detector (Mettler Toledo DT-2G/3G) was used to ensure that the microwave exposure was below the safety limit of 5 mW/cm^2 (Schiffmann and Steiner, 2012). To increase the accuracy and validity of the experimental data, three sets of samples were prepared for the temperature and weight measurements.

3.5 Effects of microwave irradiation

3.5.1 Determination of Mechanical properties of Kernel, Mesocarp and EFB

In the current milling process, sterilization aims to soften the fruits and to facilitate fruit stripping from the FFB. Mechanical properties of EFB are crucial as it determines the minimum energy required for the stripping of palm fruits from FFB. In addition, heated or dried kernel and mesocarp require further operations such as mechanical or chemical methods for oil extraction. However, microwave heating and drying could alter the mechanical properties of kernel, mesocarp and EFB. In mechanical extraction, lower mechanical properties such as elastic modulus and yield stress are preferable as the energy required to extract oil from fruits will be lowered.

In addition, an understanding of the mechanical properties of an agricultural product is necessary for the design and development of its postharvest processing machine and equipment (Akinoso and Raji, 2011).

Two types of mechanical characteristics were studied, i.e., yield stress and Young's modulus. The parameters were derived from uniaxial compression tests. The uniaxial compression tests were performed by using a universal testing machine model (Lloyds instrument model LR10K Plus Digital Control Testing). Samples of the kernel, the sliced mesocarp and the sliced EFB were evaluated using a load cell rated up to 10kN. The tests were performed at room temperature with a displacement rate of 10 mm/min. The results of these two parameters were calculated manually and compared with the data obtained from the data logger (NEXYGEN Plus 1.0). The software is able to collect the compression data, such as applied force and deformation of a sample under a displacement rate. Stress-strain curves were plotted by using the collected stress and strain data.

A yield stress indicates the stress level when a compressed sample is weakened and begins to fracture. At this point, the sample ceases to behave elasticity or return to its original shape and deforms plastically. Yield stress is the lowest stress at which a permanent deformation can be measured. On the other hand, the elastic modulus is taken as the ratio of stress to strain up to yield point when tensile or compression load is applied to a sample. When a low compression force is exerted on the sample, the sample offers little resistance towards compression and exhibits a linear relationship which can be defined as its elastic behavior. Figure 3.4 shows the stress-strain curve of a kernel at a moisture content of 10 % d.b.. OA is the elastic deformation region of the kernel and the plastic deformation takes place after the yield point of A.

In order to study the correlation between the mechanical properties with respect to the sample's moisture content, samples with known moisture contents were prepared. Table 3.2 shows the range of the samples' moisture content used in the experiment. The samples were dried to different moisture content and the weights were calculated according to the following equation:

$$W_t = \frac{W_o\left(1+MC_t\right)}{1+MC_o} \tag{3.6}$$

Table 3.2: Range of sample's moisture content used in the mechanical strength experiment

Sample	Moisture range (% kg/kg d.b.)
Kernel	0 – 23
Mesocarp	0 – 24
EFB	0 – 398.9

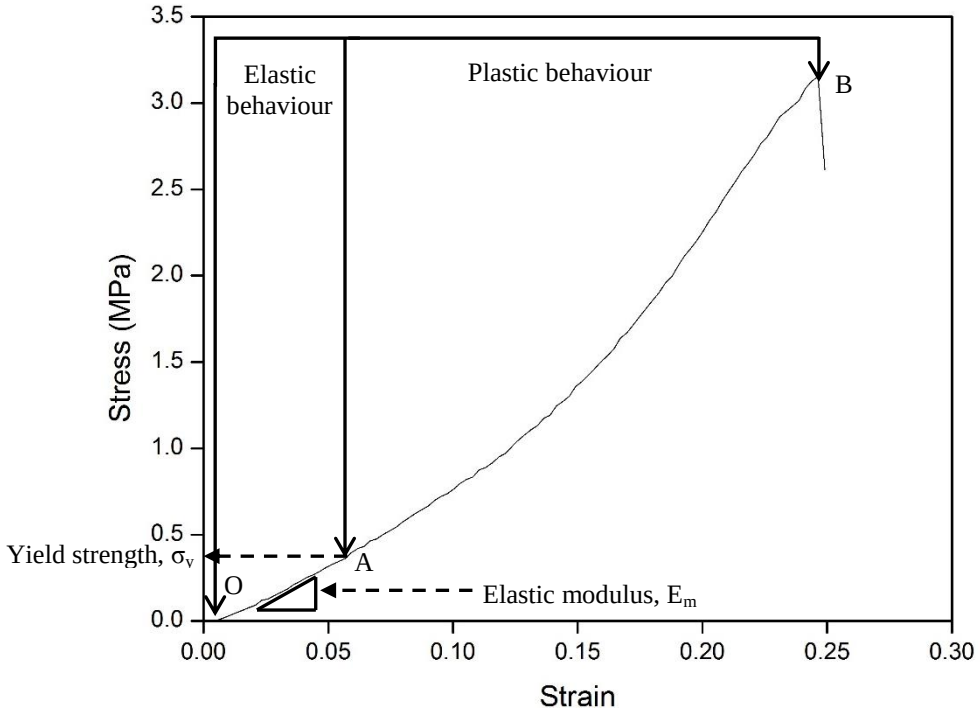

Figure 3.4: Stress-strain curve of kernel at moisture content of 10 % dry basis

3.5.2 Microstructure analysis

The surfaces of fresh and microwave-treated samples were investigated under a scanning electron microscope (Hitachi TM3000 TableTop Microscope) to characterize the effects of microwave on the physical structure of the mesocarp, kernel and EFB. In this analysis, microstructure of microwave-treated kernel, mesocarp and EFB samples subjected to a microwave drying of 100 W and 200 W for two minutes were studied after considering the visual inspective of microwave-treated kernel, mesocarp and EFB as reported in Section 4.3.2.

The samples were then grinded and placed in a desiccator before the SEM analysis was conducted. The morphological structures of the fresh and treated samples were examined using a SEM. Each sample was mounted on a stud using double-sided adhesive carbon tabs and gold coated in a sputter coater (Quorum SC7620). Accelerating voltage of 15 kV with magnifications of 500x, 1000x, 1500x and 5000x were used to take the SEM images. The surface structure of each sample was measured using the ImageJ Java image processing program.

3.6 Summary

In this chapter, the experimental procedures to determine the permittivity, mechanical and thermal properties of the kernel, mesocarp and EFB are described. These included drying kinetics, dielectric constants and loss factor, thermal conductivities, thermal stability analysis, Young's modulus and yield stress as well as microstructural analysis. The results of these experimental studies are discussed in the next chapter.

CHAPTER 4

EXPERIMENTAL RESULT AND DISCUSSION

This chapter presents the results and discussions of the experimental work discussed in the previous chapter. This chapter is divided into three main sections, namely the experimental characterizations, the microwave heating and drying and the corresponding effects of fresh fruit bunches (FFB). The characterizations included permittivity and thermal conductivity as well as the thermal behavior studies of FFB. The microwave heating and drying experiments provide drying kinetic data of FFB. These are then used for the validation of the mathematical models. The effects of microwave heating on the mechanical properties and microstructures of the FFB are also examined.

4.1 Characterizations

4.1.1 Initial moisture content

The initial moisture content of the samples is determined by the oven-drying method according to ASAE Standard S352.1 (ASAE, 1982). The determination of the initial moisture content is crucial because it affects the sample drying rate as reported by Walde et al. (2002). Drying rate is an important information for estimating total drying time to achieve the required moisture content. Initial moisture content of the fresh kernel, mesocarp and EFB of *Elaeis Guineensis* species obtained in this study is compared to the literatures as shown in Table 4.1. The initial moisture content of the kernel, the mesocarp and the EFB used in the experiments is found to be 28.2 kg/kg d.b, 25.9 kg/kg d.b and 485.49 kg/kg d.b respectively. Based on Table 4.1, the moisture contents obtained in this study are comparable with the published data despite the fruits and EFBs are grown at different locations.

Table 4.1: Initial moisture content of kernel, mesocarp and EFB (*Elaeis Guineensis*)

Sample	**Initial moisture content, MC_o (% kg/kg d.b.) (in this study)**	**Initial moisture content, MC_o (% kg/kg d.b.) (literature)**
Kernel	28.2 $\pm$ 0.85	28 (Asr et al., 2012)
Mesocarp	25.9 $\pm$ 0.85	23.75 (Tagoe et al., 2012)
EFB	485.49 $\pm$ 17.8	468 (Abdullah and Sulaiman, 2013)

4.1.2 Permittivity measurement

To adopt microwave technology in the oil palm industry, it is important to identify the interaction of microwave energy on drying samples. The interaction of microwave energy in sample is strongly related to the sample's dielectric properties. Generally, domestic and industrial microwave heating devices operate at 2.45 GHz. For this reason, dielectric properties in this frequency are investigated. Dielectric properties of oil palm kernel, mesocarp and EFB with different moisture contents at 2.45 GHz are shown in Figure 4.1, 4.2 and 4.3 respectively. These graphs show a similar pattern that dielectric constant and dielectric loss factor increase with the increase in moisture content. EFB is found to have a wider range of dielectric constant and loss factor, which are 3.09-24.4 and 0.68-12.8 respectively, compared to kernel ($2.88 \leq \varepsilon_r^{'} \leq 6.2$, $0.36 \leq \varepsilon_r^{''} \leq 1.08$) and mesocarp ($3.28 \leq \varepsilon_r^{'} \leq 4.7$, $0.29 \leq \varepsilon_r^{''} \leq 1.10$). This shows that EFB has the greater ability to store electrical energy and dissipate energy (converting electrical energy to heat), which results in greater heat generation compared to kernel and mesocarp.

According to Calay et al. (1995), the dielectric properties are dependent on the free and bound water contents in food materials so the dielectric properties of fruits increase with increasing moisture content (Sólyom et al., 2013). The influence of moisture content on the dielectric properties is observed, that higher moisture content lead to the higher magnitudes of dielectric constants and dielectric loss factors for the kernel (Figure 4.1), mesocarp (Figure 4.2) and EFB (Figure 4.3).

At the microwave frequency of 2.45 GHz, the dielectric constant and loss factor for kernel increase from 0.41 to 0.93 and 3.21 to 4.14 respectively when moisture content increases from 0 % to 17.1 % d.b. As for the mesocarp, dielectric constant increases from 3.09 to 5.29 and dielectric loss factor increases from 0.37 to 1.02 when the moisture content increases from 0 % to 12.7 % d.b.. Furthermore, dielectric constant and loss factor of EFB increase from 3.18 to 20.71 and 0.61 to 10.32 respectively, with an increase of EFB moisture content from 26.7 % to 465 % d.b..

The dielectric properties increase with moisture content is also observed on palm mesocarp and stalk reported by Tan (1981) when microwave energy is supplied at 9.5 GHz. Tan (1981) suggested that the dielectric properties are influenced by the dipolar orientation of the water molecules present in the sample (Feng et al., 2002, Ryynänen, 1995). At the higher moisture content, more free water is in the sample, thus higher the microwave absorption and energy dissipation (Metaxas and Meredith, 1983).

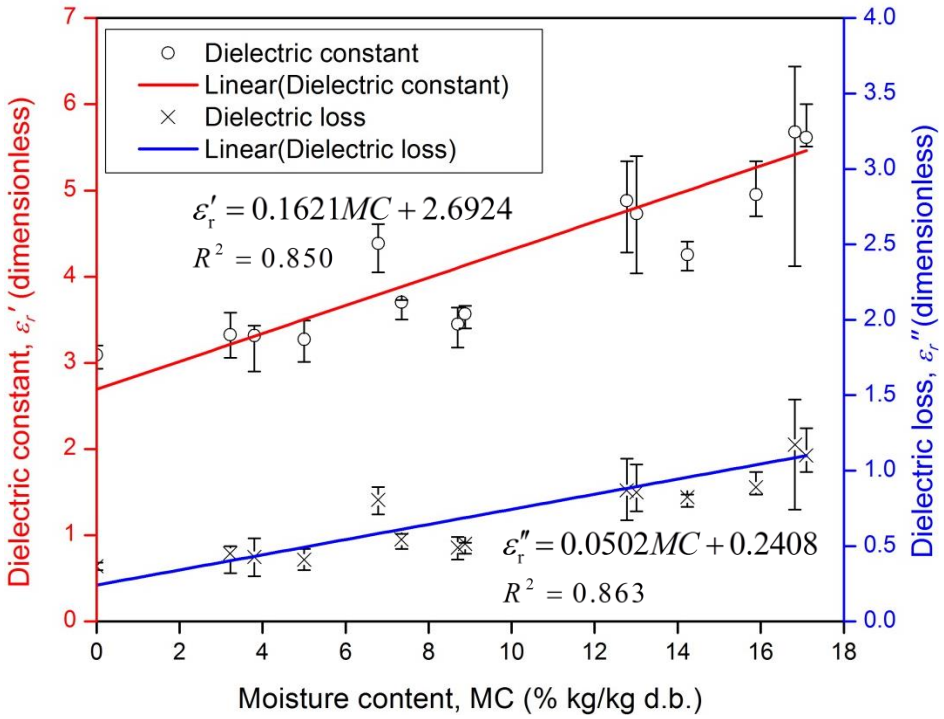

Figure 4.1: Dielectric properties of the kernel at various moisture contents at 2.45 GHz.

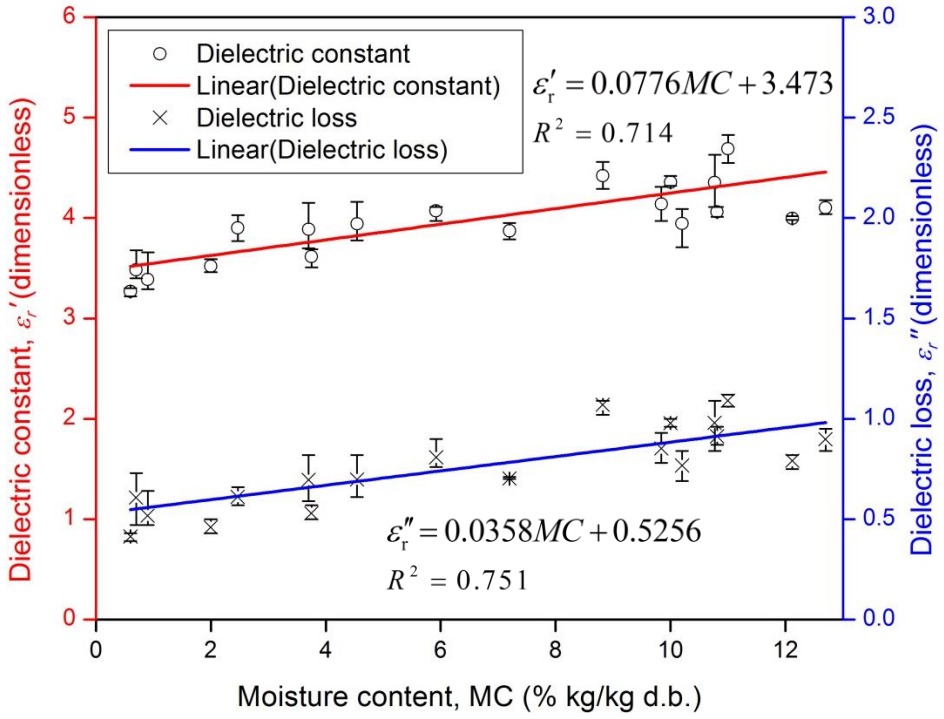

Figure 4.2: Dielectric properties of mesocarp at various moisture contents at 2.45 GHz.

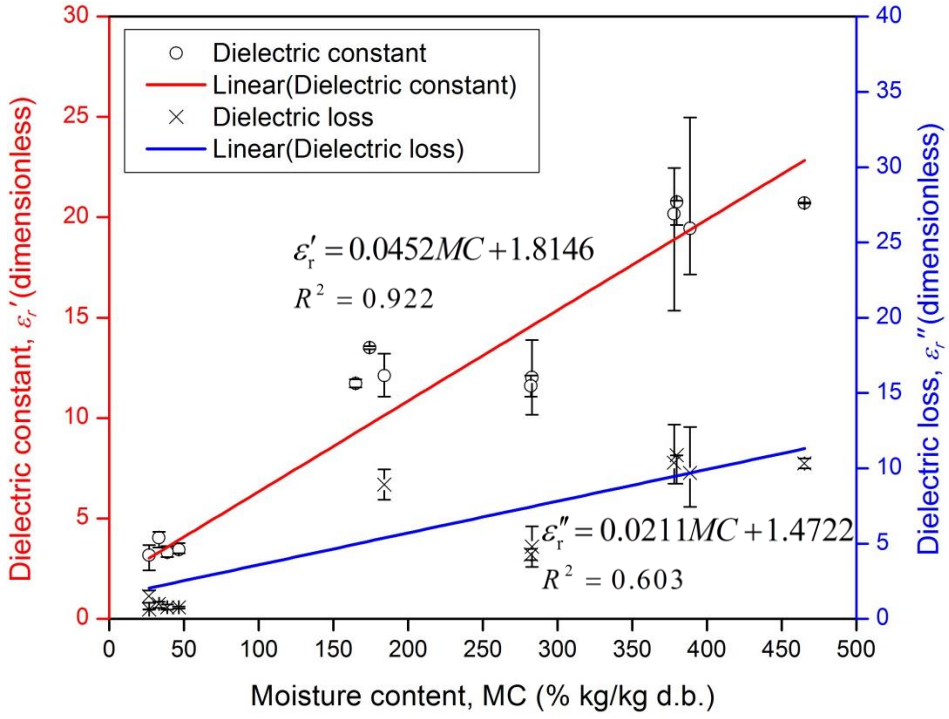

Figure 4.3: Dielectric properties of EFB at various moisture contents at 2.45 GHz.

Linear model is fitted for dielectric properties of kernel, mesocarp and EFB at a microwave frequency of 2.45 GHz for a range of respective moisture contents as shown in Figure 4.1-4.3. The linear coefficient of determination (R^2) values between the predicted and measured dielectric constant are 0.8497, 0.7139 and 0.9222 for the kernel, mesocarp and EFB respectively. In addition, 0.8633, 0.751 and 0.6025 of R^2 values are achieved for dielectric loss factors of the kernel, mesocarp and EFB respectively. The higher amount of moisture content should result in higher values of dielectric constant and loss factor (Lee et al., 2010). Consequently, this resulted a higher impedance mismatch between the sensor probe and sample. The impedance mismatch leads to multi-reflection error (Yee et al., 2011). Hence, the dielectric properties data of the kernel, mesocarp and EFB has a high deviation at a higher range of moisture content. The correlations between the dielectric properties of kernels, mesocarps and EFB as a function of moisture content are shown in Table 4.2.

Table 4.2: Regression equations relating dielectric properties to the moisture content in the kernel, mesocarp and EFB at 2.45 GHz.

Sample	**Regression equations**	R^2	**Equation number**
Kernel	$\varepsilon_r' = 0.1621MC + 2.692$	0.850	(4.1)
	$\varepsilon_r'' = 0.0502MC + 0.241$	0.863	(4.2)
Mesocarp	$\varepsilon_r' = 0.0776MC + 3.473$	0.740	(4.3)
	$\varepsilon_r'' = 0.0357MC + 0.526$	0.751	(4.4)
EFB	$\varepsilon_r' = 0.0452MC + 1.8146$	0.922	(4.5)
	$\varepsilon_r'' = 0.0211MC + 1.4722$	0.603	(4.6)

Figure 4.4 shows the loss tangents and penetration depths of kernels, mesocarps and EFB as a function of moisture content at 2.45 GHz. Dielectric properties are associated with the characteristics of material when subjected to microwave heating such as loss tangent and penetration depth.

Loss tangent is defined as the absorbability of the electromagnetic wave and changes on a material. The loss tangent is greatly affected by the moisture content of

the material. Figure 4.4 shows that the EFB (0.50-0.80) has the better absorbability properties compared to the kernel (0.09-0.225) and mesocarp (0.145-0.265). The higher absorbability properties which are correspond to the heat generation are observed when higher moisture content is present in the kernel and the mesocarp. The loss tangent increased with increasing moisture content trend was also observed in flaxseeds (Sacilik et al., 2006) and corn seeds (Sacilik and Colak, 2010b). Conversely, EFB sample has the weak absorbability properties at high moisture content but with a greater electromagnetic absorption at lower moisture content. The decreases in loss tangent are resulted from the greater magnitude of dielectric constant against the dielectric loss at the higher moisture content. This pattern is in agreement with other fibrous products such as aspen and birch (Koubaa et al., 2008) popcorn grains (Novak, 2013) and tomato and strawberries (Ghanem, 2010).

In addition, generated microwave power density within a sample is also highly dependent on penetration depth. The penetration depth denotes the depth at which the microwave power density has decreased to 37 % (e^{-1}) of its initial value at the surface that is 63 % ($1-e^{-1}$) of incident microwave power density is generated in the sample. Penetration depth is one of the important criterions for designing of any microwave heating system. Microwave is absorbed by the sample when the penetration depth is smaller than sample's (Ku et al., 2001). Thus a material with high microwave power density generation will have a lower penetration depth. The penetration depth is dependent on the dielectric properties of the sample and is calculated according to equation (2.7). The penetration depth of EFB ranged from 0.0085 to 0.019 m for moisture content from 0 to 485 % kg/kg d.b., whereas mesocarp has the penetration depth of 0.032 to 0.068 m at moisture content from 0 to 26.9 % and is lower to that of kernel at 0.03 to 0.13 m at moisture content from 0 to 28.5 %. The penetration depths of these samples exhibit the same relationship that the penetration depth increases with reduced moisture content. The similar penetration depth trend that increases with reduced moisture content was also observed for organic compounds such as egg white (Boreddy and Subbiah, 2016), chestnut flour (Zhu et al., 2012) and almond shells (Gao et al., 2012). This indicates that penetration depth is highly dependent on loss tangent than dielectric constant. Kernel, mesocarp and EFB could be heated effectively by microwave heating at a higher moisture content with low penetration depth.

(a)

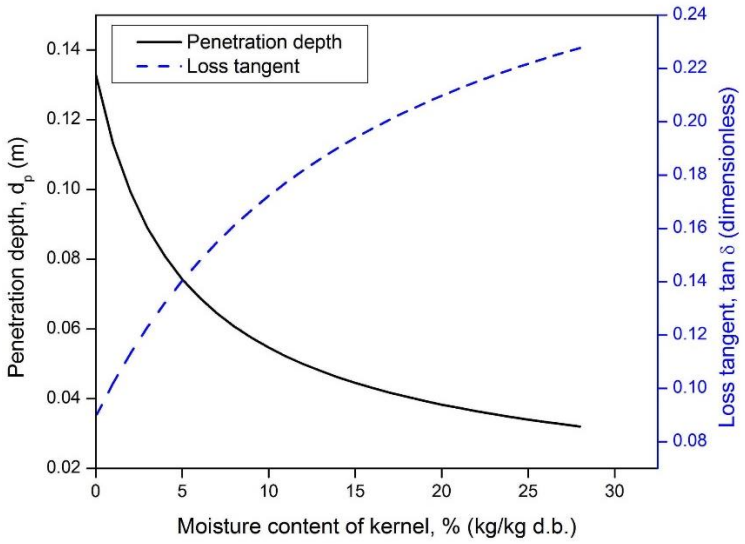

(b)

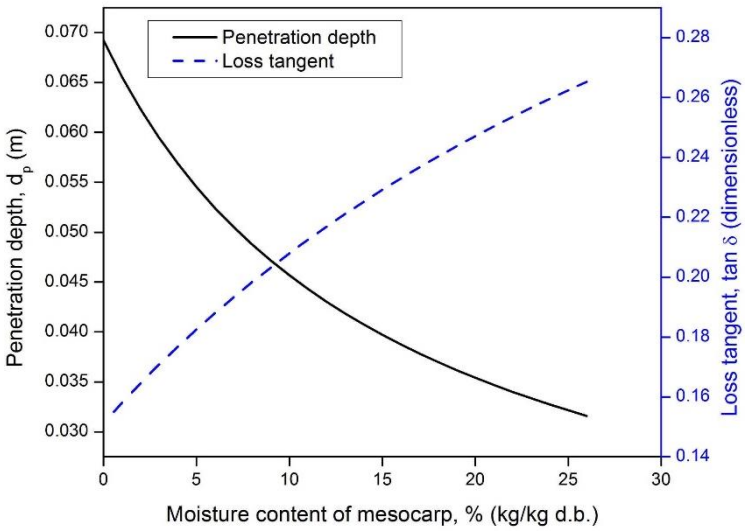

(c)

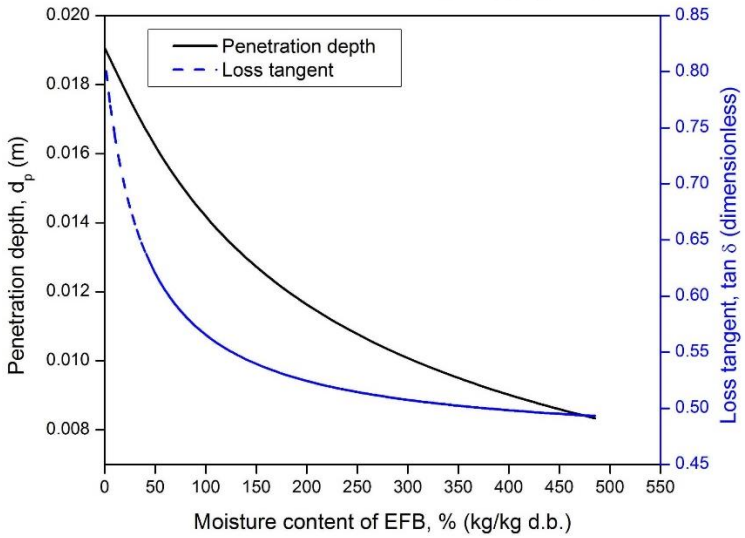

Figure 4.4: Loss tangent and penetration depth of (a)kernel, (b)mesocarp and (c)EFB at various moisture contents at a frequency of 2.45 GHz.

This study reckons that the dielectric properties of the fresh oil palm kernel, mesocarp and EFB are greatly dependent on the moisture content. The dielectric properties define the abilities of sample such as penetration depth and loss tangent. During microwave drying, the dielectric properties of the kernel, mesocarp and EFB samples decrease when their moisture content are reduced, hence change their penetration depth and loss tangent. The penetration depth of kernel, mesocarp and EFB increases with reducing moisture content whereby the loss tangent decreases with reducing moisture content. However, the loss tangent of EFB increases at lower moisture content. This information are crucial for the simulation of microwave heating studies. Therefore, the correlations between the dielectric properties of kernel, mesocarp and EFB as a function of moisture content are fitted in linear model. These data could also improve the design effectiveness of a commercial microwave system in calculating the requirements of microwave power and time to achieve the desired product's specification.

4.1.3 Thermal conductivity measurement

Thermal conductivity is one of the important parameters used in the heat transfer analysis in a sample. The thermal conductivity of kernel was found and reported to be 0.68W/(m·K) by Koya and Fono-Tamo (2013). Chan (1985) reported that the thermal conductivity of mesocarp of *Tenera* variety was 0.347W/(m·K). Nevertheless, there is lack of information on the thermal conductivity of the fresh mesocarp and EFB of *Elaeis guineensis* species in the literatures till date. Therefore, the thermal conductivity of fresh mesocarp and EFB is to be then determined this section. The thermal conductivity of the fresh oil palm mesocarp and EFB slices is determined based on transient heat source method. The dimensions of the tested samples are as reported in Section 3.3.2. The thermal conductivity values are presented in Table 4.3.

Table 4.3: Thermal conductivity of mesocarp and EFB slices

Sample	**Average thermal conductivity value, k (W/(m·K))**	**Estimated thermal conductivity from literature**
Mesocarp	0.458 ± 0.022	0.347 (Chan, 1985)
EFB	0.0285 ± 0.001	0.01 – 0.03 (Hassan et al., 2014)

In this analysis, the average thermal conductivity of the oil palm mesocarp and EFB is 0.458 and 0.028W/(m·K) respectively. The obtained thermal conductivity is compared with the estimated values and the comparison shows the experimentally determined values are close to the estimated values. The higher thermal conductivity of mesocarp leads to a greater thermal energy transfer compared to EFB. This is because the fresh EFB consists of a small amount of solid matter and a large proportion of voids namely gas or air bubbles due to the presence of high moisture hence thermal conductivity is lowered.

4.1.4 Thermal behavior characterization

TGA is conducted to study the decomposition and thermal stability of fresh kernel, mesocarp and EFB. It is done by heating the kernel, the mesocarp and the EFB from 30 °C to 900 °C at a rate of 20 °C/min in the presence of nitrogen gas. Figure 4.5-4.7 show the weight losses of the samples as a function of temperature and its derivative weight curve to illustrate the rate of mass loss. The derivative weight curve shows four degradation steps. Decomposition of natural fibers is generally attributed by the moisture evaporation and the lignocellulose decompositions such as lignin, hemicellulose and cellulose decompositions (Suardana et al., 2011, Methacanon et al., 2010, Martin et al., 2010, Lee and Wang, 2006).

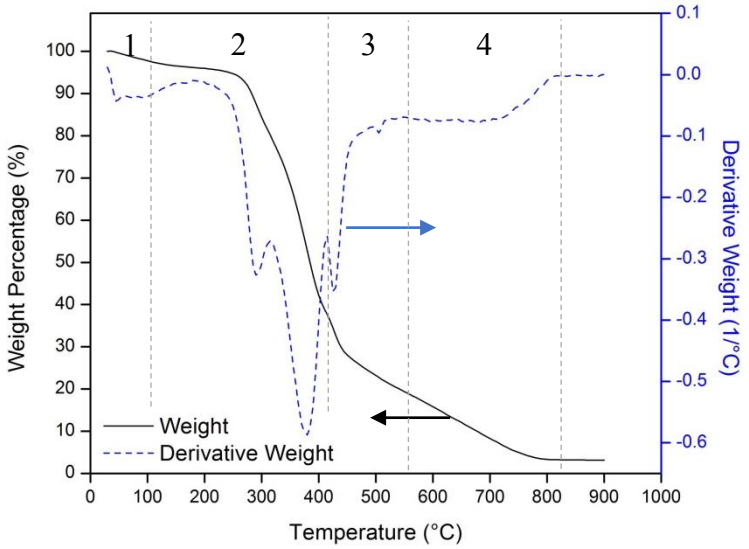

Figure 4.5: TGA and derivative weight analysis of fresh kernel

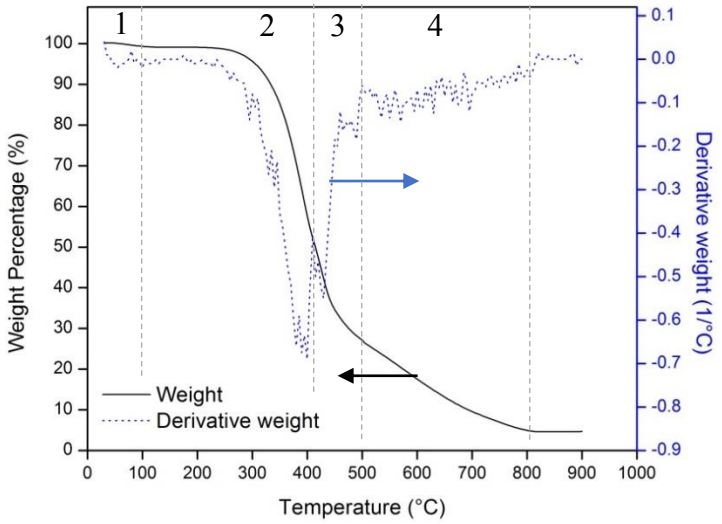

Figure 4.6: TGA and derivative weight analysis of fresh mesocarp

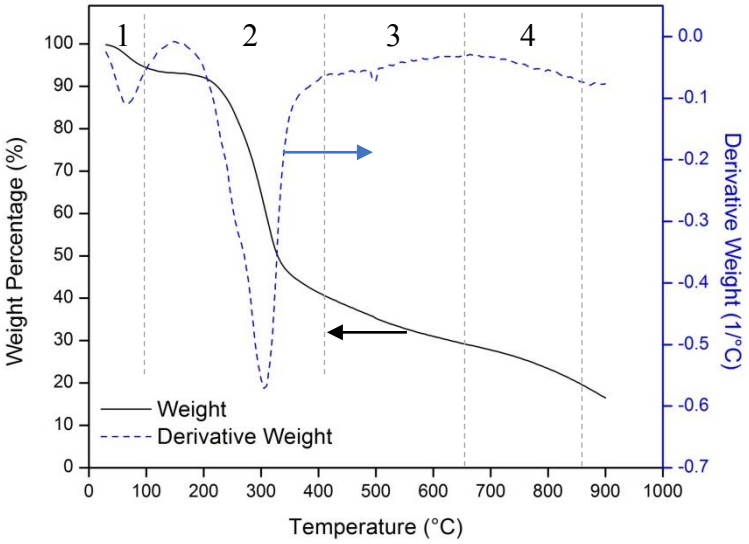

Figure 4.7: TGA and derivative weight analysis of fresh EFB

Table 4.4 shows the stages of weight loss for fresh kernel, mesocarp and EFB calculated based on Figure 4.5-4.7. The first degradation stage is occurred due to the moisture evaporation in the samples (Norul Izani et al., 2013). In the first stage, moisture is evaporated from the room temperature to 100 °C for kernel, mesocarp and EFB. Then, a massive thermal degradation due to the decomposition of lignocellulose in the sample is observed and leads to maximum rate of weight loss.

Table 4.4: Analysis of weight loss of mesocarp, kernel and EFB in four stages with its chemical constituents

Sample	**Stage 1**		**Stage 2**		**Stage 3**		**Stage 4**		**Char**
	Moisture evaporation		**Lignin and hemicellulose decomposition**		**Cellulose decomposition**		**Lignin decomposition**		**% dry sample**
	T (°C)	**W_t (%)**	**T (°C)**	**W_t (%)**	**T (°C)**	**W_t (%)**	**T (°C)**	**W_t (%)**	
Kernel	30-100	3.84	100-416	32.16	416-555	44.92	555-835	15.87	3.21
Mesocarp	30-100	1.15	100-410	46.73	410-500	24.98	500-815	22.53	4.61
EFB	30-100	6.85	100-415	52.81	415-660	11.50	660-870	10.06	18.78

The second stage happens from 100 °C to 416 °C with a mass loss of 32.16 % and 100 °C to 410 °C with a mass loss of 46.73 % for kernel and mesocarp respectively. The second stage corresponds to the decomposition of lignin and hemicellulose. The third stage occurs from 416 °C to 555 °C and 410 °C to 500 °C with mass losses of 44.92 % and 24.98 % respectively for kernel and mesocarp which corresponds to the decomposition of cellulose. The decomposition of lignin, hemicellulose and cellulose (Stage 2 and Stage 3) in EFB happens simultaneously at 100 °C to 415 °C with a huge mass loss of 52.81 %. As reported by Nabinejad et al. (2015), the decomposition of lignin starts after the end of cellulose decomposition. The decomposition of lignin starts from 555 °C to 835 °C, 500 °C to 815 °C and 415 °C to 870 °C for kernel, mesocarp and EFB respectively. The decompositions of fresh kernel, mesocarp and EFB ends at 835 °C, 815 °C and 870 °C with char of dried the samples of 3.21 %, 4.61 % and 18.78 % respectively. During the microwave drying experiments in Section 4.2, maximum temperatures of 77 °C,

68 °C and 78 °C respectively were recorded after the microwave treatment on kernel, mesocarp and EFB samples. Based on Table 4.4, the decompositions of the fibers for kernel, mesocarp and EFB happen at temperature above evaporation point (100 °C). During the microwave heating experiments, maximum temperatures of 84 °C and 96 °C respectively were recorded after the microwave treatment on kernel and mesocarp samples for 14 mins. Therefore, the weight losses of the heated kernel and EFB samples during the microwave drying experiment are only due to moisture evaporation. However, the temperature of EFB increased beyond 100 °C after 5 mins of microwave treatment. Subsequently, the lignocellulose of the EFB decomposed.

4.2 Microwave heating and drying

Figure 4.8(a), 4.8(b) and 4.8(c) show the temperature profiles of the kernel, mesocarp and EFB at P1 and P2 respectively. P1 and P2 are located on the samples as described in Section 3.4. The temperature fluctuations are due to the microwave cyclic operation. The corresponding drying curves are shown in Figure 4.9(a1), 4.9(b1) and 4.9(c1). It is observed that the EFB has the highest rate of heating compared to mesocarp and EFB when subjected to microwave heating. From the temperature profiles of the two probes, P1 and P2, it is observed that the top surface of the sample achieved a higher temperature than those at the side of the sample.

The rapid heating of EFB is contributed by its small penetration depth and high loss tangent compared to the kernel and mesocarp. The small penetration depth of EFB (0.0085 - 0.019 m) allow microwave absorption in the sample. On the other hand. The penetration depths of kernel (0.03 - 0.13 m) and mesocarp (0.032 - 0.068 m) are larger than the respective sizes. Therefore, microwave is able to penetrate through the kernel and mesocarp samples. Water droplets are observed on the wall of the conical flask in the heated sample at the end of the heating process, particularly on the EFB. This is due to evaporation of water followed by the condensation of water vapor to the cooler flask's wall.

The drying kinetics of the kernel, mesocarp and EFB at different microwave powers are depicted in Figure 4.9(a), 4.9(b) and 4.9(c) respectively. Similar drying trend was observed during microwave drying of FFB abscission layer (Sukaribin and

Khalid, 2009), oil palm leaf (Mielke, 2017) and palm fruits (Puangsuwan et al., 2015) where two stages of drying are observed in sample drying; namely the constant drying rate period and the falling drying rate period. The two drying rate period of sample at 180 W are shown in Figure 4.9(a2), 4.9(b2) and 4.9(c2). During the constant drying rate period, the mass transfer rate is constant and moisture content is dried from initial to critical moisture content. Lüle and Koyuncu (2015) stated that the rate of removal of moisture content during the constant drying period was highly dependent on the surrounding conditions and only affected slightly by the nature of the product. A decrease in the rate of moisture removal is observed at the end of constant drying as it is correlated to the rate of moisture migration within the sample. As the drying continues, the falling drying rate period is observed, where the drying rate and temperature decrease slowly until it approaches equilibrium moisture content. At this point, moisture diffuses from the sample to its surface, then followed by moisture removal from the surface to the air surrounding. The falling drying rate period is dependent on the rate of diffusion of moisture. As the drying rate decreases at the end of the falling rate drying period, progressive decrease in microwave absorption is observed as agreed by Constant et al. (1996). Hence it can concludes that power absorption is largely dependent on the moisture content.

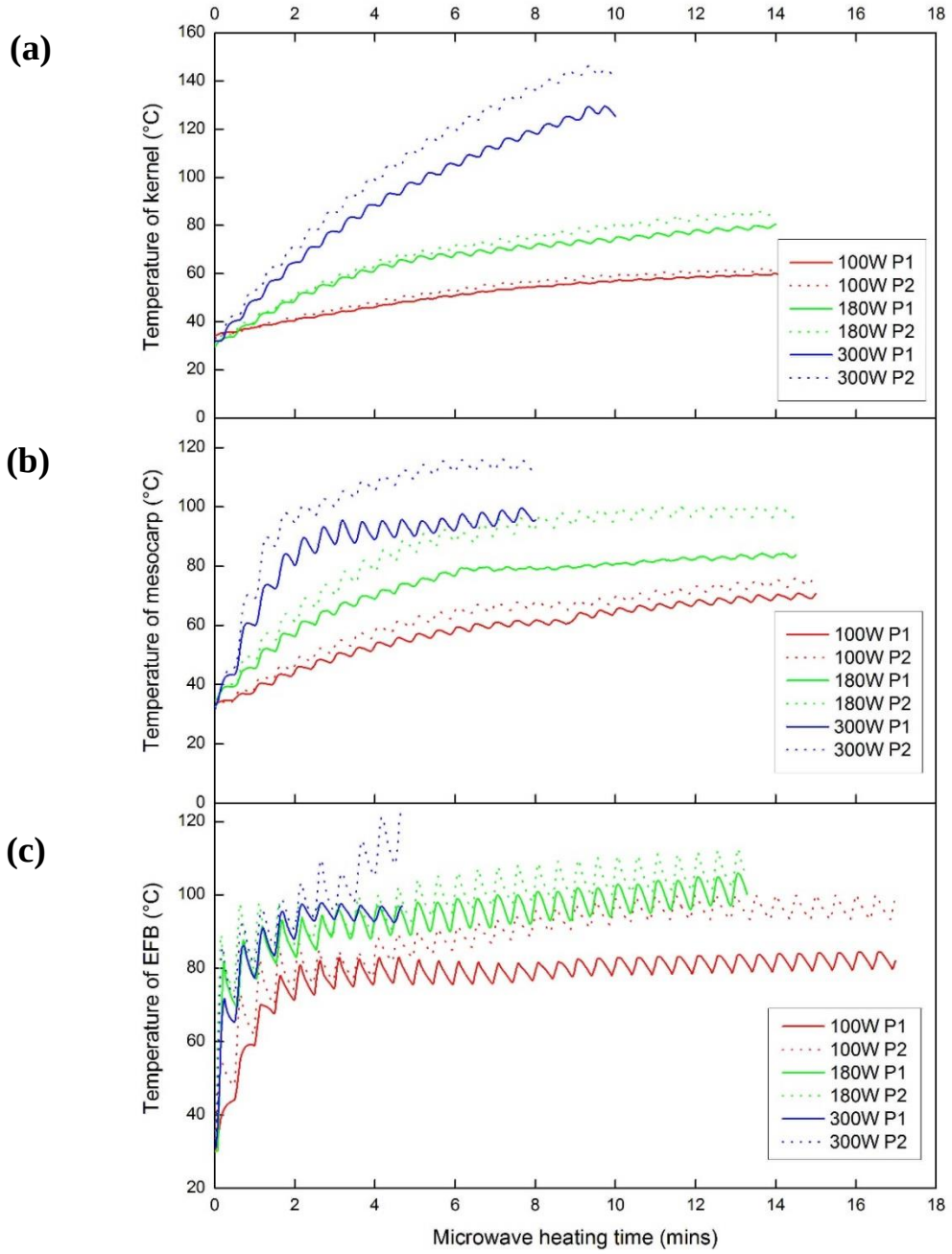

Figure 4.8: Temperature of (a)kernel, (b)mesocarp and (c)EFB subject to various microwave power levels

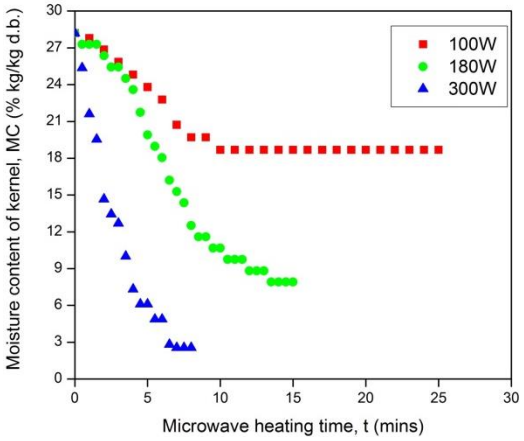

(a1)

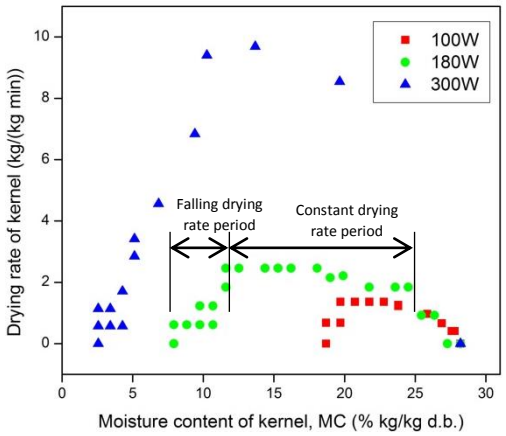

(a2)

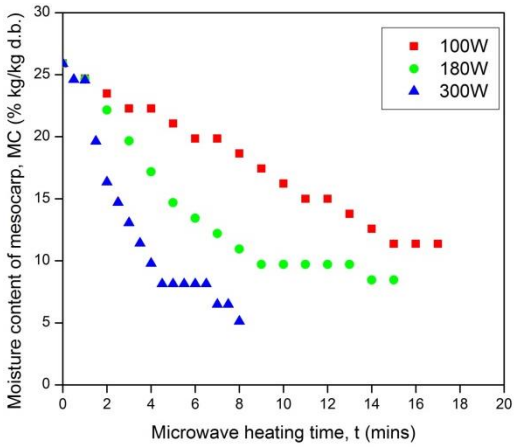

(b1)

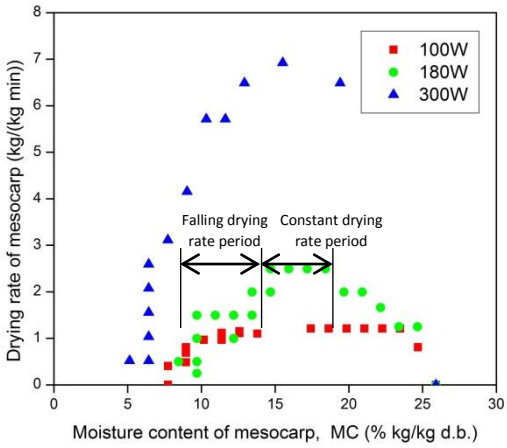

(b2)

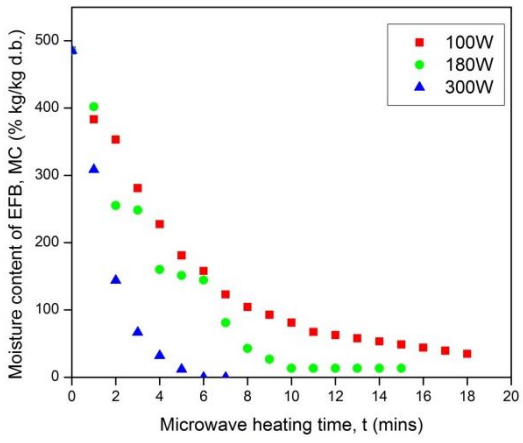

(c1)

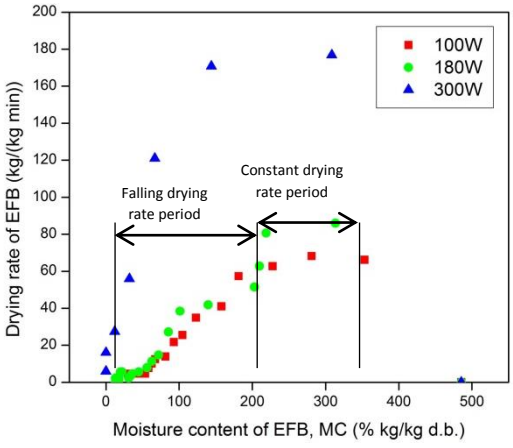

(c2)

Figure 4.9: (1) Moisture content and (2) drying rate of (a)kernel, (b)mesocarp and (c)EFB subject to various microwave power levels

Table 4.5 presents the total moisture loss and the drying time needed for the kernel, mesocarp and EFB to achieve equilibrium moisture content at various microwave powers. It is observed from Table 4.5 that a longer drying time is required at a lower microwave power level. The microwave treatment of the kernel at 300 W requires 7 mins of heating to achieve its equilibrium moisture content, whereas the equilibrium moisture content can be achieved after 13.5 and 10 mins at microwave power of 180 W and 100 W, respectively. For the mesocarp heated at 300 W, 8 mins is needed to achieve its equilibrium moisture content, whereas the equilibrium moisture content can only be attained after 14 and 15 mins when subject to 180 W and 100 W, respectively.

On the other hand, 6, 10 and 18 mins of microwave treatment are needed for an EFB to reach its equilibrium at 300 W, 180 W and 100 W, respectively. These emphasize a reduction in drying time with the increase of the applied microwave power level. The greater heating effect is provided by the higher power density to overcome the intermolecular attraction of the bound water, as a result, the bound water evaporates.

Table 4.5: Total moisture loss and drying time required to dry oil palm mesocarp, kernel and EFB to reach equilibrium.

Microwave power level, P (W)	**Kernel**		**Mesocarp**		**EFB**	
	Heating time, t (min)	**Total moisture loss, % (kg/kg d.b.)**	**Heating time, t (min)**	**Total moisture loss, % (kg/kg d.b.)**	**Heating time, t (min)**	**Total moisture loss, % (kg/kg d.b.)**
300	7	25.6	8	20.8	6	485.49
180	13.5	20.3	14	17.5	10	472.2
100	10	9.5	15	14.5	18	450.7

A rapid mass transfer is occurred at a higher microwave power level. For instance, the moisture content of kernel, mesocarp and EFB are reduced to 27.1 %, 23 % and 350 % respectively after 2 mins of microwave treatment at 100 W. On the other hand, the moisture content of the kernel, mesocarp and EFB at 300 W are reduced to be around 13.9 %, 16 %, and 140 % respectively.

However, moisture content reduction was reported to cause fruit hardening. Therefore, quantitative relationship between the moisture content and the mechanical

strength of kernel, mesocarp and EFB is essential to estimate the energy requirement in the milling process and hence it is analysed in Section 4.3.1.

Similarly after 2 mins of heating, the temperature of microwave-treated kernel, mesocarp and EFB at 300 W is increased to 75, 84 and 94 °C respectively from room temperature and the temperature is 87.5 %, 78 % and 23.7 % higher than when the treated samples are heated at 100 W. As reported by Izli and Isik (2015), high microwave exposure resulted damage at the materials' microstructure which in turn affected the quality of fruits. Hence, it is crucial to investigate the microwave drying effects on the microstructure of kernel, mesocarp and EFB to ensure minimal damages. This aspect will be further discussed in Section 4.3.2. Theoretically, heating or drying at a high microwave power level may result in intensive evaporation of water which leads to external structure destruction of the sample. Cheng et al. (2011) observed that cracking and burning effect occurred on microwave heated kernel and mesocarp when 800W was subjected. Figure 4.10-4.12 show the physical appearances of fresh and microwave-treated kernels, mesocarp and EFB. It is noticed that the burning effect starts when kernel is subjected to 180 W (Figure 4.10(c)) and 300 W (Figure 4.10(d)). From Figure 4.10(c), the burning of the kernel occurs at the center of the kernel whereby it is completely burnt at the end of the drying period after being subjected to 300 W (Figure 4.10(d)). As pointed out by Chow and Ma (2007), the burnt occurred in kernels were undesirable as it affected the quality and color of the kernel oil. However, the kernel which is microwave-treated at 180 W for 2 mins (Figure 4.10(e)) shows no major changes on the physical appearance. Therefore, kernel, mesocarp and EFB samples subjected to microwave irradiation for 2 mins are chosen for SEM analysis which is presented in Section 4.3.2.

The appearances of the fresh and microwave-treated mesocarp and EFB samples are shown in Figure 4.11 and Figure 4.12 respectively. The mesocarp and EFB are hardened after microwave heating and drying. However, minimal changes in terms of appearance and size are observed on the surfaces of the microwave treated mesocarp (Figure 4.11(b)-(e)) and EFB (Figure 4.12(b)-(e)). Nevertheless, the size reduction is observed on the microwave-treated EFBs (Figure 4.12(b)-(d)). With regard to the mesocarp (Figure 4.11(e)) and EFB (Figure 4.12(e)) subject to microwave heating at 180 W for 2 mins, the samples show no dissimilarity compare to the fresh samples.

(a) **(b)** **(c)**

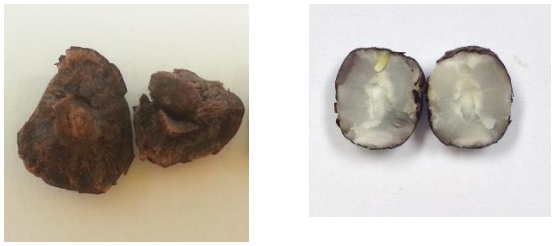

(d) **(e)**

Figure 4.10: Physical appearance of microwave treated oil palm kernel (a) before and after exposure to (b)100 W, (c)180 W, (d)300 W and (e)2 mins at 180 W.

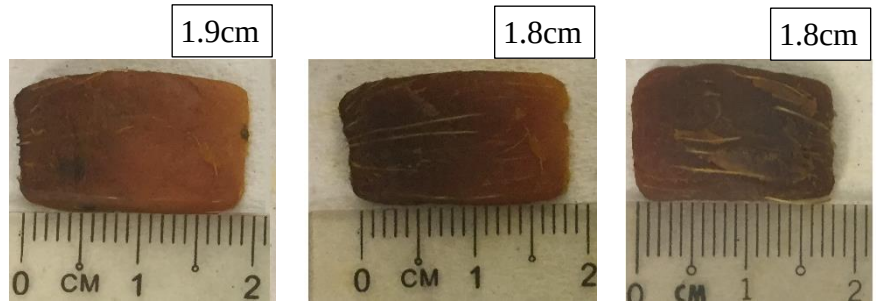

(a) **(b)** **(c)**

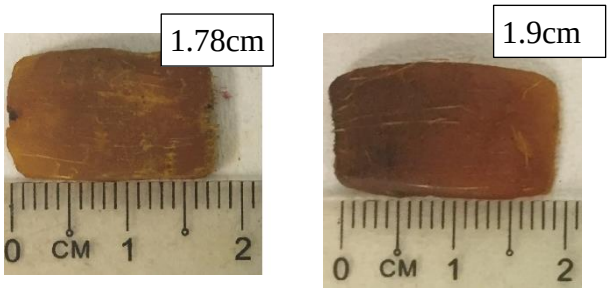

(d) **(e)**

Figure 4.11: Physical appearance of microwave treated oil palm mesocarp (a) before and after exposure to (b)100 W, (c)180 W, (d)300 W and (e)2 mins at 180 W.

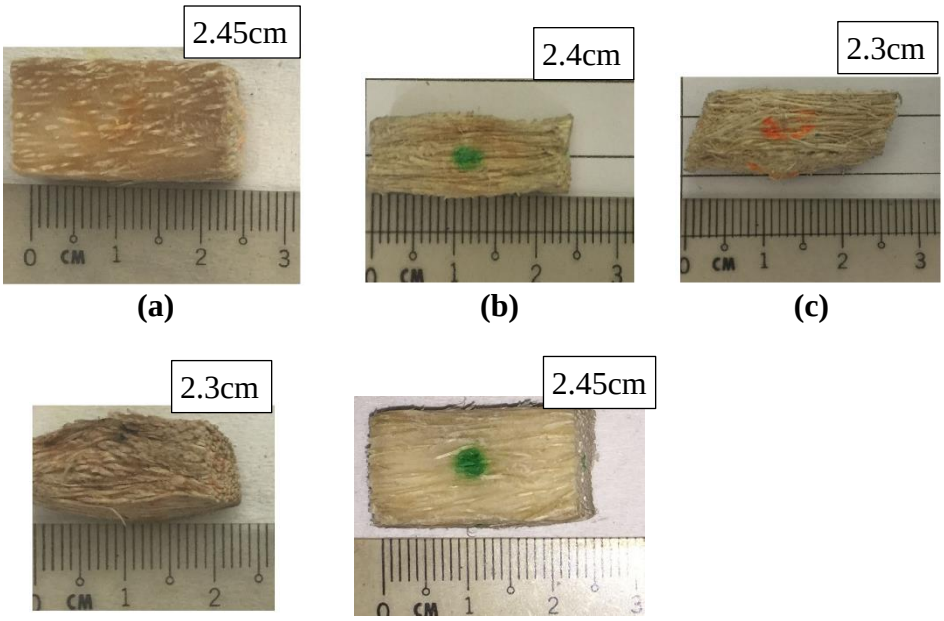

Figure 4.12: Physical appearance of microwave treated oil palm EFB (a) before and after exposure to (b)100 W, (c)180 W, (d)300 W and (e)2 mins at 180 W.

4.3 The effects of microwave heating and drying

4.3.1 Mechanical behaviour characterization

The empirical correlations between the moisture content and the mechanical strength of the dried kernel, mesocarp and EFB are essential to oil palm industry to optimize the energy requirement for fruits detachment, as well as palm oil extraction. In the fruit detachment and oil extraction processes, lower elastic modulus and yield stress of the EFB and palm fruits are desired as lower energy is required to detach the fruits from the bunches and to extract the oil from the fruits.

Figure 4.13(a), 4.14(a) and 4.15(a) show the elastic modulus of the kernel, mesocarp and EFB at various moisture contents respectively. The elastic modulus decreases when the moisture content of kernel, mesocarp and EFB increased. The observation is consistent with the findings reported by Krokida and Maroulis (1999) that the microwave drying increased the elasticity of biological products due to decrease in moisture content. The highest elastic moduli obtained for the kernel, mesocarp and EFB are 24.62 MPa at 5 % d.b., 1.21 MPa at 0 % d.b. and 0.86 MPa at 50 % d.b. respectively. The lowest elastic modulus is found to be 4.9 MPa at 24.7 % d.b., 0.22 MPa at 23.2 % d.b. and 0.22 MPa at 420 % d.b. for kernel, mesocarp and

EFB respectively. Figure 4.13(b), 4.14(b) and 4.15(b) show the yield stresses of the kernel, mesocarp and EFB at various moisture contents. The yield stress reduces with the increases of sample's moisture content. The lowest yield strength for kernel, mesocarp and EFB are found to be 0.22 MPa at 24.7 % d.b., 0.02 MPa at 24.9 % d.b. and 0.015 MPa at 420 % d.b. respectively, whereas the highest value is obtained to be 0.88 MPa at 5 % d.b., 0.105 MPa at 0 % d.b. and 0.105 MPa at 50 % d.b. respectively.

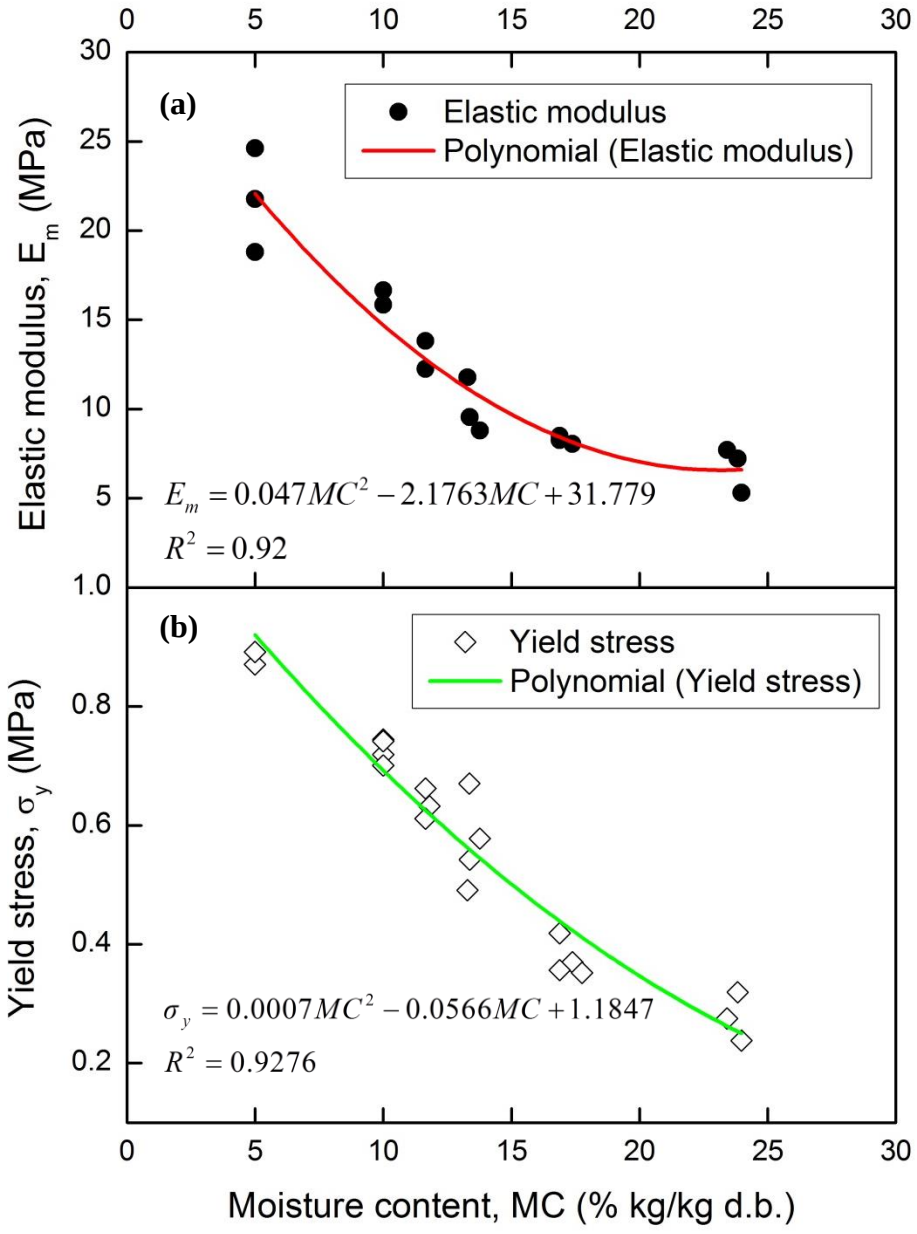

Figure 4.13: (a) Elastic modulus and (b) Yield stress of kernel at different moisture content levels dried at 180 W

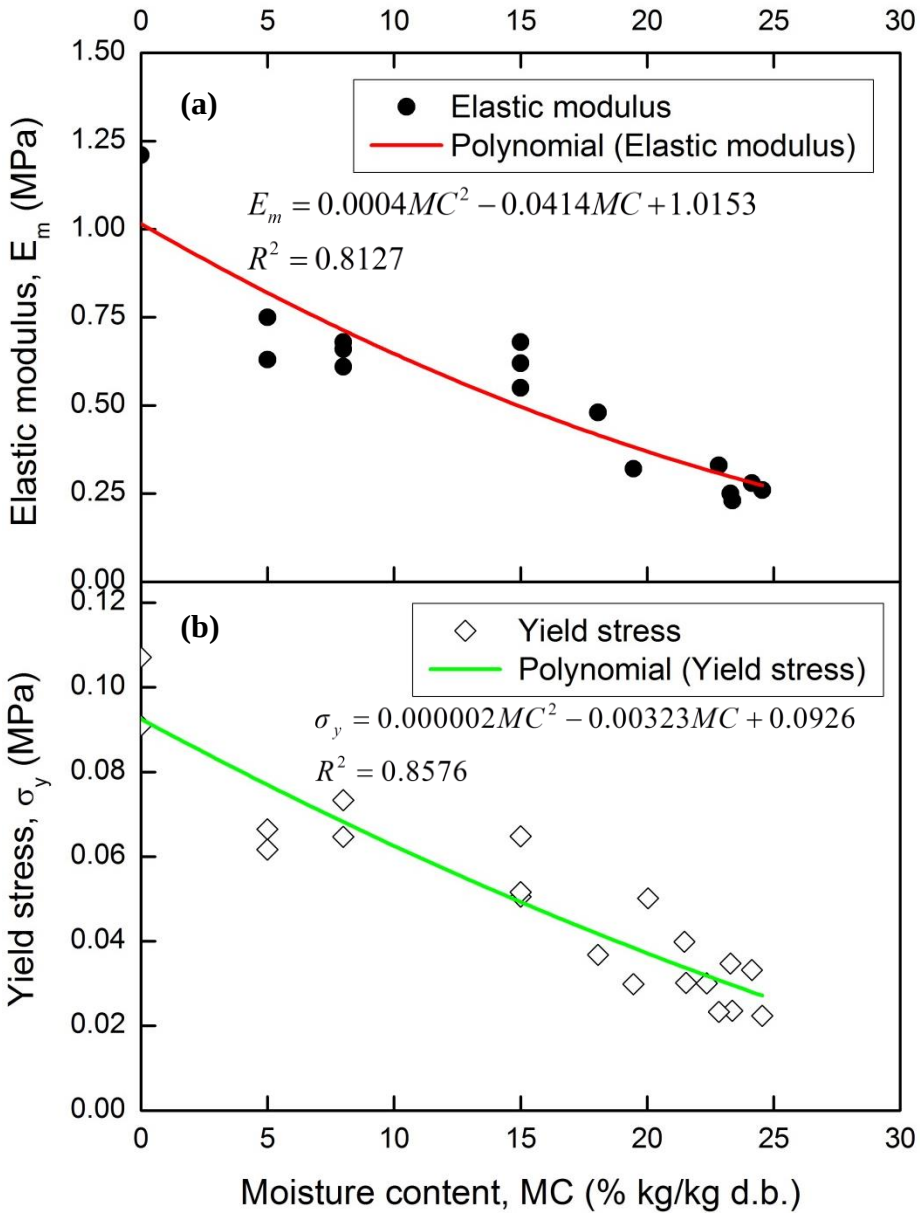

Figure 4.14: (a) Elastic modulus and (b) Yield stress of mesocarp at different moisture content levels dried at 180 W

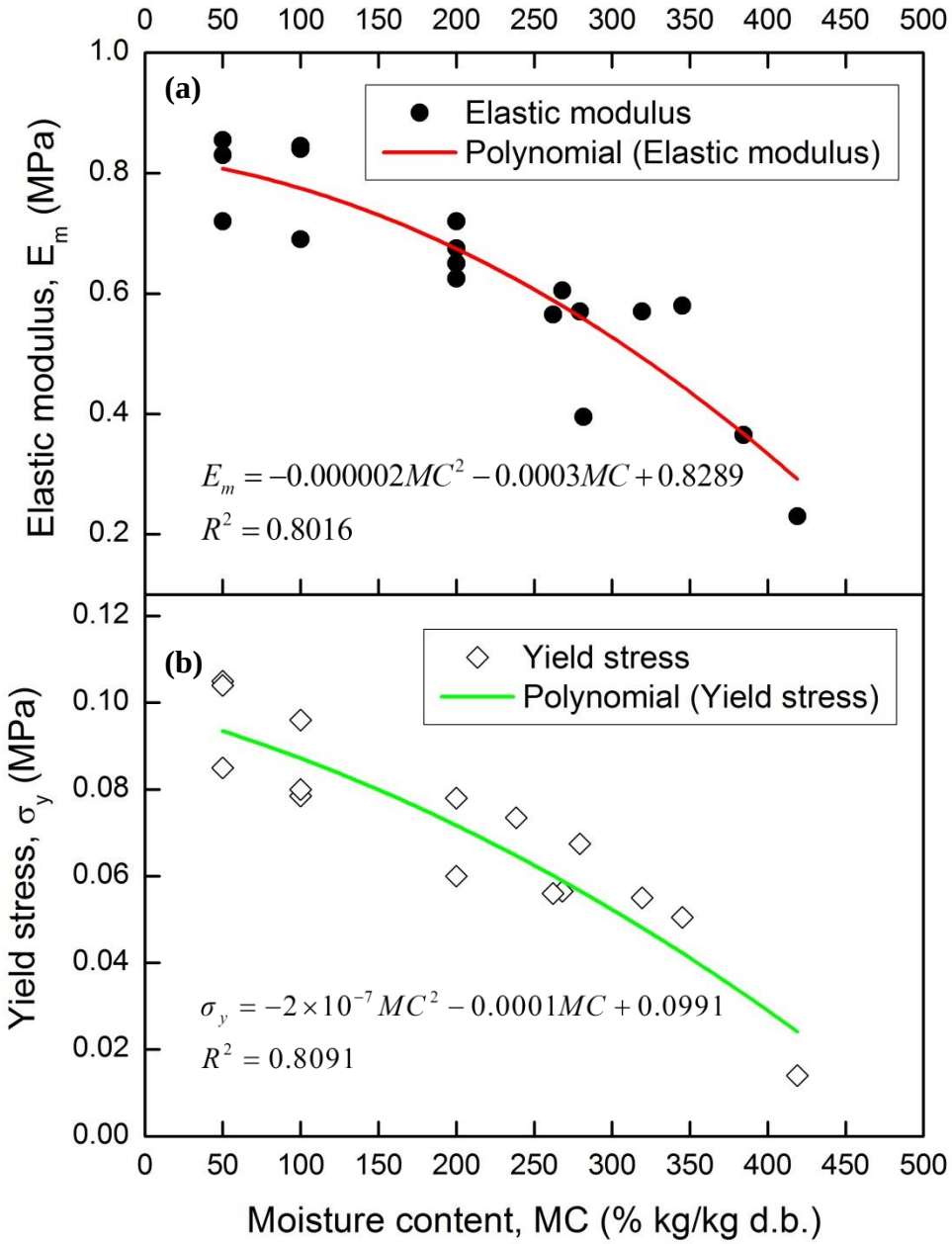

Figure 4.15: (a) Elastic modulus and (b) Yield stress of EFB at different moisture content levels dried at 180 W

The increased mechanical strength was also investigated on oil palm trunk (Sulaiman et al., 2012) and EFB composites (Ali, 2008). Contreras et al. (2008) stated that drying process promoted the mechanical rigidity and resistance to fracture and deformation of the dried samples. In addition, in order to facilitate a lower energy requirement of the stripping, pressing and extraction processes, a lower mechanical properties of the EFB and mesocarp is desired. In this analysis, the low

mechanical properties of the kernel, mesocarp and EFB can be obtained at a higher moisture content.

The microwave drying process is capable of drying the fruits to the desired moisture content, however, the mechanical strength experiments show that the microwave drying process increases the elastic modulus and yield stress of the kernel and mesocarp. Thus, a higher mechanical energy is required to extract the oil from the dried kernel and mesocarp and to detach the fruits from the dried EFB.

The correlations of the elastic modulus and the yield stress with the moisture content of kernel, mesocarp and EFB are fitted with second-order polynomial regression model. The regression equations with their coefficient of determination (R^2) are shown in Table 4.6. The equations are beneficial for designing the capacity of the oil extraction and the thresher equipment and also for further investigation on the mechanical-related behaviors such as dimensional stability and shrinkage studies.

Table 4.6: Regression equations relating the mechanical strength to the moisture content in the kernel, mesocarp and EFB.

Sample	**Regression equations**	R^2	**Equation number**
Kernel	$E_m = 0.047MC^2 - 2.1763MC + 31.779$	0.920	(4.7)
	$\sigma_y = 0.0007MC^2 - 0.0566MC + 1.1847$	0.928	(4.8)
Mesocarp	$E_m = 0.0004MC^2 - 0.0414MC + 1.0153$	0.813	(4.9)
	$\sigma_y = 0.0002MC^2 - 0.00323MC + 0.0926$	0.868	(4.10)
EFB	$E_m = -0.000002MC^2 - 0.0003MC + 0.8289$	0.802	(4.11)
	$\sigma_y = -2\times10^{-7}MC^2 - 0.0001MC + 0.0991$	0.810	(4.12)

4.3.2 SEM analysis

Figure 4.16 shows the surface structure of the fresh and treated oil palm kernels investigated at magnifications of 500x and 1500x. It has clearly shown that oil glands and cell structures are presence on the surface of the kernel which is also observed by Zaidul et al. (2007). On the other hand, the morphology of the mesocarp pulp as shown in Figure 4.17 shows a wrinkled shaped texture which is also observed Ho et al. (2014) and Shinoj et al. (2011). The surface of the treated kernel and mesocarp are found deposited with oil, as a result of microwave treatment. There is no significant critical change in the oil gland and cell structure of the treated kernels under 1500x magnificent (Figure 4.16(b), 4.16(c) and 4.16(d)) as compared to the fresh kernel (Figure 4.16(a)). However, under 500x magnification, shrinkage due to the moisture loss are observed on the surface of the treated kernels (Figure 4.16(b), 4.16(c) and 4.16(d)) and mesocarp (Figure 4.17(b), 4.17(c) and 4.17(d)). The shrinkage has increased the width of cell structure of the kernel and the mesocarp as listed in Table 4.7 and Table 4.8 respectively. The cell structures are larger and further apart when the kernel and the mesocarp are subjected to microwave heating and drying at 200 W than those treated at 100 W. The width of the cell structure of the fresh kernel has increased from 0.145 mm to 0.263 mm and 0.388 mm after microwave pre-treatment at 100 W and 200 W respectively. On the other hand, the width of the cell structure of the fresh mesocarp has increased from 0.128 mm to 0.143 mm and 0.1698 mm after microwave exposure at 100 W and 200 W respectively.

(a)

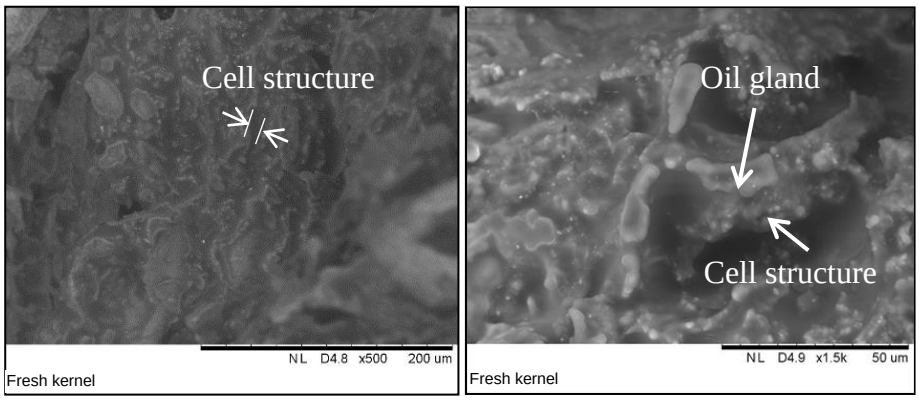

x500 x1500

(b)

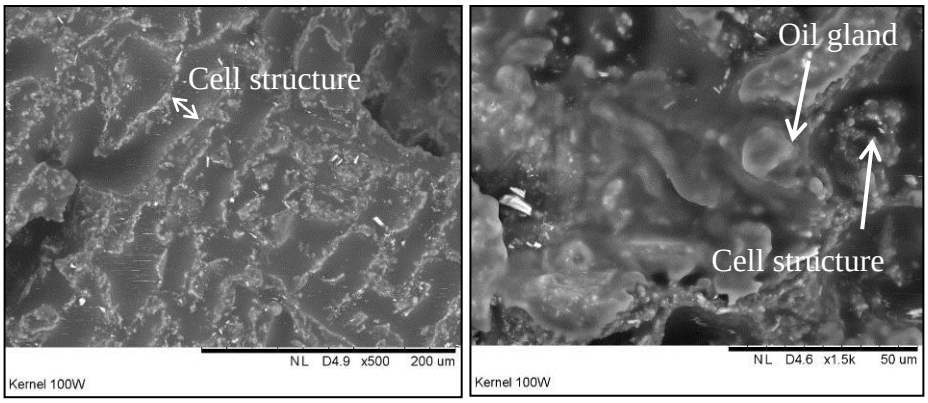

x500 x1500

(c)

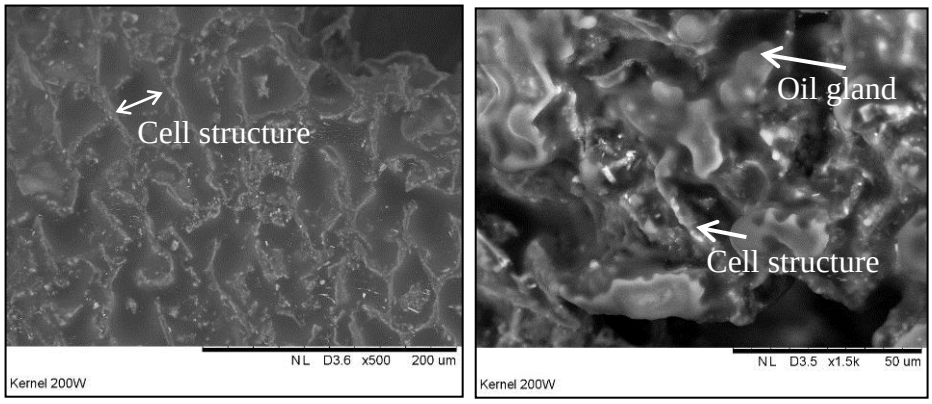

x500 x1500

Figure 4.16: SEM micrographs at 500x and 1500x magnifications of (a) fresh and microwave treated kernel at powers of (b) 100 W and (c) 200 W under 500x and 1500x magnifications.

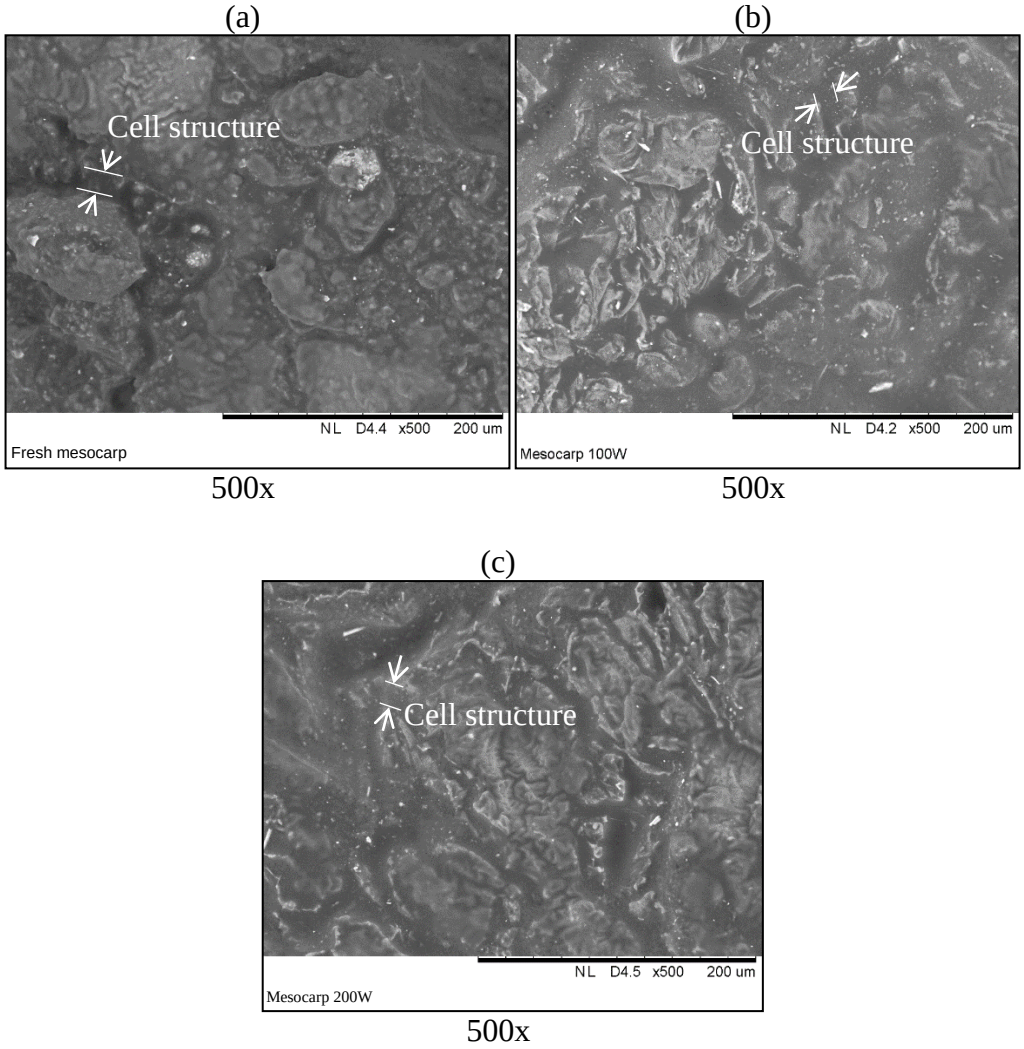

Figure 4.17: SEM micrographs of (a) fresh mesocarp and that subjected to (b) 100 W and (c) 200 W under 500x magnification.

Table 4.7: Width of the cell structure of the fresh and microwave treated kernel.

Sample	**Width of cell structure, w_{cell} (mm)**
Fresh kernel	0.145 $\pm$ 0.001
Treated kernel at 100 W for 2 mins	0.263 $\pm$ 0.001
Treated kernel at 200 W for 2 mins	0.388 $\pm$ 0.001

Table 4.8: Width of the cell structure of the fresh and microwave treated mesocarp.

Sample	**Width of cell structure, w_{cell} (mm)**
Fresh mesocarp	0.128 ± 0.001
Treated mesocarp at 100 W for 2 mins	0.143 ± 0.001
Treated mesocarp at 200 W for 2 mins	0.169 ± 0.001

Figure 4.18 shows the surface structures of the fresh and microwave-treated EFB of under magnifications of 1000x and 5000x. The fresh EFB has a similar surface structure as observed by other researchers (Norul Izani et al., 2013, Nasri et al., 2013, Law et al., 2007, Baharuddin et al., 2013, Shinoj et al., 2011). In the micrographs, pores that are round in shape are found on the fiber strand. The presence of pores on the fresh and treated EFB indicates that it is a fibrous material, as reported by Sabil et al. (2013).

From the micrograph, it is shown that the round-shaped granular starch remains deposited after the microwave treatment, but the size of granular starch is reduced after the treatment (Table 4.9). The size of granular starch is reduced from 0.115 mm to 0.009 mm and 0.006 mm after treated at 100 W and 200 W respectively. A smaller size of the granular starch is desirable as it could facilitate the removal of starch. The removal of starch could then increase the surface area of the fiber for biomass treatment (Zheng et al., 2009, Law et al., 2007). In the current sterilization process, starchs which present in fruit and EFB are removed through hydrolysis, where it has to be broken down by supplying wet steam (Pradeepkumar et al., 2008). Hence, it is believed that microwave treatment could be used to replace the conventional steam sterilization which produces undesired POME.

The fresh EFB has a rough surface with a great number of spiky and round-shaped globular protrusions at the fiber strands. Previous studies identified the globular protrusions as silica bodies (Law et al., 2007). The attached silica bodies in the circular crater are distributed uniformly along the surface of the strand. Silica bodies are observed to remain attach to the surface after the microwave treatment. Silica bodies are undesirable in industrial processes as the silica bodies are inert to most chemicals. In addition, the silica bodies are hard and could only be removed by

alkali treatment or by mechanically or at high temperature (Law et al., 2007). Figure 4.18(c) showed that a small portion of the silica bodies of EFB treated at 200 W is disrupted. Table 4.9 shows the diameters of the silica body and the circular crater before and after the microwave drying process. The drying process has increased the diameter of the circular crater from 0.112 mm to 0.134 mm and 0.171 mm after being exposed to microwave treatment for two minutes. Increase in the diameter of the circular crater could facilitates the removal of silica bodies from the crater and hence resulted in a better fiber-matrix interfacial adhesion of the EFB for further composite fabrication. Figure 4.18(b) and 4.18(c) suggested that microwave treatment has the potential to remove and disrupt the silica bodies. In spite of the reduction of the circular crater, the diameter of the silica body remains constant after being exposed to microwave treatment.

Table 4.9: Diameter of the silica bodies, circular crater and granular starch in fresh and microwave treated EFB

Sample	**Diameter of circular crater, d_{cater} (mm)**	**Diameter of the silica body in the circular crater, d_{silica} (mm)**	**Diameter of granular starch, d_{starch} (mm)**
Fresh EFB	0.112 $\pm$ 0.001	0.088 $\pm$ 0.001	0.115 $\pm$ 0.001
Treated EFB at 100 W for 2 mins	0.134 $\pm$ 0.001	0.087 $\pm$ 0.001	0.009 $\pm$ 0.001
Treated EFB at 200 W for 2 mins	0.171 $\pm$ 0.001	0.089 $\pm$ 0.001	0.006 $\pm$ 0.001

(a)

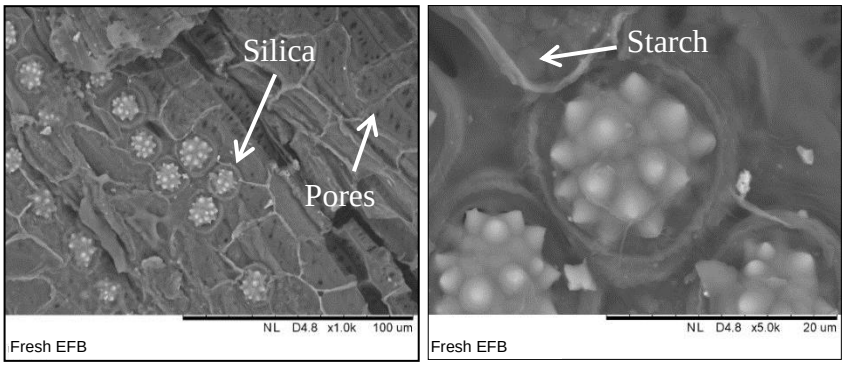

1000x 5000x

(b)

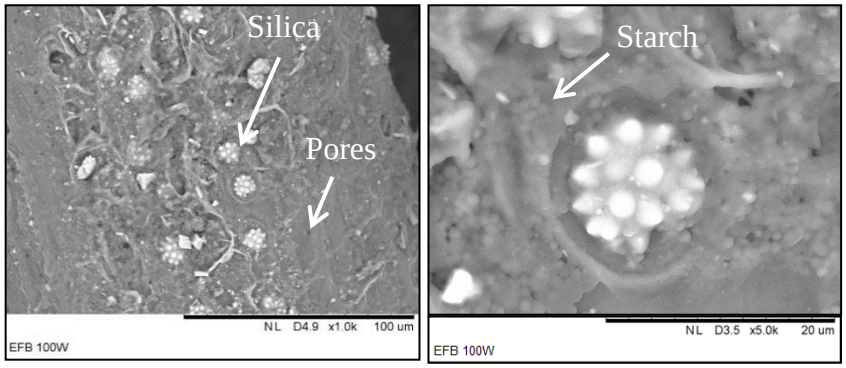

1000x 5000x

(c)

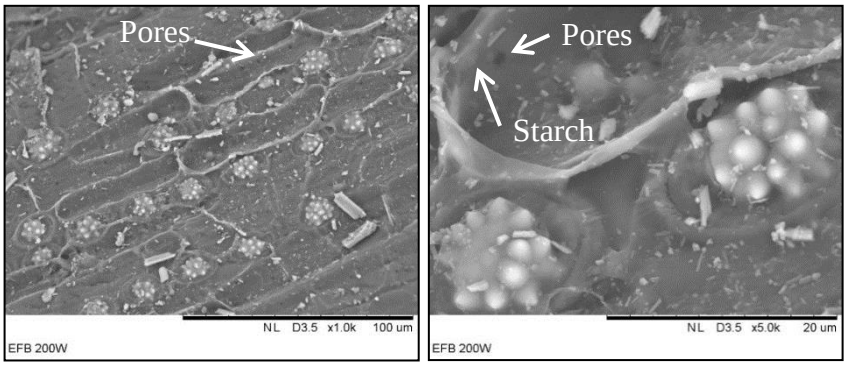

1000x 5000x

Figure 4.18: SEM micrographs at x1000 and x5000 magnifications of (a) fresh, microwave treated EFB at power level of (b) 100 W and (c) 200 W under 1000x and 5000x magnifications.

From this study, SEM micrographs confirm that visible changes have been found on the surface of EFB after the microwave drying process but there was no significant effect on the kernel and mesocarp. In comparison to the fresh samples, insignificant change of the physical structure of the dried kernel and mesocarp has ensured the minimal deterioration (Kong and Singh, 2011). The oil glands deposit on the surface of treated kernels and mesocarps are not influenced by the microwave treatment. However, the microwave treatment on EFB has reduced the size of granular starch, increase the crater size which surrounded the silica bodies and disrupted the silica bodies, and these are beneficial for the further EFB biomass treatment. Effects of microwave power on the drying process are investigated on the EFB, mesocarp and kernel.

4.4 Summary

The microwave heating and drying experiments are carried out and the experimental results such as temperature profiles and drying curves of the kernel, mesocarp and EFB at 100 W, 180 W and 300 W are obtained. The experimental works quantify the moisture content and the TGA confirms thermal degradation and mass losses of kernel, mesocarp and EFB at various stages. The experiment shows that only moisture evaporation occurs during microwave treatment because of the temperature of samples are below the decomposition temperature as identified in thermogravimetric analysis. The removal of moisture content leads to the internal burning and volume change of the kernel, the mesocarp and the EFB, which might alter its surface structure and degrade its quality. However, the microstructure analysis has verified that insignificant disruption has occurred on the surface of the treated mesocarp, kernel and EFB. Furthermore, the characterization such as thermal conductivity and permittivity of the kernel, mesocarp and EFB are experimentally determined for the use in the simulation studies in Chapter 6 and 7.

CHAPTER 5
MODELING METHODOLOGY

This chapter introduces the governing equations and modeling procedure for microwave heating and drying of fresh fruit bunches (FFB). The equations are to predict the electric field intensity, temperature and moisture distributions within the sample. The computational domain, mesh generation and the numerical procedures of the simulation will be presented in this chapter as well.

5.1 Introduction

The electromagnetic equations for a general computational domain cannot be solved by analytical methods. Therefore, the equations have to be solved using numerical methods. In this study, COMSOL, based on finite element method is used to develop a coupled electromagnetics and heat-mass transfer model. The specific objectives of this study are to:

i. Develop a coupled electromagnetic and heat-mass transfer model for the microwave heating for the individual kernel, mesocarp and EFB.
ii. Validate the developed model with experimental data.
iii. Develop a microwave heating model of FFB (consists of kernel, mesocarp and EFB)

5.2 Assumptions and limitations

Several assumptions have been made in developing the current mathematical model. These assumptions are follows:

i. The frequency of microwave used in this study is 2.45 GHz.
ii. Airflow inside the oven cavity is not modelled.
iii. Air temperature in the oven cavity is not influenced by the microwave heating. Therefore, the air temperature in the oven cavity remains constant.
iv. Evaporation only occurs on the surface of the heated samples.
v. The heat and mass transfer coefficients at the surface are constant.

vi. The temperature and moisture content are initially uniform throughout the samples.

vii. Only liquid water in the samples is considered in the model.

viii. Diffusion is purely due to concentration gradient and no interaction with other compounds.

ix. The kernel, mesocarp and EFB are assumed to be isotropic in composition.

x. The heating of samples is not affected by the magnetic field strength, i.e. the samples are not magnetic materials.

xi. Shrinkage of the heated kernel, mesocarp and EFB are ignored.

5.3 Computational domain

The geometry of the model was based on the modified domestic microwave oven (ME711K, Samsung). The computational domain is shown in Figure 5.1. The domain includes the cavity (30.8 cm width x 29 cm depth x 18.5 cm height), a rectangular waveguide (10 cm width x 5.7 cm height x 10 cm depth), a conical flask in the middle of the cavity and the sample. The microwave feed port was located at the right wall of the cavity and the sample was positioned in the middle of conical flask. The microwave heating of an ellipsoid-shaped kernel, a rectangular-shaped mesocarp and a cube-shaped EFB were simulated in this study. Two temperature points (as shown in Figure 5.2) and the average moisture content were used to compare the simulation results with the experimental data.

Two cross-sectional planes in the x-y (Figure 5.3) and the x-z (Figure 5.4) directions were used to study the simulation results. Both the planes were set at the center of the samples. As shown in Figure 5.3, the horizontal planes in x–y direction for the kernel, mesocarp and EFB were at z=0.0062 m (denoted as x–y plane 1), z=0.001775 m (denoted as x–y plane 2) and z=0.0049 m (denoted as x–y plane 3) respectively. Figure 5.4 shows the vertical planes in the x-z direction at y=0.145m for the kernel, mesocarp and EFB.

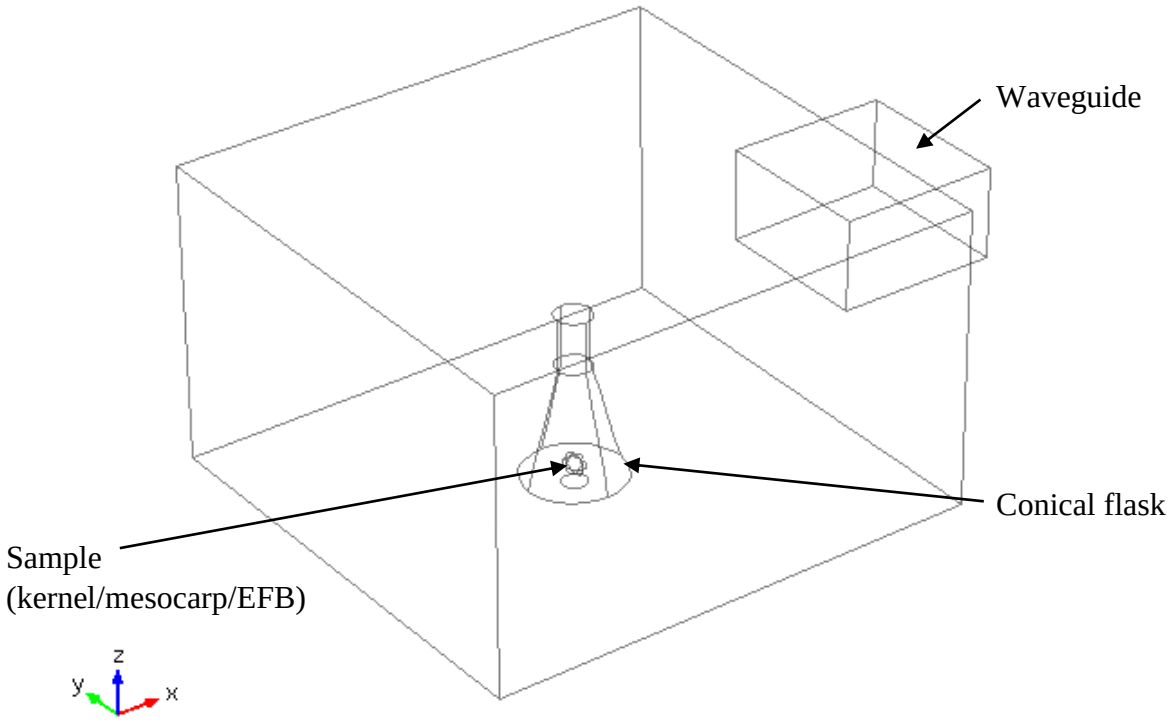

Figure 5.1: Computational domain of model

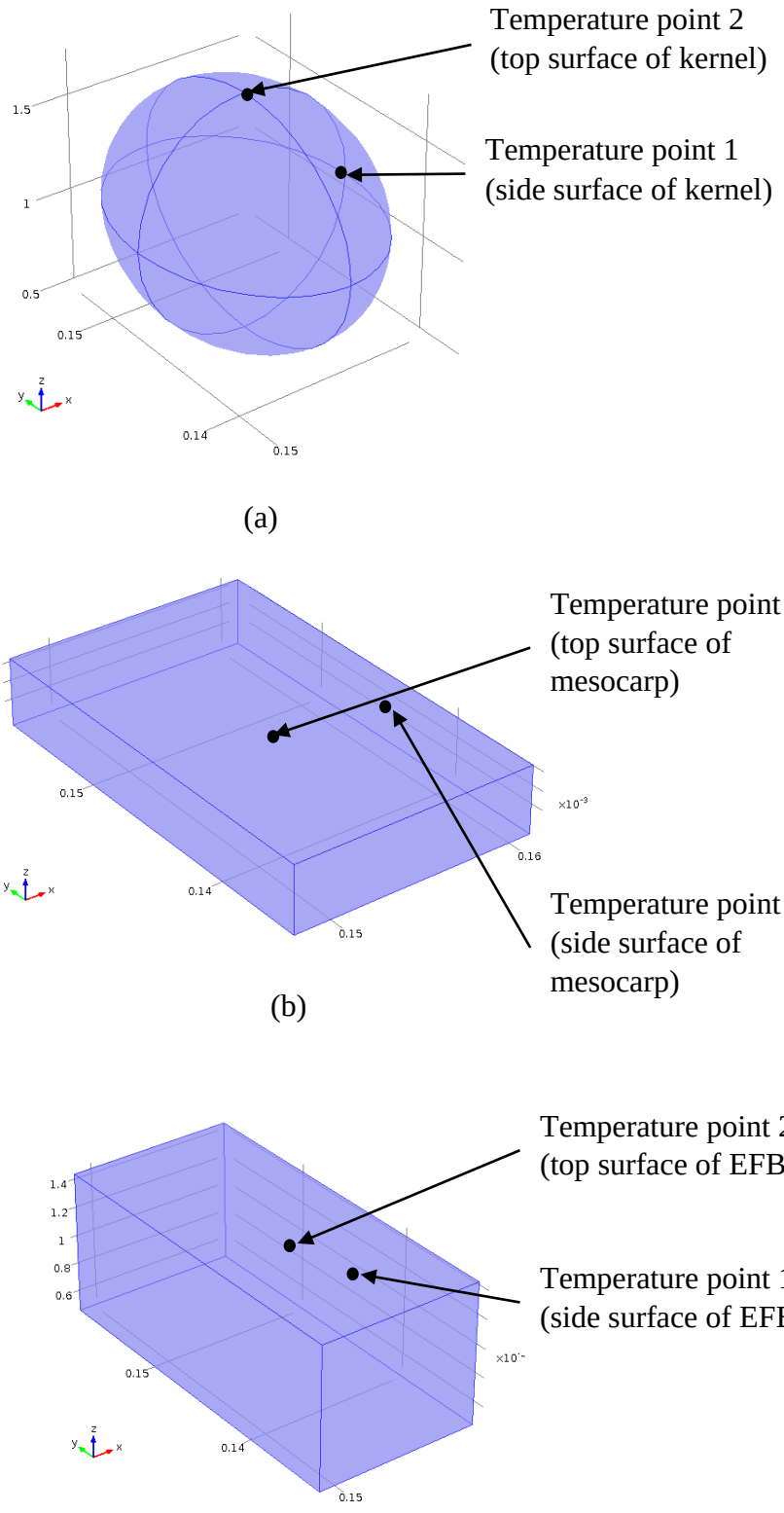

Figure 5.2: Temperature points of (a) kernel, (b) mesocarp and (c) EFB measured in simulation

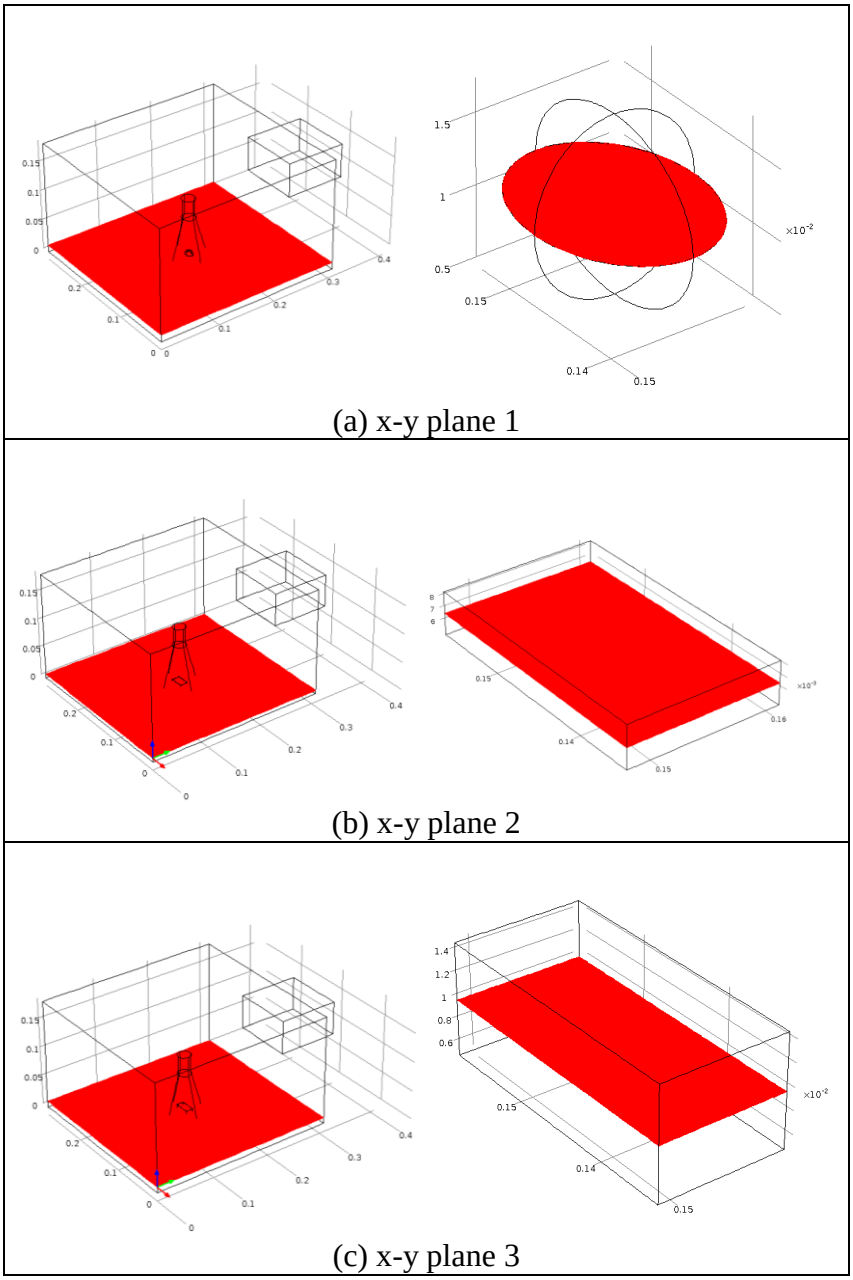

(a) x-y plane 1

(b) x-y plane 2

(c) x-y plane 3

Figure 5.3: Cut plane 1 of the kernel, mesocarp and EFB models. The horizontal plane is set at the center of the samples; the plane taken for (a) kernel at z=0.0062 m (x–y plane 1), (b) mesocarp at z=0.001775 m (x–y plane 2) and (c) EFB at z=0.0049 m (x–y plane 3) from the conical flask surface.

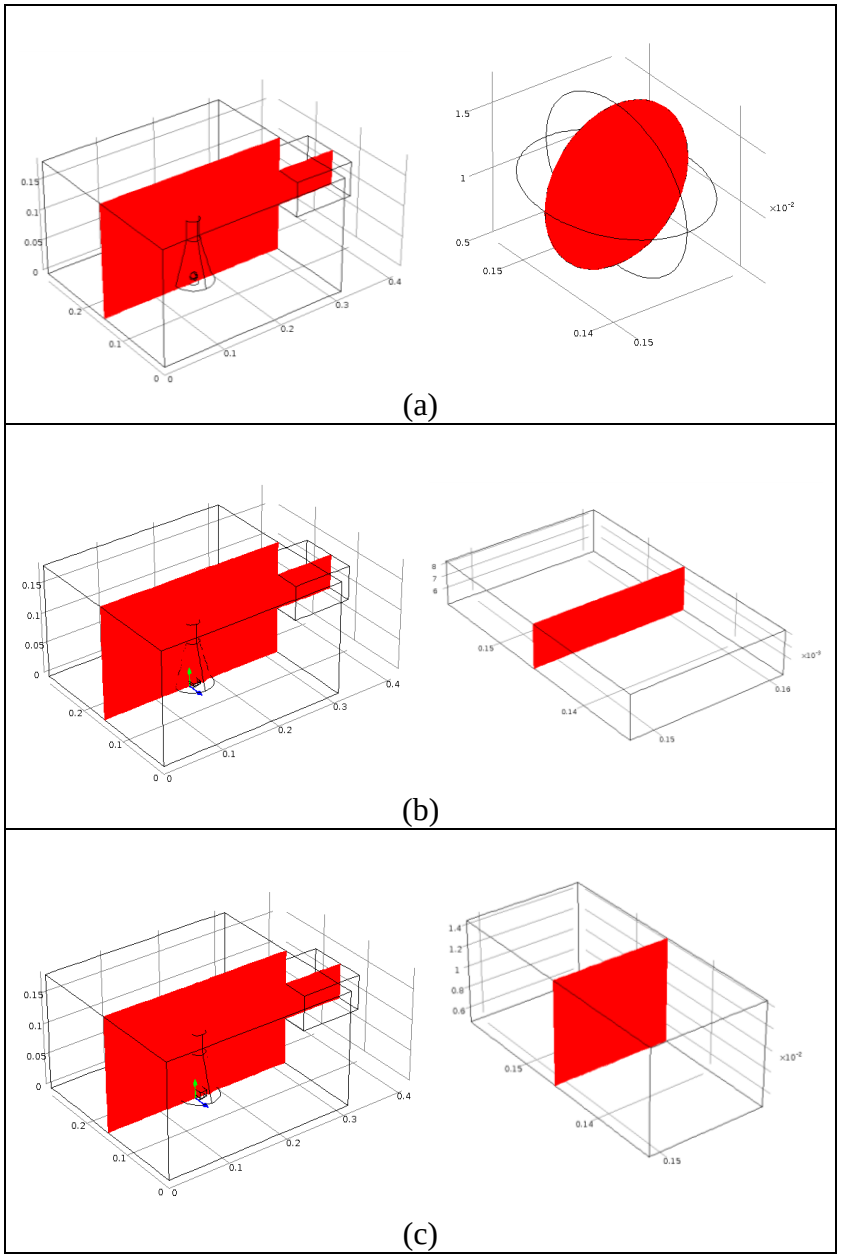

Figure 5.4: Cut plane 2 of the kernel, mesocarp and EFB models. The vertical plane is set at the center of the samples; the plane taken for (a) the kernel, (b) the mesocarp and (c)the EFB at y=0.145 m (x-z plane).

5.4 Governing equations

5.4.1 Electromagnetics field

The electromagnetic field distribution inside the microwave oven was governed by Maxwell equations as given in equations (2.1) to (2.4). The derived governing wave equation (Kumar et al., 2014) from the Maxwell's equation for a rectangular waveguide in frequency domain can be written as:

$$\nabla \cdot (\nabla \times \mathbf{E}) - \frac{\omega^2}{c_o} \mu \varepsilon_r \mathbf{E} = 0 \tag{5.1}$$

where ω is angular wave frequency ($2\pi f$, rad/s) and c_o is the speed of light in free space (3×10^8 m/s). In this study, the domestic oven microwave frequency is used, i.e. f = 2.45 GHz.

When the oil palm kernel, mesocarp and EFB were exposed to microwave in an oven, their interaction with electromagnetic wave results in the volumetric heat generation. The heat generation, $\dot{Q}_{MW}$, was generated when electromagnetic wave travel through a lossy dielectric material. This is given as (Salvi et al., 2011):

$$\dot{Q}_{MW} = \pi f \varepsilon_o \varepsilon_r^{''} |\mathbf{E}|^2 \tag{5.2}$$

The microwave power absorbed in a solid is proportional to the square of the electric field strength, $\mathbf{E}$.

5.4.2 Conservation of moisture content

Moisture diffusion was the main mass transfer mechanism in a solid from the inner body of a sample to the surface and followed by convective and evaporative moisture transfers to the air. The change in species concentration with time was determined by diffusion due to concentration gradient (Fick's diffusional model) and the evaporation reaction due to the non-equilibrium condition between liquid water and water vapor (Gottschalk et al., 2007). Evaporation was assumed to take place on the surface of the material. This lowers the solid's surface temperature (Metaxas and Meredith, 1983). A temperature gradient was formed due to the temperature difference between the surface and interior temperature.

The conservation of moisture concentration, c in the samples is given as (Malafronte et al., 2012):

$$\frac{\partial c}{\partial t} = \nabla \cdot \left(D_{eff} \nabla c \right) \tag{5.3}$$

where D_{eff} is the diffusion coefficient. The moisture concentration, c (mol/m^3) is related to the moisture content, *MC*, by:

$$MC = \frac{cM_{\mathrm{H_2O}}}{\rho} \tag{5.4}$$

where M_{H_2O} is the molecular weight of water vapor (18.02, g/mol) and ρ is the density of the sample (kg/m^3).

5.4.3 Conservation of energy

The heat transfer model included the internal heat generation by microwave, conduction heat transfer in a solid and convection heat transfer from the surface of the sample to the air as well as the evaporative cooling.

The energy balance is given by Fourier's energy balance equation (Malafronte et al., 2012) as follows:

$$\rho C_p \frac{\partial T}{\partial t} = \nabla \cdot \left(k \nabla T \right) + \dot{Q}_{MW} \tag{5.5}$$

where C_p and k are the specific heat capacity (J/(kg·K)) and thermal conductivity (W/(m·K) of the sample.

5.4.4 Initial and boundary conditions

Uniform initial conditions were considered in the sample and oven cavity. The initial conditions of the electric field, sample temperature and moisture content of the kernel, mesocarp and EFB are 0 V/m, 30 °C and the initial moisture content were obtained experimentally as shown in Table 5.1.

Table 5.1: Initial moisture content of kernel, mesocarp and EFB.

Sample	**Initial moisture content, MC_o (% kg/kg d.b.)**
Kernel	25.9
Mesocarp	28.2
EFB	485.49

5.4.4.1 Electromagnetic field

The inlet port was prescribed by the magnitude of microwave power. In this study, cyclic heating was employed. The microwave heating period is 30 s but the 'ON' and 'OFF' durations vary which are depending on the prescribed input power of the modified microwave oven used. The boundary condition for each power level was summarized as follows:

$$P(t)=\begin{cases}100\text{ W} & t\le 10\text{s}\\ 0\text{ W} & 10<t\le 30\text{s}\end{cases} \tag{5.6}$$

$$P(t)=\begin{cases}180\text{ W} & t\le 12\text{s}\\ 0\text{ W} & 12<t\le 30\text{s}\end{cases} \tag{5.7}$$

$$P(t)=\begin{cases}300\text{ W} & t\le 13\text{s}\\ 0\text{ W} & 13<t\le 30\text{s}\end{cases} \tag{5.8}$$

The heating occurs every 30s, i.e. $P(t+30s)=P(t)$.

The impedance boundary condition was used to describe the resistive metal heat losses from the metallic waveguide and cavity walls, which was

$$\frac{1}{\mu}\mathbf{n}\times(\nabla\times\mathbf{E})-\frac{jk_o}{\eta}\mathbf{n}\times(\mathbf{n}\times\mathbf{E})=0 \tag{5.9}$$

where $k_o=\omega\sqrt{\varepsilon_o\mu_o}$, μ_o is the permeability of free spaces (1.257×10^{-6} H/m) and $\eta=\sqrt{\mu/\varepsilon}$. This boundary condition was used at the waveguide and cavity walls where the electric field penetrates only a short distance outside the boundary.

5.4.4.2 Conservation of moisture concentration

The surface of a sample was subjected to the convective mass transfer and evaporation, where the following boundary condition was applied:

$$-\mathbf{n}\cdot\left(D\nabla c\right)=\dot{c}_{evap}\left(c-c_e\right)+h_m\left(c_e-c\right) \tag{5.10}$$

where h_m is the mass transfer coefficient (m/s) and the first term of the right-hand side of the equation (5.10) is the moisture evaporation, $\dot{c}_{evap}=-AT\exp(-E_a/RT)$. A and E_a are frequency factor (1/s) and activation energy (J/mol) of the sample's evaporation process, R is the universal gas constant (8.314 J/(K·mol)) and c_e is the equilibrium moisture concentration. According to Peters et al. (2002) and Caccavale et al. (2016), evaporation is considered as a heterogeneous reaction which the rate constants include effects of pure diffusion and heat-mass transfer. Hence, the evaporation can be explained and represented by Arrhenius equation. Equilibrium moisture content was obtained from the experimental data when the sample reaches equilibrium that no further weight or moisture lost after further drying through microwave irradiation.

The convective mass transfer coefficient was obtained from Equation (5.12) (Malafronte et al., 2012):

$$h_t=\frac{\mathrm{Nu}\times k_{air}}{L} \tag{5.11}$$

$$h_m=\frac{\mathrm{Sh}\times D_{air}}{L} \tag{5.12}$$

where Nu, Sh, k_{air}, D_{air} and L are Nusselt number, Sherwood number, thermal conductivity of air, diffusivity of air (m^2/s) and characteristic length of sample (m) respectively. Thermal conductivity and diffusivity of air based on room temperature were 0.02624 W/m·K and 2.19×10^{-5} m^2/s repectively. The characteristic length is also defined as the longest length of sample. The Nusselt number and Sherwood number are obtained through the following equations:

$$\mathrm{Nu}=2+0.552Re^{0.53}Pr^{1/3} \tag{5.13}$$

$$\mathrm{Sh}=2+0.552Re^{0.53}Sc^{1/3} \tag{5.14}$$

where Prandlt number, Pr, and Schmidt number, Sc, are based on room temperature are 0.713 and 0.61, respectively. By solving the equations, the estimated mass transfer coefficient of kernel, mesocarp and EFB is listed in Table 5.2.

Table 5.2: Mass transfer coefficient of the kernel, mesocarp and EFB.

Sample	**Mass transfer coefficient, h_m (m/s)**
Kernel	4.24×10^{-3}
Mesocarp	4.06×10^{-3}
EFB	2.38×10^{-2}

An Arrhenius type relationship was used to model the effective moisture diffusivity, D_{eff}, of the kernel, mesocarp and EFB (Gómez-de la Cruz et al., 2015):

$$D_{eff} = D_0 \exp\left(-E_d / RT\right) \tag{5.15}$$

where D_o is the pre-exponential factor (m^2/s) and E_d is the activation energy for moisture diffusivity (J/mol). In this model, effective moisture diffusivity was dependent on the temperature, where moisture diffusivity increased with an increase of sample's temperature.

No flux boundary condition was applied between the contact point of the sample's surface and conical flask:

$$\mathbf{n}\cdot\left(D\nabla c\right) = 0 \tag{5.16}$$

5.4.4.3 Conservation of energy

In this study, heat loss occurred at the surface of sample when the heat exchanged with surrounding air by convection and radiation. Thus,

$$-\mathbf{n}\cdot k\nabla T = h_t\left(T_S - T\right) + \dot{Q}_{rad} + \dot{Q}_{evap} \tag{5.17}$$

where surface convective heat transfer coefficient, h_t was assumed to be 5W/(m^2·K) for kernel and mesocarp which was often used for natural convective heat transfer in a typical microwave oven (Verboven et al., 2003). On the other hand, the convective heat transfer coefficient of EFB was assumed to be 30 W/(m^2·K) which was used for fibrous biological material (Zhang and Datta, 2004, Yang and Gunasekaran, 2004, Rakesh et al., 2011, Kumar et al., 2014).

The heat loss due to radiation, $\dot{Q}_{rad}$, was given by:

$$\dot{Q}_{rad} = \gamma_T \sigma_T \left(T_S^4 - T^4 \right) \tag{5.18}$$

where γ_T is the emissivity of the samples which is assumed to be 0.8 in the simulation. σ_T is the Stefan-Boltzmann constant (5.67×10^{-8} W m/K^4) and T_s is the ambient and sample temperatures.

On the other hand, the evaporative moisture cooling, $\dot{Q}_{evap}$, was given by:

$$\dot{Q}_{evap} = \dot{c}_{evap} H_{evap} \tag{5.19}$$

where H_{evap} is the enthalpy of evaporation which is represented by:

$$H_{evap} = -0.0469T^2 - 13.493T + 52202 \tag{5.20}$$

5.5 Input parameters

The input parameters for the current study are summarized in Table 5.3.

Table 5.3: Properties of oil palm kernel, mesocarp and EFB

Parameter	**Value**		
	Kernel	**Mesocarp**	**EFB**
Dielectric constant, $\varepsilon_r^{'}$	0.1621 MC +2.692 (refer to section 4.1.1)	0.0776 MC +3.473 (refer to section 4.1.1)	0.0452 MC +1.815 (refer to section 4.1.1)
Dielectric loss factor, $\varepsilon_r^{"}$	0.0502 MC +0.241 (refer to section 4.1.1)	0.0358 MC +0.526 (refer to section 4.1.1)	0.0211 MC +1.4722 (refer to section 4.1.1)
Specific heat capacity, C_p (J/kg K)	4227 (Ismail et al., 2009)	2816 (Hadi et al., 2015)	2832.46 (Nyakuma et al., 2014)
Density, ρ (kg/m^3)	1125 (Raji and Favier, 2004)	995 (Owolarafe et al., 2007)	800 (Ibrahim et al., 2014)
Pre-exponential factor, D_o (m^2/s)	3×10^{-3} (Estimated)	1×10^{-3} (Estimated)	5×10^{-3} (Estimated)
Thermal conductivity, k (W/m K)	0.68 (Koya and Fono-Tamo, 2013)	0.458 (refer to section 4.1.3)	0.028 (refer to section 4.1.3)
Activation energy of sample's evaporation process, E_a (J/mol)	34000 (Estimated)	43000 (Estimated)	41000 (Estimated)
Activation energy of sample's moisture diffusivity, E_d (J/mol)	34000 (Estimated)	36000 (Estimated)	39000 (Estimated)
Frequency factor, A (1/s)	0.0013 (Estimated)	0.005 (Estimated)	0.0023 (Estimated)

5.6 Numerical procedures

The computational domain (Figure 5.1) along with the governing equations was solved using finite element software COMSOL Multiphysics® 5.2 (COMSOL, Burlington, MA). The steps involve in the modeling are outlined in Figure 5.5.

Figure 5.5 shows the flow chart of the simulation. The model consists of two steps. Maxwell equations were solved using direct solver in frequency domain while the energy and mass balance equations were solved in a segregated way in the time domain.

Refer to Section 4.1.2, dielectric properties changed with the moisture content of the sample. As moisture was lost from the sample during a drying process, the dielectric properties of the sample changed. This led to the changes of the source term in the heat transfer equation. Furthermore, the sample's temperature changed the drying reaction rate and the enthalpy of evaporation, which affected the temperature and moisture content estimation in the samples. Therefore, the estimations of temperature distribution and moisture content in the sample require simultaneously solving the electromagnetic, heat transfer and mass transfer equations. Thus, the values of temperature-dependent and moisture-dependent properties were updated using the local temperature and moisture content at the beginning of each time step. The simulation ended when a complete heating time was reached.

In order to obtain a precise result from the model, a sufficient number of iterations have to be allowed. In this study, the modules were solved using multi-frontal massively parallel sparse direct solver (MUMPS) direct solver, which is suitable for both symmetric and unsymmetric matrices (Amestro and Du, 2000). A sampling time step was set to be 1s throughout a complete microwave heating process. The segregated method necessities an output solution with a tolerance limit of 0.001.

The simulation was performed on a Dell Precision T1700 workstation with a 32GB DDR3 RAM running on quad-core Intel Xeon i7-4790 3.60 GHz processor. The model consisted of 305,810 free tetrahedral mesh elements.

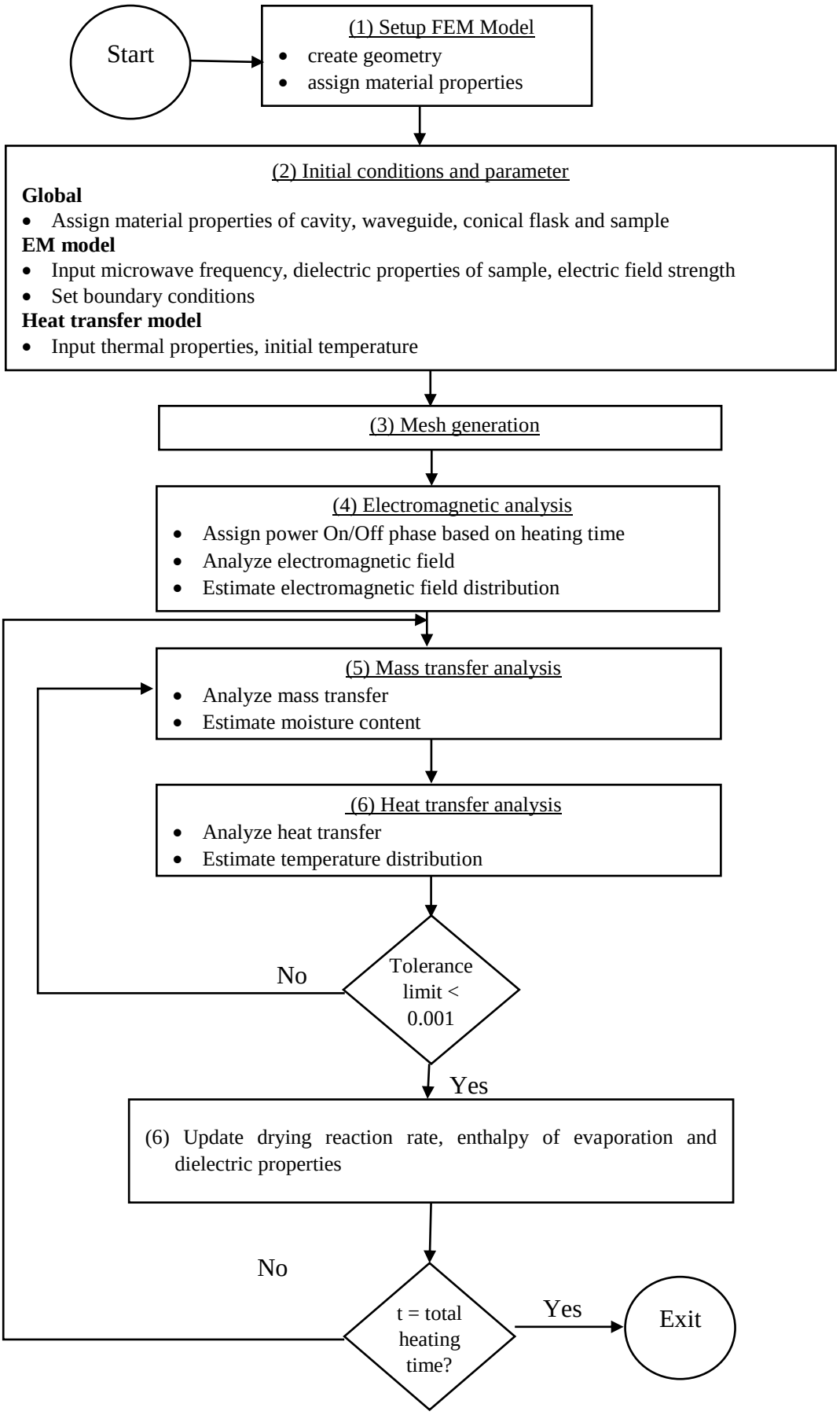

Figure 5.5: Flow chart of simulation steps

5.7 Mesh generation

The accuracy of a simulation increases with smaller mesh sizes. However, this results in large number of elements and a longer computational time. The purpose of this mesh independence study is to obtain an optimum mesh size with an optimum accuracy in the simulation studies. Five element sizes which were categorized as "coarser", "coarse", "normal", "fine" and "finer" were used in this study. Table 5.4 shows the element sizes and total element numbers of the kernel, mesocarp and EFB by using the different mesh options.

Table 5.4: Element size and total element numbers of the kernel, mesocarp and EFB case studies for various mesh options.

Mesh option	**Maximum**	**Total elements**		
	Element size (m)	**Kernel**	**Mesocarp**	**EFB**
Coarser	0.0775	15634	9196	18370
Coarse	0.0612	19090	11651	20543
Normal	0.0408	26997	16796	25742
Fine	0.0326	35741	24468	43909
Finer	0.0224	59271	47793	69584

Figure 5.6 shows the average temperatures and moisture contents of the kernel, mesocarp and EFB at 600 s for different element sizes. The solutions did not vary significantly for element size larger than 0.0326 m thus, "fine" mesh option with a maximum element size of 0.0326 m is selected for the case studies. In order to get an accurate result, the maximum element size of the kernel, mesocarp and EFB samples was further refined to $1/4^{th}$.

The total number of tetrahedral elements used for the kernel, mesocarp and EFB case studies were 233446, 51558 and 147353 elements, respectively while the microwave cavity had total tetrahedral elements of 41226.

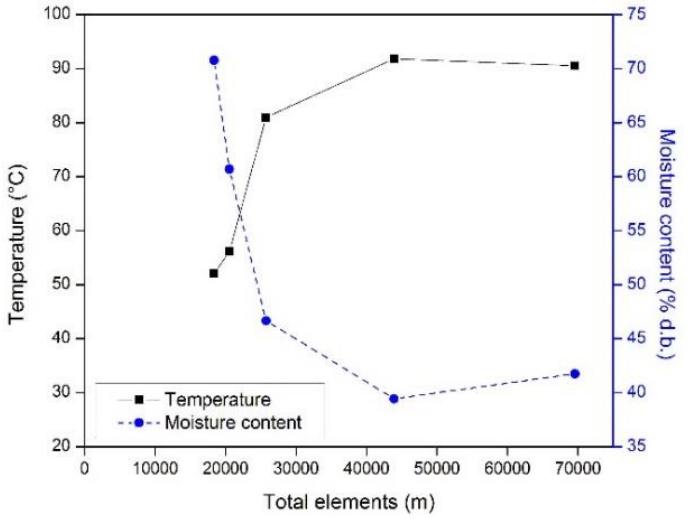

(a)

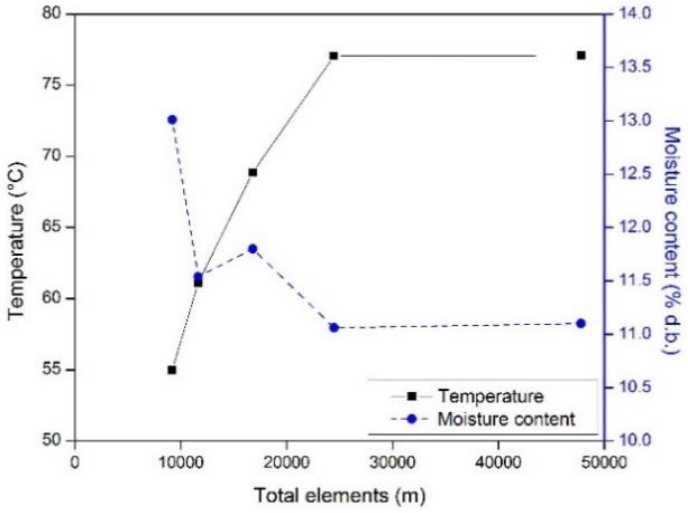

(b)

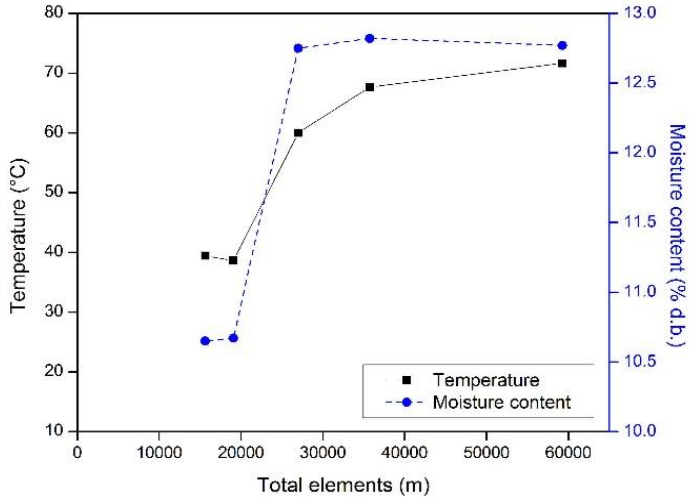

(c)

Figure 5.6: Temperature and moisture content of (a) kernel, (b)mesocarp and (c)EFB at t=600 s, with a total number of elements in the model.

5.8 Summary

This chapter describes a multiphysics model of microwave heating of kernel, mesocarp and EFB. The model solves for Maxwell's electromagnetic wave distribution, energy and moisture content inside a sample is discussed. The solution methodology is presented and grid independence studies are also performed. The optimum mesh sizes and element numbers are recommended.

CHAPTER 6
SIMULATION RESULTS

The previous chapter described the modeling methodology for the microwave heating of individual kernel, mesocarp and EFB. In this chapter, the simulation results are compared with the experimental temperature profiles and drying curves of the afore-mentioned samples. The validated models can be used to further understand the microwave heating process.

6.1 Model validations

Figure 6.1-6.6 show the comparisons between the experimental and simulation results of the heated kernel, mesocarp and EFB samples for microwave powers of 100 W, 180 W and 300 W. The simulation results are compared with experimental obtained temperatures at P1 and P2, as well as the average moisture content, MC. The points, P1 and P2 are located at the side and the top of the sample. The Root Mean Square Error ($RMSE$) was used to compare the simulation and experimental results and is given by:

$$RMSE = \sqrt{\frac{1}{n}\sum_{i=1}^{n}\left(T_{sim} - T_{exp}\right)^2} \tag{6.1}$$

where T_{sim} and $T_{\exp}$ represent the simulated and experimental transient temperatures respectively, and n is the sampling number taken during the microwave heating process. Similarly, the $RMSE$ between the simulated and experimental moisture content were also calculated. A low $RMSE$ indicates a good fit between the generated simulated results and the experimental data.

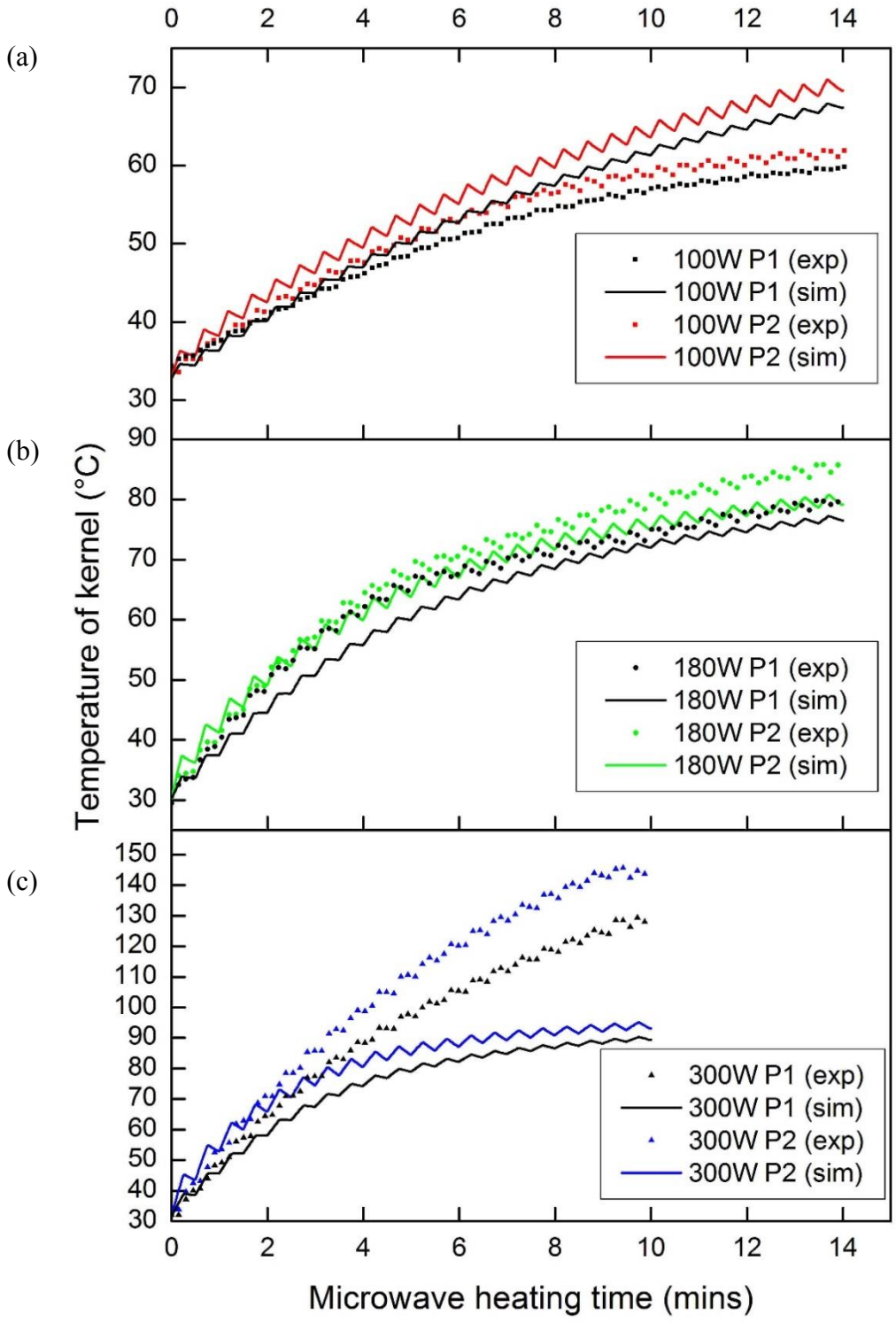

Figure 6.1: Simulated and experimental temperature of kernel subject to microwave power of (a)100 W, (b)180 W and (c)300 W

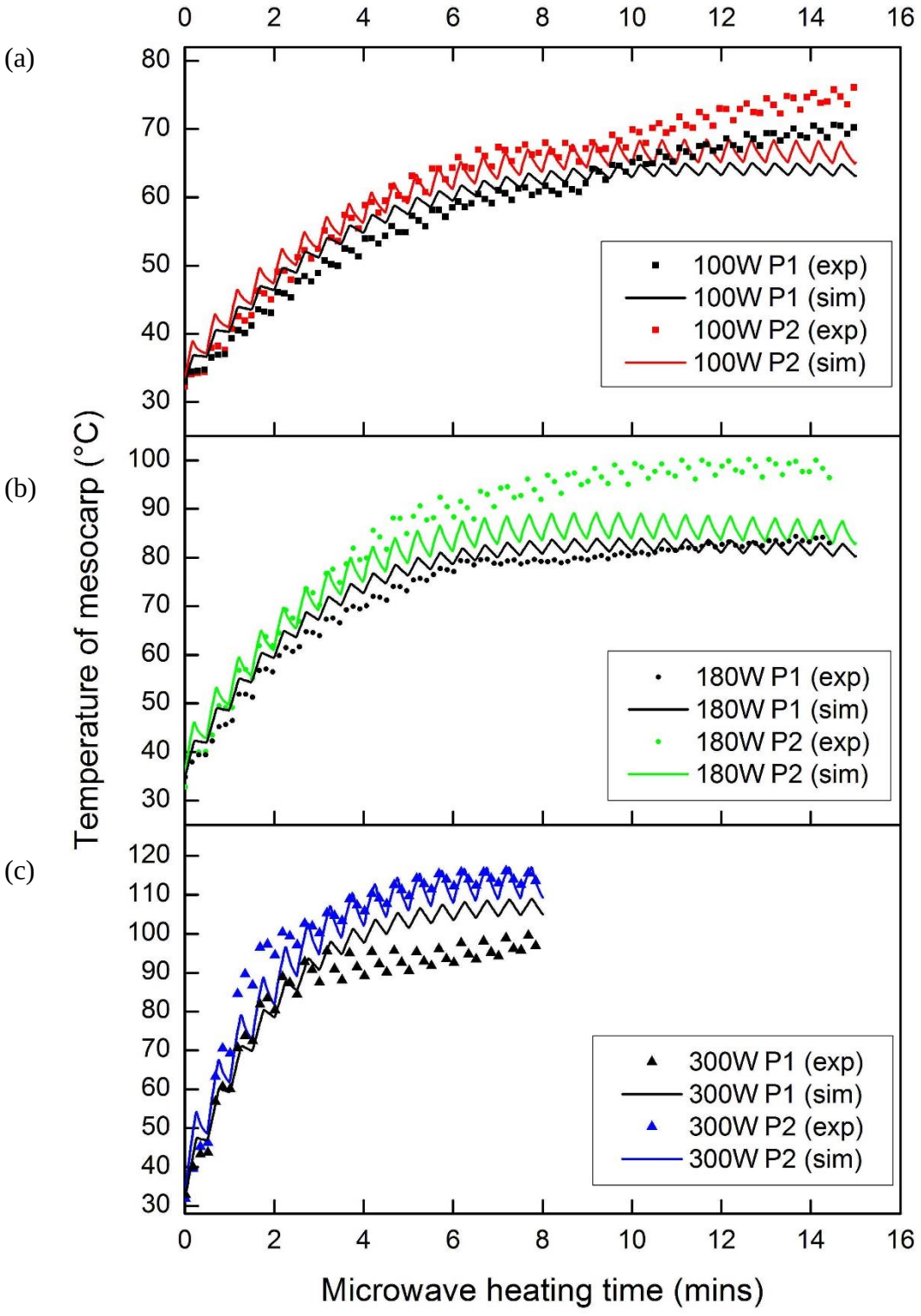

Figure 6.2: Simulated and experimental temperature of mesocarp subject to microwave power of (a)100 W, (b)180 W and (c)300 W

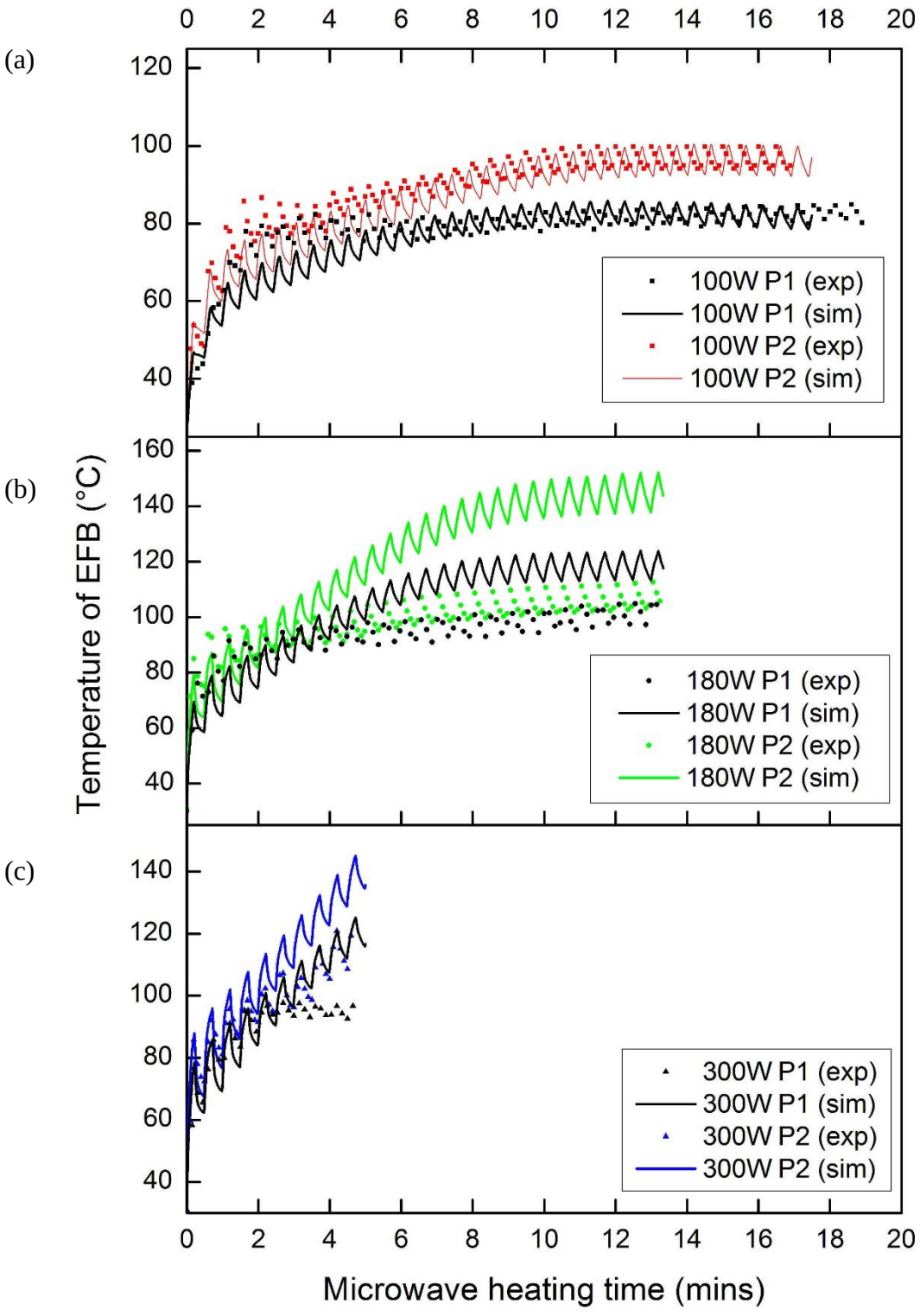

Figure 6.3: Simulated and experimental temperature of EFB subject to microwave power of (a)100 W, (b)180 W and (c)300 W

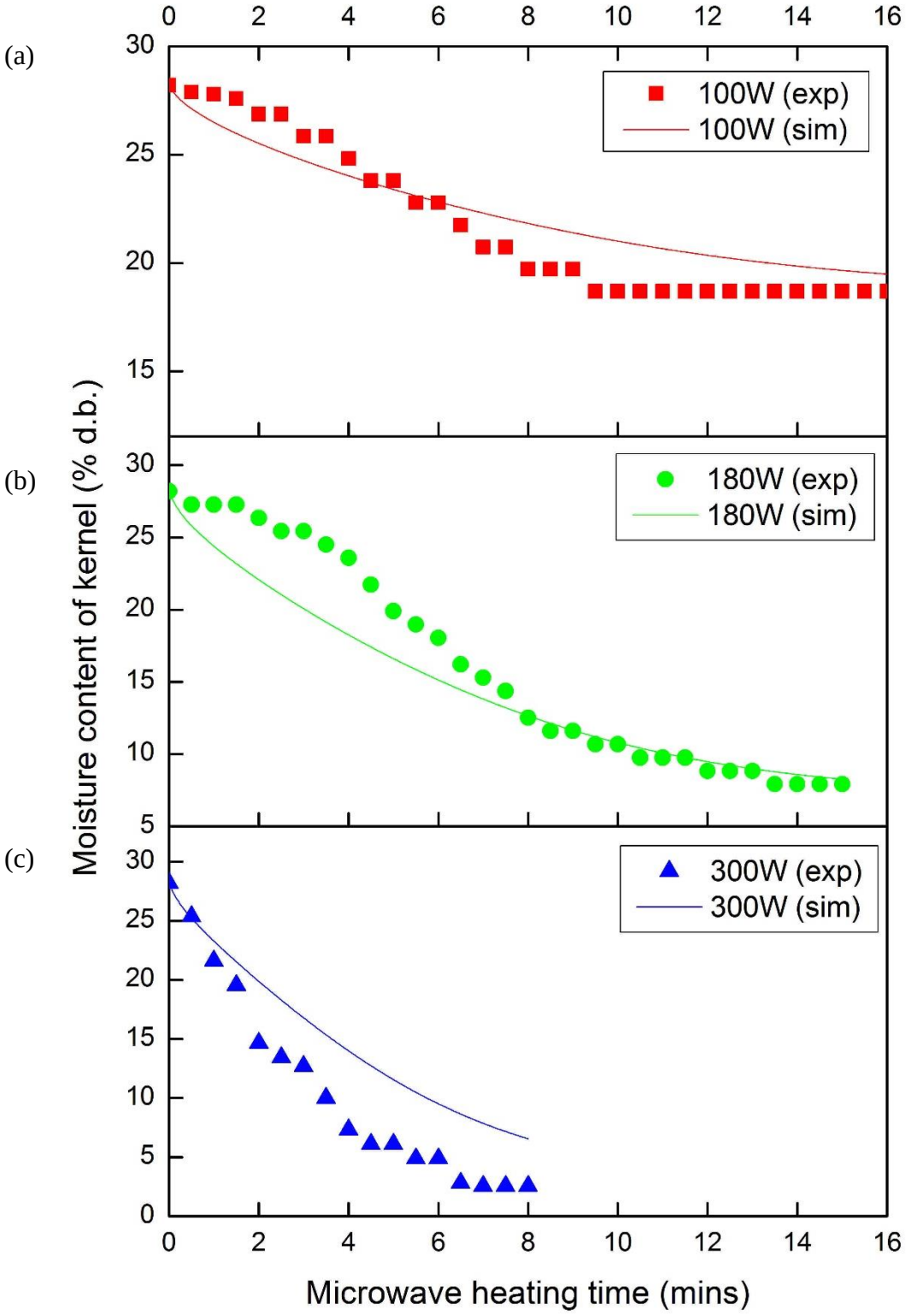

Figure 6.4: Simulated and experimental moisture content of kernel subject to microwave power of (a)100 W, (b)180 W and (c)300 W

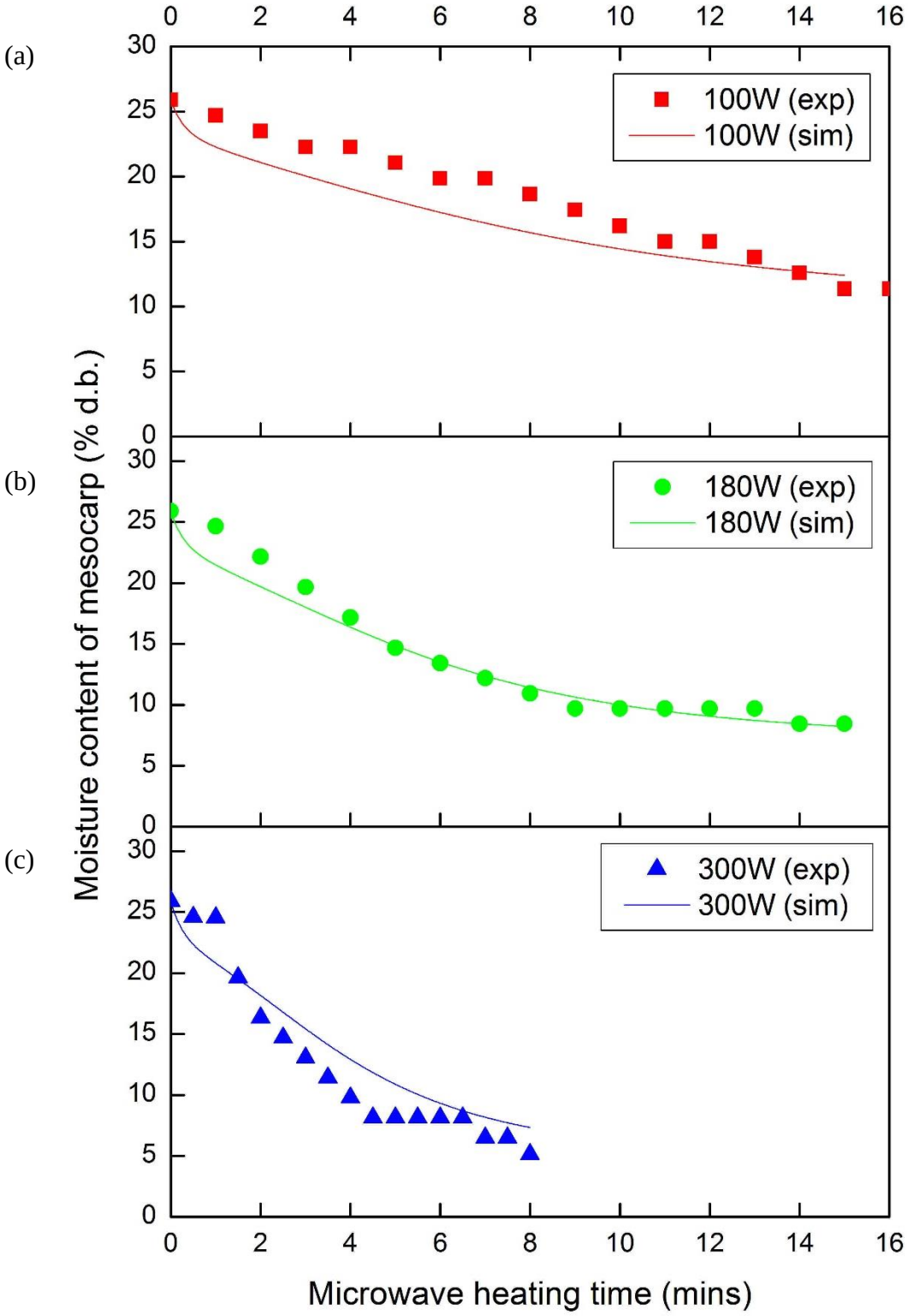

Figure 6.5: Simulated and experimental moisture content of mesocarp subject to microwave power of (a)100 W, (b)180 W and (c)300 W

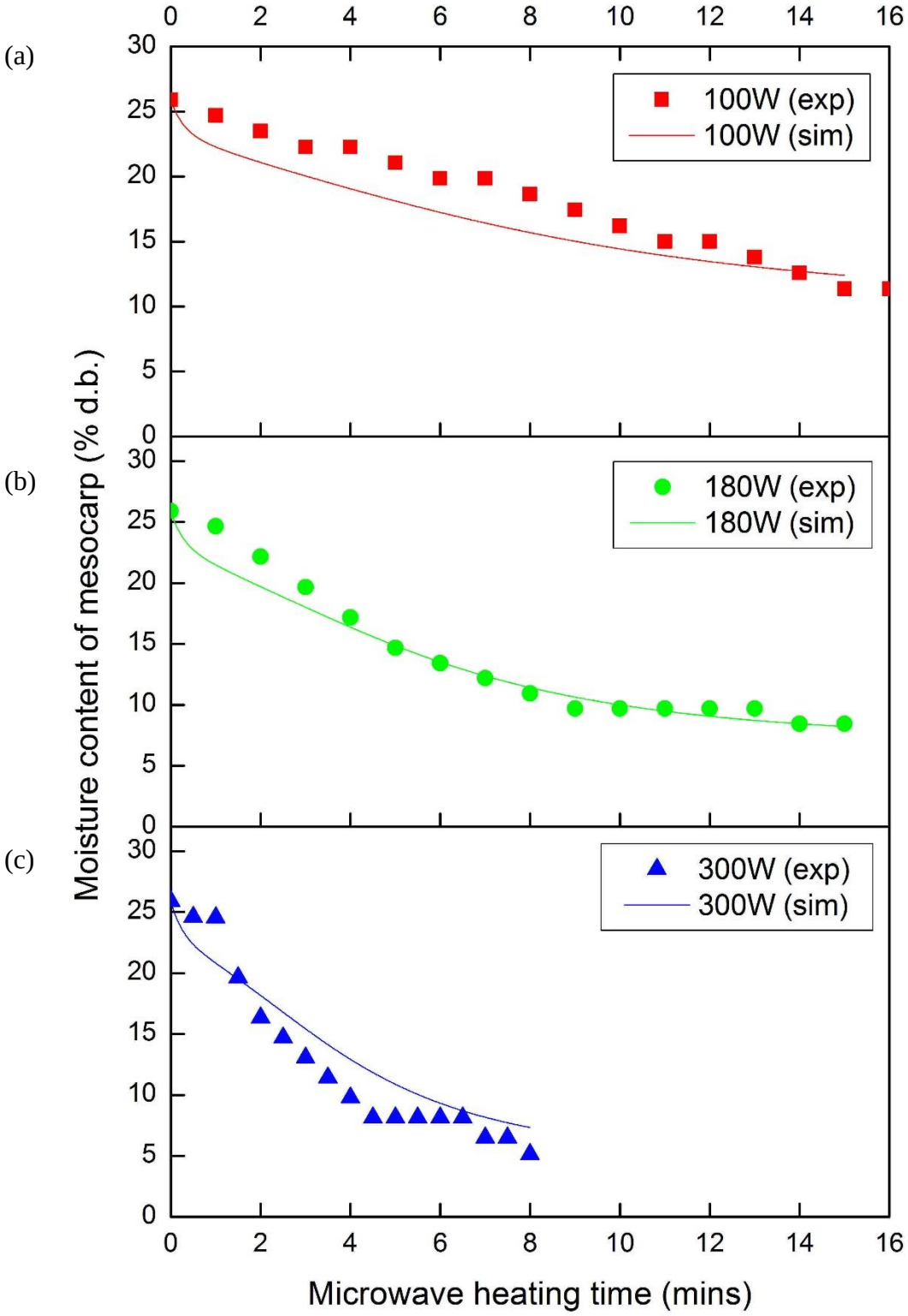

Figure 6.6: Simulated and experimental moisture content of EFB subject to microwave power of (a)100 W, (b)180 W and (c)300 W

The *RMSE* of the sample's temperatures and averaged moisture contents are calculated and are listed in Table 6.1 and 6.2 respectively. The higher *RMSE* values of the kernel at 300 W indicate the poorer kernel temperature correlation which is due to the overheating (burns) inside the kernels. Therefore, the change of the physical structure due to burns in the kernels does not accounted for in the current work.

Table 6.1: Correlation analysis for the simulated and experimental results of samples' temperatures.

Power, P	***RMSE* of temperature**					
	Kernel		**Mesocarp**		**EFB**	
	P1 (°C)	**P2 (°C)**	**P1 (°C)**	**P2 (°C)**	**P1 (°C)**	**P2 (°C)**
100	7.0	6.5	7.9	5.9	5.2	5.3
180	3.7	3.4	2.7	10.5	18.7	14.8
300	22.3	30.5	3.2	4.0	11.5	13.4

Table 6.2: Correlation analysis for the simulated and experimental results of samples' averaged moisture content.

Power, P	***RMSE* of averaged moisture content (%, kg/kg d.b.)**		
	Kernel	**Mesocarp**	**EFB**
100	1.17	2.28	21.7
180	2.59	1.18	21.7
300	7.07	3.86	15.9

Figure 6.1-6.3 show the temperature of the kernel, mesocarp and EFB subjected to microwave powers of 100 W, 180 W and 300 W. Generally, the temperature of the samples increases rapidly until a steady state is reached. The steady state temperature of a sample varies with locations. For instance, location at top surface of the sample (P1) had the higher temperature compared to the location at side of the sample (P2). From the simulation results, the steady state temperatures of the top surfaces of the kernel, mesocarp and EFB at 100 W, 180 W and 300 W microwave power levels are shown in Table 6.3. The kernels attain steady state

temperatures at 23 mins at 79 °C, 14 mins at 81 °C and 8 mins at 92 °C when subjected to microwave powers of 100 W, 180 W and 300 W respectively. The steady state temperature of mesocarp are around 66 °C at 7.5 mins, 86 °C at 6 mins and 115 °C at 3 mins when subjected to microwave power levels of 100 W, 180 W and 300 W, respectively. As for the EFB, the steady state temperature are 95 °C at 8 mins**,** 150 °C at 7 mins and 142 °C at 5 mins when subjected to microwave power levels of 100 W, 180 W and 300 W respectively. Generally, a higher microwave power results in a higher steady state temperature in the samples. Nevertheless, the high temperature is not recommended, particularly for kernels, which the temperature of the kernel is suggested to be kept below 100 °C to prevent the vitamin E of kernel oil from being destroyed (Chow and Ma, 2007).

Among the samples, EFB achieved the highest steady state temperature followed by the mesocarp and the kernel. The varied steady state temperature values between the samples are affected by their thermal and physical properties such as specific heat capacity, thermal conductivity and density. A higher value of the thermal conductivity or a lower value of the specific heat capacity and the density can increase the steady state temperature of the samples. Moreover, this is also caused by the greater microwave absorption of the EFB compared to the cooling mechanisms such as convection, radiation and evaporation that lead to the greater increased temperature within the EFB samples. These mechanisms within the kernel, mesocarp and EFB will be discussed.

Table 6.3: Steady state simulated temperature of the kernel, mesocarp and EFB subjected to 100 W, 180 W and 300 W microwave power levels.

Microwave power, P (W)	**Steady-state Temperature (°C)**					
	Kernel		**Mesocarp**		**EFB**	
	Top	**Side**	**Top**	**Side**	**Top**	**Side**
100	79	76	66	64	95	82
180	81	77	86	84	150	118
300	92	88	115	108	142	124

Furthermore, the results show that lower applied microwave power could attain a lower temperature within the kernel, mesocarp and EFB samples, however, it limits the range of their moisture lost. Figure 6.4-6.6 show the moisture content of the kernel, mesocarp and EFB subjected to microwave powers of 100 W, 180 W and 300 W. The 100 W power could only reduce the moisture content of the kernel, mesocarp and EFB to 16 % d.b., 8 % d.b. and 50 % d.b. respectively. The 180 W power dried the kernel, mesocarp and EFB to 7 % d.b., 9 % d.b. and 30 % d.b. respectively. However, 300 W power could almost fully dry the kernel, mesocarp and EFB samples. A higher sample temperature is desirable to increase the moisture diffusivity rate and to attain a higher moisture lost from the sample's surface (Chen et al, 2016). However, EFBs with a higher moisture content are desirable due to their lower mechanical properties. This promotes the stripping of palm fruits from EFBs.

Furthermore, in practice, kernels have to be dried to 7 % d.b. to ensure its good quality before undergoing further processes such as kernel oil extraction and oil recovery (Ibrahim et al., 1997). Among the three applied microwave powers, only 180 W and 300 W were able to reduce the moisture content of a kernel to below 7 % d.b.. The microwave irradiation takes approximately 13.5 mins to dry a kernel from 28.2 % d.b. to 7 % d.b. at 180 W, and it took only 3 mins at 300 W. In a conventional milling process, drying process required more than 16 hours to lower the moisture content of kernel to the desired moisture content (Ibrahim et al., 1997). By adopting the microwave heating process, the moisture content of kernel has reduced to 7 % d.b. with the reduction of the process time by approximately 98.6-99.6% of the conventional drying process. Although a great reduction in process time was achieved, the impact on oil quality is crucial. The impact will again be discussed in section 8.6.

Among the microwave power levels, 100 W could not reduce the kernel moisture content below 7 % d.b., while the 300 W had burnt the kernel and EFB samples during the experiments. Therefore, the following discussions and the case study presented in Chapter 7 is subject to microwave power level of 180 W.

6.2 Electric field distributions

The kernel, mesocarp and EFB are not magnetic materials, thus, the heating of samples is not affected by strength of the magnetic field but by the electric field (Luan et al., 2016). Therefore, the electric field distributions and the heating patterns within the cavity and samples will be presented next.

Figure 6.7 shows the simulated electric field distribution of the kernel, mesocarp and EFB inside the microwave cavity on the x-y plane, whereas Figure 6.8 shows the distribution on the x-z plane. Arrows in the figures indicate the direction of the electric fields for the 2.45 GHz incident wave. In the figures, the electric field in the microwave cavity appeared to have resonated patterns of high and low electric field intensity in the microwave cavity. The highest and lowest intensity spots are represented as the wave crests and troughs. These crest and trough spots are caused by standing waves. The standing wave is formed due to the interference of electromagnetic waves in the microwave cavity.

In Figure 6.7 and 6.8, the distances between the two wave crests or troughs in x-axis and y-axis are observed to be around 15 cm and 10 cm respectively. The distances vary from the microwave wavelength at 2.45 GHz (12.2 cm). As stated by Chen et al. (2006), the microwave propagation is different from that in free space.

However, according to Hossan and Dutta (2012), the formation of the crests and troughs of the resonance is directly related to the wavelength of the electromagnetic wave. Figure 6.9 shows the electric field distributions in the microwave cavity viewed on x-y plane at the heights of 0.62 cm, 6.2 cm and 14.2 cm. It is observed that the crests and troughs of the standing wave are changed with height. Their locations are identical at heights of 0.62 cm and 14.2 cm, but turned out to be completely opposite at the height of 6.2 cm. Since the wavelength at a microwave frequency of 2.45 GHz is 12 cm, thus the standing waves of 0.62cm and 14.2 cm at z-axis had the similar wave pattern.

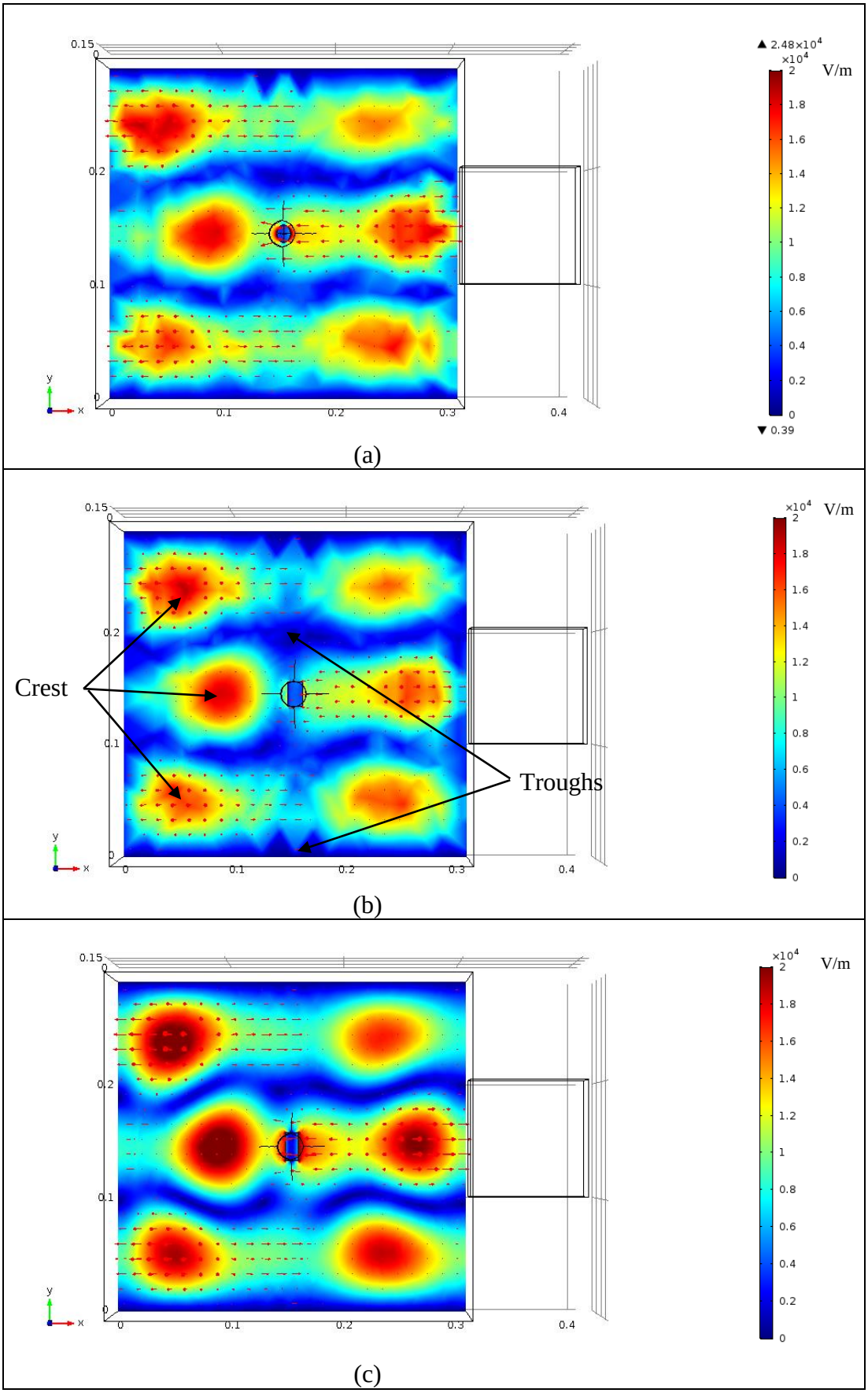

Figure 6.7: Distribution of electric field inside the microwave cavity with (a) kernel, (b) mesocarp and (c) EFB viewed on x-y plane.

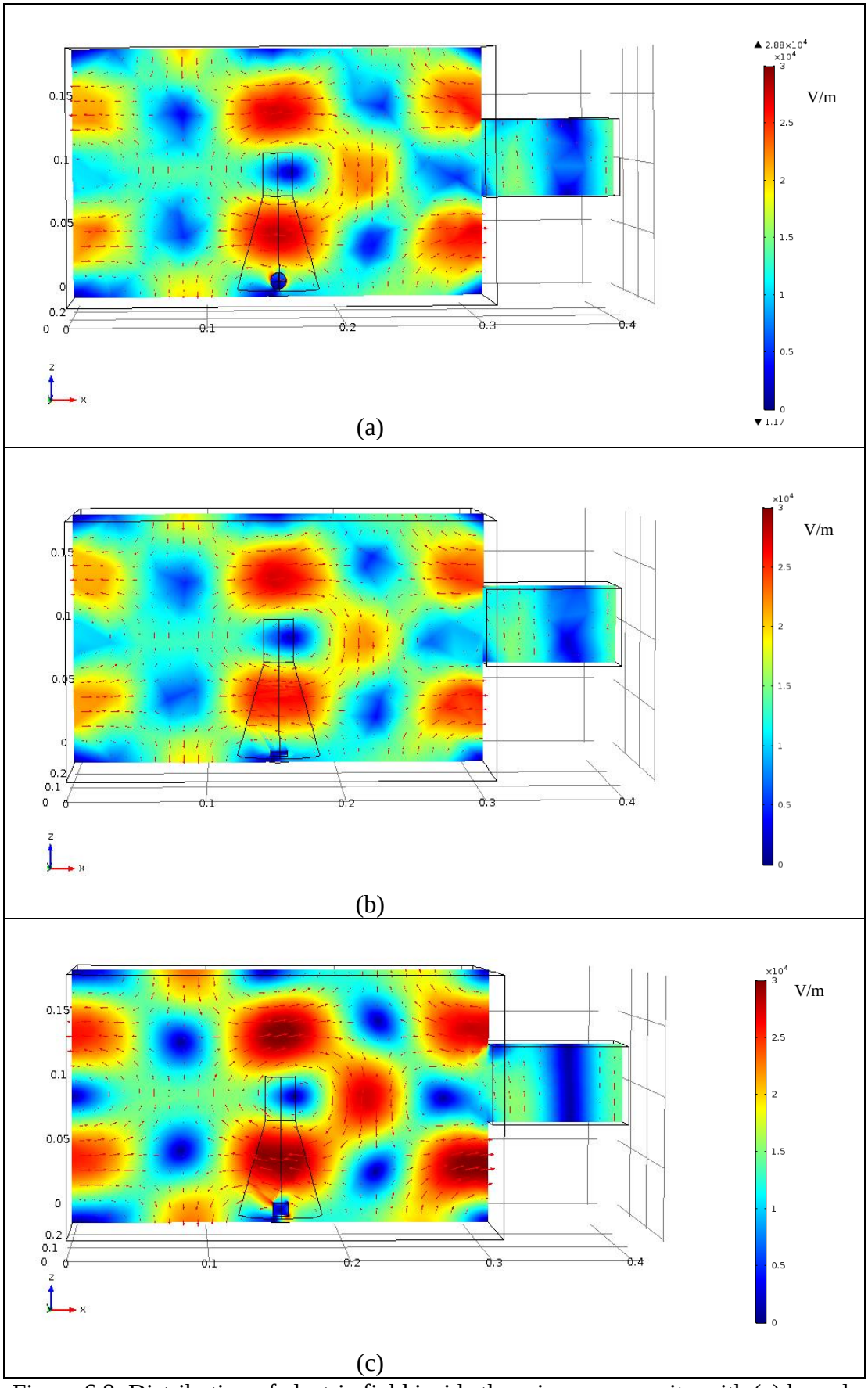

Figure 6.8: Distribution of electric field inside the microwave cavity with (a) kernel, (b) mesocarp and (c) EFB viewed on x-z plane.

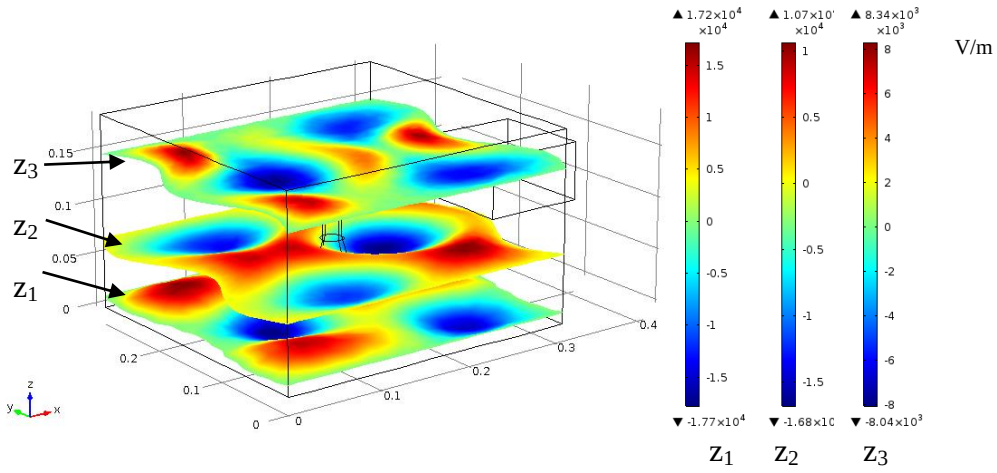

Figure 6.9: Standing waves in the microwave cavity at z_1=6.2mm, z_2=62mm and z_3=142mm.

It can be observed from the Figure 6.7 and 6.8 that the similar electric field distributions occurred in the cavity for the kernel, mesocarp and EFB. Different shape of samples affected the electromagnetic distribution in the cavity. However, the samples are very small compared to the cavity's size, hence similar intensity and distribution of electric field inside the cavity are observed for these three cases. Therefore, this is agreed by Hong et al. (2016) who stated that the sample's position did not significantly influenced the electric field distribution. However, changing the sample's position and shape resulted in the variation of electric field distribution in the sample, which leads to different heating pattern in the sample. According to Curet et al. (2008), electric field distribution was required in order to predict the temperature distribution into the product. The authors showed that hotspot was found at the location where the magnitude of electric field was maximal. Figure 6.10-6.12 show the simulated electromagnetic field in the x-y plane and x-z plane at the middle of the heated kernel, mesocarp and EFB at 180 W. During the microwave exposure, electric fields are found interacted in the kernel, mesocarp and EFB, as shown in Figure 6.10(b), 6.11(b) and 6.12(b). The electric field intensity in the samples is strongly influenced by the electric field distribution surround the sample. The electric field intensities of the surrounding air in the microwave cavity can go up to 2.88×10^4 V/m while the electric field intensity in the kernel, the mesocarp and the EFB are 7.28×10^3 V/m, 9.4×10^3 V/m and 1.82×10^4 V/m, respectively. The electric field strength is noticeably different for the kernel, mesocarp and EFB samples. Among the samples, the highest electric field strength is found in the EFB followed by the mesocarp and the kernel.

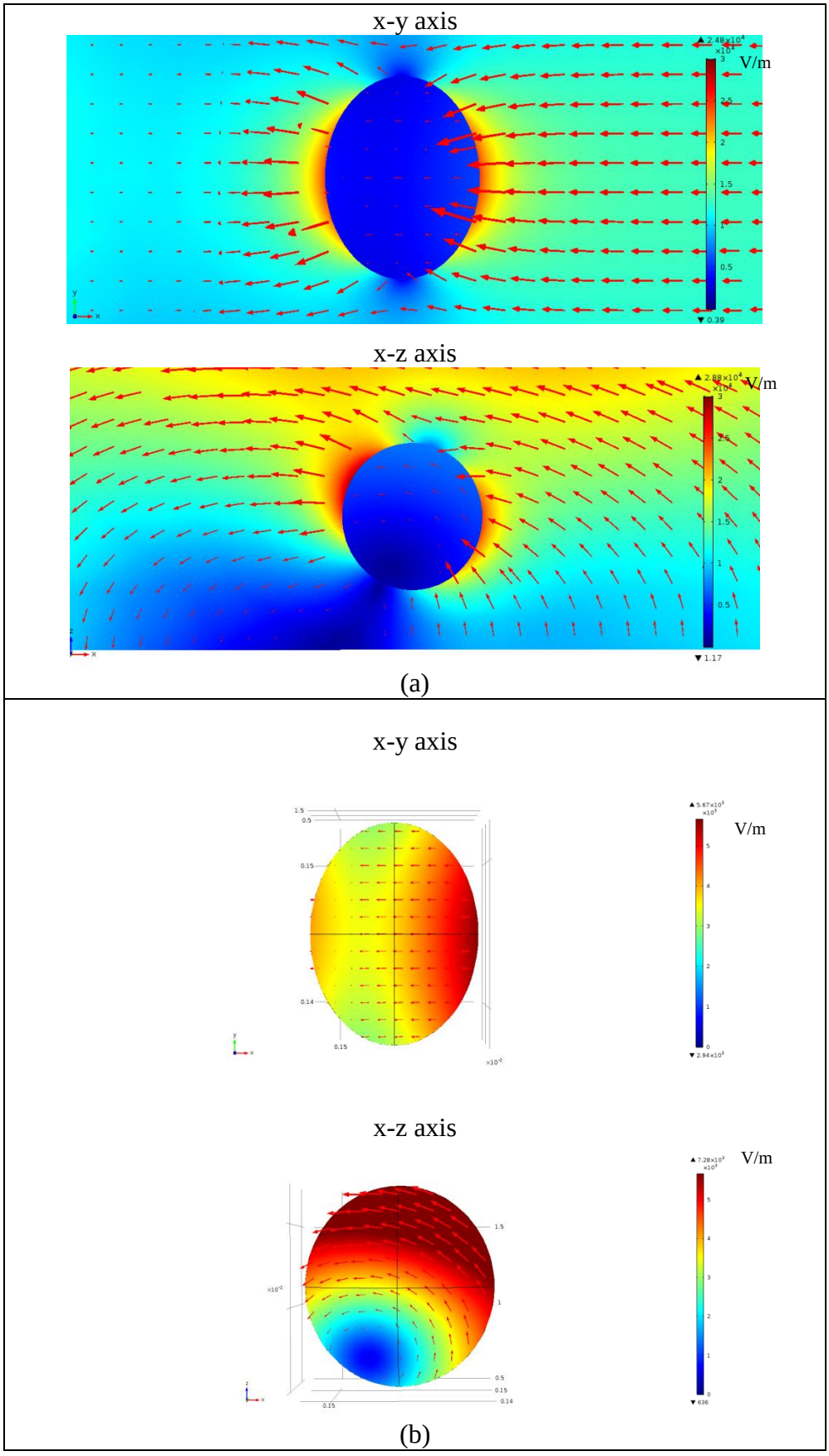

Figure 6.10: The electric field intensity which is (a) around and (b) inside the kernel through the microwave exposure.

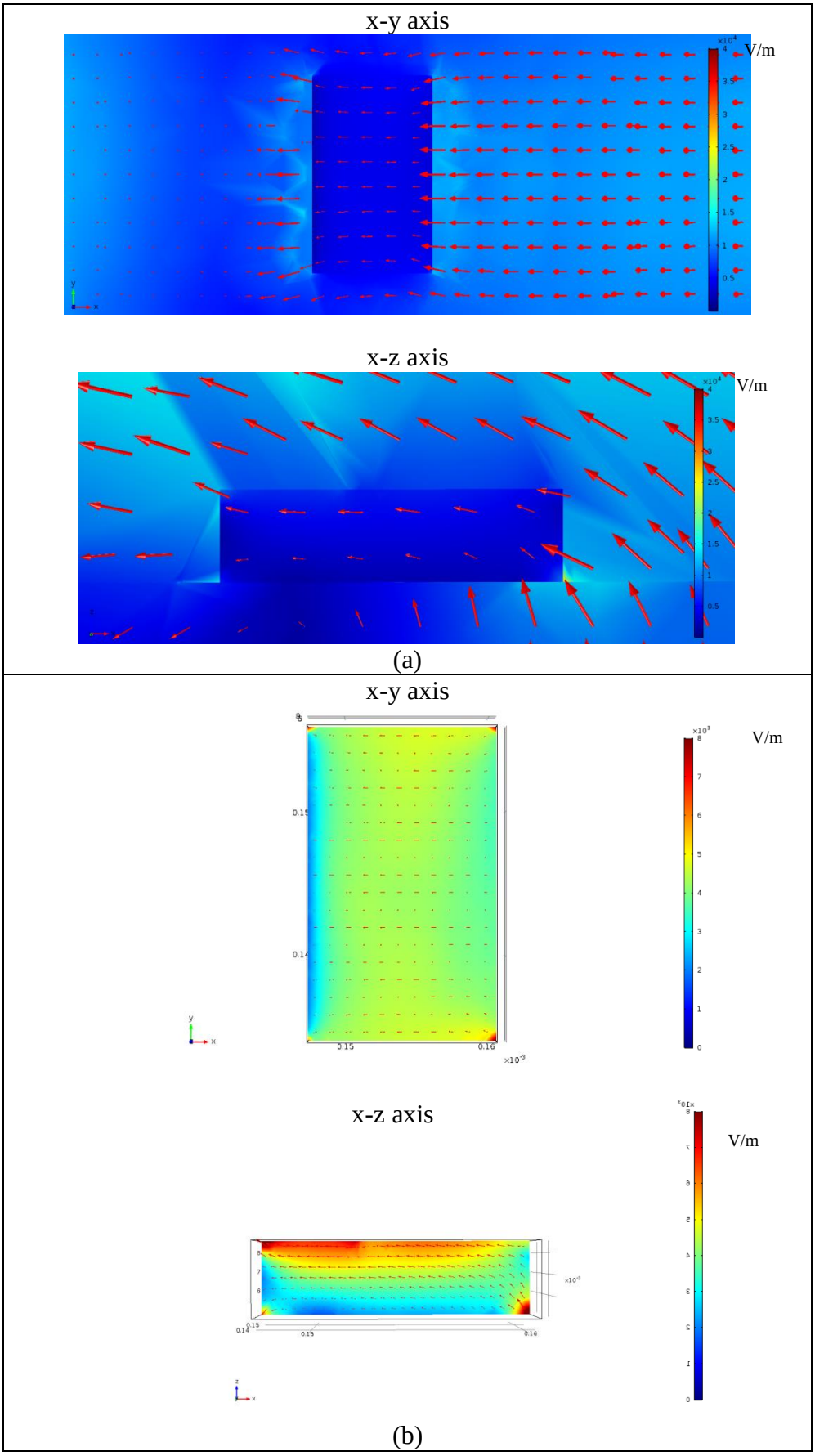

Figure 6.11: The electric field intensity which is (a) around and (b) inside the mesocarp through the microwave exposure.

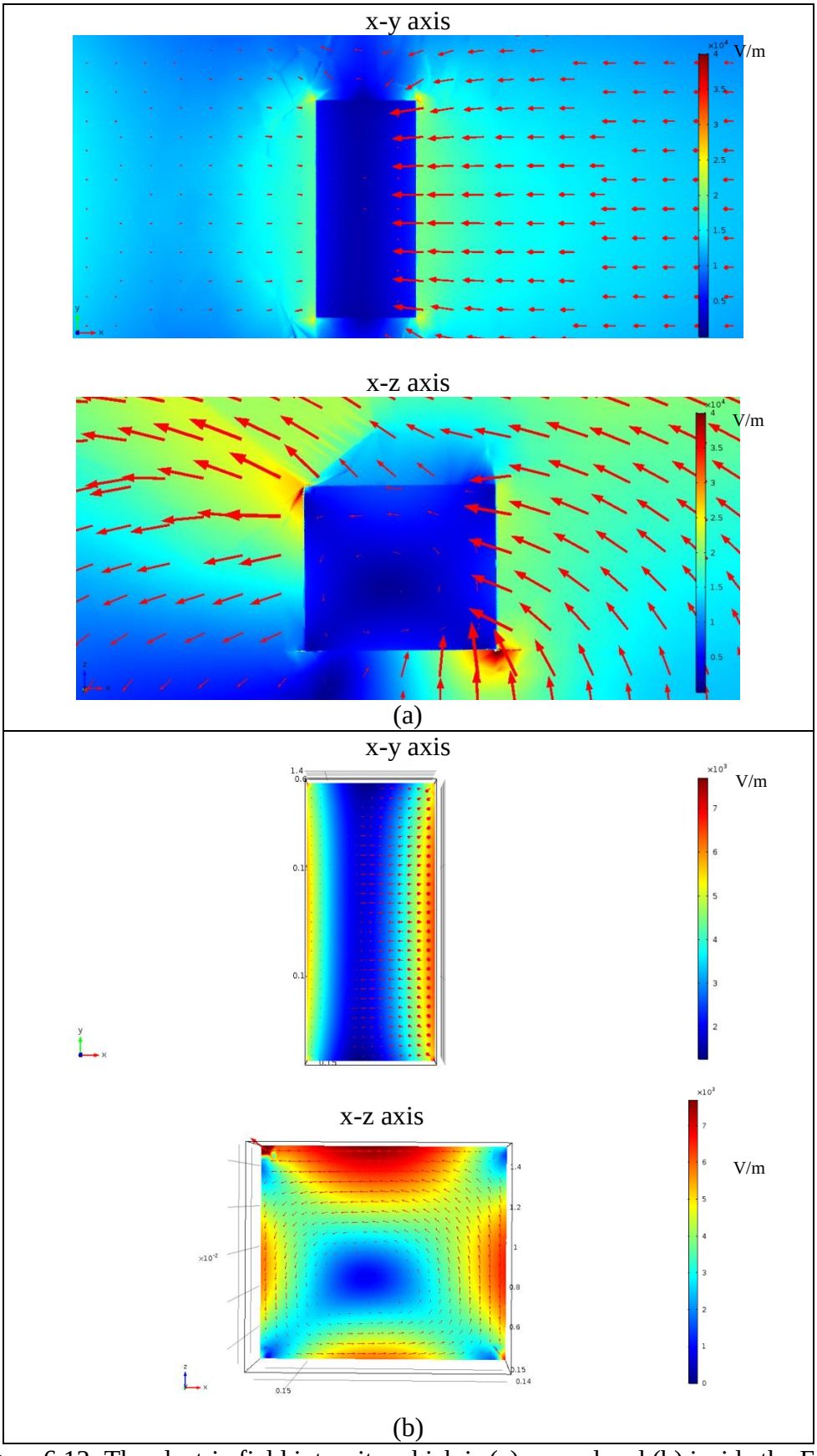

Figure 6.12: The electric field intensity which is (a) around and (b) inside the EFB through the microwave exposure.

This variation can be explained by the greater dielectric properties of EFB compared to the mesocarp and kernel. In addition, the differences in geometry and dimensions of the samples could be one of the factors affecting the electric field strength.

Besides, due to reflections of the incident electromagnetic wave, only part of the wave is transmitted into the sample. The reflection and transmission components at interfaces between the air and top surface of the samples contribute to the standing-wave pattern. In this case, such pattern leads to a greater electric field concentration at those interfaces. As shown in Figure 6.10(b), 6.11(b) and 6.12(b), a high intensity of electric field is observed to surround the top and the elongated sections of the kernel, and at the edges of the mesocarp and EFB. The high electric field intensity is resulted from the great electric field surrounding the mentioned regions.

In addition, the ellipsoid shaped kernel is observed to have more electric field deposition compared to the cubical shaped mesocarp and EFB. This observation is agreed with Birla, Wang, and Tang (2008)'s finding where a more uniform electric field distribution was obtained within the spherical object than the cubed object. Hence, spherical object is expected to heat more evenly compared to cubical objects. Birla, Wang, and Tang (2008) stated that the uniform distribution is due to the propagation of electric wave which enter the rounded edges of the spherical object from one direction, rather than converging from multi-directions from the sharp edges of the rectangular shaped sample. As a result, the electric field intensity at the rounded edges of the kernel is reduced. Therefore, a more uniform electric field intensity is obtained in the ellipsoid shaped kernel than the cubical shaped mesocarp and EFB.

On the other hand, Figure 6.10(b), 6.11(b) and 6.12(b) show that the lowest electric field intensity is occurred in the central regions of the three samples. Gradual increases of electric fields from the center towards the surface of the samples are observed, indicating that there are more energy depositions near the surface. Birla, Wang, and Tang (2008) mentioned that regions with a high intensity of electromagnetic field resulted in high microwave energy absorptions, thus contributed to uneven heating. Therefore, the microwave power absorption, heating and drying patterns associated with the electric field intensity are discussed next.

6.3 Microwave power density generation and power lost

The temperature in the kernel, mesocarp and EFB are increased by the heat generation due to microwave energy, but are also reduced by the surface cooling mechanisms such as convection, radiation and evaporation. Figure 6.13(a)-(c) show the generated microwave power density and power lost per unit are due to convection, radiation and evaporation for kernel, mesocarp and EFB throughout the microwave heating process.

Based on the generated microwave power densities as shown in Figure 6.13, the power absorbed by the samples are obtained by integrating the power absorption density over a sample's volume. The microwave power absorbed by the kernel, mesocarp and EFB are found to be 0.95-2.4 W, 1.05-1.7 W and 5-37 W respectively. The low microwave power density generated by the kernel and mesocarp can be explained by their lower dielectric loss factors compared to the EFB as the power density generation is dependent on the dielectric loss factor of sample. The greater dielectric loss factors of EFB ($\varepsilon_r^{"}$=1.472-11.7) in comparison with the kernel ($\varepsilon_r^{"}$ =0.241-1.656) and mesocarp ($\varepsilon_r^{"}$ =0.526-1.453) results in a higher generated microwave power density of the EFB (refer to Section 4.1.1). As the volume of the mesocarp sample is smaller than that of kernel, it absorbs and dissipates less heat compared to kernel.

Despite the temperature in the samples increases after further microwave heating, lower generated microwave power densities are observed in Figure 6.13. This observation could be explained by the changes of dielectric loss factor of the samples. In this work, the dielectric loss factors of the kernel, mesocarp and EFB are a function of moisture content. The dielectric loss factor decreases with the reduction in moisture content and thus, lesser microwave power can be absorbed by the dried samples.

(a)

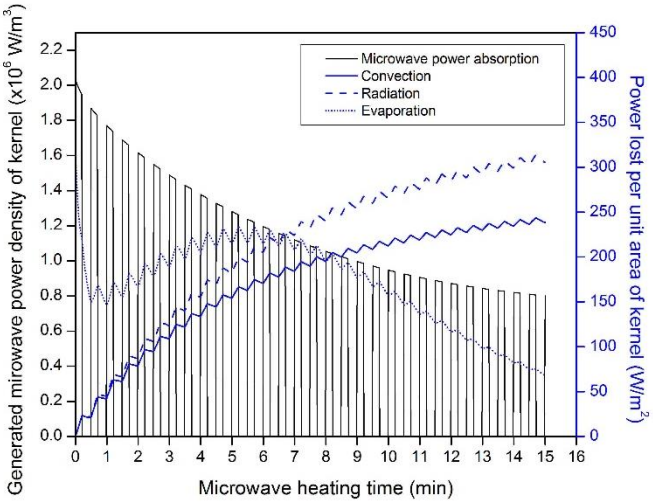

(b)

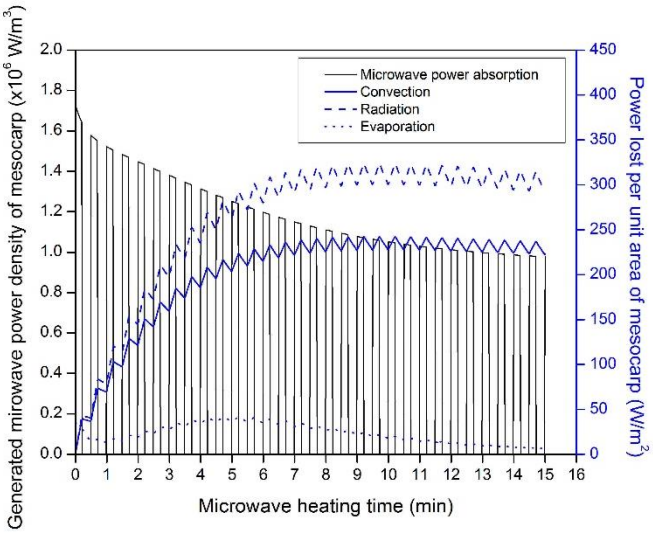

(c)

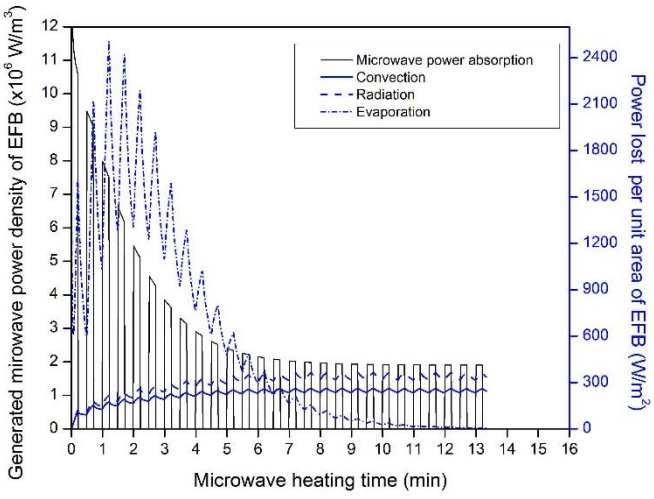

Figure 6.13: Generated microwave power density and power lost per unit area of (a) a kernel, (b) a mesocarp and (c) an EFB due to various mechanisms when subject to 180 W microwave power.

From Figure 6.13(a) and 6.13(b), the power lost per unit area due to evaporation decreases rapidly at the initial stage. The initial decrease of the power loss is due to rapid moisture evaporation at the surfaces of kernel and mesocarp while the surface temperature is relatively low. The surface temperatures of the kernel and mesocarp are around 40 - 50 ^{0}C at t = 1 min ((Figure 6.1(b) and 6.2(b)). After the initial decrease of evaporative power loss, it is followed by a gradual increase until it reaches a maximum power loss. The maximum evaporative power loss occurs at around t = 5 - 6 min when the surface temperatures of kernel and mesocarp are approximately 70 ^{0}C (Figure 6.1(b)) and 90 ^{0}C (Figure 6.2 (b)). On the other hand, EFB achieved the maximum evaporative power lost at t=2 mins when its surface temperature are approximately 100 ^{0}C (Figure 6.3(b)). The increase of evaporative power loss is also due to the steady moisture diffusion from inner part of the samples to the surface. As the moisture in the sample decreases, the evaporative power loss decreases for the remaining heating duration, despite a higher sample temperature is attained. Moreover, the evaporation rate decreases as the moisture content of the samples is further reduced. This is caused by the slower moisture migration from the interior of the solid towards its surface, thus, reduces the amount of moisture content to be evaporated at the sample's surface (Metaxas and Meredith, 1983).

In addition, the power loss due to radiation is 2.4-4.4 times higher than the power loss due to convection. This is attributed to the low heat transfer coefficient (5 W/(m^2·K)) is used for kernel and mesocarp, and a relatively higher heat transfer coefficient (30 W/(m^2·K)) is used for EFB to model in the microwave cavity. 5 W/(m^2·K) for kernel and mesocarp which is often used for natural convective heat transfer in a typical microwave oven. However, a relatively higher heat transfer coefficient (22.5-40W/(m^2·K)) is typically represented for fibrous material (Zhang and Datta, 2004, Yang and Gunasekaran, 2004, Rakesh et al., 2011, Kumar et al., 2014), therefore, the relatively higher heat transfer coefficient, 30 W/(m^2·K), is used to represent for the fibrous EFB. Radiation and convection of kernel, mesocarp and EFB are increased with time and the rate of increment has slowed down gradually which is dependent on the surface temperature of the samples, as shown in equations (5.19) and (5.20).

In this study, the heat loss of kernel, mesocarp and EFB due to evaporation is relatively small compared to the power loss due to radiation and convection. Besides, the microwave power absorptions are gradually decreases within the kernel, mesocarp and EFB due to the reduction of dielectric loss factor of the dried samples.

6.4 Temperature and moisture distributions

Although Figure 6.1-6.3 show the temperature of two point locations of the samples, the temperature distribution in the sample are necessary to identify the hot spots to avoid the overheating of the sample.

In microwave heating, temperature distribution in a sample is dependent on the electric field intensity and generated microwave power density. Figure 6.14-6.22 show the electric field distributions, microwave power absorption densities and temperature distributions in the kernel, mesocarp and EFB after microwave heating for 1 min and 5 mins. The generated microwave power density (Figure 6.15, 6.18 and 6.21) have the same pattern with the electric field intensity in the kernel (Figure 6.14), mesocarp (Figure 6.17) and EFB (Figure 6.20). The occurrence of the resonances during microwave heating results in local hotspots which causes temperature non uniformity in the samples. A higher temperature is found at the upper central surface and a lower temperature occurs at edges and side surfaces of mesocarp (Figure 6.19) and EFB (Figure 6.22). On the other hand, Figure 6.16 shows a hotspot is found at the top region of the kernel and its lower part is generally colder. Hossan and Dutta (2012) reported that the temperature distribution of a rectangle shaped salmon fillet was closely related to the generated microwave power density distribution except for areas which are closer to the surface where the influence of surface cooling is presented in Section 6.3.

The temperature distribution of kernel (Figure 6.16) has the same pattern as the generated microwave power density distribution where the hotspot is located at the maximum generated microwave power density (Figure 6.15). However, the temperature distributions in the mesocarp and EFB are not the same as the corresponding generated microwave power densities. The mesocarp (Figure 6.19) and EFB (Figure 6.22) have central hotspots which are not located in the regions with maximum generated microwave power densities (Figure 6.18 and 6.21).

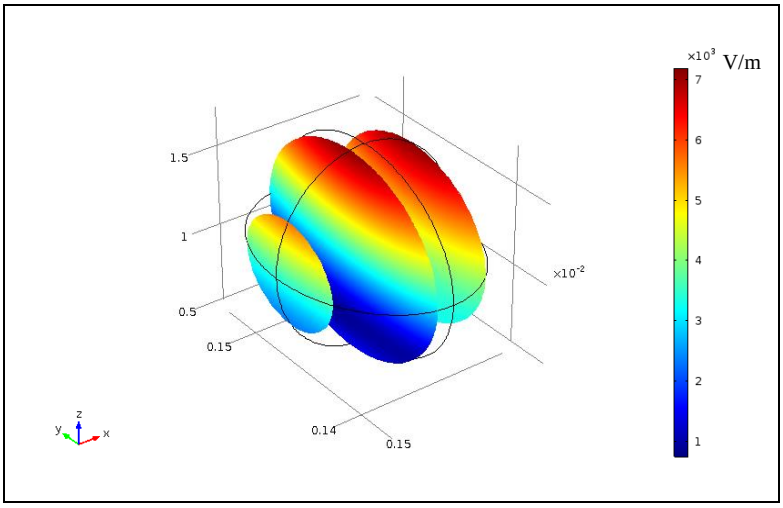

Figure 6.14: Electric field intensity in the kernel throughout the microwave heating and drying durations.

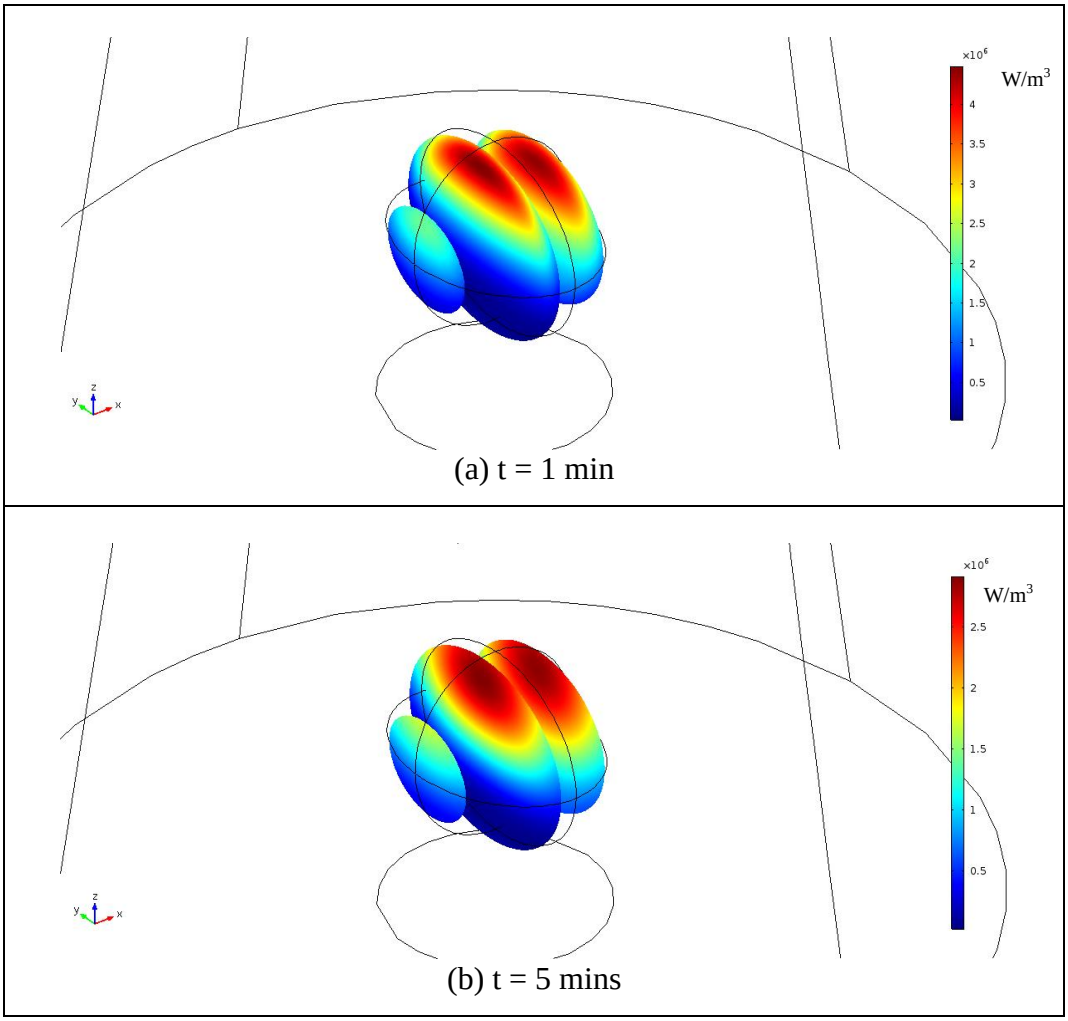

Figure 6.15: Generated microwave power density in the kernel after (a) 1 min and (b) 5 mins of microwave heating and drying.

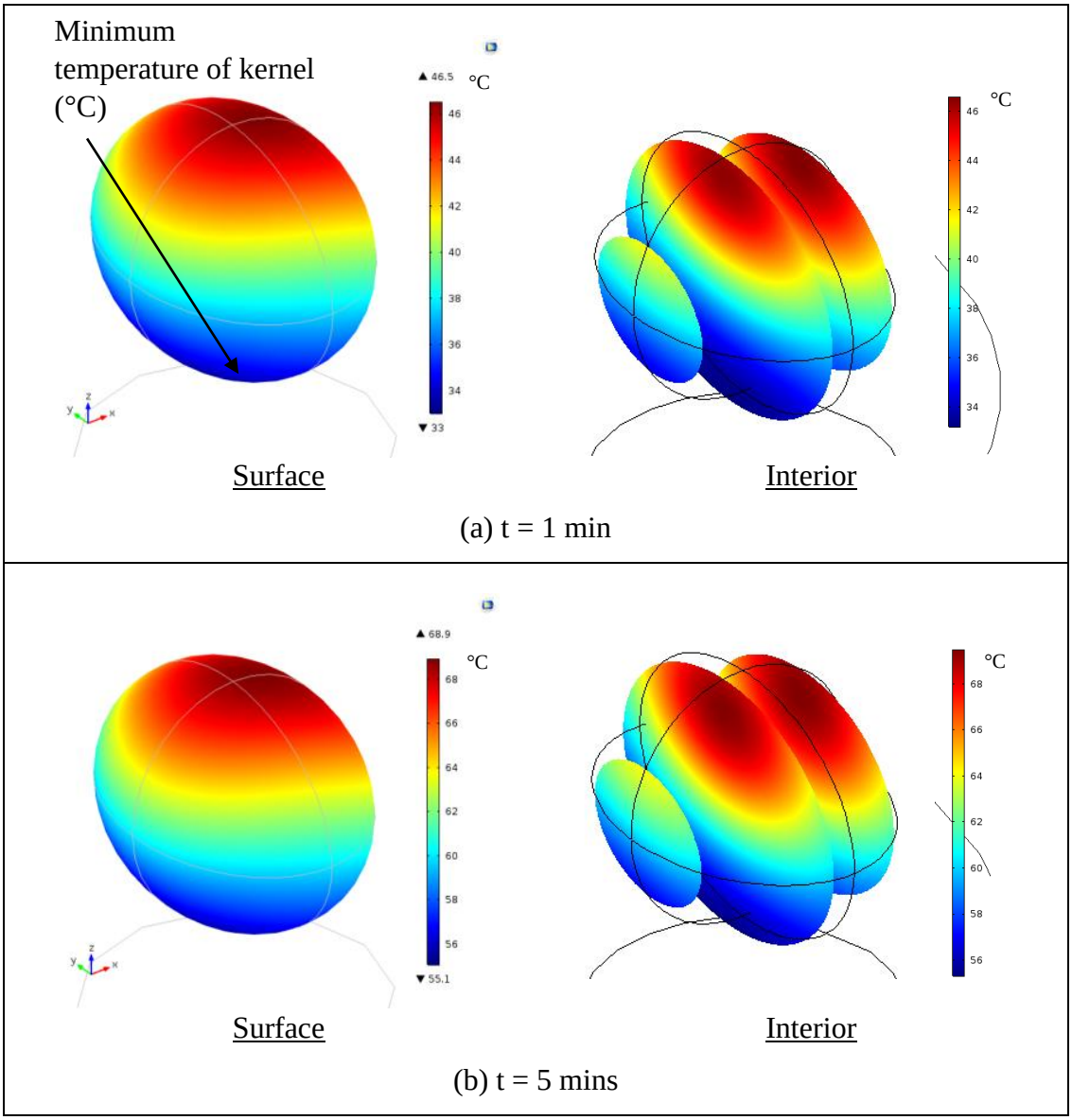

Figure 6.16: Surface and interior temperature distributions in the kernel after (a) 1 min and (b) 5 mins of microwave heating.

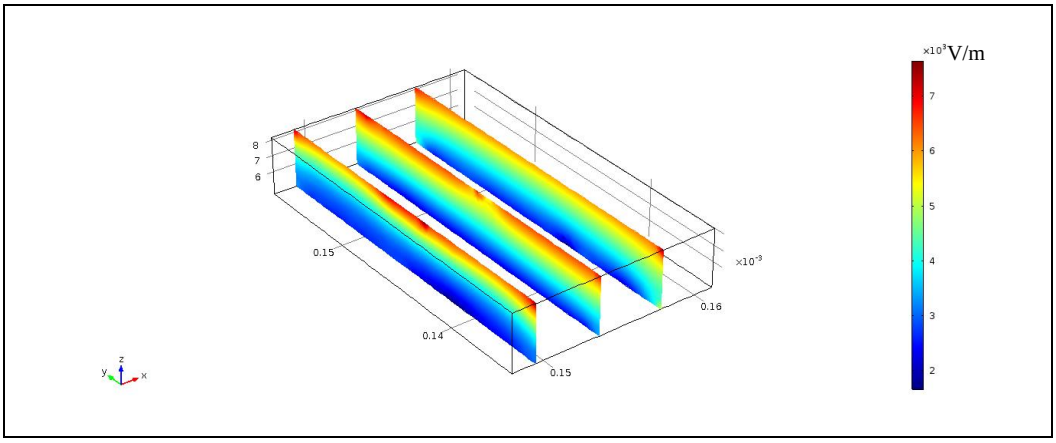

Figure 6.17: Electric field intensity in the mesocarp throughout the microwave heating and drying durations.

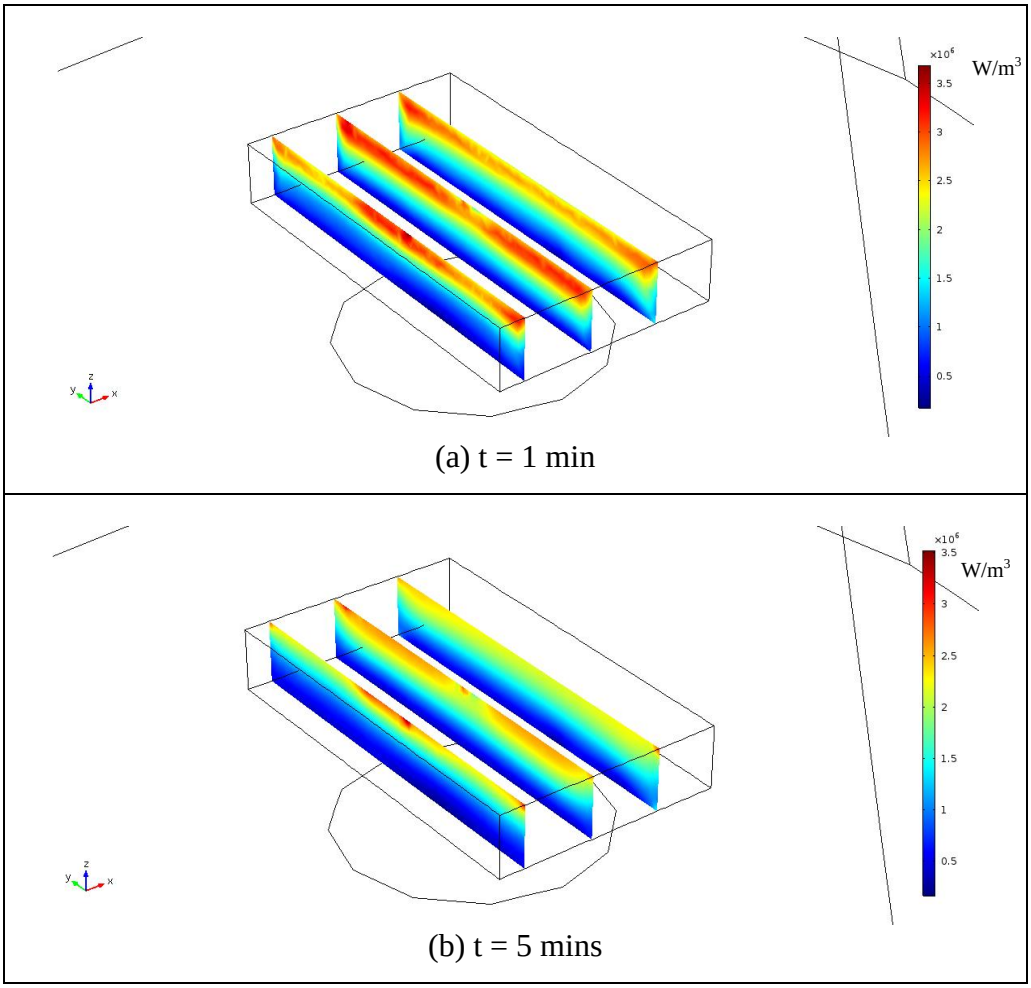

Figure 6.18: Generated microwave power density in the mesocarp after (a) 1 min and (b) 5 mins of microwave heating and drying.

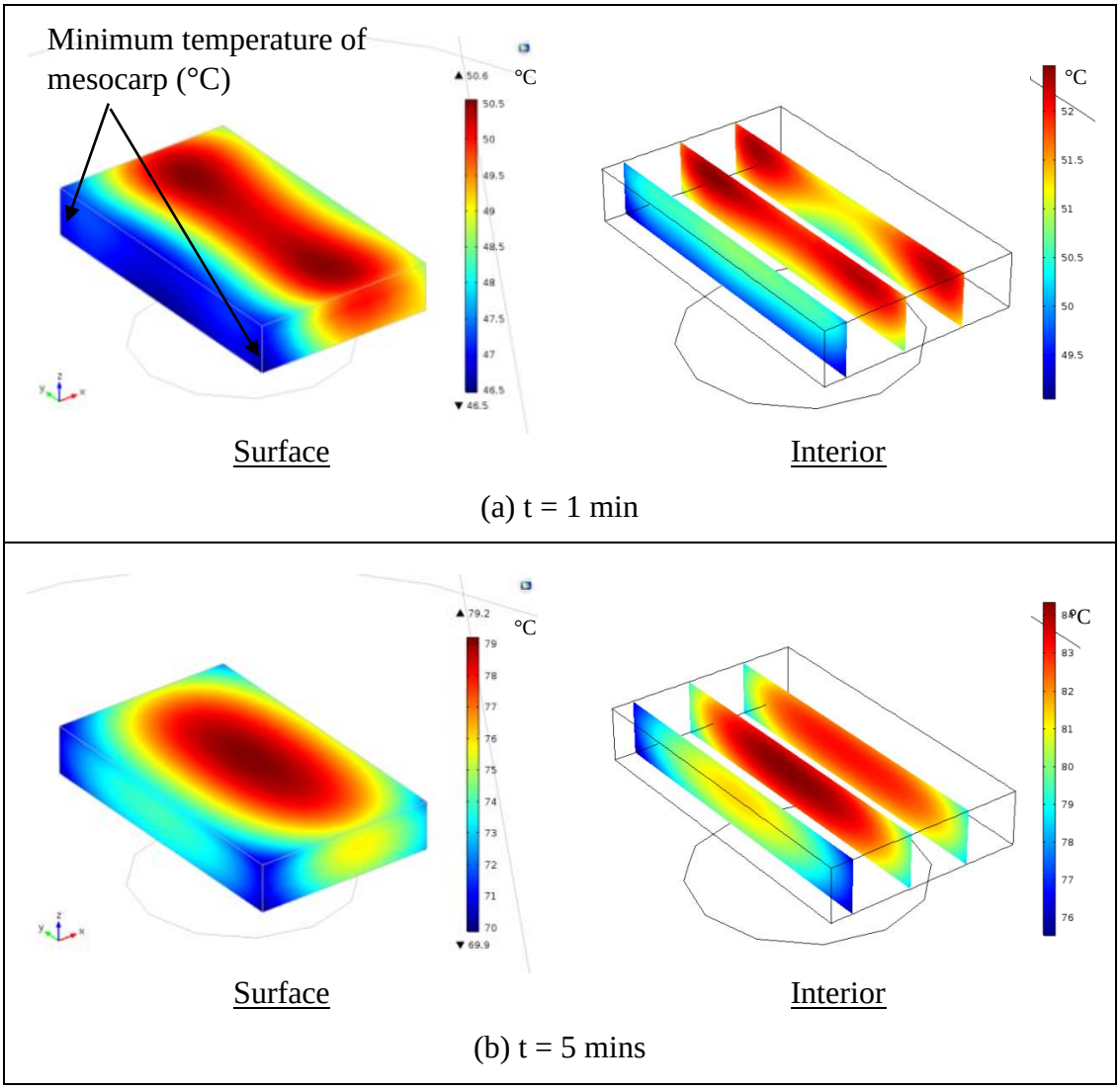

Figure 6.19: Surface and interior temperature distributions in the mesocarp after (a) 1min and (b) 5 mins of microwave heating.

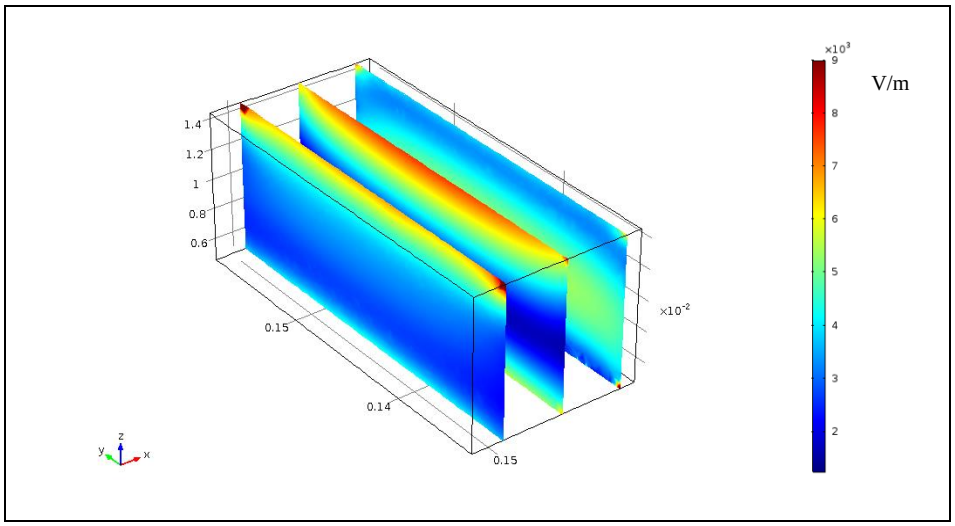

Figure 6.20: Electric field intensity in the EFB throughout the microwave heating and drying durations.

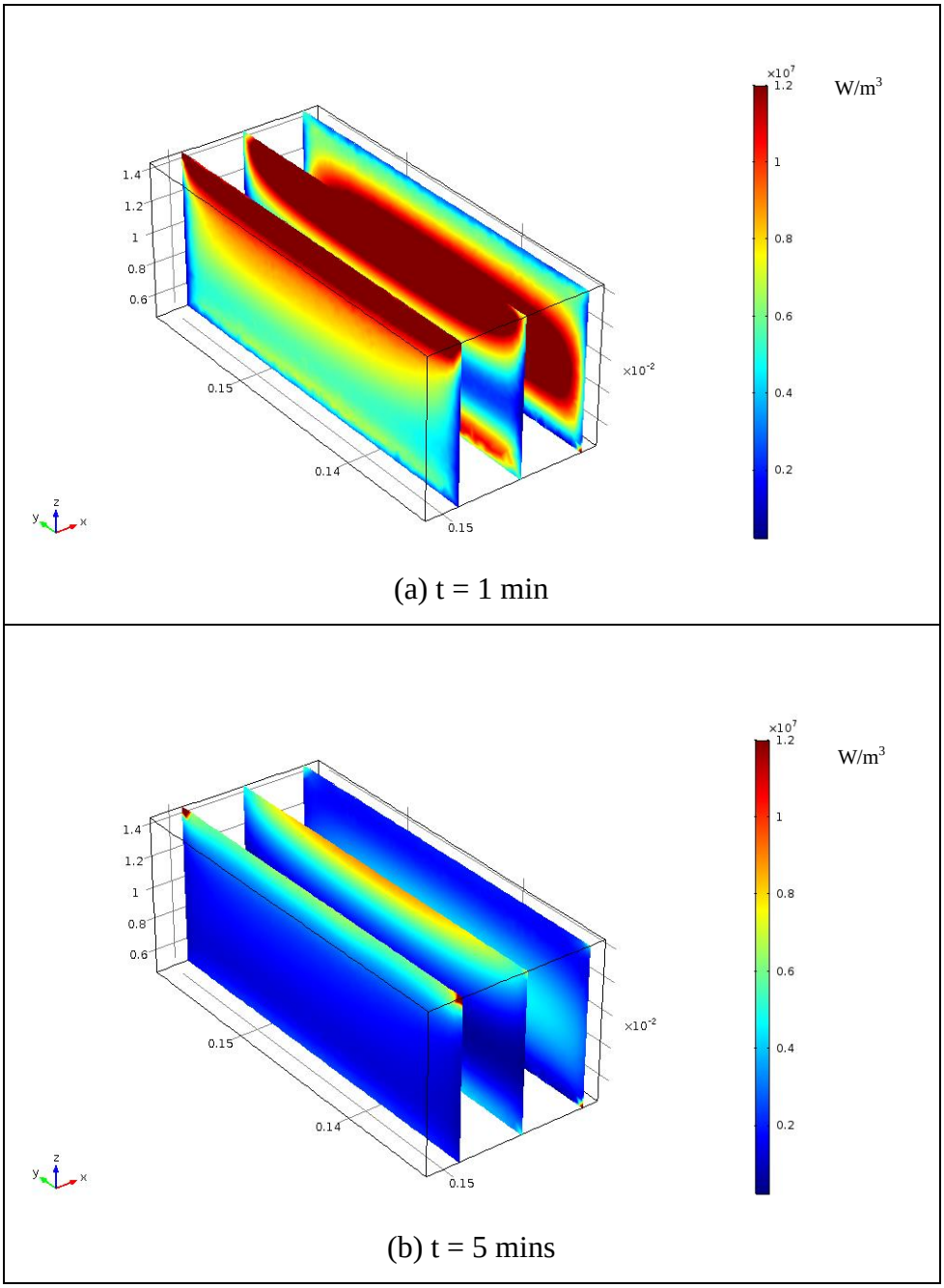

(a) t = 1 min

(b) t = 5 mins

Figure 6.21: Generated microwave power density in the EFB after (a) 1 min and (b) 5 mins of microwave heating and drying.

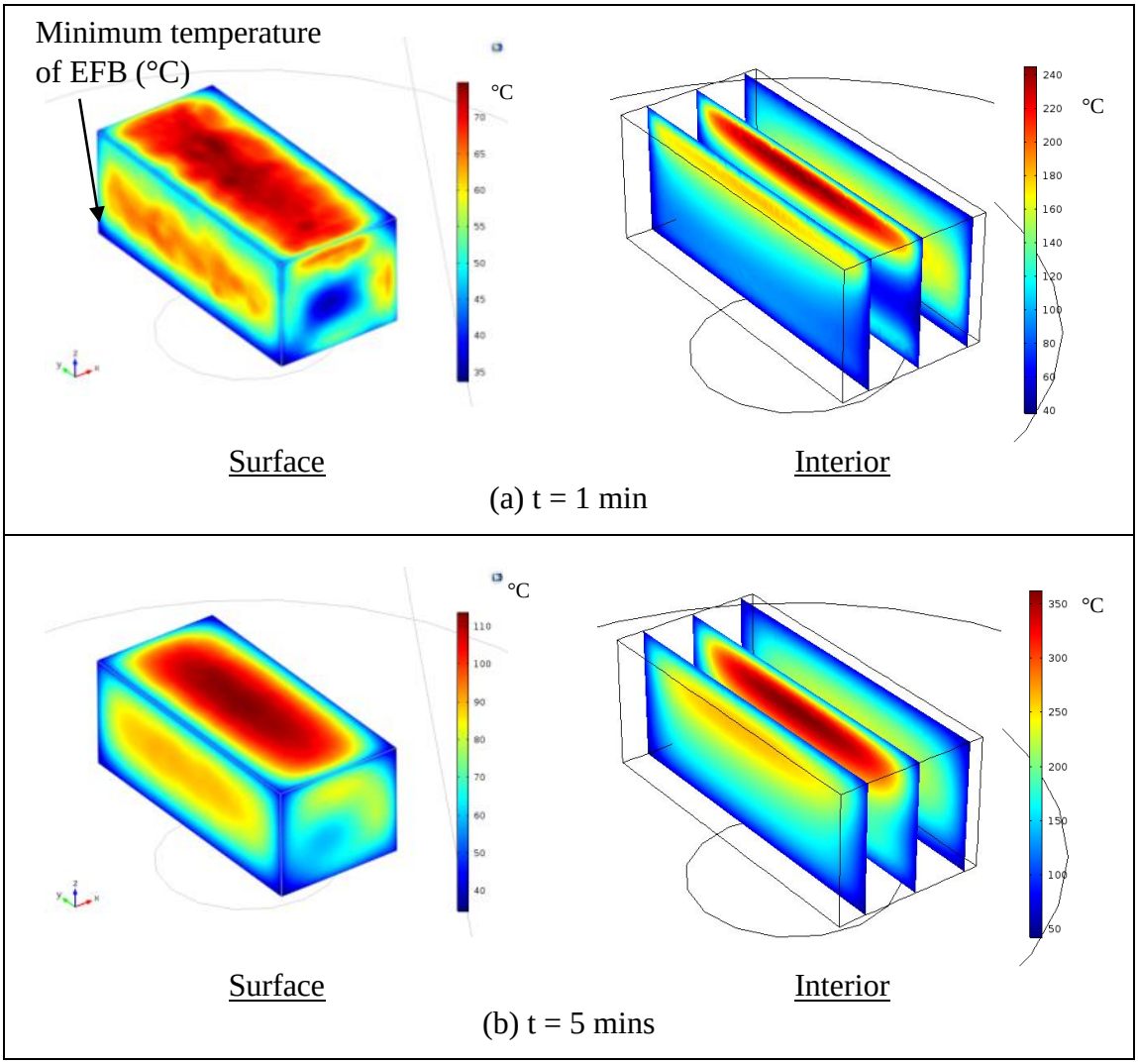

Figure 6.22: Surface and interior temperature distributions in the EFB after (a) 1min and (b) 5 mins of microwave heating.

The temperature of the hotspot, however, has reduced during the OFF phase. The microwave oven supplies microwave irradiance intermittently. A full cycle has a period of 30 s. In the case of 180 W microwave power, microwave supply is switched on (ON phase) for 12 s and switched off for the next 18 s (OFF phase) in every cycle. Figure 6.23 shows the temperature distributions of the samples during the cooling stage. The cooling stage reduces the peak temperature and also allows more uniform temperature distribution within the samples.

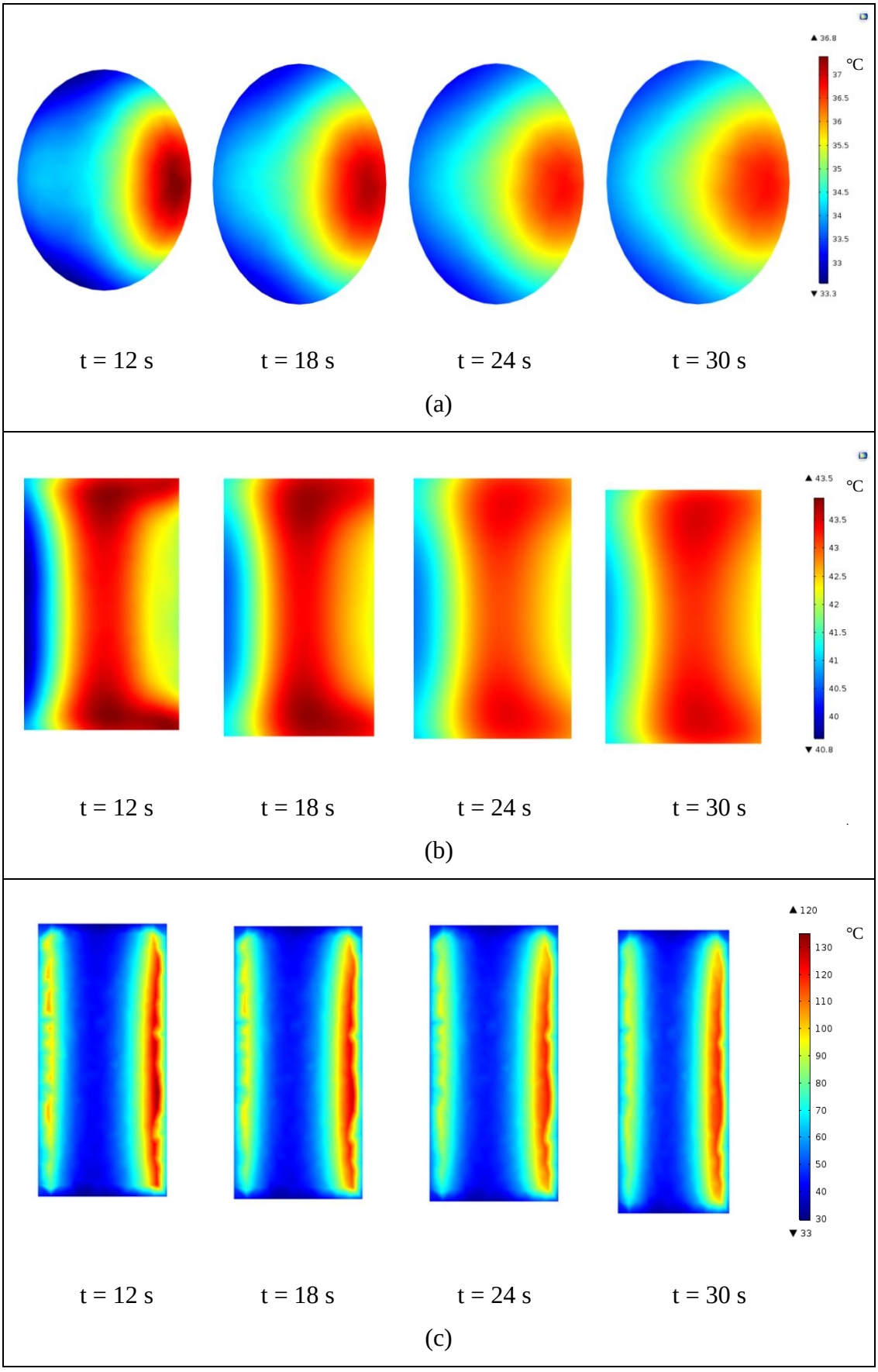

Figure 6.23: Temperature distribution in the center (h/2) of the (a) kernel, (b) mesocarp and (c) EFB during the microwave OFF phase, t = 12-30s.

Besides, according to equation (5.2), heat generation within a sample is directly proportional to the sample's dielectric loss factor. Figure 6.24-6.26 show the distributions of dielectric loss factor of kernel, mesocarp and EFB after 1 min (60s) and 5 mins (300s) of microwave heating. The dielectric loss factor is higher at the center and is lower the surface. As the dielectric loss factor follows closely with that of moisture content distribution as it is modeled as a function of moisture content as presented in Chapter 4.

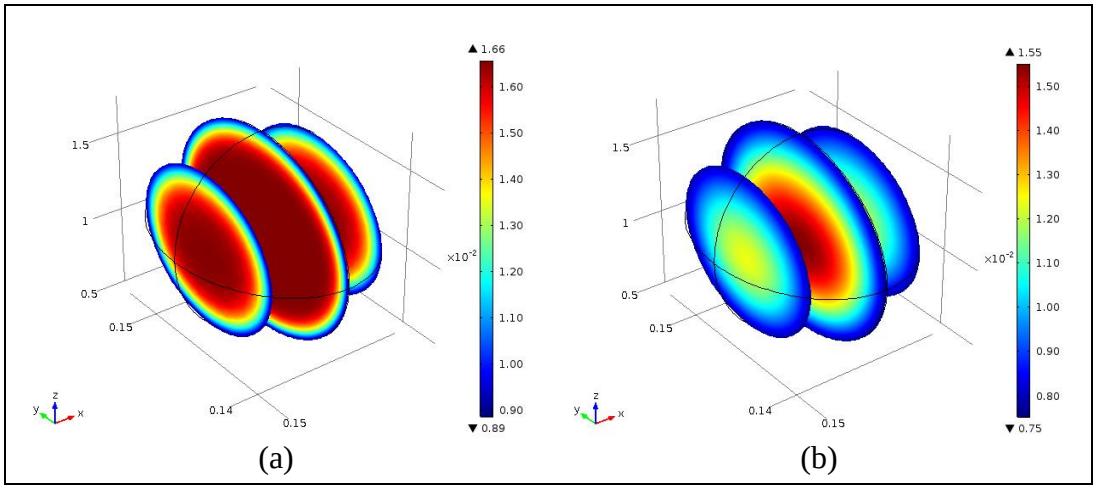

(a) (b)

Figure 6.24: Dielectric loss factors of the kernel on the viewed after (a) 1 min (60 s) and (b) 5 mins (600 s) of microwave heating.

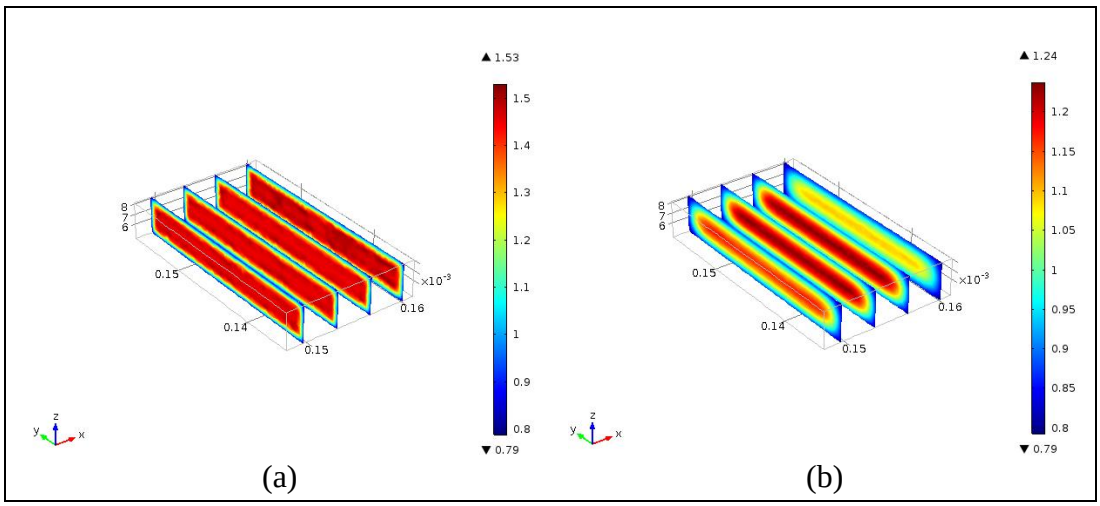

(a) (b)

Figure 6.25: Dielectric loss factors of the mesocarp viewed on after (a) 1 min (60 s) and (b) 5 mins (300 s) of microwave heating.

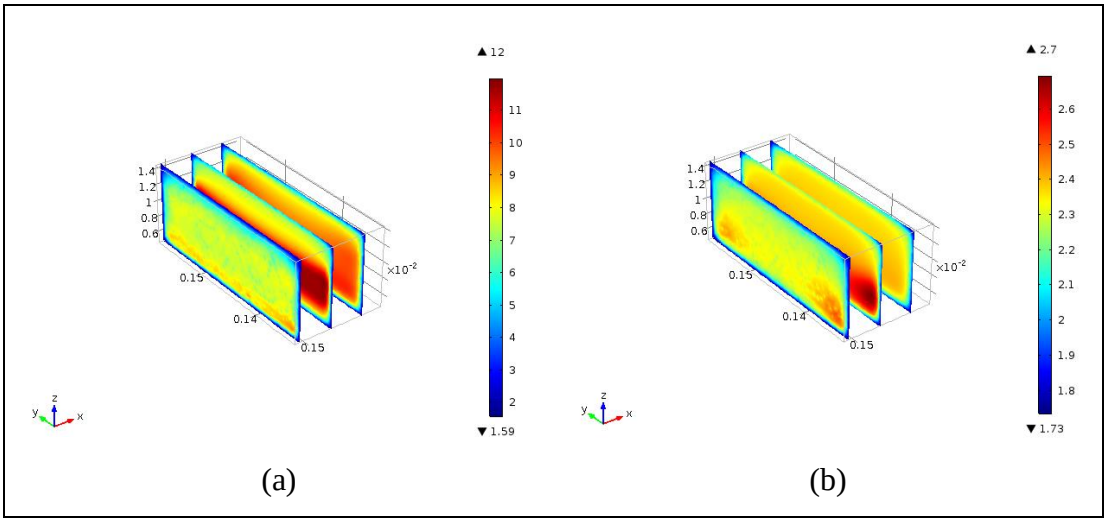

(a) (b)

Figure 6.26: Dielectric loss factors of the EFB viewed on after (a)1 min (60 s) and (b)5 mins (300 s) of microwave heating.

The maximum, minimum, volume-averaged and surface-averaged temperature profiles of the kernel, mesocarp and EFB are shown in Figure 6.27. In the temperature history, the surface-averaged temperatures of the kernel, mesocarp and EFB are lower than the volume-averaged temperature. The low surface temperature is attributed to the cooling effect due to evaporation, radiation and convection at the sample's surface. The volume-averaged temperatures of the kernel and mesocarp are 3 % and 2 % higher than their surface-averaged temperatures, respectively. This small difference suggests that surface temperature of kernel and mesocarp could be used as an approximation to volumetric temperature. On the other hand, the volume-averaged temperature of the EFB is greater than its surface-averaged temperature by 150 %. The large difference can be caused by two factors which are its small thermal conductivity and also the larger sample size. Due to these two factors, a larger thermal gradient exists between EFB core and the surface.

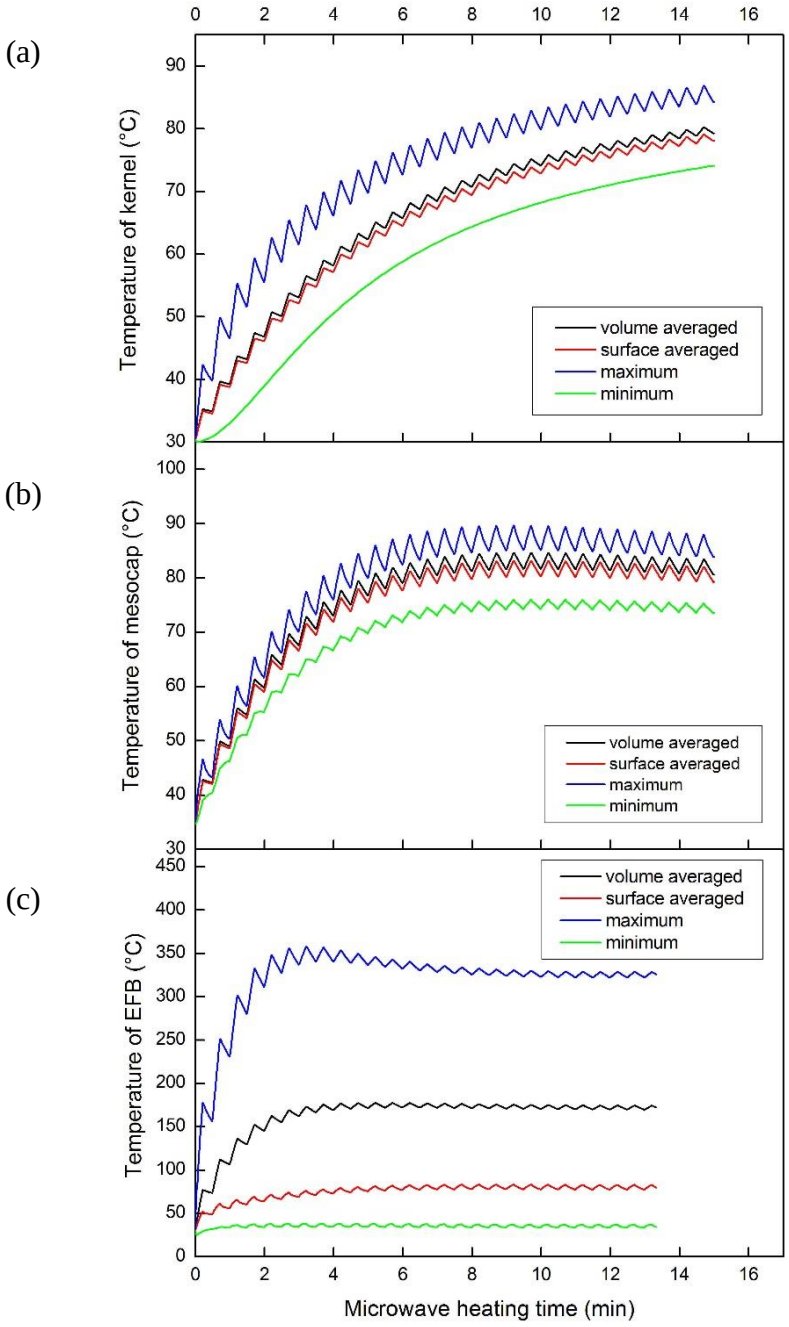

Figure 6.27: Temperature history of (a) a kernel, (b) a mesocarp and (c) an EFB subject to microwave power of 180 W.

Figure 6.28 shows the comparisons between the volume-averaged and surface-averaged moisture contents of the kernel, mesocarp and EFB that are subjected to microwave power of 180 W. The moisture content at the surface and within the kernel, mesocarp and EFB decrease exponentially. Similarly, the moisture contents at the surfaces of the kernel, mesocarp and EFB are dried more rapidly than the interior. The drier surface is caused by the convective air flow and the evaporation of liquid vapor from the samples' surfaces.

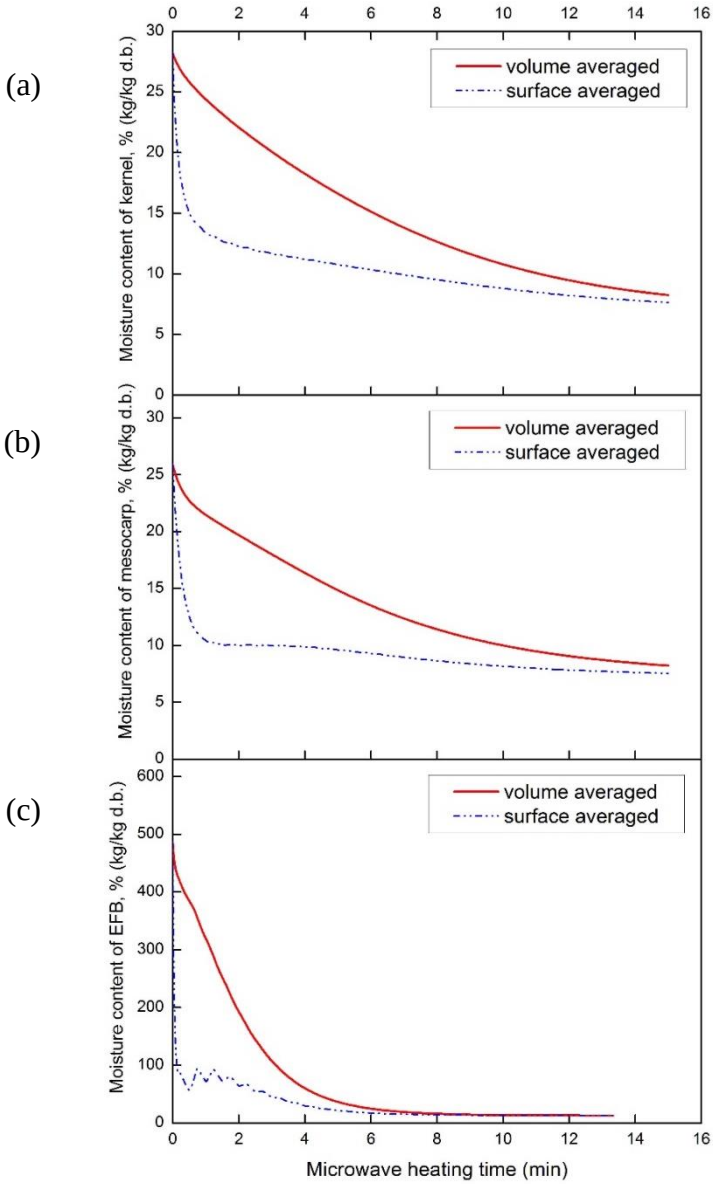

Figure 6.28: Moisture content history of (a) a kernel, (b) a mesocarp and (c) an EFB subject to microwave power of 180 W.

Based on the equation (5.15) and the equation (5.20), the diffusion rate and the evaporation of the moisture content are dependent on the sample's temperature. A higher sample's interior temperature (see Figure 6.27) promotes the moisture diffusion process to the sample's dry surface. To have an overall view of the mass transport phenomena, Figure 6.29-6.31 illustrate the moisture distributions within the kernel, mesocarp and EFB subjected to cyclic microwave heating at 180 W for 1 min, 5 mins and 10 mins.

The moisture content has a different distribution pattern during its pre-heating period (1 min) compared to the constant period (5 mins) and the falling period (10 mins). The moisture content of the samples is not distributed evenly. The maximum moisture content of the kernel (Figure 6.29), mesocarp (Figure 6.30) and EFB (Figure 6.31) samples are centrally located throughout the microwave irradiation process. The moisture distribution during the constant period and failing are almost identical, where moisture on the surface started to separate the dry and wet regions, which also described by Ip and Wan (2012).

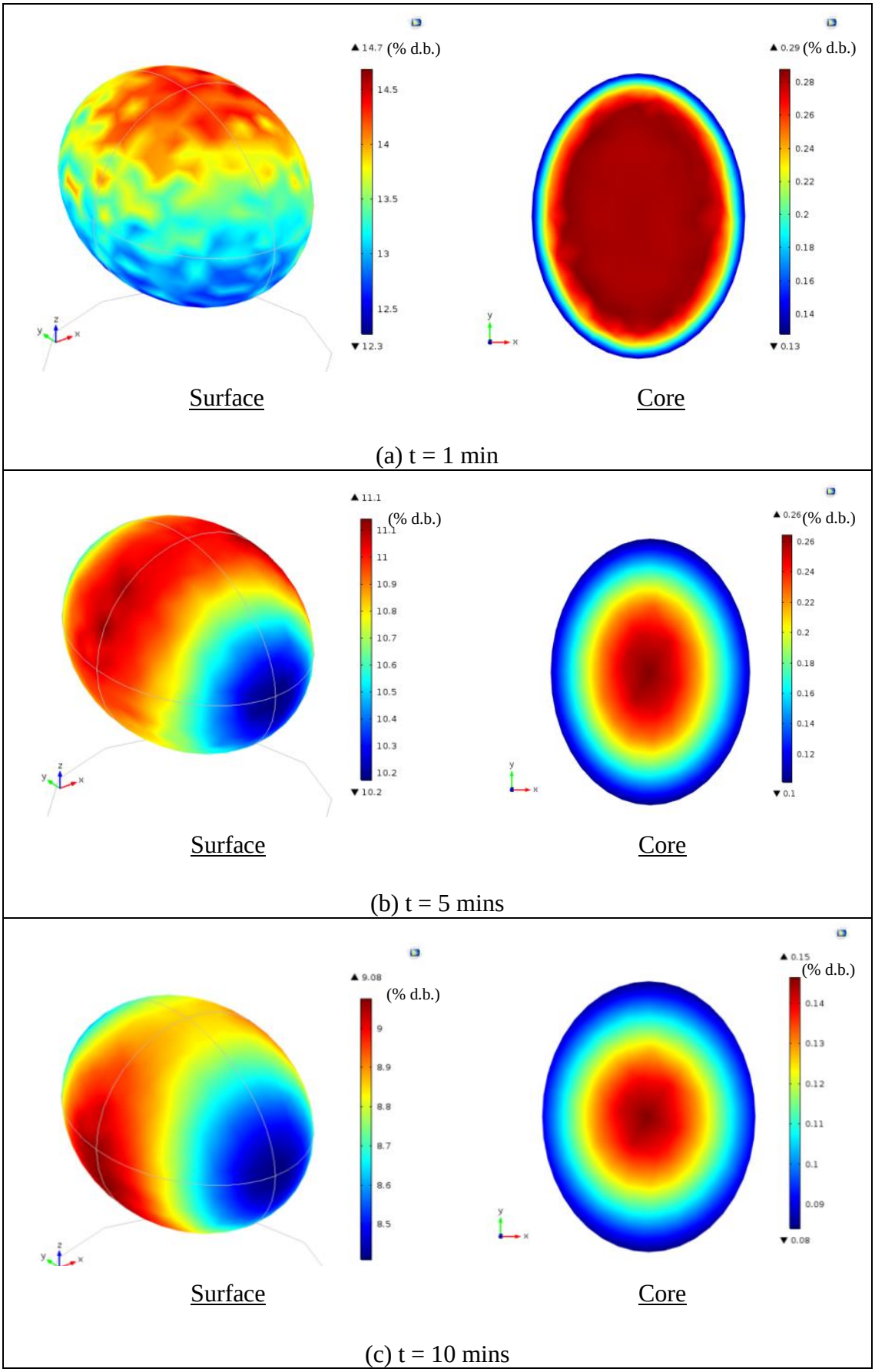

Figure 6.29: Moisture content profiles of kernel after subject to cyclic microwave heating at 180 W for (a) 1 min, (b) 5 mins and (c) 10 mins.

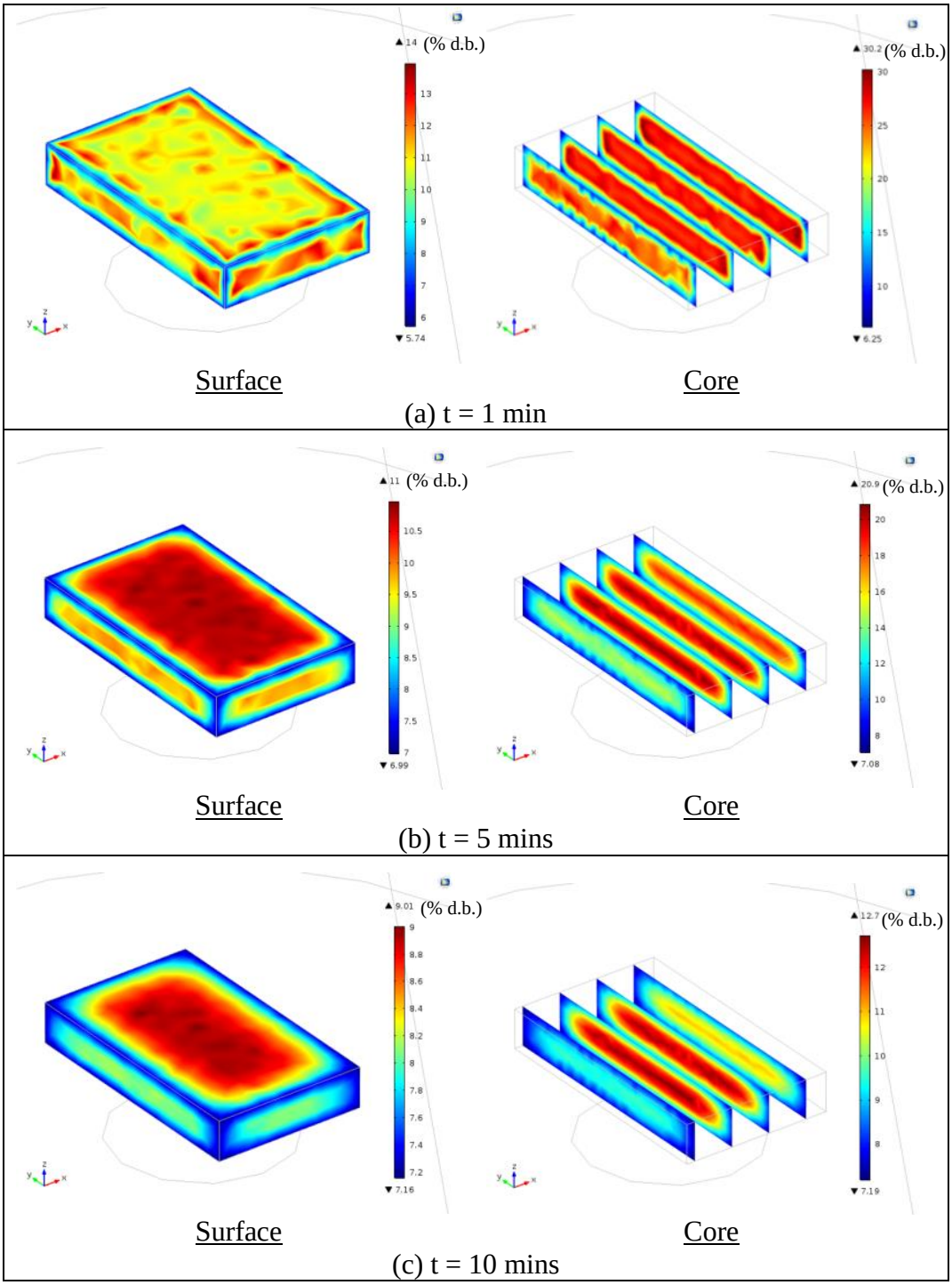

Figure 6.30: Moisture content profiles of mesocarp after subject to cyclic microwave heating at 180 W for (a) 1 min, (b) 5 mins and (c) 10 mins.

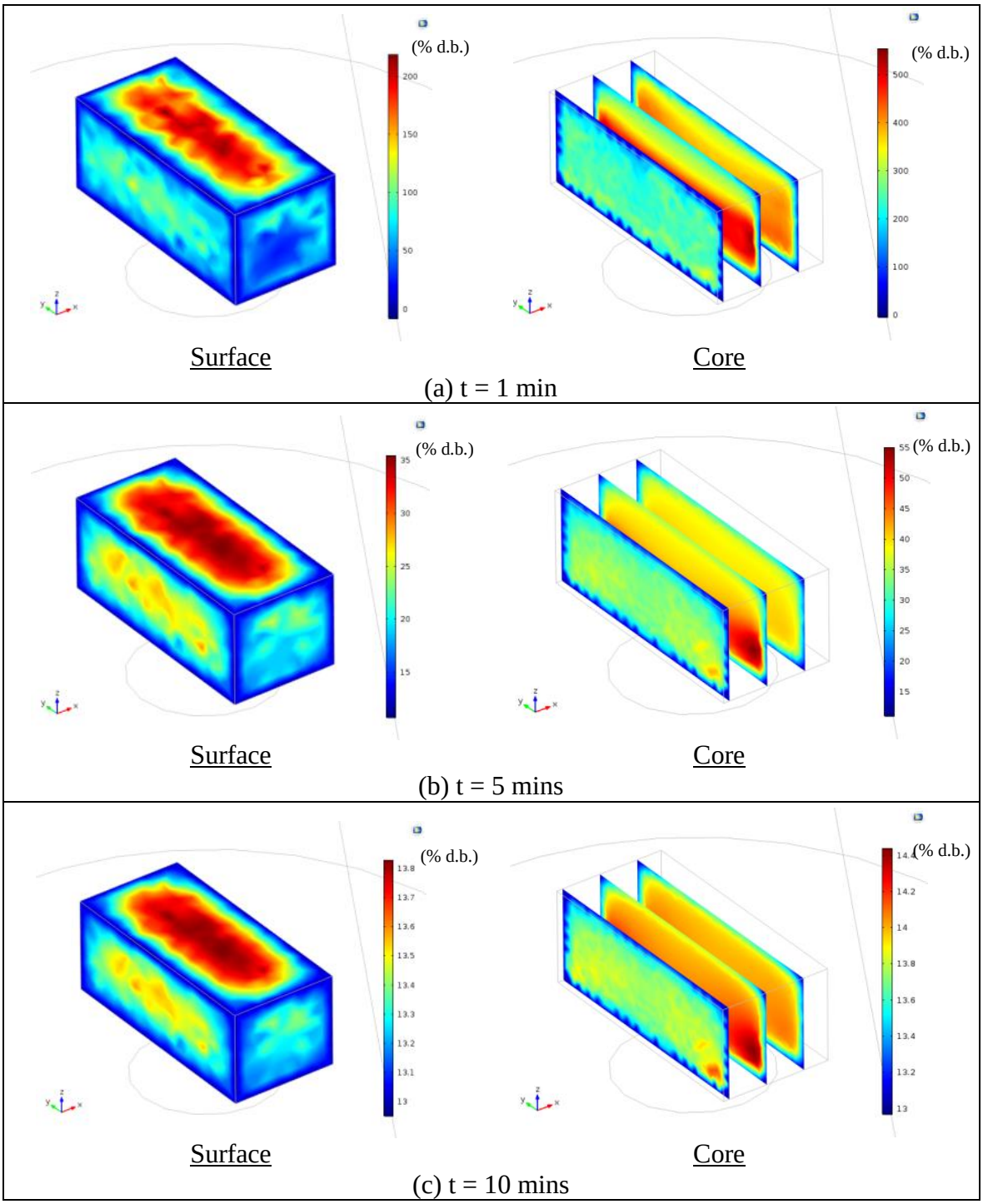

Figure 6.31: Moisture content profiles of EFB after subject to cyclic microwave heating at 180 W for (a) 1 min, (b) 5 mins and (c) 10 mins.

6.5 Summary

In this study, three microwave power levels (100 W, 180 W and 300 W) are simulated and the temperature and moisture content results are compared with experimental data for model validation. The temperature and moisture content histories of the kernel, mesocarp and EFB are discussed. The study of the electromagnetic distributions in the ellipsoid shaped kernel and the cubical shaped mesocarp and EFB showed that the temperature distribution are directly related to the electric field intensity and the generated microwave power density in the samples. However, the total generated microwave power density are highly dependent on the dielectric properties of the samples. In this work, EFB has the largest dielectric properties followed by the mesocarp and kernel. Therefore, EFB is capable of absorbing more microwave energy and generates more heat than the mesocarp and the kernel.

Besides, the temperature history shows that the minimum temperature of the samples occurr on the surface. This is caused by the surface cooling from evaporation, convection and radiation effects. Among the heat transfer mechanisms, convection and radiation are the dominant cooling mechanisms to reduce the surface temperature of the heated sample. Therefore, the surface of the heated sample has a lower temperature than the interior. The hot spots are observed to occur at the centers of the mesocarp and EFB and on the top surface of the kernel. The hotspots can be avoided by applying cyclic heating. The cyclic operation reduces the temperature and provides a better temperature uniformity in the kernel, the mesocarp and the EFB samples.

CHAPTER 7
MODELING OF FRESH FRUIT BUNCH

In this chapter, the microwave heating of a simplified fresh fruit bunches (FFB) is simulated which the FFB consist of kernel, mesocarp and EFB. The purpose of this simulation is to study the heat and mass transfer behaviors of FFB when microwave energy is provided. The modelling procedure of the FFB is similar to that discussed in Chapter 5. The computational domain, the meshing scheme and the microwave heating behavior of the FFB are presented.

7.1 Computational domain

In this case study, a small part of FFB exposed to microwave irradiation is modelled (as shown in Figure 7.1(a)). The FFB in this model (Figure 7.1(b)) consists of a palm fruit and EFB. The EFB is attached to the fruit.

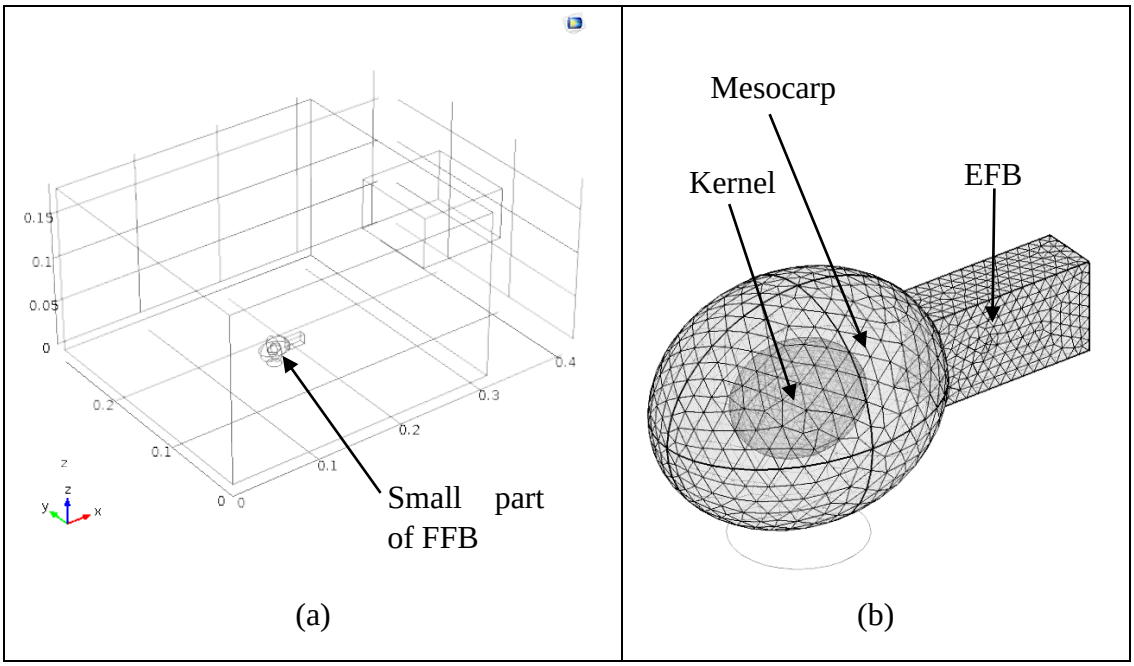

Figure 7.1: (a) Computational model of FFB and the (b) details of FFB.

Based on the volume assessment conducted by Noerhidajat et al. (2015), palm fruit is well represented as an ellipsoidal shape. Thus, kernel and mesocarp are modelled as an ellipsoid shape and a rectangular shape for EFB. The dimensions and the total volume of the modelled FFB are listed in Table 7.1. The dimensions of mesocarp and kernel are based on values reported by Hazir and Shariff (2011) and

the EFB is assumed as a rectangular block of 25.7 mm (length) x 10.8 mm (width) x 6.75 mm (height).

Table 7.1: Dimensions of the kernel, mesocarp and EFB constructed in the model.

Layer	Shape	Dimension			Total volume (mm^3)
		Length (mm)	Width (mm)	Height (mm)	
Kernel	Ellipsoid	15.5	11.8	12.4	1086.4
Mesocarp	Ellipsoid	33.75	25.7	27	11175.34
EFB	Rectangular	25.7	6.75	10.8	1385.9

Figure 7.2 is a three dimensional view of a FFB. A red color line (line 1) as indicated in this figure is placed at the center of the FFB.

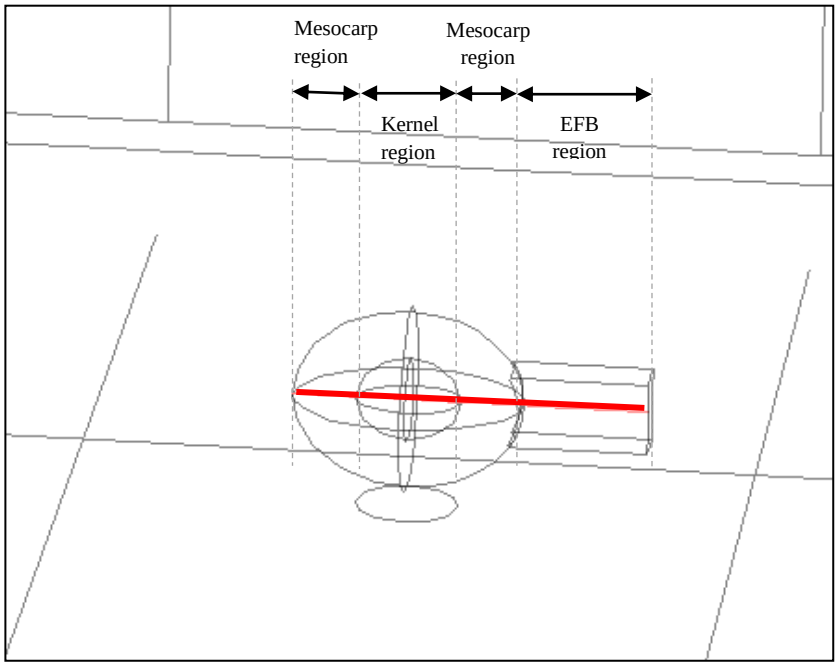

Figure 7.2: The red line (line 1) as indicated is used for result comparisons.

Besides, two cross-sectional planes in the x-y (Figure 7.3) and x-z (Figure 7.4) directions are used to study the results of the simulations. Both the planes pass through the center of the samples. As shown in Figure 7.3, the horizontal plane in x–y direction is at z = 0.0162 m (denoted as x–y plane 4). On the other hand, Figure 7.4 shows the vertical plane in the x-z direction at y = 0.145 m.

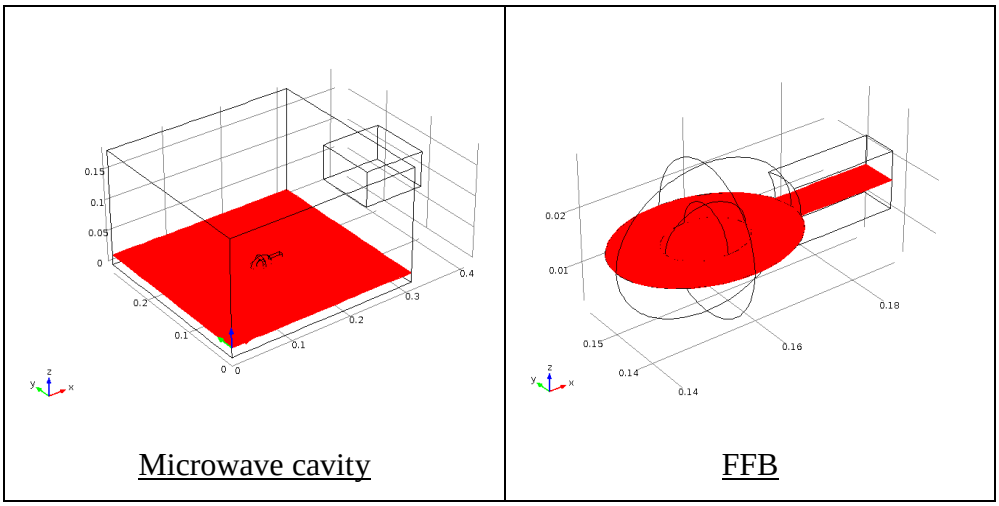

Figure 7.3: Cut plane 1 of the FFB models. The horizontal plane is set at the center of the samples; the plane is located at z = 0.0162 m (x-y plane 4) from the cavity surface.

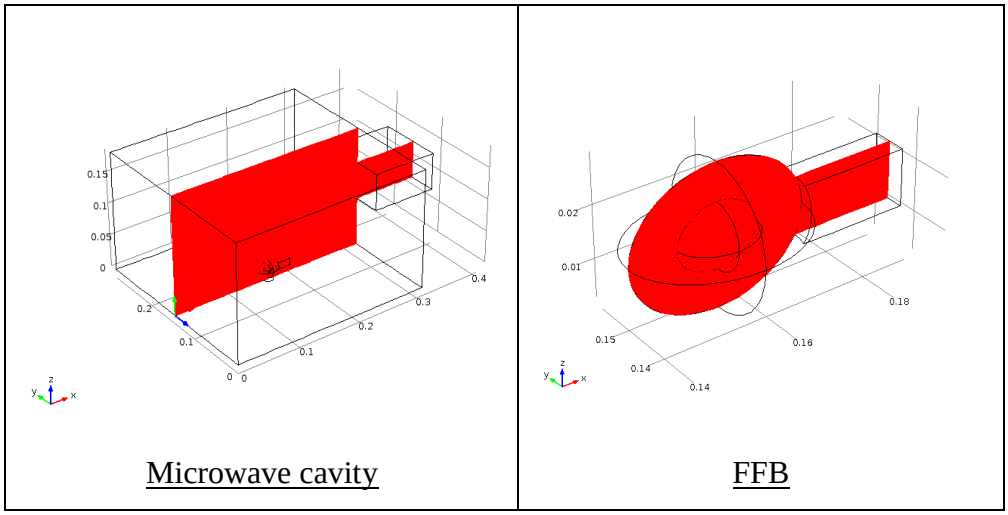

Figure 7.4: Cut plane 2 of the FFB models. The vertical plane is set at the center of the samples; the plane is located at y = 0.145 m (x-z plane 4) from the cavity surface.

7.2 Mesh generation

Since the shape and the dimensions of the kernel, mesocarp and EFB are changed according to Table 7.1, a mesh generation study is needed to be carried out on the modified geometries. Similar meshing options are applied in the mesh independent test, namely "coarser", "coarse", "normal", "fine" and "finer" meshing options. Table 7.2 shows the maximum element sizes and the total number of tetrahedral elements for different mesh options.

Table 7.2: Element sizes and total element numbers of the geometry for various mesh options.

Mesh option	**Maximum Element size (m)**	**Total elements**
Coarser	0.0775	34440
Coarse	0.0612	36802
Normal	0.0408	42256
Fine	0.0326	47916
Finer	0.0224	66725

The simulated averaged temperatures and moisture contents of the kernel, mesocarp and EFB at 600s with different element sizes are shown in Figure 7.5. The comparisons indicate that the temperature and moisture content of the kernel, mesocarp or EFB have reached almost constant values for the "fine" meshing option thus, the "fine" mesh option is used to refine the meshes in the case study. In this case study, the same initial conditions, boundary conditions, input parameters and numerical procedure as described in Sections 5.3, 5.5 and 5.6 are applied.

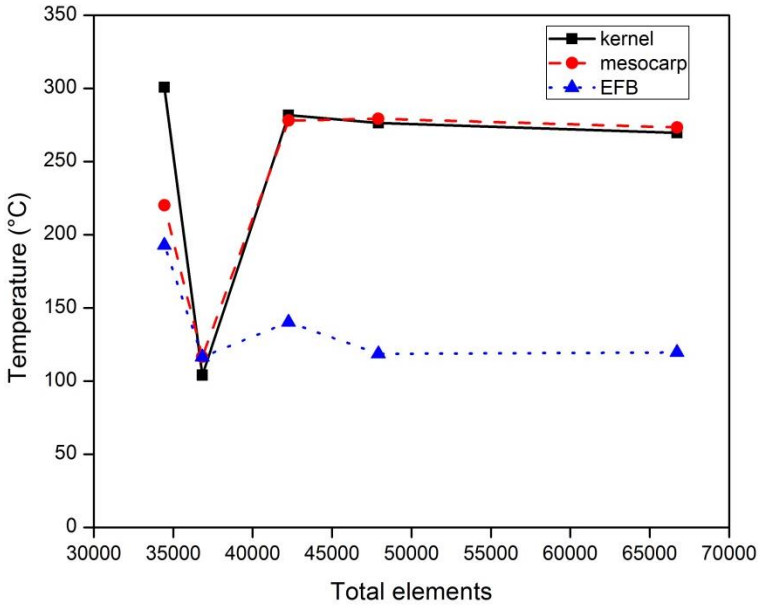

(a)

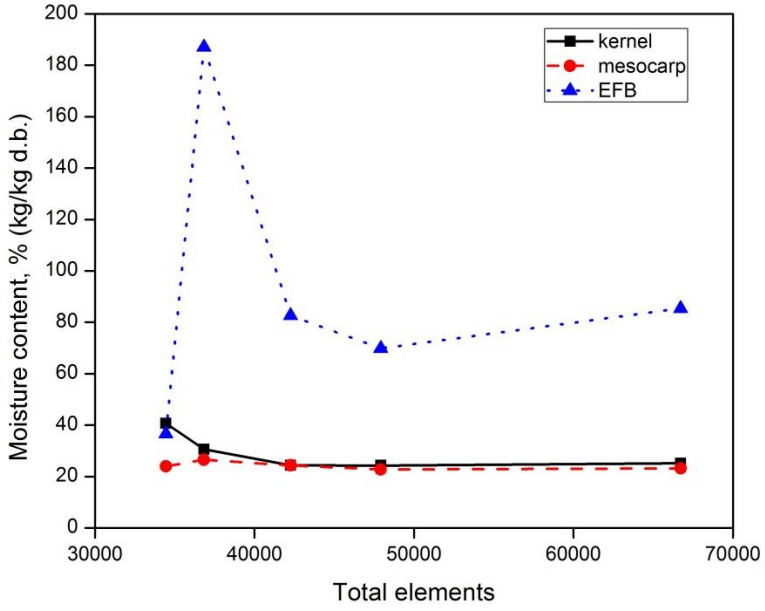

(b)

Figure 7.5: Effects of element numbers on estimated (a) temperature and (b) moisture content of kernel, mesocarp and EFB at t=600s.

7.3 Electric field distributions

Figure 7.6 and 7.7 show the electric field distribution in the microwave cavity viewed on x-y plane 4 and x-z plane 4. In Figure 7.6(a) and 7.7(a), high and low electric field intensity spots are observed and the formation of these spots is explained in Section 6.2 and is due to the interference of electromagnetic waves in the cavity. The electric field intensity around the FFB ranges from 0.3×10^4 to 2.3×10^4 V/m on the x-y plane 4 (Figure 7.6(b)) and from 0.3×10^4 to 2.8×10^4 V/m at the x-z plane 4 (Figure 7.7(b)). In Figure 7.6(a) and 7.7(a), the highest electric field intensities in the microwave cavity are observed to surround the edges and surfaces of the mesocarp and EFB of the FFB. Among the three individual materials, the EFB experiences the strongest field strength (2.25×10^3-2.15×10^4 V/m), followed by the mesocarp (853-2.14×10^4 V/m) and kernel (2.6×10^3-9.84×10^3 V/m). The strongest field strength (2.14×10^4-2.15×10^4 V/m) in EFB and mesocarp is located in the interface between the EFB and mesocarp. The arrows in Figure 7.6(c) and 7.7(c) indicate more electric field is deposited at the interface between EFB and mesocarp compared to other regions. The lowest electric field intensities are found at the top and the bottom of the mesocarp and the kernel, whereas low electric field intensity is located at the center of the EFB. The field intensity distribution is affected by size, geometry and location of the kernel, mesocarp and EFB of the FFB.

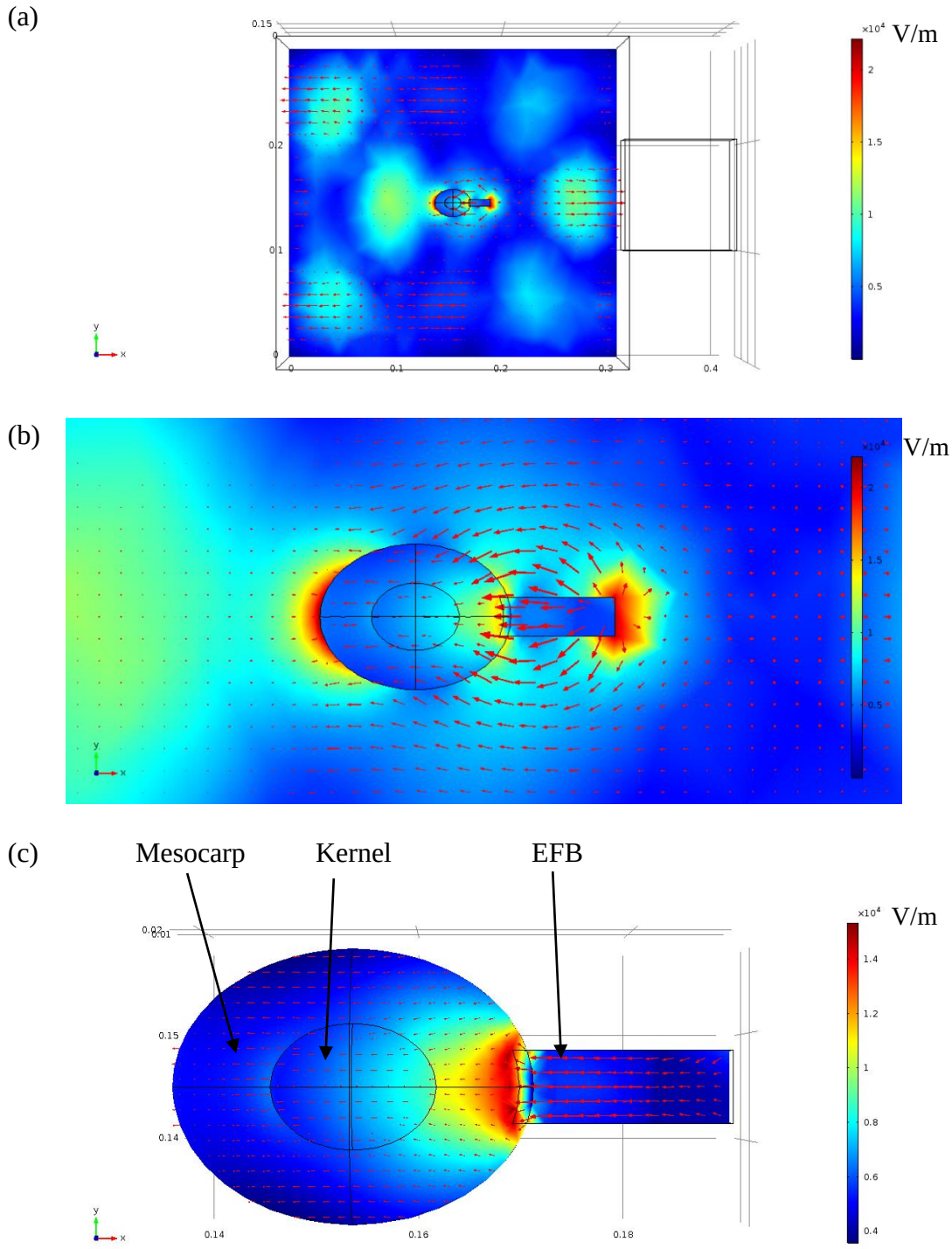

Figure 7.6: Electric distribution (a)in the microwave cavity, (b)around the FFB and (c)within the FFB viewed on x-y plane. The arrows in the figures indicate the direction of the electric fields for the 2.45 GHz incident waves.

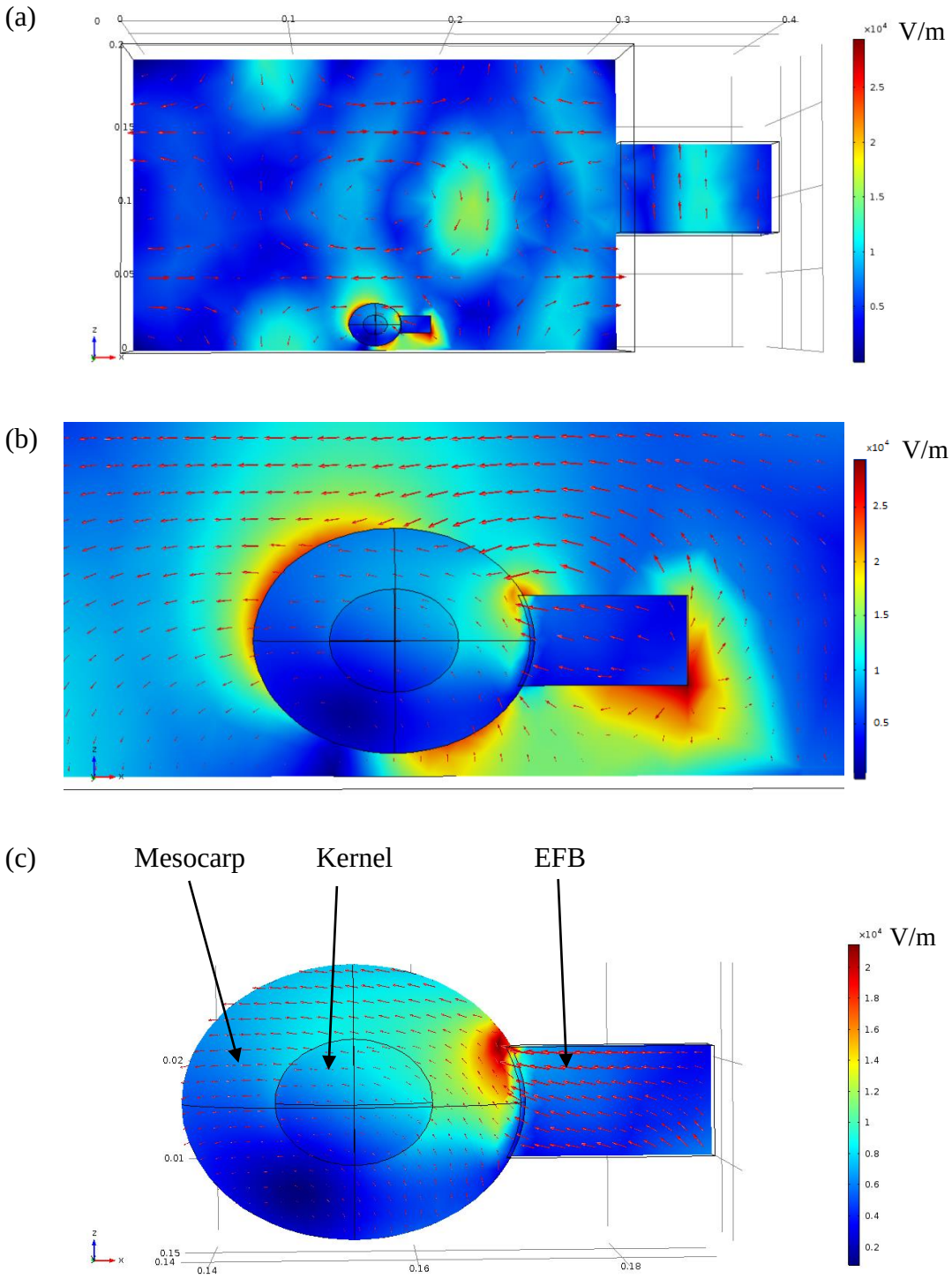

Figure 7.7: Electric distribution (a)in the microwave cavity, (b)around the FFB and (c)within the FFB viewed on x-z plane. The arrows in the figures indicate the direction of the electric fields for the 2.45 GHz incident waves.

7.4 Microwave power density generation and power lost

Figure 7.8(a) shows only microwave power density is generated within the kernel since evaporation, radiation and convection mechanisms are assumed to occur at the fruit (mesocarp) surface. In addition, comparing with Figure 6.13(a), generated microwave power density of kernel in a FFB does not manifest an exponential decrease; instead, it shows a gradual decrease at the beginning of microwave heating. The microwave absorption is dependent on the moisture content and dielectric properties. Therefore, the moisture diffusion in the kernel has significantly affected the microwave absorption since the kernel is encapsulated by mesocarp.

Evaporation, radiation and convection occurred on both the mesocarp and EFB. Their generated microwave power density showed a decreasing trend, due to the removal of moisture content. The generated microwave power density of the mesocarp in FFB is 25 times greater than the heated sliced mesocarp as shown in Figure 5.1. This is because the mesocarp in FFB has a larger volume for microwave power generation and it is yet placed at the location with stronger electric field intensity.

As shown in Figure 7.8(c), the generated microwave power of the EFB had greater density compared to the cooling mechanisms (convection, radiation and evaporation). This is due to a larger volume of EFB is exposed to the microwave energy. Thus, generated microwave power density into the FFB is significant. In EFB, power loss due to convection and radiation is relatively high compared to the power lost due to evaporation.

High generated microwave power density is initially observed in EFB region at t = 5 s (Figure 7.9(a)). As the drying continues, the high microwave power density moves to the interface region between EFB and mesocarp as shown in Figure 7.9(b) and 7.9(c).

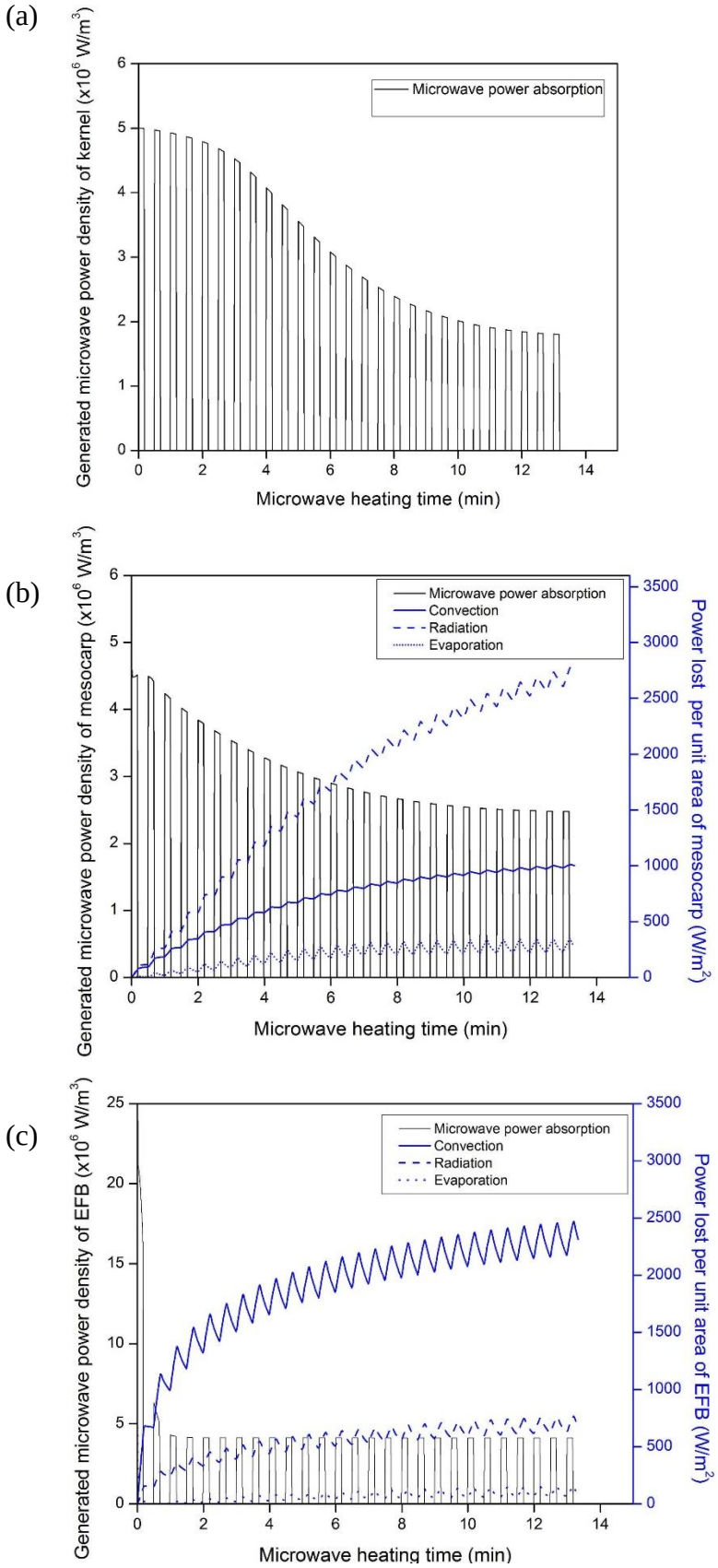

Figure 7.8: Power absorbed and lost for (a) a kernel, (b) mesocarp and (c) EFB due to various mechanism when subject to 180 W microwave power.

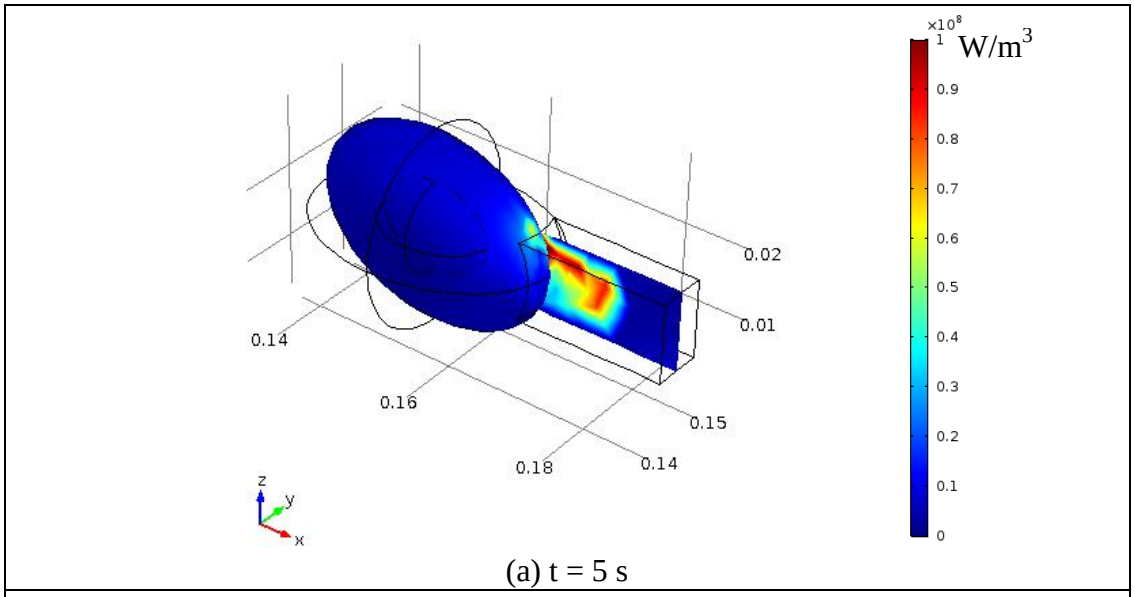

(a) t = 5 s

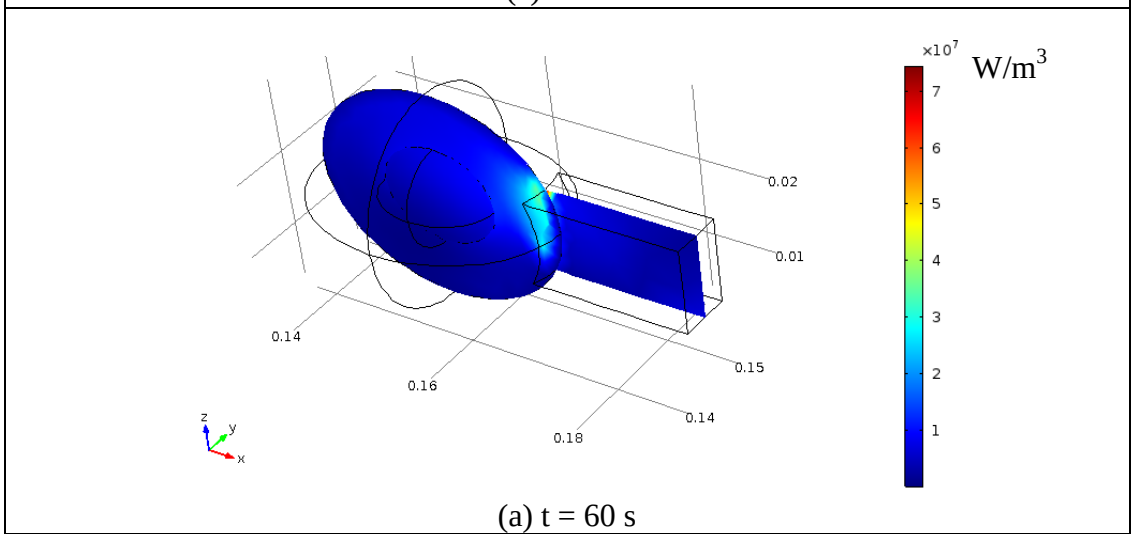

(a) t = 60 s

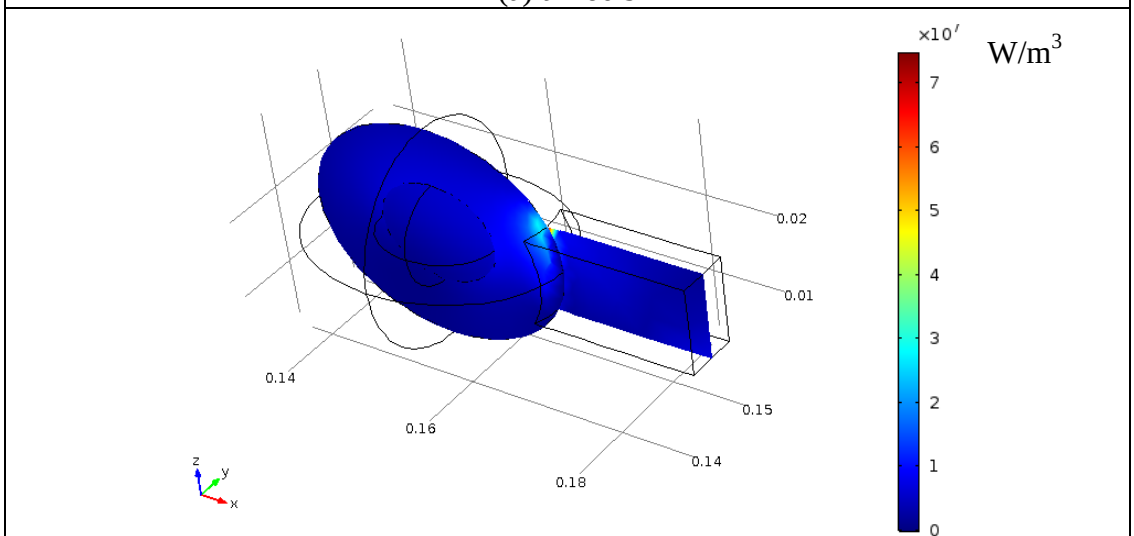

(c) t = 300 s

Figure 7.9: The microwave power density of FFB after (a) 5 s, (b) 1 min (60 s) and (c) 5 mins (300 s) of microwave heating.

Figure 7.10 shows the variation of electric field intensity and microwave power density along line 1 (Figure 7.2) at different times. The electric field intensity during ON phase is shown. The power density in EFB region changes sharply from t = 5 s to t = 60 s while in mesocarp and kernel regions, the power density change is relatively small. Although EFB is located at the location with the weak electric field intensity, it generates more microwave heat source at t = 5 s (0.1-8.8 W) compared to the kernel (0.2-1 W) and the mesocarp (0.1-2 W). This is due to EFB's higher dielectric properties determined from Section 4.1.2.

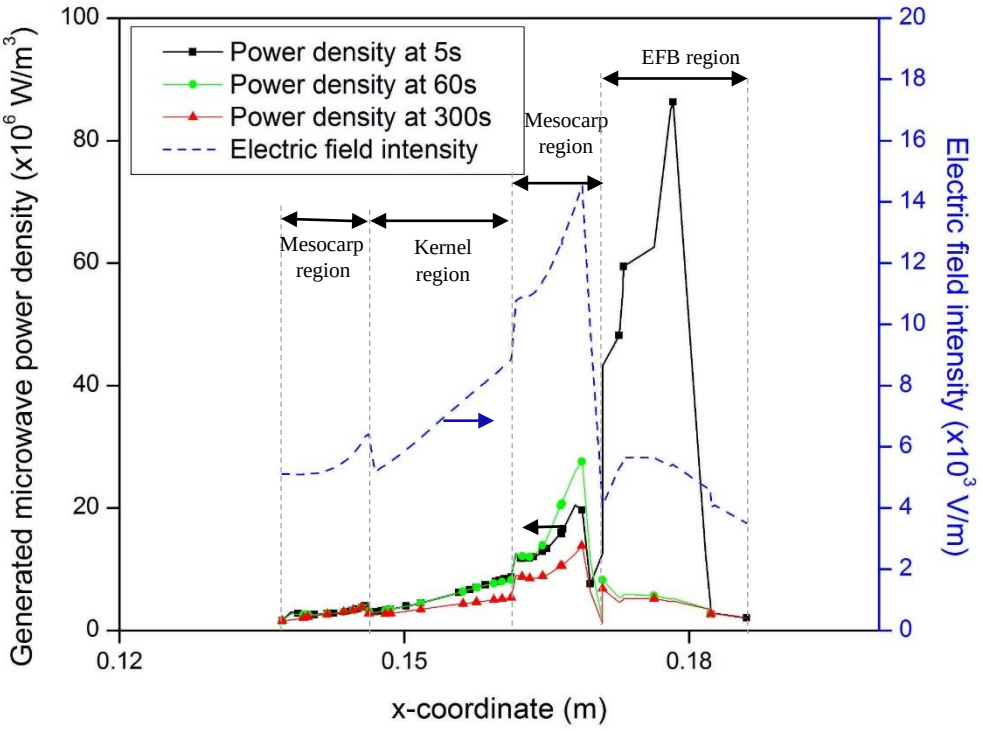

Figure 7.10: Electric field intensity and microwave power density absorbed by mesocarp, kernel and EFB at microwave exposure for 5 s, 60 s and 300 s.

7.5 Temperature and moisture distributions

Figure 7.11(a) shows that high temperature is found in EFB region at t = 5 s. As the microwave heating continues, the temperature continues to rise and mesocarp temperature is found to increase as shown in Figure 7.11(b)-(c). In comparison with the generated microwave power density, the temperature increase is resulted by the power density at 5 s. However, after 60 s and 300 s of microwave heating, the temperature in the mesocarp and kernel are distributed despite minimal generation of power density. In addition, it is interesting to note that mesocarp temperature

increases much quicker compared to the colder region of EFB. It is mainly because mesocarp has a higher thermal conductivity than EFB. Thus, it is easier for heat to be transported to region with a high thermal conductivity. Therefore, conduction plays a significant role in temperature distribution when the microwave irradiation is halted.

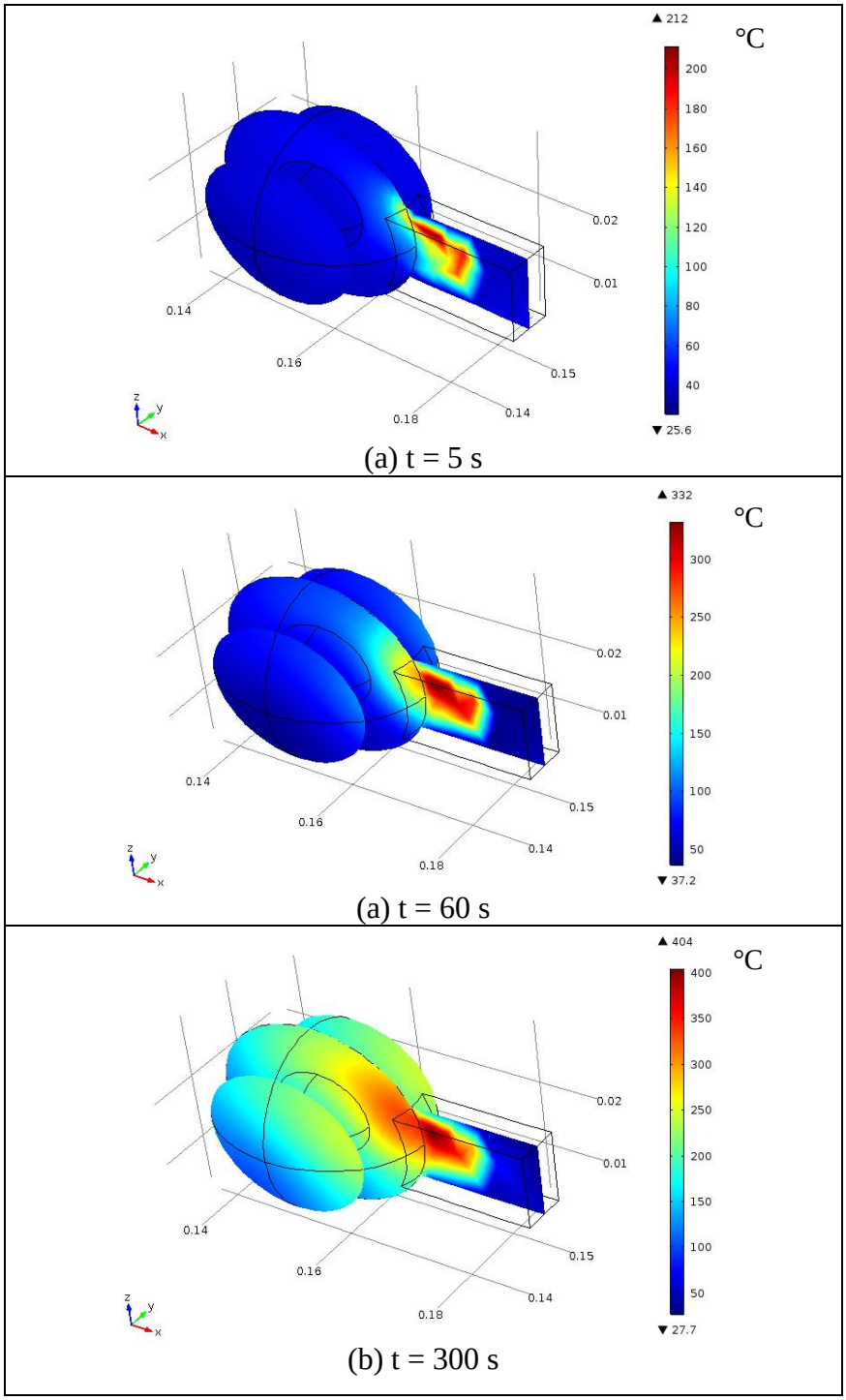

Figure 7.11: The temperature distributions in the FFB after (c) 1 min (60 s) and (d) 5 mins (300 s) of microwave heating.

Figure 7.12 and Figure 7.13 show the average temperatures and moisture contents of the kernel, the mesocarp and the EFB in the FFB. As shown in Figure 7.12 and 7.15, the temperature of the EFB reached a maximum temperature of 230 °C at 15 mins, where the EFB lost a total moisture content of 468 % d.b.. Mesocarp lost around 19 % d.b. of the average moisture content with an increased temperature up to 260 °C. The moisture content of the kernel is reduced to 7 % d.b. with the temperature increased up to 260 °C, after microwave irradiation for 10 mins. Nevertheless, EFB and mesocarp, are natural fibers and can decompose at temperature above 100 °C. Moreover, the quality of the oil in the mesocarp would be degraded. Furthermore, as mentioned, the temperature of the kernel and mesocarp should not exceed 100 °C, otherwise the vitamin E of kernel oil and palm oil would be destroyed. In this study, kernel and mesocarp reach 100 °C after being heated for 2 mins and 1.8 mins respectively, with the average moisture loss of 2.85 % and 4 %. In addition, a drastic drop of moisture content is observed at the beginning of the microwave drying process of the mesocarp and the EFB but this does not occur for the kernel. The sudden drop is owing to the rapid moisture lost from the surface of the mesocarp and the EFB by evaporation.

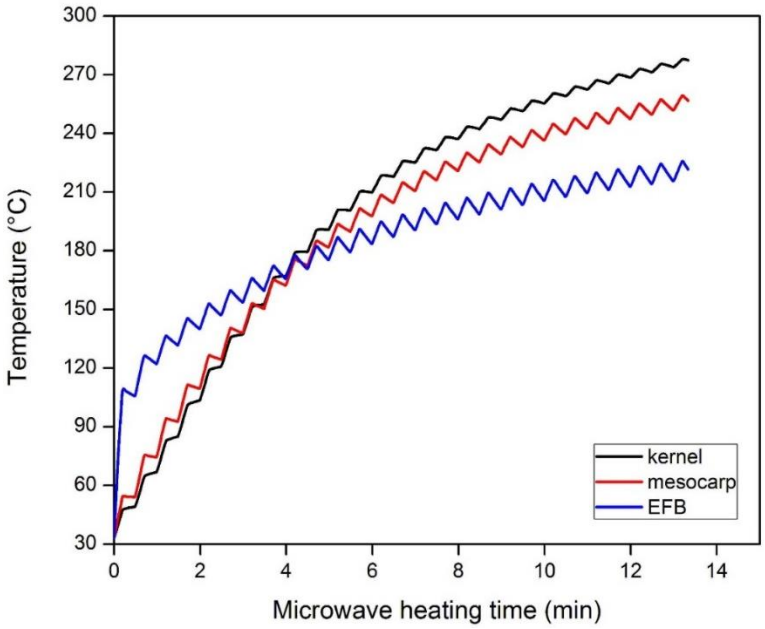

Figure 7.12: Average temperature of the kernel, mesocarp and EFB subjected to 180 W microwave power.

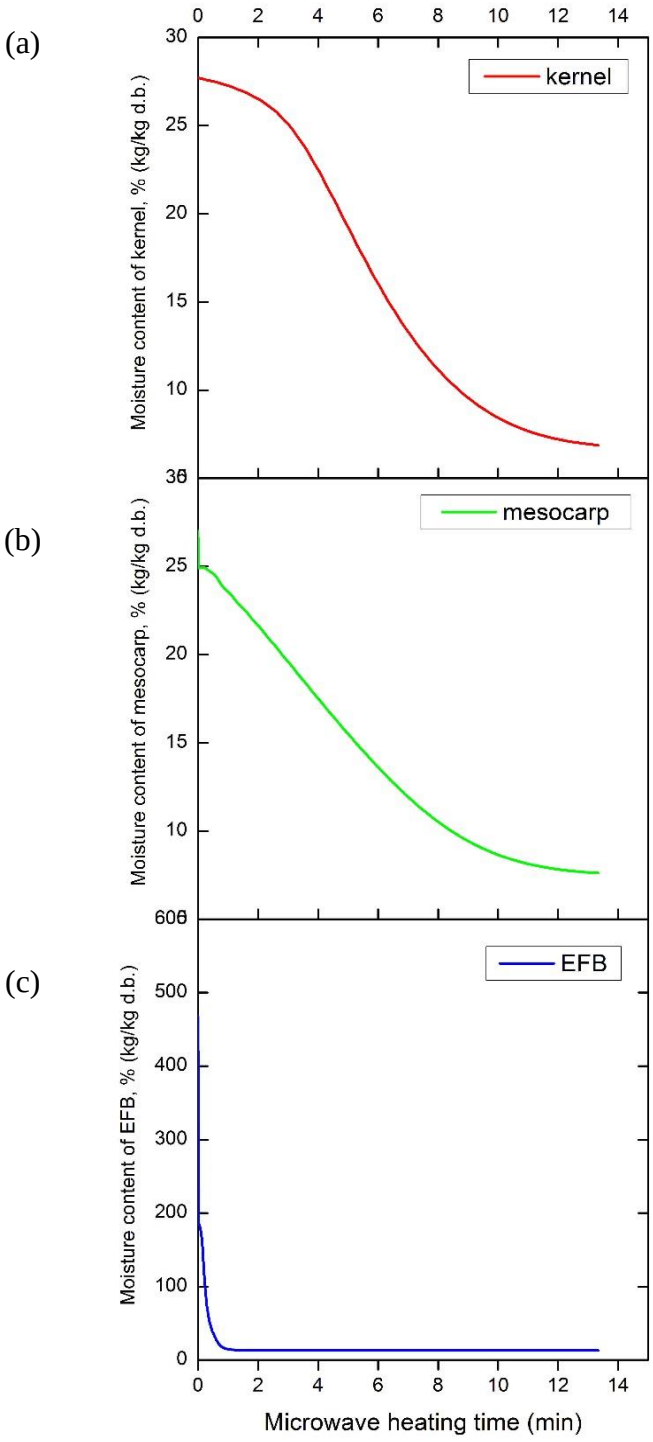

Figure 7.13: Average moisture content of (a) kernel, (b) mesocarp and (c) EFB subjected to 180 W microwave power.

Figure 7.14 shows the moisture contents along the FFB (red line in Figure 7.2) after exposed to intermittent microwave irradiation for 0 s, 50 s, 300 s and 600 s. Before the microwave heating commences, the moisture content of the kernel, the mesocarp and the EFB are 25.9 %, 28.2 % and 485.5 % respectively. After 50 s of microwave heating, it is observed that the moisture content of mesocarp has increased tremendously at the contact point between the mesocarp and EFB. The sudden increase of moisture content is due to the rapid moisture diffusion from the EFB to the mesocarp. The smaller generated microwave power density in the mesocarp (as shown in Figure 7.10) have lowered the heating process hence lower moisture diffusion compared to the EFB, thus resulted in the higher moisture content in the mesocarp. However, after 300 s of microwave heating, the moisture content of the above mentioned region has significantly reduced. The reduction of the moisture content is due to the evaporation, convection and moisture diffusion between the dried EFB and wet mesocarp. The differences in moisture concentrations between the mesocarp and EFB have caused the moisture diffusion.

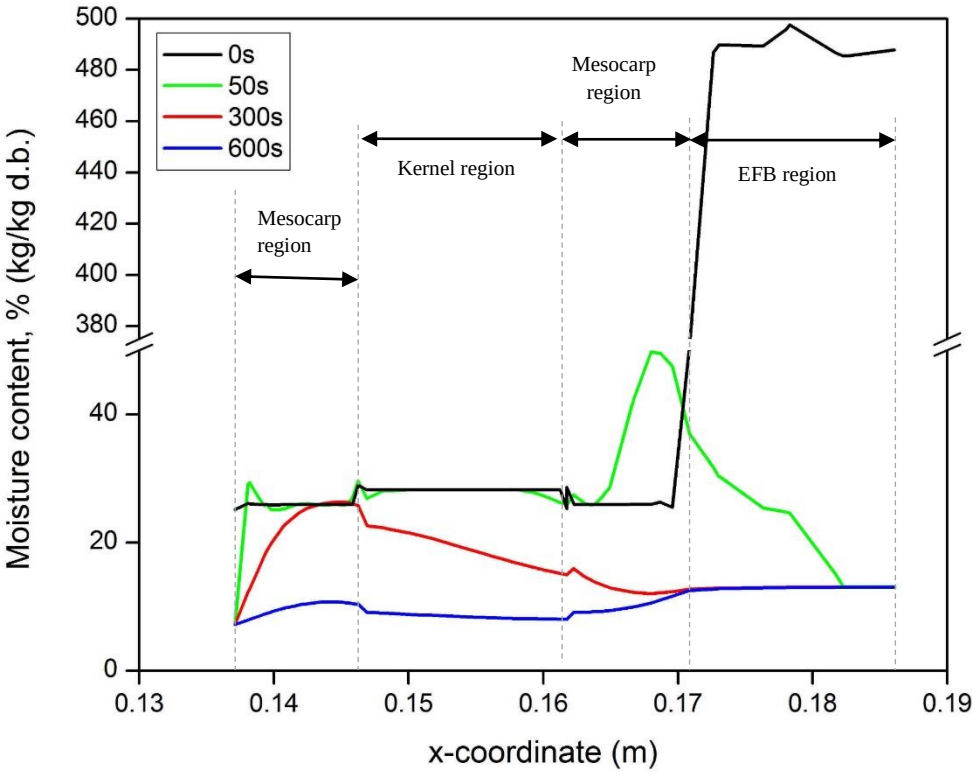

Figure 7.14: Moisture content in mesocarp, kernel and EFB at microwave exposure for the 50 s, 100 s and 300 s.

During the microwave heating of the FFB, the average penetration depths of kernel, mesocarp and EFB, as shown in Figure 7.15, are increased during microwave drying when the moistures of the samples are lost. The increase of the penetration depth on decreasing moisture content implies that the kernel, mesocarp and EFB at lower moisture content are not capable of absorbing the microwave radiation compared to the higher moisture content.

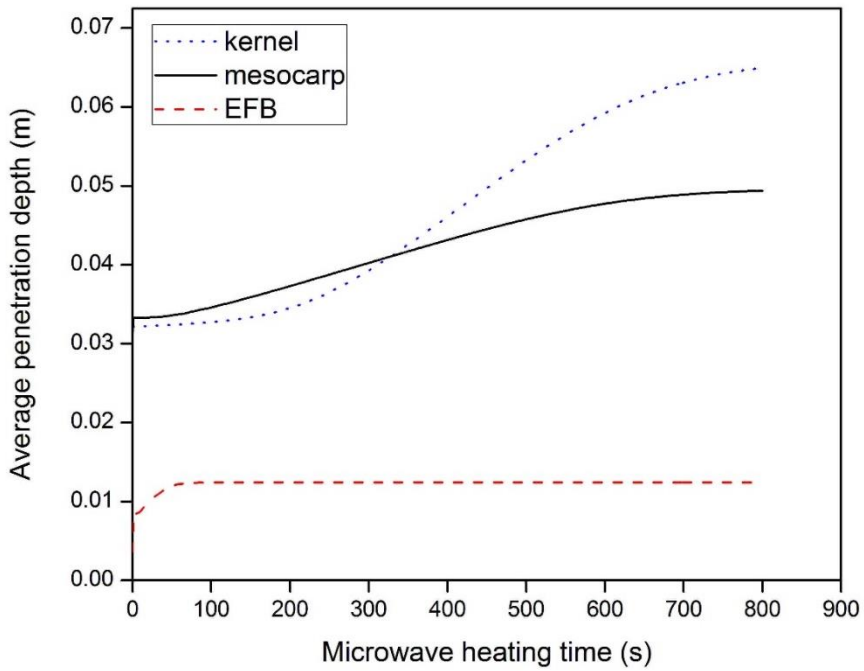

Figure 7.15: Average penetration depth of kernel, mesocarp and EFB during microwave heating and drying.

In this study, the values of dielectric constants and dielectric loss factor are seen to be decreasing as the moisture content is further reduced which leads to an increasing penetration depth. The penetration depth of fresh kernel, mesocarp and EFB is 50.8 %, 34.7 % and 76 % lower than the completely dried kernel, mesocarp and EFB respectively. Higher moisture content makes it more suitable to be used in microwave heating. In general, penetration depth should not be larger than the sample size in order to absorb the microwave energy. However, a very small penetration depth implies that the heating is dominant on the surface. The comparisons reveal that the EFB has better dielectric properties than the kernel and mesocarp. In addition, lower moisture content also shows a higher value of penetration depth.

Figure 7.16 shows the loss tangent for the heated and dried kernel, mesocarp and EFB. The loss tangent for kernel, mesocarp and EFB are decreased during microwave heating and drying. The loss tangent of the kernel, mesocarp and EFB ranges from 0.1-0.22, 0.19-0.25 and 1.36-2.4 respectively. With the reduction of moisture content of EFB to 48 %, the loss tangent of EFB decreases sharply to 1.4 and then decreases gradually to 1.36. On the other hand, the loss tangent of the kernel and mesocarp gradually decreases during the microwave heating and drying. The reduction of loss tangent is related to the decrease of the dielectric properties of the samples. As the dielectric loss factor increases more rapidly compared to the dielectric constant, this implies that loss tangent is more sensitive to the variation in dielectric loss factor in comparison to dielectric constant. EFB has a higher loss tangent relative to the kernel and mesocarp and due to the selective absorption of the electromagnetic energy, the EFB will undergo a greater degree of heating than the kernel and mesocarp. Therefore, during heating, heat will be transferred from the EFB to other regions by convection or conduction.

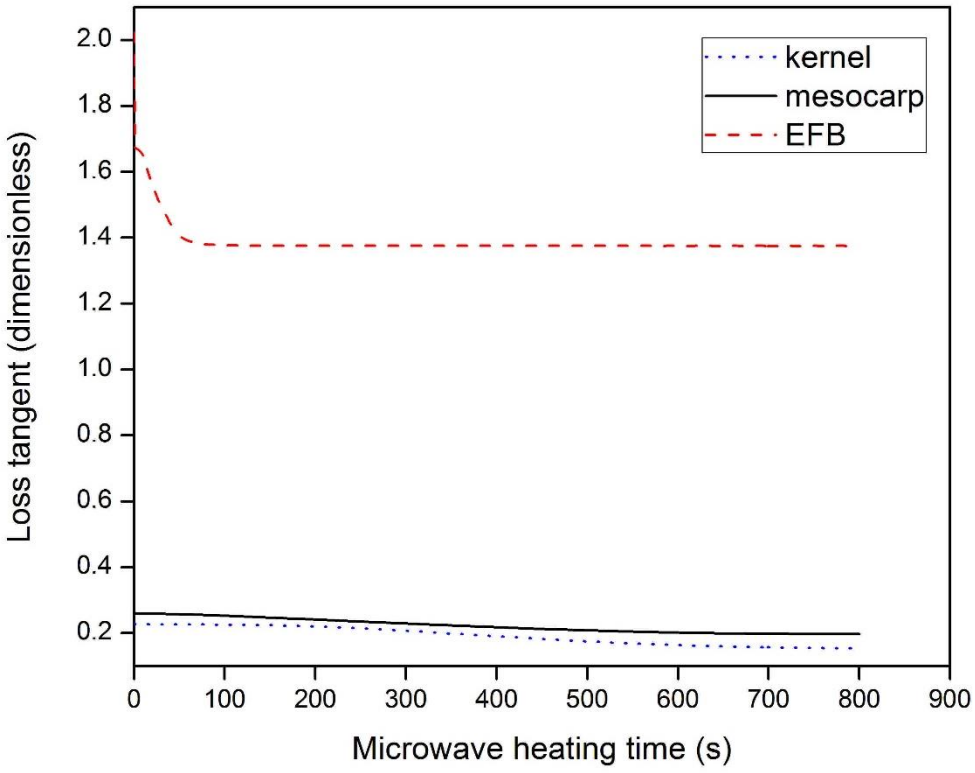

Figure 7.16: Loss tangent of kernel, mesocarp and EFB during microwave heating

The penetration depth of kernel, mesocarp and EFB is large at lower moisture content. The loss tangent of kernel, mesocarp and EFB decreases with moisture content. However, the penetration depth increases with it. The reduced loss tangent in the samples implies that a reduction of the heat generation rate during its interaction with microwave. The results show that EFB has better microwave power absorption and heat dissipation rate than the kernel and mesocarp. The determination of dielectric properties is essential to identify the penetration depth and loss tangent parameters which are important to understand the interactions between the microwave power absorption, heat dissipation and microwave energy.

7.6 Summary

A simulation study of FFB is carried out in this study. The generated microwave power density of the FFB is found to be positively correlated to the electric field strength in the microwave cavity. It is dependent on the dielectric properties. In the FFB, EFB is able to generate more heat compared to the kernel and mesocarp due to its greater dielectric properties. In addition to overheating, the low thermal conductivity of EFB also results in uneven temperature distribution.

CHAPTER 8
CONCLUSION AND RECOMMENDATION

This chapter concludes the key findings on the characterizations, the heating and drying behaviors and the effects of microwave heating on the oil palm kernel, mesocarp and EFB. In addition, findings from the simulation of microwave heating on the heat and mass transfer behavior of kernel, mesocarp, fresh empty fruit bunches (EFB) and fresh fruit bunches (FFB) are summarized. This chapter also covers the recommendations for future work in this area.

8.1 Characteristics of kernel, mesocarp and EFB

The initial moisture content of the kernel, mesocarp and EFB of *Elaeis guineensis* species are 28.2 % d.b., 25.9 % d.b. and 485.5 % d.b respectively. It is found that the moisture content strongly influences on the dielectric properties of the samples. The fresh EFB are found to have the greatest range of dielectric constant ($3.09 \leq \varepsilon_r' \leq 24.4$) and loss factor ($0.68 \leq \varepsilon_r'' \leq 12.8$) compared to mesocarp ($3.28 \leq \varepsilon_r' \leq 4.7$, $0.29 \leq \varepsilon_r'' \leq 1.10$) and kernel ($2.88 \leq \varepsilon_r' \leq 6.2$, $0.036 \leq \varepsilon_r'' \leq 1.08$). The results indicated that EFB has great dielectric properties to absorb microwave energy, followed by mesocarp and kernel. However, slower temperature elevation can preserve the extracted oil quality from the mesocarp and kernel.

On the other hand, the thermal conductivity is compared to the estimated values from the literature. The thermal conductivity is found to be 0.458 and 0.028 W/(m·K) for the mesocarp and the EFB, whereas the kernel is found to be 0.68 W/(m·K). Furthermore, TGA is conducted to avoid the decomposition of the oil palm fruits and bunches. The analysis showed the decomposition of the kernel, mesocarp and EFB started from 100 °C. Therefore, the heated sample must keep below 100 °C to avoid sample degradation.

8.2 Effects of microwave heating and drying on kernel, mesocarp and EFB

In order to ease the fruit detachment and oil extraction, a low mechanical strength, i.e. elastic modulus and yield strength, is preferable. However, the

microwave heating process has been shown to increase the elastic modulus and yield stresses of the kernel, mesocarp and EFB. The increasing elasticity of modulus is an unavoidable consequence of microwave heating. A low mechanical strength is obtained at a higher moisture content. Correlations of elastic modulus and yield stress as a function of moisture content are obtained for kernel, mesocarp and EFB. The correlations are useful for the shrinkage study of the kernel, mesocarp and EFB. In addition, no significant change and physical damages occur on the surface of the kernel, mesocarp and EFB samples.

8.3 Heat and mass transfers of oil palm kernel, mesocarp and EFB

A multiphysics model which account for electromagnetic wave, conservation of energy and moisture content is developed in the current work. The developed model shows good agreement between the experimental and simulation results.

The temperature increase in the sample not only depends on the electric field intensity and the dielectric properties of the samples but also on the physical properties determined from the characterization studies such as thermal conductivity, specific heat capacity and density. Low specific heat capacity and density of EFB cause the higher temperature rise in the EFB compared to the kernel and the mesocarp. Furthermore, a small difference between the volume-averaged and surface-averaged temperature suggests that the surface temperature of kernel and mesocarp can be used as an approximation as their average volumetric temperature.

Minimum temperature occurs on the sample surface which is due to the surface cooling mechanisms. Among the mechanisms, radiation and convection are dominant cooling mechanisms to reduce the surface temperature, whereby evaporation is significant when sample has high moisture content. In addition, surface convection and evaporation lead to rapid moisture loss on the sample surface and result in low moisture content on sample surface. A higher sample temperature and moisture concentration gradient promotes the moisture diffusion process to sample's dry surface.

Both the moisture concentration and temperature gradients have contributed to the heat and mass transfer fluxes. Therefore, both the heat and mass transfers must be

modelled simultaneously in order to predict the temperature and moisture content distributions accurately.

8.4 Heat and mass transfers of FFB

The interaction of microwave with the FFB is studied. The microwave power generation is dependent on the electric field intensity and dielectric loss factor on the FFB. The electric field intensity is affected by size, geometry and location of the sample whereby the dielectric loss factor is affected by the moisture content of the sample.

In addition, the penetration depth and the loss tangent which are dependent on the dielectric properties of the samples reveal that low penetration depth and high loss tangent of the samples are obtained at high moisture content. A higher loss tangent in EFB explains that the EFB undergoes a greater degree of heating than the kernel and mesocarp.

In the case study, EFB generates more microwave heat source compared to the kernel and the mesocarp, despite EFB is placed at the location with weaker electric field intensity. Therefore, the dielectric properties of the sample are dominant in microwave power generation. Hence, EFB achieves a high temperature and rapid moisture lost compared to the kernel and the mesocarp. Heat energy in EFB is transferred quicker to the mesocarp than to the colder region in the EFB because of the higher thermal conductivity of mesocarp. In addition, the differences in moisture concentrations between the mesocarp and EFB have caused their moisture diffusion, and leads to the quicker reduction in moisture content of the mesocarp and the kernel. Although microwave heating of the FFB provides a faster heating and drying for the mesocarp and kernel, overheating might be an issue.

8.5 Significance of the current work

The significance of this work is the fundamental study of microwave heating of kernel, mesocarp, EFB and FFB through experimental characterization and multiphysics modeling. The dielectric properties is a function of moisture content,

thus the dielectric properties of the samples changes during microwave heating and drying. Hence the microwave power generation is affected throughout the microwave heating and drying processes.

This study indicates the location of the heated sample is important to be identified in order to avoid thermal runaway in the sample.

In addition, this study also determines the characteristics of the kernel, mesocarp and EFB such as dielectric properties, thermal conductivity and thermal behavior. Furthermore, the effect of microwave energy on kernel, mesocarp and EFB towards the mechanical behavior and the microstructure changes are examined. The parameters such as penetration depth and loss tangent which are important in characterizing the temperature distribution in microwave heated samples are investigated. These findings provide a better illustration of the interaction of oil palm fruit components with microwave energy.

8.6 Recommendations for future work

The recommendations for future work are categorized into three sections; characterization, quality evaluations and improvements in modeling.

First, for the sample characterizations, the dielectric properties which are the essential parameters, depend on various parameters such as temperature (Lovás et al., 2010, Hossan and Dutta, 2012, Uyar et al., 2016) and density (Nelson and Trabelsi, 2012) of the samples. In addition, mechanical properties of the samples were also found to be influenced by the temperature. Therefore, future studies could be carried out to determine the dielectric and mechanical properties as a function of temperature. for kernels, mesocarp and EFB.

Besides, the chemical compositions of the fruit and oil such as fatty acid and vitamin E should also be determined after microwave heating. This analysis would help to determine the optimum temperature and moisture content to produce a better quality of palm oils. In addition, researchers could pay attention to provide microwave heating to the kernels, mesocarp and EFB individually because the high dielectric properties of EFB leads to a more rapid heat generation and moisture loss. The temperatures of kernels and mesocarp should be kept at optimum level to

preserve the oil quality. Furthermore, parameters such as the oven cavity size, location of microwave port, microwave frequency and the location of samples in the microwave oven cavity are important factors and should be considered to obtain an optimum sample's temperature and moisture content.

Moreover, researchers discovered that the temperature and moisture content are also influenced by shrinkage of an object, which can be predicted from its mechanical strength. Mathematical models which incorporate the shrinkage effect could predict a more accurate temperature and moisture content history. Furthermore, various microwave frequencies shall be compared as the microwave frequency can affect the electric field distributions and thus, changing the heating pattern. In addition, since the heat generation of the FFB is highly dependent on the electric field strength, various conditions such as locations, sizes, application of turntable and duration of microwave on-off supplies should be included in order to avoid hotspots and to provide a more uniform temperature and moisture distribution of the FFB.

REFERENCE

Abbas, S. A., S. Ali, S. I. M. Halim, A. Fakhrul-Razi, R. Yunus, and T. S. Y. Choong. 2006. "Effect of thermal softening on the textural properties of palm oil fruitlets." *Journal of Food Engineering* 76 (4):626-631. doi: 10.1016/j.jfoodeng.2005.06.013.

Abdullah, M. A., M. S. Nazir, M. R. Raza, B. A. Wahjoedi, and A. W. Yussof. 2016. "Autoclave and ultra-sonication treatments of oil palm empty fruit bunch fibers for cellulose extraction and its polypropylene composite properties." *Journal of Cleaner Production* 126:686-697. doi: 10.1016/j.jclepro.2016.03.107.

Abdullah, N., and F. Sulaiman. 2013. "The properties of the washed empty fruit bunches of oil palm." *Journal of Physical Science* 24 (2):117-137.

Akinoso, R., and A. G. O. Raji. 2011. "Physical properties of fruit, nut and kernel of oil palm." *International Agrophysics* 25:85-88.

Ali, S. b. M. 2008. "Effect of Moisture on Tensile Properties of Oil Palm Empty Fruit Bunch (EFB) Unsaturated Polyster Composites." Bachelor Degree, Faculty of Engineering, University Malaysia Sarawak.

Alibas, I. 2007. "Energy Consumption and Colour Characteristics of Nettle Leaves during Microwave, Vacuum and Convective Drying." *Biosystems Engineering* 96 (4):495-502. doi: 10.1016/j.biosystemseng.2006.12.011.

Alibas, I. 2009. "Microwave, Vacuum, and Air Drying Characteristics of Collard Leaves." *Drying Technology* 27 (11):1266-1273. doi: 10.1080/07373930903267773.

Altan, A., and M. Maskan. 2005. "Microwave assisted drying of short-cut (ditalini) macaroni: Drying characteristics and effect of drying processes on starch properties." *Food Research International* 38:787-796.

Amestro, P. R., and I. S. Du. 2000. "Multifrontal parallel distributed symmetric and unsymmetric solvers." *Comput. Methods Appl. Mech. Eng.* 184:501-520.

Anazodo, U. G. N., and E. R. Norris. 1981. "Effects of genetic and cultural, on the mechanical properties of corncobs." *Journal of Agricultural Engineering Research* 26:97-107.

Arballo, J. R., L. A. Campañone, and R. H. Mascheroni. 2010. "Modeling of Microwave Drying of Fruits." *Drying Technology* 28 (10):1178-1184. doi: 10.1080/07373937.2010.493253.

Aremu, A. K., and O. K. Fadele. 2011. "Study of some properties of doum palm fruit (Hyphaene thebaica Mart.) in relation to moisture content " *African Journal of Agricultural Research* 6 (15):3597-3602.

ASAE. 1982. Standard: ASAE S352.1. Moisture measurement-Grains and seeds. Michigan, USA.

Asr, M. H., M. N. Ibrahim, M. N. Mokhtar, K. F. M. Yunos, and N. A. B. Ibrahim. 2012. "Selected properties of oil palm kernel." International Conference on Agricultural and Food Engineering for Life (Cafei2012), Selangor, Malaysia.

Ayappa, K. G., H. T. Davis, G. Crapiste, E. A. Davis, and J. Gordon. 1991. "Microwave heating: an evaluation of power formulations." *Chemical Engineering Science* 46 (4):1001-1016.

Baharuddin, A. S., A. Sulaiman, D. H. Kim, M. N. Mokhtar, M. A. Hassan, M. Wakisaka, Y. Shirai, and H. Nishida. 2013. "Selective component degradation of oil palm empty fruit bunches (OPEFB) using high-pressure

steam." *Biomass and Bioenergy* 55:268-275. doi: 10.1016/j.biombioe.2013.02.013.

Barba, A. A., and M. d'Amore. 2012. Relevance of Dielectric Properties in Microwave Assisted Processes Croatia, European Union: InTech.

Barbosa-Cánovas, G. V., and H. Vega-Mercado. 1996. *Dehydration of Foods*. 1 ed: Springer.

Berk, Z. 2013. "Chapter 3 - Heat and Mass Transfer: Basic Principles." In *Food Process Engineering and Technology (Second Edition)*, 77-125. San Diego: Academic Press.

Bilbao-Sa´inz, C., A. Andre´s, A. Chiralt, and P. Fito. 2006. " Microwaves phenomena during drying of apple cylinders." *Microwaves phenomena during drying of apple cylinders* 74 (1):160-167. doi: 10.1016/j.jfoodeng.2005.02.028.

Birla, S., S. Wang, J. Tang, and G. Tiwari. 2008. "Characterization of Radio Frequency Heating of Fresh Fruits Influenced by Dielectric Properties." *Journal of Food Engineering* 89:390–398. doi: 10.1016/j.jfoodeng.2008.05.021.

Birla, S. L., S. Wang, and J. Tang. 2008. "Computer simulation of radio frequency heating of model fruit immersed in water." *Journal of Food Engineering* 84 (2):270-280. doi: 10.1016/j.jfoodeng.2007.05.020.

Boreddy, S. R., and J. Subbiah. 2016. "Temperature and moisture dependent dielectric properties of egg white powder." *Journal of Food Engineering* 168:60-67. doi: 10.1016/j.jfoodeng.2015.07.023.

Brezing, D. 1986. "African palm by-products in primary processing plants: treatment of effluents " IV Mesa Redonda Latinoamericanasobre Palma Aceitera, Valledupar Colombia, 8-12 June.

Caccavale, P., M. V. De Bonis, and G. Ruocco. 2016. "Conjugate heat and mass transfer in drying: A modeling review." *Journal of Food Engineering* 176:28-35. doi: 10.1016/j.jfoodeng.2015.08.031.

Calay, R. K., M. Newborough, D. Probert, and P. S. Calay. 1995. "Predictive equations for the dielectric properties of foods." *International Journal of Food Science and Technology* 29:699-713.

Chan, S. Y. 1985. "Modeling and Simulation of the Fresh Fruit bunches (FFB) during Sterilization Process." Master Thesis, Universiti Malaya.

Chen, H., J. Tang, and F. Liu. 2006. "Coupled Simulation of an Electromagnetic Heating Process Using the Finite Difference Time Domain Method." *Journal of Microwave Power and Electromagnetic Energy* 41 (3):50-68. doi: 10.1080/08327823.2006.11688563.

Chen, J., K. Pitchai, S. Birla, D. Jones, M. Negahban, and J. Subbiah. 2016. "Modeling heat and mass transport during microwave heating of frozen food rotating on a turntable." *Food and Bioproducts Processing* 99:116-127. doi: 10.1016/j.fbp.2016.04.009.

Cheng, J., J. Zhou, Y. Li, J. Liu, and K. Cen. 2008. "Improvement of coal water slurry property through coal physicochemical modifications by microwave irradiation and thermal heat." *Energy & Fuels* 22 (4):2422-2428. doi: 10.1021/ef7005244.

Cheng, S. F., N. L. Mohd, and C. H. Chuah. 2011. "Microwave pretreatment: A clean and dry method for palm oil production." *Industrial Crops and Products* 34 (1):967-971. doi: 10.1016/j.jfoodeng.2014.08.004.

Chow, M. C., and A. N. Ma. 2007. "Processing of fresh palm fruits using microwaves." *Journal of Microwave Power and Electromagnetic Energy* 40 (3):165-173.

Constant, T., C. Moyne, and P. Perre. 1996. "Drying with internal heat generation: Theoretical aspects and application to microwave heating." *AIChE Journal* 42 (2):359-368. doi: 10.1002/aic.690420206.

Contreras, C., M. E. Martín-Esparza, A. Chiralt, and N. Martínez-Navarrete. 2008. "Influence of microwave application on convective drying: Effects on drying kinetics, and optical and mechanical properties of apple and strawberry." *Journal of Food Engineering* 88 (1):55-64. doi: 10.1016/j.jfoodeng.2008.01.014.

Crank, J. 1975. *The mathematics of diffusion*. London: Oxford University Press.

Cui, Z.-W., C.-Y. Li, C.-F. Song, and Y. Song. 2008. "Combined Microwave-Vacuum and Freeze Drying of Carrot and Apple Chips." *Drying Technology* 26 (12):1517-1523. doi: 10.1080/07373930802463960.

Curet, S., O. Rouaud, and L. Boillereaux. 2008. "Microwave tempering and heating in a single-mode cavity: Numerical and experimental investigations." *Chemical Engineering and Processing: Process Intensification* 47 (9–10):1656-1665. doi: 10.1016/j.cep.2007.09.011.

Darby, S. 2014. "Palm Oil Facts & Figures ". Sime Darby. http://www.simedarby.com/upload/Palm_Oil_Facts_and_Figures.pdf.

Datta, A. K., and R. C. Anantheswaran. 2001. *Handbook of Microwave Technology for Food Application*. New York, New York: Marcell Dekker, Inc.

Decareau, R. V., and R. A. Peterson. 1986. *Microwave processing and engineering*: VCH.

Demirhan, E., and B. Özbek. 2009. "Color Change Kinetics of Microwave-Dried Basil." *Drying Technology* 27 (1):156-166. doi: 10.1080/07373930802566101.

Dincer, I., and S. Dost. 1995. "An analytical model for moisture diffusion in solid objects during drying." *Drying Technology* 13 (1-2):425-435.

Dincer, I., and M. M. Hussain. 2002. "Development of a new Bi-Di correlation for solids drying." *Internacional Journal of Heat and Mass Transfer* 45:3065-3069.

Dumas, C., and G. S. Mittal. 2002. "Heat and Mass Transfer Properties of Pizza during Baking." *International Journal of Food Properties* 5 (1):161-177. doi: 10.1081/JFP-120015599.

Fan, D., L. Wang, S. Ma, W. Ma, X. Liu, J. Huang, J. Zhao, H. Zhang, and W. Chen. 2013. "Structural variation of rice starch in response to temperature during microwave heating before gelatinisation." *Carbohydrate Polymers* 92 (2):1249-1255. doi: 10.1016/j.carbpol.2012.10.053.

Fazaeli, M., M. Tahmasebi, and Z. E. Djomeh. 2012. "Characterization of food texture: application of Microscopic technology." *Current Microscopy Contributions to Advances in Science and Technology* 2 (5):855-871.

Feng, H., J. Tang, and R. P. Cavalieri. 2002. "Dielectric properties of dehydrated apples as affected by moisture and temperature." *Trans. ASAE* 45 (1):129-135.

Funebo, T., and T. Ohlson. 1999. "Dielectric Properties of Fruits and Vegetables as a Function of Temperature and Moisture Content Dielectric Properties of Fruits and Vegetables as a Function of Temperature and Moisture Content."

Journal of Microwave Power and Electromagnetic Energy 34 (1):42-54. doi: 10.1080/08327823.1999.11688387.

Gao, M., J. Tang, J. A. Johnson, and S. Wang. 2012. "Dielectric properties of ground almond shells in the development of radio frequency and microwave pasteurization." *Journal of Food Engineering* 112 (4):282-287. doi: 10.1016/j.jfoodeng.2012.05.011.

Ghanem, T. H. 2010. "Dielectric Properties of Liquid Foods Affected by Moisture Contents and Temperatures." *Misr Journal Of Agricultural Engineering* 27 (2):688-698.

Ghazanfari, A., S. Emami, L. G. Tabil, and S. Panigrahi. 2006. "Thin-Layer Drying of Flax Fiber: I. Analysis of Modeling Using Fick's Second Law of Diffusion." *Drying Technology* 24 (12):1631-1635. doi: 10.1080/07373930601031430.

Gómez-de la Cruz, F. J., J. M. Palomar-Carnicero, P. J. Casanova-Peláez, and F. Cruz-Peragón. 2015. "Experimental determination of effective moisture diffusivity during the drying of clean olive stone: Dependence of temperature, moisture content and sample thickness." *Fuel Processing Technology* 137:320-326. doi: 10.1016/j.fuproc.2015.03.018.

Gottschalk, K., M. Linke, C. Mészáros, and I. Farkas. 2007. "Modeling Condensation and Evaporation on Fruit Surface." *Drying Technology* 25 (7-8):1237-1242. doi: 10.1080/07373930701438667.

Guiné, R. P. F., A. C. Cruz, and M. Mendes. 2012. "Convective Drying of Apples: Kinetic Study, Evaluation of Mass Transfer Properties and Data Analysis using Artificial Neural Networks." *International Journal of Food Engineering* 10 (2):281-299.

Güner, M., E. Dursun, and İ. G. Dursun. 2003. "Mechanical Behaviour of Hazelnut under Compression Loading." *Biosystems Engineering* 85 (4):485-491. doi: 10.1016/S1537-5110(03)00089-8.

Guo, W., Y. Liu, X. Zhu, and S. Wang. 2011. "Temperature-dependent dielectric properties of honey associated with dielectric heating." *Journal of Food Engineering* 102 (3):209-216. doi: 10.1016/j.jfoodeng.2010.08.016.

Hadi, A. b. A., P. D. I. D. A. W. Mohammad, and P. I. D. M. S. Takriff. 2015. "The study of Temperature Distribution for Fresh Fruit Bunch during Sterilization Process." *Journal of Industrial Engineering Research* 1 (6):25-32.

Hadi, N. m. A., N. M. Han, C. Y. May, and M. A. Ngan. 2012. "Dry Heating of Palm Fruits: Effect on Selected Parameters." *American Journal of Engineering and Applied Sciences* 5 (2):128-131. doi: 10.3844.

Haghighi, K., and J. J. Segerlind. 1988. "Modeling Simultaneous Heat and Mass Transfer in an Isotropic Sphere- A Finite Element approach." *American Society of Agricultural Engineers* 31 (2):629-637.

Hansen, J. D. 1992. "Heating Curve Models of Quarantine Treatments Against Insect Pests." *Journal of Economic Entomology* 85 (5):1846-1854. doi: 10.1093/jee/85.5.1846.

Hassan, S., A. Tesfamichael, and M. F. Mohd Nor. 2014. "Comparison Study of Thermal Insulation Characteristics from Oil Palm Fibre." *MATEC Web of Conferences* 13:02016.

Hawlader, M. N. A., J. C. Ho, and Z. Qing. 1999. "A mathematical model for drying of shrinking materials." *Drying Technology* 17 (1-2):27-47. doi: 10.1080/07373939908917517.

Hazir, M. H. M., and A. R. M. Shariff. 2011. "Oil Palm Physical and Optical Characteristics from Two Different Planting Materials." *Journal of Applied Sciences, Engineering and Technology* 3 (9):953-962.

Hemis, M., C. B. Singh, and D. S. Jayas. 2011. "Microwave-Assisted Thin Layer Drying of Wheat." *Drying Technology* 29 (10):1240-1247. doi: 10.1080/07373937.2011.584999.

Hii, C. L., C. L. Law, and M. C. Law. 2013. "Simulation of heat and mass transfer of cocoa beans under stepwise drying conditions in a heat pump dryer." *Applied Thermal Engineering* 54 (1):264-271. doi: 10.1016/j.applthermaleng.2013.02.010.

Hippel, A. R. v. 1954. *Dielectric Properties and Waves*. New York: John Wiley.

Ho, J. C., S. K. Chou, K. J. Chua, A. S. Mujumdar, and M. N. A. Hawlader. 2002. "Analytical study of cyclic temperature drying: effect on drying kinetics and product quality." *Journal of Food Engineering* 51 (1):65-75. doi: 10.1016/S0260-8774(01)00038-3.

Ho, L. S., A. Nair, H. M. Yusof, H. Kulaveerasingam, and M. S. Jangi. 2014. "Morphometry of lipid bodies in embryo, kernel and mesocarp of oil palm: Its relationship to yield." *American Journal of Plant Sciences* 5:1163-1173.

Hong, Y.-d., B.-q. Lin, H. Li, H.-m. Dai, C.-j. Zhu, and H. Yao. 2016. "Three-dimensional simulation of microwave heating coal sample with varying parameters." *Applied Thermal Engineering* 93:1145-1154. doi: 10.1016/j.applthermaleng.2015.10.041.

Hossan, M. R., and P. Dutta. 2012. "Effects of temperature dependent properties in electromagnetic heating." *International Journal of Heat and Mass Transfer* 55 (13–14):3412-3422. doi: 10.1016/j.ijheatmasstransfer.2012.02.072.

Hussain, S. A., S. Bano, H. S. Yeoh, and O. Rozita. 2013. "Simulation on temperature distribution of oil palm empty fruit bunches during microwave prylosis process." *Asia-Pacific Journal of Chemical Engineering* 9 (1):39-49.

Ibrahim, M. H., W. R. W. Daud, and M. Z. M. Talib. 1997. "Drying characteristics of oil palm kernels." *Drying Technology* 15 (3&4):1103-1117.

Ibrahim, S. H., W. K. Sia, B. A., N. M.N.M., and A. R. 2014. "Thermal performance of oil palm fibre and paper pulp as the insulation materials." *UNIMAS e-Journal of Civil Engineering* 1:22-28.

Igwe, J. C., and C. C. Onyegbado. 2007. "A Review of Palm Oil Mill Effluent (Pome) Water Treatment." *Global Journal of Environmental Research* 1 (2):54-62.

Ip, R. W. L., and E. I. C. Wan. 2012. "The New Use of Diffusion Theories for the Design of Heat Setting Process in Fabric Drying." In *Advances in Modeling of Fluid Dynamics*, edited by Chaoqun Liu. Rijeka, Croatia: InTech.

Ismail, M. H. S., M. K. A. Aziz, and N. A. Morad. 2009. "A Systems Approach to Mathematical Modelling of Sterilisation Process in Palm Oil Mill." *European Journal of Scientific Research* 35 (4):583-592.

Izli, N., and E. Isik. 2015. "Color and microstructure properties of tomatoes dried by microwave, convective, and microwave-convective methods." *International Journal of Food Properties* 18 (2):241-249. doi: 10.1080/10942912.2013.829492.

Jie, W. S., H. Abdullah, N. Yusof, and Z. Abbas. 2015. "Dielectric properies of oil palm trunk core." *Journal of Clean Energy Technologies* 3 (6):422-427. doi: 10.7763/JOCET.2015.V3.235.

Jun, W., Z. Jing-ping, W. Jian-ping, and X. Nai-zhang. 1998. "Modeling Simultaneous Heat and Mass Transfer for Microwave Drying on Apple." *Drying Technology* 17 (9):1927-1934. doi: 10.1080/07373939908917662.

Kabutey, A., M. Divišová, L. Sedláček, W. E. Boatri, T. Svatoňová, and R. Sigalingging. 2013. "Mechanical behaviour of oil palm kernels (Elaeis Guineensis)." *Scientia Agriculturae Bohemica* 44:18-22. doi: 10.7160/sab.2013.440104.

Kamyab, H., M. F. M. Din, A. Keyvanfar, M. Z. A. Majid, A. Talaiekhozani, A. Shafaghat, C. T. Lee, L. J. Shiun, and H. H. Ismail. 2015. "Efficiency of Microalgae Chlamydomonas on the Removal of Pollutants from Palm Oil Mill Effluent (POME)." *Energy Procedia* 75:2400-2408. doi: 10.1016/j.egypro.2015.07.190.

Kang, Y. S., C. K. Spillman, J. L. Steel, and D. S. Chung. 1995. "Mechanical properties of wheat." *Transactions of the ASAE* 38:573-578.

Kemp, I. C., and D. E. Oakley. 2002. "Modelling of Particulate Drying in Theory and Practice." *Drying Technology* 20 (9):1699-1750. doi: 10.1081/DRT-120015410.

Kong, F., and R. P. Singh. 2011. "2 - Chemical deterioration and physical instability of foods and beverages." In *Food and Beverage Stability and Shelf Life*, edited by David Kilcast and Persis Subramaniam, 29-62. Woodhead Publishing.

Koubaa, A., P. Perré, R. M. Hutcheon, and J. Lessard. 2008. "Complex Dielectric Properties of the Sapwood of Aspen, White Birch, Yellow Birch, and Sugar Maple." *Drying Technology* 26 (5):568-578. doi: 10.1080/07373930801944762.

Koya, O. A., and R. S. Fono-Tamo. 2013. "Characterisation of Pulverised Palm Kernel Shell for Sustainable Waste Diversification." *Internation of Journal of Scientific & Engineering Research* 4:6-10.

Krokida, M. K., and Z. B. Maroulis. 1999. "Effect of microwave drying on some quality properties of dehydrated products." *Drying Technology* 17 (3):449-466. doi: 10.1080/07373939908917545.

Ku, H. S., E. Siores, and J. A. R. Ball. 2001. "Review - Microwave Processing of Materials: Part I." *HKIE Transactions* 8 (3):31-37. doi: 10.1080/1023697X.2001.10667855.

Kumar, C., M. U. H. Joardder, T. W. Farrell, G. J. Millar, and M. A. Karim. 2016. "Mathematical model for intermittent microwave convective drying of food materials." *Drying Technology* 34 (8):962-973. doi: 10.1080/07373937.2015.1087408.

Kumar, C., M. U. H. Joardder, A. Karim, G. J. Millar, and Z. Amin. 2014. "Temperature Redistribution Modelling During Intermittent Microwave Convective Heating." *Procedia Engineering* 90 (0):544-549. doi: 10.1016/j.proeng.2014.11.770.

Kumar, P., A. S. Mujumdar, and Z. Koran. 1990. "Microwave Drying: Effects on Paper Properties." *Drying Technology* 8 (5):1061-1087. doi: 10.1080/07373939008959936.

Law, K. N., W. R. W. Daud, and A. Ghazali. 2007. "Morphological and chemical nature of fiber strands of oil palm empty-fruit bunch (OPEFB)." *BioResources* 2 (3):351-362.

Law, M. C., E. L. Liew, S. L. Chang, Y. S. Chan, and C. P. Leo. 2016. "Modelling microwave heating of discrete samples of oil palm kernels." *Applied Thermal Engineering* 98:702-726.

Lee, K. Y., Z. Abbas, Y. K. Yeow, M. D. N. Sharizan, and C. E. Meng. 2010. "In situ measurements of complex permittivity and moisture content in oil palm fruits." *The European Physical Journal Applied Physics* 49 (3):1-5. doi: 10.1051/epjap/2010007.

Lee, S.-H., and S. Wang. 2006. "Biodegradable polymers/bamboo fiber biocomposite with bio-based coupling agent." *Composites Part A: Applied Science and Manufacturing* 37 (1):80-91. doi: 10.1016/j.compositesa.2005.04.015.

Lewis, R. W., P. Nithiarasu, and Kankanhalli. 2008. *Fundamentals of the Finite Element Method for Heat and Fluid Flow*. New Jersey: John Wiley and Sons.

Li, Z. Y., R. F. Wang, and T. Kudra. 2011. "Uniformity Issue in Microwave Drying." *Drying Technology* 29 (6):652-660. doi: 10.1080/07373937.2010.521963.

Liu, C. M., Q. Z. Wang, and N. Sakai. 2005. "Power and temperature distribution during microwave thawing, simulated by using Maxwell's equations and Lambert's law." *International Journal of Food Science & Technology* 40 (1):9-21. doi: 10.1111/j.1365-2621.2004.00904.x.

Liu, J. Y., and C. Shun. 1991. "Solutions of Luikov equations of heat and mass transfer in capillary-porous bodies." *International Journal of Heat and Mass Transfer* 34 (7):1747-1754. doi: 10.1016/0017-9310(91)90150-D.

Liu, S., M. Fukuoka, and N. Sakai. 2013. "A finite element model for simulating temperature distributions in rotating food during microwave heating." *Journal of Food Engineering* 115 (1):49-62. doi: 10.1016/j.jfoodeng.2012.09.019.

Lorenz, K., and R. V. Decareau. 1976. "Microwave heating of foods - changes in nutrient and chemical composition." *C R C Critical Reviews in Food Science and Nutrition* 7 (4):339-370. doi: 10.1080/10408397609527213.

Lovás, M., M. Kováčová, G. Dimitrakis, S. Čuvanová, I. Znamenáčková, and Š. Jakabský. 2010. "Modeling of microwave heating of andesite and minerals." *International Journal of Heat and Mass Transfer* 53 (17–18):3387-3393. doi: 10.1016/j.ijheatmasstransfer.2010.03.012.

Luan, D., J. Tang, P. D. Pedrow, F. Liu, and Z. Tang. 2016. "Analysis of electric field distribution within a microwave assisted thermal sterilization (MATS) system by computer simulation." *Journal of Food Engineering* 188:87-97. doi: 10.1016/j.jfoodeng.2016.05.009.

Luikov, A. V. 1975. "Systems of differential equations of heat and mass transfer in capillary-porous bodies (review)." *International Journal of Heat and Mass Transfer* 18 (1):1-14. doi: 10.1016/0017-9310(75)90002-2.

Lüle, F., and T. Koyuncu. 2015. "Convective and Microwave Drying Characteristics of Sorbus Fruits (Sorbus domestica L.) " *Procedia - Social and Behavioral Sciences* 195:2634-2643. doi: 10.1016/j.sbspro.2015.06.467.

Lupinska, A., M. Araszkiewicz, A. Koziol, and M. Lupinski. 2009. "Microwave Drying of Rapeseeds on a Semi-Industrial Scale with Inner Emission of Microwaves." *Drying Technology* 27:1332–1337.

Madaki, Y. S., and L. Seng. 2013. "Palm oil mill effluent (POME) from Malaysia palm oil mills: Waste or resource." *International Journal of Science, Environment and Technology* 2 (6):1138-1155.

Magee, R. K., Majeda; McMinn, Wendy. 2003. "Modelling the mass transfer during convective, microwave and combined microwave-convective drying of solid slabs and cylinders." *Food Research International* 36 (9-10):977-983.

Magee, T. R. A., W. A. M. McMinn, G. Farrell, L. Topley, Y. S. Al-Degs, G. M. Walker, and M. Khraisheh. 2013. "Moisture and temperature dependence of the dielectric properties of pharmaceutical powders." *Journal of Thermal Analysis and Calorimetry* 111:2157-2164.

Malafronte, L., G. Lamberti, A. A. Barba, B. Raaholt, E. Holtz, and L. Ahrné. 2012. "Combined convective and microwave assisted drying: Experiments and modeling." *Journal of Food Engineering* 112 (4):304-312. doi: 10.1016/j.jfoodeng.2012.05.005.

Mandal, V., Y. Mohan, and S. Hemalath. 2007. "Microwave assisted extraction-an innovative and promising extraction tool for medicinal plant research." *Pharmacognosy Reviews* 1 (1):7-18.

Maroulis, Z. B., and G. D. Saravacos. 2003. *Food Process Design*. New York: Marcel Dekker.

Martin, A. R., M. A. Martins, O. R. R. F. da Silva, and L. H. C. Mattoso. 2010. "Studies on the thermal properties of sisal fiber and its constituents." *Thermochimica Acta* 506 (1–2):14-19. doi: 10.1016/j.tca.2010.04.008.

McConnell, D. R. 1974. "Energy Consumption: A comparison between the Microwave Oven and the Conventional Electric Range." *Journal of Microwave Power* 9 (4):341-347.

Mercier, S., B. Marcos, C. Moresoli, M. Mondor, and S. Villeneuve. 2014. "Modeling of internal moisture transport during durum wheat pasta drying." *Journal of Food Engineering* 124:19-27.

Meredith, R. 1998. *Engineer's Handbook of Industrial Microwave Heating*. Vol. 25: IEE Power Series.

Metaxas, A. C., and R. J. Meredith. 1983. *Industrial Microwave Heating*: P. Peregrinus.

Methacanon, P., U. Weerawatsophon, N. Sumransin, C. Prahsarn, and D. T. Bergado. 2010. "Properties and potential application of the selected natural fibers as limited life geotextiles." *Carbohydrate Polymers* 82 (4):1090-1096. doi: 10.1016/j.carbpol.2010.06.036.

Mielke, T. 2017. "Global supply, demand and price outlook for vegetable oils as well as for palm oil." Price Outlook Conference, Kuala Lumpur, 9 March 2017.

Misra, R. N., and J. H. Young. 1981. "A model for predicting the effect of moisture content on the modulus of elasticity of soy beans." *Transactions of the ASAE* 24:1338-1341.

MPOB. 2011. "Malaysia Palm Oil Industry: Oil Palm in Malaysia." accessed 27 January 2016. http://www.palmoilworld.org/about_malaysian-industry.html.

Mudgett, R. E. 1986. "Microwave properties and heating characteristics of foods." *Food Technology* 40:84-93.

Mujumdar, A. S. 2006. *Handbook of Industrial Drying*. Boca Raton, USA: CRC Press.

Nabinejad, O., D. Sujan, M. E. Rahman, and I. J. Davies. 2015. "Effect of oil palm shell powder on the mechanical performance and thermal stability of polyester composites." *Materials and Design* 65:823-830.

Nair, K. P. P. 2010. "7 - Oil Palm (Elaeis guineensis Jacquin)." In *The Agronomy and Economy of Important Tree Crops of the Developing World*, 209-236. London: Elsevier.

Nascimento, T. A., V. Calado, and C. W. P. Carvalho. 2012. "Development and characterization of flexible film based on starch and passion fruit mesocarp flour with nanoparticles." *Food Research International* 49 (1):588-595. doi: 10.1016/j.foodres.2012.07.051.

Nasri, N. S., U. D. Hamza, A. Abdulkadir, S. N. Ismail, and M. M. Ahmed. 2013. "Utilization of sustainable palm empty fruit bunch sorbents for carbon dioxide capture." 6th International Conference on Process Systems Engineering (PSE ASIA), Kuala Lumpur.

Nasrin, A. B., N. Ravi, W. S. Lim, Y. M. Choo, and A. M. Fadzil. 2011. "Assessment of the performance and potential export renewable energy (RE) from typical cogeneration plants used in palm oil mills." *JEAS - Journal of Engineering & Applied Sciences* 6 (6):433-439.

Navarrete, A., R. B. Mato, and M. J. Cocero. 2012. "A predictive approach in modeling and simulation of heat and mass transfer during microwave heating. Application to SFME of essential oil of Lavandin Super." *Chemical Engineering Science* 68 (1):192-201. doi: 10.1016/j.ces.2011.09.026.

Nelson, S. O., and S. Trabelsi. 2012. "Factors Influencing the Dielectric Properties of Agricultural and Food Products." *Journal of Microwave Power and Electromagnetic Energy* 46 (2):93-107. doi: 10.1080/08327823.2012.11689828.

Noerhidajat, R. Yunus, Z. Z.A., S. Syafiie, and T. S. Chang. 2015. "Modeling and Simulation of Heat and Mass Transfer in Oil Palm Fruit Digestion Process." *Journal of Emerging Trends in Engineering and Applied Sciences (JETEAS)* 6 (2):136-143.

Nor'aini, S., and W. L. Siew. 1990. "Quality control measures in the palm oil industry." *Palm Oil Developments Malaysia* 12:9-17.

Norul Izani, M. A., M. T. Paridah, U. M. K. Anwar, M. Y. Mohd Nor, and P. S. H'ng. 2013. "Effects of fiber treatment on morphology, tensile and thermogravimetric analysis of oil palm empty fruit bunches fibers." *Composites Part B: Engineering* 45 (1):1251-1257. doi: 10.1016/j.compositesb.2012.07.027.

Novak, J. 2013. "Electrical Properties of Popcorn Grains." *Acta Technologica Agriculturae* 2. doi: 10.2478/ata-2013-0011.

Nyakuma, B. B., A. Johari, A. Ahmad, and T. A. T. Abdullah. 2014. "Comparative Analysis of the Calorific Fuel Properties of Empty Fruit Bunch Fiber and Briquette." *Energy Procedia* 52:466-473. doi: 10.1016/j.egypro.2014.07.099.

Ohimain, E. I., and S. C. Izah. 2014. "Energy self-sufficiency of smallholder oil palm processing in Nigeria." *Renewable Energy* 63:426-431. doi: 10.1016/j.renene.2013.10.007.

Oliveira, M. E. C., and A. S. Franca. 2002. "Microwave heating of foodstuffs." *Journal of Food Engineering* 53:347-359.

Oloso, A. O., and B. Clarke. 1993. "Some Aspects of Strength Properties of Cashew Nuts." *Journal of Agricultural Engineering Research* 55 (1):27-43. doi: 10.1006/jaer.1993.1030.

Oloyede, A., and P. Groombridge. 2000. "The influence of microwave heating on the mechanical properties of wood." *Journal of Materials Processing Technology* 100 (1–3):67-73. doi: 10.1016/S0924-0136(99)00454-9.

Omar, R., A. Idris, R. Yunus, K. Khalid, and M. I. Aida Isma. 2011. "Characterization of empty fruit bunch for microwave-assisted pyrolysis." *Fuel* 90 (4):1536-1544. doi: 10.1016/j.fuel.2011.01.023.

Otálora, M. C., J. G. Carriazo, L. Iturriaga, M. A. Nazareno, and C. Osorio. 2015. "Microencapsulation of betalains obtained from cactus fruit (Opuntia ficus-indica) by spray drying using cactus cladode mucilage and maltodextrin as encapsulating agents." *Food Chemistry* 187:174-181. doi: 10.1016/j.foodchem.2015.04.090.

Owolarafe, O. K., T. M. Olabige, and M. O. Faborode. 2007. "Macro-structural characterisation of palm fruit at different processing conditions." *Journal of Food Engineering* 79 (1):31-36. doi: 10.1016/j.jfoodeng.2006.01.024.

Özbek, B., and G. Dadali. 2007. "Thin-layer drying characteristics and modelling of mint leaves undergoing microwave treatment." *Journal of Food Engineering* 83 (4):541-549. doi: 10.1016/j.jfoodeng.2007.04.004.

Pandey, R. N., S. K. Srivastava, and M. D. Mikhailov. 1999. "Solutions of Luikov equations of heat and mass transfer in capillary porous bodies through matrix calculus: a new approach." *International Journal of Heat and Mass Transfer* 42 (14):2649-2660. doi: 10.1016/S0017-9310(98)00253-1.

Papargyris, D. A., R. J. Day, A. Nesbitt, and D. Bakavos. 2008. "Comparison of the mechanical and physical properties of a carbon fibre epoxy composite manufactured by resin transfer moulding using conventional and microwave heating." *Composites Science and Technology* 68 (7–8):1854-1861. doi: 10.1016/j.compscitech.2008.01.010.

Pappas, G., E. Skinner, and V. N. M. Rao. 1988. "Effect of imposed strain and moisture content on some viscoelastic characteristics of cowpea (*Vigna unguiculata*)." *Journal of Agricultural Engineering Research* 39:209-219.

Peters, B., E. Schröder, C. Bruch, and T. Nussbaumer. 2002. "Measurements and particle resolved modelling of heat-up and drying of a packed bed." *Biomass and Bioenergy* 23 (4):291-306. doi: https://doi.org/10.1016/S0961-9534(02)00052-1.

Plumb, O. A., G. A. Spolek, and B. A. Olmstead. 1985. "Heat and mass transfer in wood during drying." *International Journal of Heat and Mass Transfer* 28 (9):1669-1678. doi: 10.1016/0017-9310(85)90141-3.

Prabhu, G., N. Arvind Kumar, M. Sankaranarayana, and T. K. Nandy. 2014. "Tensile and impact properties of microwave sintered tungsten heavy alloys." *Materials Science and Engineering: A* 607 (0):63-70. doi: 10.1016/j.msea.2014.03.130.

Pradeepkumar, T., B. S. Jyothibhaskar, and K. N. Satheesan. 2008. *Management of Horticultural Crops*. Edited by K. V. Peter. Vol. 11. New Delhi: New India Publishing.

Puangsuwan, K., M. Chongcheawchamnan, and C. Tongurai. 2015. "Effective Moisture Diffusivity, Activation Energy and Dielectric Model for Palm Fruit Using a Microwave Heating." *Journal of Microwave Power and Electromagnetic Energy* 49 (2):100-111.

Rahman, M. S. 2007. *Handbook of Food Preservation*. Florida: CRC Press.

Raji, A. O., and J. F. Favier. 2004. "Model for the deformation in agricultural and food particulate materials under bulk compressive loading using discrete element method. II: compression of oilseeds." *Journal of Food Engineering* 64:373-380.

Rakesh, V., A. K. Datta, J. H. Walton, K. L. McCarthy, and M. J. McCarthy. 2011. "Microwave Combination Heating: CoupledElectromagnetics- Multiphase Porous MediaModeling and MRI Experimentation." *Bioengineering, Food and Natural Products* 58 (4):1262-1278. doi: 10.1002/aic.12659.

Ramasamy, S., and B. Moghtaderi. 2010. "Dielectric Properties of Typical Australian Wood-Based Biomass Materials at Microwave Frequency." *Energy Fuels* 24 (8):4534-4548. doi: 10.1021/ef100623e.

Ranjan, R., J. Irudayaraj, and J. Mahaffy. 2002. "Modeling Simultaneous Heat and Mass Transfer using the Control-volume Method." *Numerical Heat Transfer, Part B: Fundamentals* 41 (5):463-476. doi: 10.1080/104077902753725911.

Rattanadecho, P. 2006. "The simulation of microwave heating of wood using a rectangular wave guide: Influence of frequency and sample size." *Chemical Engineering Science* 61 (14):4798-4811. doi: 10.1016/j.ces.2006.03.001.

Rodríguez, R., J. I. Lombraña, M. Kamel, and C. de Elvira. 2005. "Kinetic and Quality Study of Mushroom Drying under Microwave and Vacuum." *Drying Technology* 23 (9-11):2197-2213. doi: 10.1080/07373930500212685.

Rossen, J. L. H., K. 1977. "Simultaneous Heat and Moisture Transfer in Dehydrated Food: A Review of Theoretical Models." *AIChE Symposium Series* 163:71-81.

Ryynänen, S. 1995. "The electromagnetic properties of food material: a review of the basic principles." *Journal of Food Engineering* 26 (4):409-429.

Sabil, K. M., M. A. Aziz, B. Lal, and Y. Uemura. 2013. "Effects of torrefaction on the physiochemical properties of oil palm empty fruit bunches, mesocarp fiber and kernel shell." *Biomass and Bioenergy* 56 (0):351-360. doi: 10.1016/j.biombioe.2013.05.015.

Sacilik, K., and A. Colak. 2010a. "Determination of dielectric properties of corn seeds from 1 to 100 MHz." *Powder Technology* 203 (2):365-370. doi: 10.1016/j.powtec.2010.05.031.

Sacilik, K., and A. Colak. 2010b. "Determination of dielectric properties of corn seeds from 1 to 100 MHz." *Powder Technology* 203:365-370.

Sacilik, K., C. Tarimci, and A. Colak. 2006. "Dielectric Properties of Flaxseeds as affected by Moisture Content and Bulk Density in the Radio Frequency Range." *Biosystems Engineering* 93 (2):153-160. doi: 10.1016/j.biosystemseng.2005.11.001.

Salema, A. A., Y. K. Yeow, K. Ishaque, F. N. Ani, M. T. Afzal, and A. Hassan. 2013. "Dielectric properties and microwave heating of oil palm biomass and biochar." *Industrial Crops and Products* 50:366-374. doi: 10.1016/j.indcrop.2013.08.007.

Salvi, D., D. Boldor, G. M. Aita, and C. M. Sabliov. 2011. "COMSOL Multiphysics model for continuous flow microwave heating of liquids." *Journal of Food Engineering* 104 (3):422-429. doi: 10.1016/j.jfoodeng.2011.01.005.

Sarah, M., and M. R. Taib. 2013. "Microwave Sterilization of Oil Palm Fruits: Effect of Power, Temperature and D-value on Oil Quality." *Journal of Medical and Bioengineering* 2 (3):153-156. doi: 10.12720.

Schiffmann, R. F., and R. Steiner. 2012. "Inexpensive Microwave Leakage Detectors - Are They Worth It? (A Performance Evaluation Report)." *Journal of Microwave Power and Electromagnetic Energy* 46 (3):128-138.

Sharma, G. P., and S. Prasad. 2001. "Drying of garlic (Allium sativum) cloves by microwave–hot air combination." *Journal of Food Engineering* 50 (2):99-105. doi: 10.1016/S0260-8774(00)00200-4.

Shepherd, H., and R. K. Bhardwaj. 1986. "Thermal properties of pigeon pea." *Cereal Foods World* 31:466-470.

Shinoj, S., R. Visvanathan, S. Panigrahi, and M. Kochubabu. 2011. "Oil palm fiber (OPF) and its composites: A review." *Industrial Crops and Products* 33 (1):7-22. doi: 10.1016/j.indcrop.2010.09.009.

Singh, R. P., and D. R. Heldman. 2014. "Chapter 4 - Heat Transfer in Food Processing." In *Introduction to Food Engineering (Fifth Edition)*, 265-419. San Diego: Academic Press.

Sipahioglu, O., and S. A. Barringer. 2003. "Dielectric Properties of Vegetables and Fruits as a Function of Temperature, Ash, and Moisture Content." *Journal of Food Science* 68 (1):234-239. doi: 10.1111/j.1365-2621.2003.tb14145.x.

Sivasothy, K., and M. H. Rohaya. 2000. "Crushing and sterilization of fresh fruit bunches: a promising approach for continuous sterilization." International Planters Conference, Kuala Lumpur, 17-20 May.

Sobhy, A., and J. Chaouki. 2010. "Microwave-assisted Biorefinery." *Chemical Engineering Transactions* 19:25-31.

Sólyom, K., S. Kraus, R. B. Mato, V. Gaukel, H. P. Schuchmann, and M. J. Cocero. 2013. "Dielectric properties of grape marc: Effect of temperature, moisture content and sample preparation method." *Journal of Food Engineering* 119 (1):33-39. doi: 10.1016/j.jfoodeng.2013.05.005.

Sosa-Morales, M. E., L. Valerio-Junco, A. López-Malo, and H. S. García. 2010. "Dielectric properties of foods: Reported data in the 21st Century and their potential applications." *LWT - Food Science and Technology* 43 (8):1169-1179. doi: 10.1016/j.lwt.2010.03.017.

Soysal, Y., S. Öztekin, and Ö. Eren. 2006. "Microwave Drying of Parsley: Modelling, Kinetics, and Energy Aspects." *Biosystems Engineering* 93 (4):403-413. doi: 10.1016/j.biosystemseng.2006.01.017.

Stanisławski, J. 2005. "Drying of Diced Carrot in a Combined Microwave–Fluidized Bed Dryer." *Drying Technology* 23 (8):1711-1721. doi: 10.1081/DRT-200065129.

Suardana, N. P. G., M. S. Ku, and J. K. Lim. 2011. "Effects of diammonium phosphate on the flammability and mechanical properties of bio-composites." *Materials & Design* 32 (4):1990-1999. doi: 10.1016/j.matdes.2010.11.069.

Sukaribin, N., and K. Khalid. 2009. "Effectiveness of sterilisation of oil palm bunch using microwave technology." *Industrial Crops and Products* 30 (2):179-183. doi: 10.1016/j.indcrop.2009.05.001.

Sulaiman, O., M. F. Awalludin, R. Hashim, and M. I. H. Mondal. 2012. "The effect of relative humidity on the physical and mechanical properties of oil palm trunk and rubberwood." *Cellulose Chemistry and Technology* 46 (5):401-407.

Sumnu, G., E. Turabi, and M. Oztop. 2005. "Drying of carrots in microwave and halogen lamp–microwave combination ovens." *LWT - Food Science and Technology* 38 (5):549-553. doi: 10.1016/j.lwt.2004.07.006.

Tagoe, S. M. A., M. J. Dickinson, and M. M. Apetorgbor. 2012. "Factors influencing quality of palm oil produced at the cottage industry level in Ghana." *International Food Research Journal* 19 (1):271-278.

Tan, H. S. 1981. "Microwave heating of oil-palm fresh fruit samples." *United Nations Educational, Scientific and Cultural Organization* 16:1-16.

Thostenson, E. T., and T. W. Chou. 1999. "Microwave processing: fundamentals and applications." *Composites: Part A* 30:1055-1071.

Torgovnikov, G. I. 1993. "Dielectric Properties of Wood and Wood-Based Materials." In. Berlin: Springer.

Ujang, Z., S. Salmiati, and M. R. Salim. 2010. Microbial Biopolimerization Production from Palm Oil Mill Effluent (POME). In *Biopolymers*, edited by Magdy Elnashar. Rijeka, Croatia: InTech.

Umesh Hebbar, H., and N. K. Rastogi. 2012. "Chapter 12 - Microwave Heating of Fluid Foods." In *Novel thermal and non-thermal technologies for fluid foods*, edited by P. J. CullenBrijesh K. TiwariVasilis P. Valdramidis, 369-409. San Diego: Academic Press.

Umudee, I., M. Chongcheawchamnan, M. Kiatweerasakul, and C. Tongurai. 2013. "Sterilization of oil palm fresh fruit using microwave technique." *International Journal of Chemical Engineering and Applications* 4 (3):111-113. doi: 10.7763/IJCEA.2013.V4.274.

Uyar, R., F. Erdogdu, F. Sarghini, and F. Marra. 2016. "Computer simulation of radio-frequency heating applied to block-shaped foods: Analysis on the role of geometrical parameters." *Food and Bioproducts Processing* 98:310-319. doi: 10.1016/j.fbp.2016.02.009.

Vázquez, G., F. Chenlo, R. Moreira, and A. Costoyas. 1999. "The dehydration of garlic 2: The effects of pretreatments on drying kinetics." *Drying Technology* 17 (6):1109-1120. doi: 10.1080/07373939908917597.

Verboven, P., A. K. Datta, N. T. Anh, N. Scheerlinck, and B. M. Nicolaï. 2003. "Computation of

airflow effects on heat and mass transfer in a microwave oven." *J. Food Eng.* 59:181-190.

Vincent, C. J., R. Shamsudin, and A. S. Baharuddin. 2014. "Pre-treatment of oil palm fruits: A review." *Journal of Food Engineering* 143:123-131. doi: 10.1016/j.jfoodeng.2014.06.022.

Waananem, K. M., and M. R. Okos. 1988. "Failure properties of yellow dent corn kernels." *Transactions of the ASAE* 31:1816-1823.

Walde, S. G., K. Balaswamy, V. Velu, and D. G. Rao. 2002. "Microwave drying and grinding characteristics of wheat (Triticum aestivum)." *Journal of Food Engineering* 55 (3):271-276. doi: 10.1016/S0260-8774(02)00101-2.

Wang, J., and Y. S. Xi. 2005. "Drying characteristics and drying quality of carrot using a two-stage microwave process." *Journal of Food Engineering* 68 (4):505-511. doi: 10.1016/j.jfoodeng.2004.06.027.

Wang, J., Z. Zhou, and J. Zhao. 2016. "A method for the steady-state thermal simulation of district heating systems and model parameters calibration." *Energy Conversion and Management* 120:294-305. doi: 10.1016/j.enconman.2016.04.074.

Wang, W., G. Chen, and F. Gao. 2005. "Effect of Dielectric Material on Microwave Freeze Drying of Skim Milk." *Drying Technology* 23 (1-2):317-340. doi: 10.1081/DRT-200047896.

Wang, W., G. Chen, and A. Mujumdar. 2007. "Physical interpretation of solids drying: An overview on mathematical modeling research." *Drying Technology* 25 (4):659-668. doi: 10.1080/07373930701285936.

Wang, W., B. N. Thorat, G. Chen, and A. S. Mujumdar. 2002. "Simulation of Fluidized-bed Drying of Carrot with Microwave Drying." *Drying Technology* 20 (9):1855-1867. doi: 10.1081/DRT-120015418.

Whitaker, S. 1977. "Simultaneous Heat, Mass, and Momentum Transfer in Porous Media: A Theory of Drying." In *Advances in Heat Transfer*, edited by P. Hartnett James and F. Irvine Thomas, 119-203. Elsevier.

Xanthopoulos, G., D. Mitropoulos, and G. Lambrinos. 2012. "Estimation of Heat and Mass Transfer Coefficients During Air-Freezing of Cucumber." *International Journal of Food Properties* 15 (2):221-235. doi: 10.1080/10942911003778006.

Yang, H. W., and S. Gunasekaran. 2004. "Comparison of temperature distribution in model food cylinders based on Maxwell's equations and Lambert's law during pulsed microwave heating." *Journal of Food Engineering* 64 (4):445-453. doi: 10.1016/j.jfoodeng.2003.08.016.

Yanyang, X., Z. Min, A. S. Mujumdar, Z. Le-qun, and S. Jin-cai. 2004. "Studies on Hot Air and Microwave Vacuum Drying of Wild Cabbage." *Drying Technology* 22 (9):2201-2209. doi: 10.1081/DRT-200034275.

Yee, L. K., Z. Abbas, M. A. Jusoh, Y. K. Yeow, and C. E. Meng. 2011. "Determination of Moisture Content in Oil Palm Fruits Using a Five-Port Reflectometer." *Sensors* 11 (4):4073-4085.

Younsi, R., D. Kocaefe, S. Poncsak, and Y. Kocaefe. 2007. "Computational modelling of heat and mass transfer during the high-temperature heat treatment of wood." *Applied Thermal Engineering* 27 (8–9):1424-1431. doi: 10.1016/j.applthermaleng.2006.10.025.

Zaidul, I. S. M., N. A. N. Norulaini, A. K. M. Omar, Y. Sato, and R. L. Smith Jr. 2007. "Separation of palm kernel oil from palm kernel with supercritical carbon dioxide using pressure swing technique." *Journal of Food Engineering* 81 (2):419-428. doi: 10.1016/j.jfoodeng.2006.11.019.

Zhang, J., and A. K. Datta. 2004. "Some Considerations in Modeling of Moisture Transport in Heating of Hygroscopic Materials." *Drying Technology* 22 (8):1983-2008. doi: 10.1081/DRT-200032740.

Zhao, J., Z. Fu, X. Jia, and Y. Cai. 2016. "Modeling conventional drying of wood: Inclusion of a moving evaporation interface." *Drying Technology* 34 (5):530-538. doi: 10.1080/07373937.2015.1060999.

Zheng, Y., Z. Pan, and R. Zhang. 2009. "Overview of biomass pretreatment for cellulosic ethanol production " *International Journal of Agricultural and Biological Engineering* 2 (3):51-67.

Zhou, L., V. M. Puri, R. C. Anantheswaran, and G. Yeh. 1995. "Finite element modeling of heat and mass transfer in food materials during microwave heating-Model development and validation." *Journal of Food Engineering* 25 (4):509-529.

Zhu, X., W. Guo, X. Wu, and S. Wang. 2012. "Dielectric properties of chestnut flour relevant to drying with radio-frequency and microwave energy." *Journal of Food Engineering* 113 (1):143-150. doi: 10.1016/j.jfoodeng.2012.04.014.

APPENDIX

Appendix 1 Experiment Set-up

Modified domestic microwave oven (Samsung ME711K) and weight balance (AA-160 Denmer)

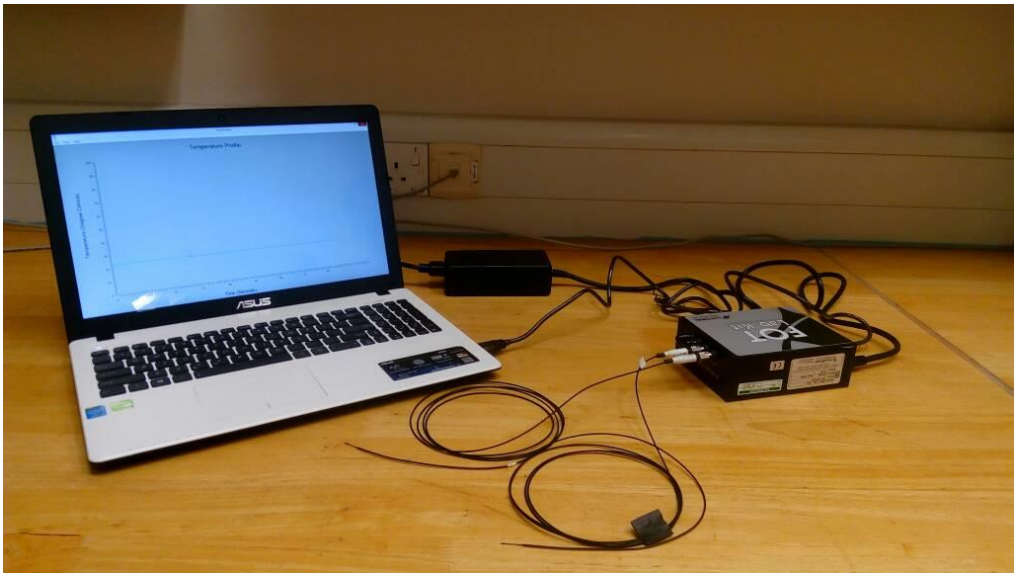

Fiber optic thermometers (Luxtron, USA) are connected to computer through FOT lab kit 4-channel fiber optic thermometry system